Non-equilibrium dynamics of driven low-dimensional quantum systems

Stefano Scopa

Université de Lorraine - École doctorale C2MP

Thèse

présentée pour obtenir le grade de

Docteur en Physique

par

Stefano Scopa

LPCT - Université de Lorraine, Nancy

Non-equilibrium dynamics of driven low-dimensional quantum systems

Membres du Jury:

Président du jury:	
Malte Henkel,	LPCT - Université de Lorraine, Nancy
Rapporteurs :	
Tomaž Prosen,	University of Ljubljana
Cécile Monthus,	IPhT CNRS-CEA - Université Paris-Saclay
Examinateurs :	
Rosemary J. Harris,	Queen Mary University of London
Denis Bernard,	ENS Paris
Guillaume Roux,	LPTMS - Université Paris Sud
Directeur de Thèse :	
Dragi Karevski,	LPCT - Université de Lorraine, Nancy

Nancy September 30, 2019

Acknoledgements

I would like to sincerely thank Dragi for his guidance and his help during the development of the thesis. If I look backwards to three years ago, I really understand how much I got from his supervision. On the same footing, I would like to thank also my collaborators Jérémie Unterberger and Gabriel Landi. They have strengthened and enlarged my background in mathematics and in quantum physics. Much of my formation is due to them as well.

I am thankful to Tomaž Prosen and Cécile Monthus for their role of rapporteurs on the manuscript and to Rosemary Harris, Guillaume Roux, Malte Henkel and Denis Bernard for completing the thesis committee.

I am grateful to Chiara Animali and Thierry Platini for their suggestions and for the remarks on the thesis draft. A special thanks goes also to Yannis Brun, with which I have shared this PhD experience every day, from the beginning up to these last stages. Without him, my PhD time would not have been the same. Not less, I would like to thank also the other (former and fellow) students Dimitrios Voliotis, Hugo Tschirhart, Frankie Azevedo, Sascha Wald, Marjana Krasnytska, Alekos Segalina and Claude Dimo.

I am thankful to Jérôme Dubail, Malte Henkel and Ettore Vicari for physical insights and for their help in finding a Post-Doc position.

Lastly, I would like to thank the whole LPCT lab for their warm welcome and for letting me feel an active part of the group at any time.

A great thanks goes also to my family, that encouraged and supported me during these years.

Contents

Acronyms

AD Adiabatic
BCH Baker-Campbell-Hausdorff
BH Bose Hubbard
CPTP Complete-Positive-Trace-Preserving
EL Ermakov-Lewis
FSS Finite-Size Scaling
HO Harmonic Oscillator
JW Jordan Wigner
KZ Kibble-Zurek
LDA Local Density Approximation
MI Mott-Insulator
QAD Quasi-Adiabatic
QPT Quantum Phase Transition
RG Renormalization Group
SF Superfluid
TD Thermodynamical
TG Tonks-Girardeau
TSS Trap-Size Scaling
US Unitarily Stable
UU Unitarily Unstable

List of publications

One-dimensional Bose gas driven by a slow time-dependent harmonic trap
authors: Stefano Scopa and Dragi Karevski
journal ref: J. Phys. A: Math. Theor. 50, (42) 425301 (2017)
doi: 10.1088/1751-8121/aa890f
arXiv: 1706.00723

Exact dynamics of a one dimensional Bose gas in a periodic time-dependent harmonic trap
authors: Stefano Scopa, Jérémie Unteberger and Dragi Karevski
journal ref: J. Phys. A: Math. Theor. 51, (18) 185001 (2018)
doi: 10.1088/1751-8121/aab8a5
arXiv: 1801.07462

Lindblad-Floquet description of finite-time quantum heat engines
authors: Stefano Scopa, Gabriel T. Landi and Dragi Karevski
journal ref: Phys. Rev. A 97, 062121 (2018)
doi: 10.1103/PhysRevA.97.062121
arXiv: 1803.11180

Exact solution of time-dependent Lindblad equations with closed algebras
authors: Stefano Scopa, Gabriel T. Landi, Adam Hammoumi and Dragi Karevski
journal ref: Phys. Rev. A 99, 022105 (2019)
doi: 10.1103/PhysRevA.99.022105
arXiv: 1811.05490

Other works:

Dynamical off-equilibrium scaling across magnetic first order phase transitions
authors: Stefano Scopa and Sascha Wald
journal ref: J. Stat. Mech. 113205 (2018)
doi: 10.1088/1742-5468/aaeb46
arXiv: 1806.00866

Introduction & Summaries

Summaries

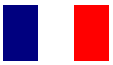

Résumé

Cette thèse analyse certains aspects de la dynamique hors équilibre de systèmes quantiques unidimensionnels lorsqu'ils sont soumis à des champs externes dépendant du temps. Nous considérons plus particulièrement le cas des forçages périodiques, et le cas d'une variation temporelle lente d'un paramètre de l'Hamiltonien qui permet de traverser une transition de phase quantique.
La première partie contient une présentation des notions, des modèles et des outils nécessaires pour comprendre la suite de la thèse, avec notamment des rappels sur les modèles quantiques critiques (en particulier sur les chaines de spin et sur le modèle de Bose-Hubbard), le mécanisme de Kibble-Zurek, et la théorie de Floquet.
Ensuite, nous étudions la dynamique hors équilibre des gaz de Tonks-Girardeau dans un potentiel harmonique dépendant du temps par différentes techniques: développements perturbatifs, diagonalisation numérique exacte et solutions analytiques exactes basées sur la théorie des invariants dynamiques d'Ermakov-Lewis.
Enfin, nous analysons la dynamique hors équilibre des systèmes quantiques ouverts markoviens soumis à des variations périodiques des paramétres du système et de l'environnement. Nous formulons une théorie de Floquet afin d'obtenir des solutions exactes des équations de Lindblad périodiques. Ce formalisme de Lindblad-Floquet est utilisé pour obtenir une caractérisation exacte du fonctionnement en temps fini des machines thermiques quantiques.

Abstract

This thesis analyzes some aspects regarding the dynamics of one-dimensional quantum systems which are driven out-of-equilibrium by the presence of time-dependent external fields. Among the possible kinds of driven systems, our

focus is dedicated to the slow variation of a Hamiltonian's parameter across a quantum phase transition and to the case of a time-periodic forcing. To begin with, we prepare the background and the tools needed in the following. This includes a brief introduction to quantum critical models (in particular to the XY spin chain and to the Bose-Hubbard model), the Kibble-Zurek mechanism and Floquet theory.
Next, we consider the non-equilibrium dynamics of Tonks-Girardeau gases in time-dependent harmonic trap potentials. The analysis is made with different techniques: perturbative expansions, numerical exact diagonalization and exact methods based on the theory of Ermakov-Lewis dynamical invariants.
The last part of the thesis deals instead with the non-equilibrium dynamics of markovian open quantum systems subject to time-periodic perturbations of the system parameters and of the environment. This has led to an exact formulation of Floquet theory for a Lindblad dynamics. Moreover, within the Lindblad-Floquet framework it is possible to have an exact characterization of the finite-time operation of quantum heat-engines.

Introduction

The non-equilibrium statistical physics is a wide and far-reaching subject. In its broadest interpretation, it includes any statistical system which is driven out-of-equilibrium because of some external perturbations. From stochastic processes, transport phenomena and phase-ordering kinetics to relaxation problems in quantum physics and, also, from inflationary times to the control of many-body wave functions in modern quantum devices, non-equilibrium behaviors appear in different contexts at any time of our history.
In contrast with equilibrium statistical mechanics, the non-equilibrium counterpart lacks of a general framework and it requires the development of specific tools depending on the problem that is faced. As a consequence, the study of non-equilibrium behaviors is typically focused on specific problems. Nevertheless, the large use of the term *non-equilibrium* over the last decades is due to shared questions and aims, such as the discovery of new states of matter, the analysis of unconventional dynamical behaviors and the technological advances that can be achieved. From its beginnings up to nowadays, this interest has been constantly fed thanks to the progress of numerical techniques and to the experimental possibility of testing the theoretical predictions regarding the non-equilibrium dynamics. Such a path has led to several important results, among which we may mention the relaxation towards generalized Gibbs ensembles [Rig07], the development of generalized hydrodynamics [Ber12a, Ber16, CA16] or the novel studies in quantum information, see e.g. [Wee12, Wil17], and quantum thermodynamics, see e.g. [Gem10, Bin18].

In this thesis, the focus is on those non-equilibrium situations that are realized by a proper time-variation of physical parameters (e.g. the temperature, the magnetic field or the pressure). In fact, even though a system typically manages to relax towards new equilibrium situations (corresponding to the current values of the parameters), there exist some cases in which the relaxation time of a certain perturbation exceeds the time variations of the perturbation itself and thus the system collectively falls out-of-equilibrium. These cases include a sudden and sharp variation of the parameters, namely the *quench protocols*, or the driving across critical points, where the emergence of large-scale modes prevents the equilibration.
Similarly, non-equilibrium behaviors can emerge when the system is coupled to

an oscillating parameter: because of the time periodicity of the perturbation, the system is unable to relax towards a steady-state and it will (possibly) converge towards a cyclic evolution only after a long time.
Our analysis mainly deals with one-dimensional quantum systems, for which several techniques (such as *bosonization* or *fermionization*) have been developed in order to obtain exact predictions regarding their equilibrium and non-equilibrium properties. The quantum physics in one dimension shows interesting peculiarities due to the special character of the particles interactions: no quasi-free excitations exist since the motion of any particle inevitably affects the behavior of its neighbors; any individual displacement results therefore into a collective motion [Gia03]. Moreover, the improvements in the experimental manipulation of quantum platforms (such as cold atoms or quantum spin chains) have led to the experimental realizations of quasi-1d geometries, pushing the physics community to look into the 1d world not only for theoretical interest.

The thesis is organized in two main parts. **Part I** is dedicated to the construction of the background and of the tools that we need for later discussions. Indeed, our idea is to guide *any* reader (even those that are not familiar with the topic) through the whole manuscript and to provide the information that are required for a complete understanding. However, in order to cover in brief many arguments, these chapters will not give a comprehensive view on the treated topics. In details,

> **Chapter 1** is an introduction to quantum phase transitions and to their appearance in well-known quantum critical models.
> We recall the general idea of quantum transitions, renormalization group and the emergence of scaling behaviors; we mention the problem of having a zero temperature. Afterwards, we present two paradigmatic quantum critical models, namely the quantum XY spin chain and the Bose-Hubbard Hamiltonian. For the XY model, we discuss the possible experimental realization with ions crystals, the properties of the ground state in the different regions of the phase diagram and its quantum phase transitions. The exact solution of the model by means of a Jordan-Wigner transformation is explicitly shown. Concerning the Bose-Hubbard Hamiltonian, we move from its experimental realization with gases of cold atoms in optical lattices to the theoretical analysis of the ground state on varying of the lattice depth. A qualitative phase diagram is derived with mean-field approximation.
>
> In **Chapter 2**, we consider the dynamical behavior of quantum critical

models that are slowly driven across a quantum phase transition by time-dependent parameters. We discuss the emergence of non-equilibrium behaviors due to the breakdown of the adiabaticity, the formation of topological defects, the Kibble-Zurek approximation and the non-equilibrium scaling limit. Next, we talk about Kibble-Zurek in space for the analysis of inhomogeneous systems; this leads to the breakdown of local approximation and to a trap-size scaling regime.

Chapter 3 gives a twofold analysis on Floquet theory, from both physical and mathematical perspectives. First, we introduce the Floquet dynamics for time-periodic Schrödinger equations, including high-frequency expansions for fast-oscillating drivings and an exact algebraic approach. After that, we turn into math and we recall the general ideas about Floquet theorem; for later purposes, we also discuss the application of Floquet theorem to the study of the stability intervals of the Hill operators.

The **Part II** of the thesis is devoted to the analysis of specific problems. The discussion mostly follows the published research papers. More precisely,

In **Chapter 4**, we investigate the non-equilibrium dynamics of Bose-gases in time-dependent harmonic traps. In particular, we focus on the Tonks-Girardeau limit of the Bose-Hubbard model, that is for strong repulsive interaction where it is reduced to a XX spin chain. Next, we consider a slow trap release protocol which corresponds to an inhomogeneous protocol across the XX criticality driven by an effective chemical potential (induced by the trap). We analyze the problem with different approaches: numerical exact diagonalization, quasi-adiabatic perturbation theory and with exact Ermakov-Lewis theory; the case of a Efimov expansion is explicitly considered. Afterwards, we move to the case of a periodic variation of the trap amplitude. With the use of Floquet theory, together with Ermakov-Lewis invariants, we classify the possible dynamical scenarios of the bosons cloud depending on the type of periodic forcing. We find two main cases: on one hand, the emergence of breathing modes; on the other, the development of dynamical instabilities. Both the scenarios allow for a scaling description that we explicitly point out.

Chapter 5 is dedicated to the study of non-equilibrium dynamics in markovian open quantum systems. We introduce the concept of markovian master equation and we comment about the Kraus decomposition of a generic dynamical map; we derive the Lindblad master equation and its

construction from phenomenological hints. Afterwards, we move into a vectorized space. We look for exact solutions of time-dependent Lindblad equations where both the unitary parameters and the environment can depend on time. To do so, we build a super-operator basis satisfying closed algebra and we design a time-dependent map to an auxiliary time-independent frame; hence, one can solve for the dynamics of the auxiliary system and, coming back to the physical frame, the time evolution of the driven open system. Then, we analyze the case of a periodic driving and we show how the auxiliary frame technique allows for an exact Floquet description of the Lindblad evolution. Two explicit examples are provided: a single qubit system and a squeezed harmonic oscillator. As a concrete application, we make use of Lindblad-Floquet theory for the exact description of finite-time quantum heat-engines.

A short abstract is provided at the beginning of these chapters for a quick focus on the key parts and on the main results. Technical aspects and further information are found in the appendices at the end of each chapter.
General conclusions and future perspectives are drawn in the last paragraph of the manuscript.

Part I

Background & Tools

Chapter 1

Quantum critical models

A phase transition occurs when the variation of a physical parameter (such as the temperature or the pressure) leads to a rearrangement of the internal degrees of freedom of the system with a consequent qualitative change of its macroscopic properties.
The history of phase transitions dates back to the discovery of Andrews critical opalescence in carbon dioxide [And69], or even further back in the past with the pioneer studies of de la Tour [dlT22, dlT23, Ber09]. From that time, an increasing number of phenomena have been described within the theory of phase transitions [Car96, Ma00, Hen08] including e.g. the different states of water, the creation of magnets from iron samples, the opalescence of some liquids compounds up to some aspects regarding the Universe itself.
In general, a phase transition is governed by an order parameter (e.g. the magnetization of a magnet or the density fluctuations in liquid systems) that captures the properties of the system in the different regions of the phase diagram and that qualitatively changes across a phase boundary. A preliminary classification of phase transitions is made considering the way in which the order parameter is modified at the transition point: we distinguish between *continuous* (or of second-order) phase transitions, where the order parameter varies continuously across the phase boundary and *discontinuous* (or of first-order) phase transitions, where the order parameter undergoes instead an abrupt variation. Here, we shall focus mostly on the former class even though we mention that interesting physics is found at first-order transitions as well (e.g. hysteresis cycles or memory kernels related to the formation of metastable states) [Bin87].
Continuous phase transitions are said to be *critical* because they are character-

ized by the presence of fluctuations that occur over increasing distances and on an increasing time scale. This peculiarity leads to a universal description of critical phenomena, based on the symmetry properties of the model but not on its microscopic details.
The nature of the fluctuations of the order parameter leads to a second important classification of phase transitions. If the excitations are mainly thermally actived, we will say that the transition is *thermal*. On the other hand, if the main source of excitations is given by quantum fluctuations then we will speak about *quantum phase transitions* [Son97, Voj03, Sac11a, Dut15].
The role played by quantum mechanics in phase transitions is however a bit more subtle than this. More precisely, a quantum phase transition is achieved only at absolute zero temperature when a (non-thermal) parameter drives a transition of the system's ground state. Conversely, any phase transition occuring at a finite temperature $T \neq 0$ is thermal.
Indeed, scale invariance at the criticality implies that large-scale modes have a vanishing energy gap ($\varepsilon \to 0$) and thus any quantum contribution to the fluctuations of the order parameter is irrelevant on macroscopic scales (since then $\varepsilon \ll T$). This does not necessarily mean that quantum physics is unimportant for thermal transitions. For instance, one can think about the λ-point of ^{4}He which is reached at temperatures $T_\lambda \sim 4$ Kelvin [Pit16]. Here, the formation of the condensate wave function results from quantum mechanical microscopic processes but still the universal large-scale behavior is described in terms of a classical (complex-valued) field.
That being said, one might think that quantum phase transitions are of marginal interest due to the experimental impossibility to reach zero temperature. In reality, the expected behaviors at $T = 0$ have already consequences on the thermodynamic properties at low (but finite) temperatures and for a broad range of values of the non-thermal parameter around its quantum transition point. It has been shown that a *quantum critical regime* extends to low temperatures [Sac11b, Kin14, Kla14, Fré19]. In this regime, the presence of a finite temperature gives rise to unconventional power-law dependences with exponents that are governed by the physics at $T = 0$. As a consequence, unexpected physical behaviors, such as Dirac liquids [Cro16, Luc16], are observed.
Quantum phase transitions show up in a plethora of models, among which some of the best-known are transverse-field spin systems and Hubbard models. Several experiments have been testing quantum critical models in the last two decades. We can mention experiments made with ions crystals [Col10a, Bit96], cuprates [Zal04, Tsv16], heavy fermions [Si10, Wan17, Che17] and cold atomic gases [Gre02, Tak14, Kin04, Fol00, Bou09, Sch18a], as some examples.

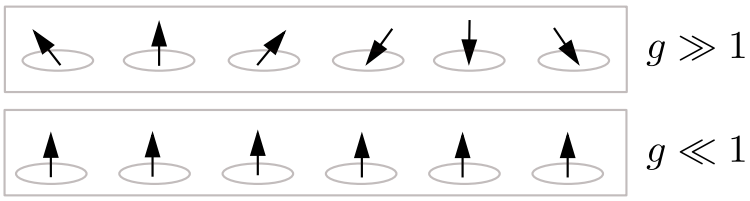

Figure 1.1: **Illustration of a phase transition.** Typical lattice configuration of the system in Eq.(1.1.1) in the limits $g \gg 1$ and $g \ll 1$. The former case is associated to a ground state Ψ_0 that is symmetric under G while in the latter Ψ_0 has a reduced symmetry $G' \subset G$.

1.1 Quantum Phase Transitions

Let $\hat{H}$ be a quantum Hamiltonian living on a 1d lattice of size L of the form

$$\hat{H}(g) = g\,\hat{H}_0 + \hat{H}_1 \tag{1.1.1}$$

with g a dimensionless (non-thermal) parameter. Suppose that $\hat{H}(g)$ is invariant under a certain symmetry group G but that the symmetry properties of the ground state Ψ_0 depend on the value of the parameter g. In particular, suppose that for $g \gg 1$ where $\hat{H} \propto \hat{H}_0$, Ψ_0 is invariant under the full symmetry group G whereas for $g \ll 1$ where $\hat{H} \simeq \hat{H}_1$, Ψ_0 reduces its symmetry to a subgroup $G' \subset G$, see Fig.1.1. This implies that there exists a transition point $g = g_c$ where we assist to a change in the macroscopic properties of the system's ground state associated with the spontaneous symmetry breaking $G \to G'$.
The transition point can be located considering the ground state energy

$$E_0(g) \equiv \langle \Psi_0 | \hat{H}(g) | \Psi_0 \rangle \tag{1.1.2}$$

as a function of g. The change in nature of the low-energy properties will be then related to a *non-analyticity* in the behavior of $E_0(g)$ arising when $g \to g_c$. For sake of simplicity, let us assume that the operators $\hat{H}_0$ and $\hat{H}_1$ are conserved quantities, i.e., $[\hat{H}_0, \hat{H}_1] = 0$ so that the system's eigenstates are independent on g. Conversely, the energy spectrum will vary with g and, for $g \to g_c$, it will generate a *level-crossing* where a low-lying excited state and the ground state exchange each other. At the level-crossing, a non-analyticity point in the ground state energy is created.
More commonly, the two parts of the Hamiltonian in Eq.(1.1.1) do not commute and what we observe is an *avoided* level-crossing where the non-analyticity of $E_0(g)$ develops only for $L \to \infty$, see Fig.1.2.

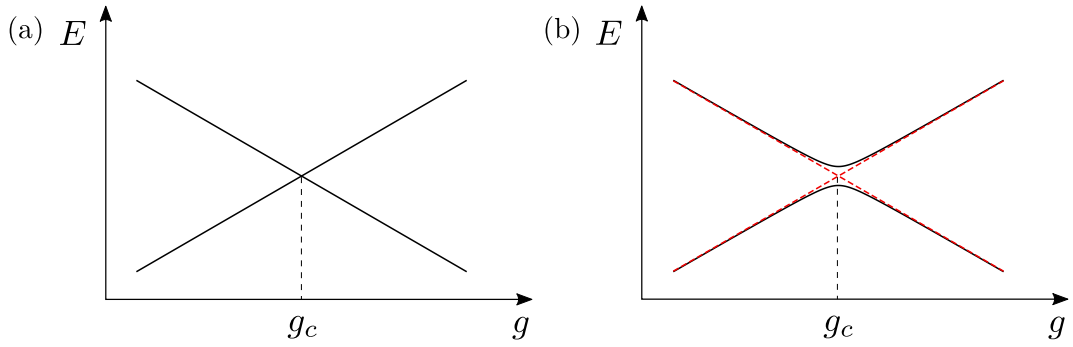

Figure 1.2: **Level-crossing of the low eigenvalues.** Plot of the low eigenvalues of $\hat{H}(g)$ in Eq.(1.1.1) on varying g. (a) If the two quantities $\hat{H}_0$ and $\hat{H}_1$ are conserved, we assist to a level crossing of the lowest levels at the transition point $g = g_c$. (b) More commonly $[\hat{H}_0, \hat{H}_1] \neq 0$, the crossing is developed only for $L \to \infty$ as a limit of an avoided one.

Spontaneous symmetry breaking is generally accompanied by the emergence of large-scale modes. Indeed, the energy gap ε of low-energy fluctuations typically closes for $g \to g_c$ with the power law:

$$\varepsilon(g) \propto J \, |g - g_c|^{z\nu}, \tag{1.1.3}$$

where J is a certain microscopic coupling that sets the energy unit and $z\nu$ is a universal[§] critical exponent. The universal physics in the gapless regime is thus governed by zero-mass quasi-particles which are able to propagate over very large distances. As a consequence, the system's correlation length ξ exhibits a power law growth for $g \to g_c$:

$$\xi(g) \propto a \, |g - g_c|^{-\nu} \tag{1.1.4}$$

up to reach macroscopically large values $\xi \sim L$; here, a denotes the lattice spacing and ν is the correlation length critical exponent.
Comparing Eq.(1.1.3) and (1.1.4) allows to define a characteristic time scale

$$\tau(g) \propto \xi^z(g) \propto \varepsilon^{-1}(g) \tag{1.1.5}$$

which is nothing but the relaxation time of the large-scale fluctuations.
The relaxation critically slows down as soon as the transition is approached (i.e.,

[§]The value of critical exponents depends on the number of spatial dimensions (here one) and on the symmetry properties (here $G \to G'$) but not on the microscopic details of the Hamiltonian.

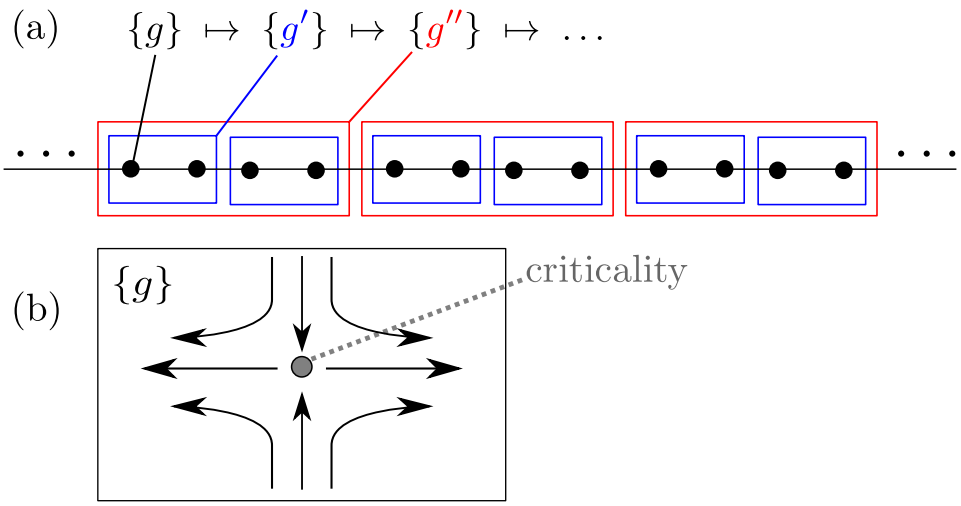

Figure 1.3: **Illustration of RG.** (a) A microscopic lattice model ($\{g\}$) can be described by a set of effective Hamiltonians at larger scales (that depend on new parameters $\{g\} \mapsto \{g'\} \mapsto \{g''\} \mapsto \dots$) by tracing out the internal degrees of freedom. (b) This procedure ultimately leads to a RG flow (illustrated for a two dimensional space of the parameters $\{g\}$) for which the criticality is a fixed point. It follows that a critical system is scale invariant.

$\tau(g) \propto |g - g_c|^{-z\nu}$) and ultimately stops[§] at $g = g_c$, leading to scale invariance in time. The different critical behavior of lengths and times is dictated solely by the exponent z, known therefore as *dynamical exponent*.

A comprehensive analysis of critical phenomena requires a renormalization group (RG) approach, see e.g. [Ma00, Car96, ZJ12].
RG consists - roughly speaking - in an iterative procedure that takes a microscopic model $\hat{H}(\{g\})$ (here the notation $\{g\}$ stands for the set of relevant coupling constants that specify the Hamiltonian) and replaces it by an effective Hamiltonian $\hat{H}'(\{g'\})$, able to capture the physics on larger scales. Doing so, the set of parameters $\{g\} \mapsto \{g'\}$ is modified by the internal degrees of freedom that have been removed, see Fig.1.3. The ensemble of RG transformations ultimately leads to a RG flow that connects the microscopic model to its effective large-scale description. Typically, one loses the microscopic nature of the model during the RG procedure. However, there can exist particular configurations $\{g\} = \{g_c\}$, namely *critical points* (that correspond to fixed points of the RG flow), for which the effective Hamiltonians look all self-similar. Such scale

[§]In finite-size systems τ will remain bounded to the value L^z.

invariance at the critical point leads to the emergence of long-range order and, consequently, to a spontaneous reduction of symmetry in the system's states. The behaviors in Eqs.(1.1.3), (1.1.4) are then expected.

1.1.1 Scaling limit

Scale invariance inevitably affects the value of correlation functions in the proximity of a critical point. In fact, away from the transition the system is typically correlated over a few lattice sites and the (connected) correlations of a local operator $\hat{O}(x,t)$ between two spatial points decay exponentially

$$\langle\Psi_0|\hat{O}(x,t)\,\hat{O}(x',t)|\Psi_0\rangle \propto \exp\left(-\frac{|x-x'|}{\xi(g)}\right), \tag{1.1.6}$$

as soon as $|x-x'| \gg a$; largely separated domains are practically uncorrelated. On the other hand, all spatial points correlate close to the transition due to a diverging correlation length $\xi(g)$. A particular regime thus emerges for $g \to g_c$, (where $\xi,\, \tau \to \infty$) at fixed x/ξ, x'/ξ and t/τ where the (connected) correlation functions show a *scaling behavior* (see e.g. [Ma00, Car96, ZJ12, Hen13])

$$\langle\Psi_0|\hat{O}(x,t)\,\hat{O}(x',t)|\Psi_0\rangle \propto \xi^{-2d_o}\,\mathcal{G}_{oo}\left(\frac{|x-x'|}{\xi}, \frac{t}{\tau}\right) \tag{1.1.7}$$

with d_o the *scaling dimension* of the operator $\hat{O}$ and $\mathcal{G}_{oo}$ a homogeneous function called *scaling function*. Notice that in the presence of a finite-size system where $\xi(g)$ can grow up to L, the system size becomes a relevant scaling variable and finite-size scaling (FSS) is observed

$$\langle\Psi_0|\hat{O}(x,t)\,\hat{O}(x',t)|\Psi_0\rangle \propto L^{-2d_o}\,\mathcal{G}_{oo}\left(\frac{|x-x'|}{L}, \frac{t}{L^z}, \frac{\xi}{L}\right) \tag{1.1.8}$$

for $g \to g_c$ and $L \to \infty$. The infinite volume behavior is recovered simply when $\xi/L \to 0$ at fixed x/ξ and t/τ. The scaling relations in Eq.(1.1.7) and (1.1.8) have straightforward extensions to n-points correlators, see e.g. [ZJ12].

1.1.2 First-order transitions

Consider again the Hamiltonian in Eq.(1.1.1) for $g < g_c$. In this case, the ground state Ψ_0 is not unique and it is selected[§] among different realizations of

[§]As follows from cluster decomposition principles.

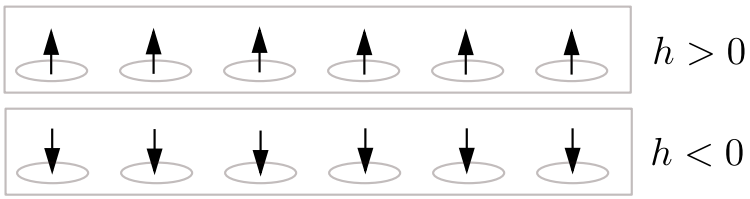

Figure 1.4: **Illustration of a first-order phase-transition.** Typical lattice configuration of the system in Eq.(1.1.9) in the cases $h > 0$ and $h < 0$ (here illustrated for $g = 0$). The two phases are different realizations of the symmetry group G' and are separated by a quantum first-order transition.

the broken symmetry G' with same ground state energy. This degeneracy can be removed e.g. by adding to $\hat{H}$ a perturbation of the form

$$\hat{H} = g\,\hat{H}_0 + \hat{H}_1 + h\,\hat{H}_2 \tag{1.1.9}$$

where $\hat{H}_2$ is symmetric under the subgroup G' and h is a dimensionless parameter. Depending on the value of h then, the low-energy properties of the system will be determined by a specific realization of G'. For instance, suppose that $E_0(g < g_c)$ is doubly degenerate and that $\hat{H}_2$ induces a split of the level where the two phases are associated with a positive (negative) value of h, see Fig.1.4. Across the line of $h = 0$, a (avoided) level-crossing is then generated and the ground state energy $E_0(g < g_c, h)$ shows a non-analytic behavior. This results into a quantum phase transition which is however protected by the presence of a finite energy gap: no critical behavior is found and the correlation length $\xi(g)$ remains finite. This kind of phase transitions are referred as (quantum) *first-order* transitions, see e.g. [Cam14, Cam15b, Cam15c, Pel18a, Pel18b, Pel18c, Ros18].

Therefore, a *safe* definition of quantum phase transitions (which includes critical phenomena as well as first-order transitions) could be:

A **quantum phase transition** (QPT) *is a non-analyticity point in the ground state energy due to a (avoided) level-crossing of the low-lying energy spectrum where macroscopically different quantum states of matter are connected.*

1.1.3 Zero temperature?

As experimentally accessible setups necessarily require a non-zero temperature, it is worth mentioning the effects of a finite temperature on the $T = 0$ critical regime. We can say that the only effect of having a finite temperature

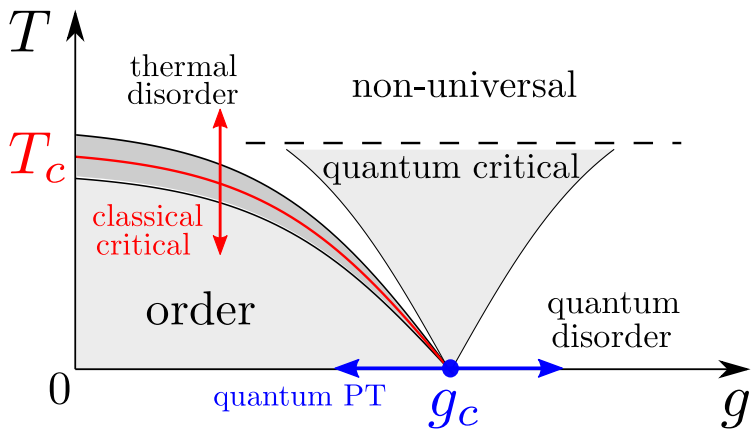

Figure 1.5: **Finite-temperature phase diagram.** Illustration of a phase diagram in the vicinity of a quantum critical point at finite temperature. The horizontal axis shows the driving parameter g of the quantum phase transition; the vertical axis is the temperature. Depending on the value of the temperature we distinguish: (i) a quantum phase transition (*in blue*) arising for $g = g_c$ at strictly zero temperature; (ii) a classical critical regime (*dark gray region*) which narrows as we decrease the temperature up to terminate in the quantum critical point. (iii) A quantum critical region for $J|g - g_c|^{z\nu} \lesssim T \ll J$ where traces of the quantum critical behavior can be detected. For high temperatures $T \gg J$, the model shows a non-universal behavior.

$T \neq 0$ is to introduce a *finite-size* dimension in time. To see this, let us consider the zero-temperature partition function of a d-dimensional quantum system:

$$\mathcal{Z} = \mathrm{tr}\left(e^{-i\Delta t\,\hat{H}}\right) = \sum_n \langle n|e^{-i\Delta t\,\hat{H}}|n\rangle\,, \tag{1.1.10}$$

where $\Delta t = t - t_0$. Defining $\Delta t \equiv -i\beta$, the imaginary-time partition function reads $\mathcal{Z} = \mathrm{tr}(\exp(-\beta\,\hat{H}))$ and it turns out to be equivalent to a $(d+1)$ effective classical system at temperature $1/\beta$. In other words, it is possible to consider the collection of (imaginary) time instants of a d-dimensional quantum model as a fictitious extra dimension and to derive its thermodynamic properties by looking into an effective $(d+1)$-dimensional classical system with temperature $1/\beta$; this observation is typically referred as *quantum-to-classical* mapping.
In the presence of a finite temperature $T \neq 0$, the effective classical description will then take place in a cylinder of sizes $d \times [0, L_T]$, where the width of the imaginary-time strip is simply $L_T \equiv 1/T$. Scaling relations (1.1.7) arising for $g \to g_c$ are consequently modified by the presence of a finite-size time

scale [Son97, Sac11a]:

$$\lim_{L_T\to\infty} \langle\Psi_0|\hat{O}(x,t,T)\,\hat{O}(x',t,T)|\Psi_0\rangle \propto L_T^{-2d_o/z}\,\mathcal{G}_{oo}\left(\frac{|x-x'|}{L_T^{1/z}}, \frac{t}{L_T}, \frac{\tau}{L_T}\right) \tag{1.1.11}$$

and the zero-temperature scaling (1.1.7) is recovered for $\tau/L_T \to 0$, as follows from standard FSS arguments. Notice that the condition $\tau/L_T \ll 1$ is equivalent to $T \ll J|g-g_c|^{z\nu}$ and thus implies that the phase transition is asymptotically governed by its zero-temperature quantum behavior. On the other hand, for $\tau/L_T \gtrsim 1$ (that is $T \gtrsim J|g-g_c|^{z\nu}$), the system will recognize the presence of a finite temperature leading to the unconventional scaling of Eq.(1.1.11). Therefore, a fan-shaped region emerges for temperatures $T \gtrsim J|g-g_c|^{z\nu}$ and for $g \to g_c$, where the presence of the zero-temperature criticality influences the value of thermodynamic observables, see Fig.1.5. This region extends as far as the condition $T \ll J$ is satisfied; conversely, at higher temperatures $T \gg J$, the quantum phase coherence is destroyed by thermal fluctuations and the behavior of the system is controlled by the microscopic model.

In the following sections, we present two important models where these features about QPTs are experimentally observed: *quantum spin chains* and *cold atomic systems*. The former are created with various type of ions crystals (e.g. $CoNb_2O_6$ [Col10a], $LiHoF_4$ [Bit96] or with cuprates [Zal04, Tsv16]), see Sec.1.2, while the latter are typically realized with gases of ^{87}Rb e.g. [Gre02, Tak14, Kin04] or more recently with atom chip devices e.g. [Fol00, Bou09, Sch18a], see Sec.1.3.

1.2 Quantum spin chains

To begin with, we consider the so-called *quantum spin $\frac{1}{2}$ chains*. In this class of models, the degrees of freedom reside on the sites of a 1d lattice where they are implemented by the Pauli operators:

$$\hat{\sigma}^x \equiv \begin{bmatrix} 0 & 1 \\ 1 & 0 \end{bmatrix}; \qquad \hat{\sigma}^y \equiv \begin{bmatrix} 0 & -i \\ i & 0 \end{bmatrix}; \qquad \hat{\sigma}^z \equiv \begin{bmatrix} 1 & 0 \\ 0 & -1 \end{bmatrix}. \tag{1.2.1}$$

These variables describe a quantum object that can have two distinct microscopic configurations, namely $|\uparrow\rangle$ and $|\downarrow\rangle$, associated with the eigenvalues ± 1 of the Pauli operators. Among the spin-chain models, the one-dimensional quantum Ising chain in a transverse magnetic field is perhaps the simplest theoretical

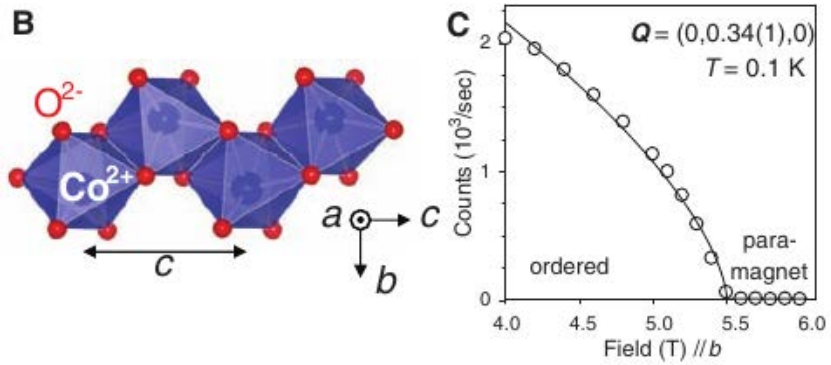

Figure 1.6: **Experimental realization of the Ising model** (Reprinted from Ref. [Col10a] with the permission of *Science*). *Left panel* (B): a zigzag crystal of $CoNb_2O_6$ realizes a 1d quantum Ising chain along the c axis. *Right panel* (C): Phase diagram built through the intensity of the Bragg peak observed by neutron diffraction as a function of the applied transverse field.

paradigm for a quantum phase transition. It is given by the Hamiltonian

$$\hat{H}_{\text{Ising}} = -J \sum_{j=1}^{L-1} \hat{\sigma}_j^z \, \hat{\sigma}_{j+1}^z - g \sum_{j=1}^{L} \hat{\sigma}_j^x \tag{1.2.2}$$

where

$$\hat{\sigma}_j^k \equiv \underbrace{\hat{\mathbb{1}} \otimes \hat{\mathbb{1}} \otimes \ldots \otimes \hat{\sigma}^k}_{j \text{ sites}} \otimes \ldots \otimes \hat{\mathbb{1}}, \qquad k = x, y, z \tag{1.2.3}$$

are the Pauli operators at the lattice site j. The first term $\propto J > 0$ is a ferromagnetic exchange coupling between nearest neighbors that does compete with an applied transverse magnetic field g. Indeed, from one side the coupling J favors a spontaneous magnetic order along the chain ($\uparrow \ \ldots \ \uparrow$ or $\downarrow \ \ldots \ \downarrow$) whereas the transverse field g forces the system to be a disordered paramagnet with respect to the z direction ($\rightarrow \ \ldots \ \rightarrow$). This competition leads to a QPTs occuring at $g/J = 1$ where the two distinct phases merge and a critical behavior is observed.

The Ising model is experimentally realizable e.g. with crystals of cobalt niobate $CoNb_2O_6$ [Col10a]. Here, the two spin configurations $\uparrow$ and $\downarrow$ correspond to the alignments of Co^{2+} ions in a quasi-1d crystal and the spins dynamics can be probed with neutron scattering experiments, see Fig.1.6 (taken from [Col10a]). Notice that there are other spin chain models suitable for experimental investi-

gations. We mention the spin $\frac{1}{2}$ antiferromagnetic Heisenberg chain,

$$\hat{H} = -J \sum_{j=1}^{L-1} \vec{\sigma}_j \cdot \vec{\sigma}_{j+1}, \qquad \vec{\sigma}_j \equiv \left(\hat{\sigma}_j^x, \hat{\sigma}_j^y, \hat{\sigma}_j^z\right); \tag{1.2.4}$$

realized with cuprates (such as $SrCuO_2$ or Sr_2CuO_3) [Zal04, Tsv16] where spinons excitations are observed in neutron scattering experiments as correctly predicted by means of Bethe ansatz [Bet30].

1.2.1 Quantum Ising model

At this point, we would like to make the general considerations about QPTs of Sec.1.1.1 more concrete with the analysis of a specific model. To do so, we come back to the 1d quantum Ising model presented in Eq.(1.2.2),

$$\hat{H}_{\text{Ising}} = -J \sum_{j=1}^{L-1} \hat{\sigma}_j^z \, \hat{\sigma}_{j+1}^z - g \sum_{j=1}^{L} \hat{\sigma}_j^x \,. \tag{1.2.5}$$

This model has the same form of the Hamiltonian (1.1.1) being invariant under a global $\mathbb{Z}_2$ transformation generated by

$$\hat{S}_x \equiv \prod_{j=1}^{L} \hat{\sigma}_j^x \;: \qquad \hat{H}_{\text{Ising}} = \hat{S}_x \, \hat{H}_{\text{Ising}} \, \hat{S}_x^\dagger \tag{1.2.6}$$

(since $\hat{\sigma}_j^z \mapsto -\hat{\sigma}_j^z$ and $\hat{\sigma}_j^x \mapsto \hat{\sigma}_j^x$ under $\hat{S}_x$), which means that the model is unable to distinguish between $\uparrow$ and $\downarrow$ configurations, regardless of the values of J and g. Conversely, the symmetry properties of the ground state change on varying the ratio g/J. In particular, for $g \gg J$, the interaction with the transverse field is dominant and $\hat{H}_{\text{Ising}} \simeq -g \sum_j \hat{\sigma}_j^x$ at the leading order in J/g. The ground state of the system is

$$|\Psi_0\rangle = \prod_{j=1}^{L} \frac{1}{\sqrt{2}} \left(|\uparrow\rangle_j + |\downarrow\rangle_j\right) \qquad (J = 0) \tag{1.2.7}$$

($|\uparrow\rangle_j$, $|\downarrow\rangle_j$ are ± 1-eigenstates of $\hat{\sigma}_j^z$) i.e., it has the form of a product state in the eigenstates of the $\hat{\sigma}^x$ operator. The spin variables on each site can be either $\uparrow$ or $\downarrow$ oriented with same probability resulting into a disordered ground state which is $\mathbb{Z}_2$ invariant. It follows that the two-point function of $\hat{\sigma}_j^z$ operators is

$$\langle \Psi_0 | \hat{\sigma}_i^z \, \hat{\sigma}_j^z | \Psi_0 \rangle = \delta_{ij} \tag{1.2.8}$$

exactly at $J = 0$, while it decays exponentially for small but finite $J \ll g$ as (compare with Eq.(1.1.6))

$$\lim_{|r_i - r_j| \to \infty} \langle \Psi_0 | \hat{\sigma}_i^z \, \hat{\sigma}_j^z | \Psi_0 \rangle \propto \exp\left(- \frac{|r_i - r_j|}{\xi(g/J)} \right), \tag{1.2.9}$$

with $r_j = a\, j$ (a is the lattice spacing). On the other hand, when $g \ll J$ the Hamiltonian is $\hat{H}_{\text{Ising}} \simeq -J \sum \hat{\sigma}_j^z \, \hat{\sigma}_{j+1}^z$ and it turns out to be diagonal in the basis of $\hat{\sigma}_j^z$. Therefore, there are two ground states:

$$|\Psi_0^+\rangle = \prod_{j=1}^{L} |\uparrow\rangle_j \quad \text{or} \quad |\Psi_0^-\rangle = \prod_{j=1}^{L} |\downarrow\rangle_j \,, \qquad (g = 0) \tag{1.2.10}$$

which spontaneously break the $\mathbb{Z}_2$ spin reversal symmetry defining a preferred orientation along the chain; linear superpositions of $\Psi_0^{\pm}$ are avoided for cluster decomposition arguments. Notice that the degeneracy of the ground state persists at any order in g/J and it is not an artifact due to the choice $g = 0$, see e.g. [Sac11a]. The change in nature of the ground state properties inevitably affects the value of the σ-σ correlator:

$$\lim_{|r_i - r_j| \to \infty} \langle \Psi_0^{\pm} | \hat{\sigma}_i^z \, \hat{\sigma}_j^z | \Psi_0^{\pm} \rangle = m_0^2 \tag{1.2.11}$$

where $m_0 \neq 0$ is called spontaneous magnetization since the expectation value

$$\sum_{j=1}^{L} \frac{1}{L} \langle \Psi_0^{\pm} | \hat{\sigma}_j^z | \Psi_0^{\pm} \rangle = \pm m_0. \tag{1.2.12}$$

Exactly at $g = 0$, $m_0 = 1$ and for small $g/J > 0$, $m_0(g, J) = (1 - (g/J)^2)^{1/8}$, see [Pfe70, Pfe71].

As anticipated, we conclude that the Ising model shows a QPT arising for $g/J = 1$ that separates the regime $g \ll J$, where the ferromagnetic tendency ($\propto J$) aligns the spins in an ordered cluster, from the regime $g \gg J$ for which the transverse magnetic field is sufficiently strong to create a disordered ground state. Numerical simulations for finite-size quantum Ising spin chains are easily done using the python package QuTip [Joh12, Joh13]. In Fig.1.7, we show the results for the two-point function $\langle \hat{\sigma}_i^z \, \hat{\sigma}_j^z \rangle$.

Scaling relations are also expected to be satisfied when $g/J \to 1$. In particular, if we consider the system magnetization,

$$\hat{m} \equiv \frac{1}{L} \sum_{j=1}^{L} \hat{\sigma}_j^z, \tag{1.2.13}$$

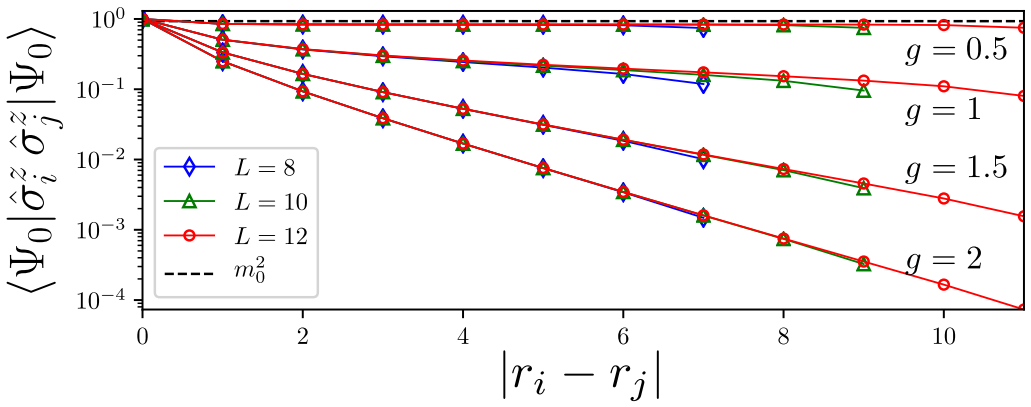

Figure 1.7: **Ising model: numerical analysis of the two-point function.** Numerical evaluation of the two-point function $\langle\Psi_0|\hat{\sigma}_i^z\,\hat{\sigma}_j^z|\Psi_0\rangle$ vs the sites distance $|r_i - r_j|$ in logarithmic scale for different sizes L. We consider several values of the transverse field g at fixed $J = 1$. Notice that for $g > 1$ the value of the correlations decays exponentially (as expected from Eq.(1.2.9)) and the slope of the curve (in log scale) defines the inverse of the correlation length ξ. On the other hand, for $g < 1$, the value of the correlation becomes a constant equal to $m_0^2 = (1 - g^2)^{1/4}$, see Eq.(1.2.11).

it is well-known that in the limit $g/J \to 1$, $L \to \infty$ one has the FSS behavior

$$\langle\Psi_0|\hat{m}|\Psi_0\rangle \propto L^{-\beta/\nu}\,\mathcal{M}(J^{-1}(g-1)\,L^{1/\nu}) \tag{1.2.14}$$

where $\mathcal{M}$ is a scaling function, β and ν are critical exponents describing the singular behavior of the magnetization ($\langle\hat{m}\rangle \propto (g-1)^{\beta}$) and of the correlation length (see Eq.(1.1.4)) respectively; for the 1d quantum Ising model, $\nu = 1$ and $\beta = 1/8$ [Sch64, Pel02][§]. Notice that, due to the $\mathbb{Z}_2$ spin-reversal symmetry, the definition of the system magnetisation in Eq.(1.2.13) leads always to a zero expectation value in the numerical simulations. This problem is known from decades and it has many possible solutions, see e.g. [Yan52, Sch64]. For our purposes, we opt for a shortcut and we just replace $\langle\hat{m}\rangle$ with the quantity:

$$\widetilde{m} \equiv \sum_{n=1}^{2^L} |\alpha_n|^2\,|m_n| \tag{1.2.15}$$

[§]It is well-known that the 1d quantum Ising model possesses the same critical exponent than the 2d classical Ising model, see e.g. [Voj03, Sac11a]

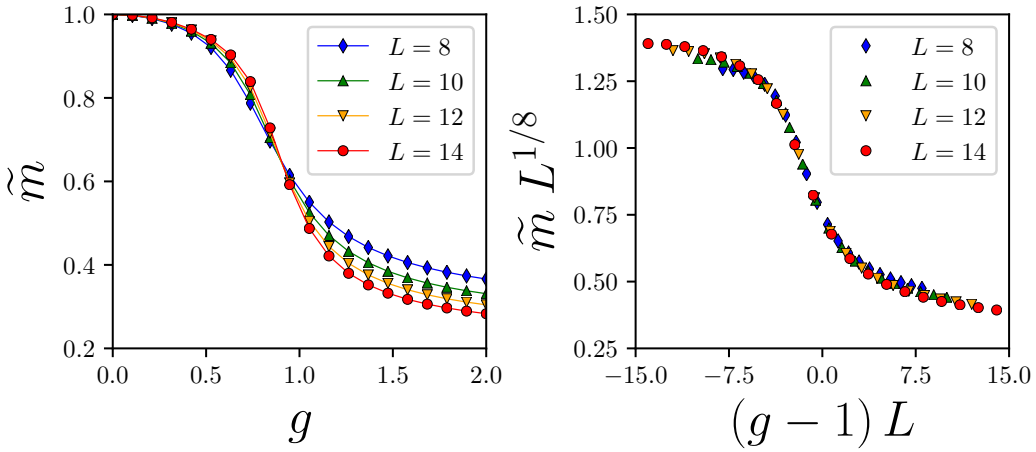

Figure 1.8: **FSS of the Ising magnetization.** Numerical analysis of a finite-size Ising chain at fixed $J = 1$ for different values of g. *Left panel*: Value of the order parameter $\widetilde{m}$ in Eq.(1.2.15) on varying of g. *Right panel:* Rescaled values of $\widetilde{m}$ for different sizes L collapse onto a single curve proving the FSS in Eq.(1.2.14).

where $m_n = \langle n|\hat{m}|n\rangle$, $\alpha_n = \langle \Psi_0|n\rangle$ and

$$\{|n\rangle\} = \{|\uparrow\uparrow \dots \uparrow\uparrow\rangle, |\downarrow\uparrow \dots \uparrow\uparrow\rangle, \dots, |\downarrow\downarrow \dots \downarrow\uparrow\rangle, |\downarrow\downarrow \dots \downarrow\downarrow\rangle\} \tag{1.2.16}$$

is the basis of the 2^L spin chain configurations. Such order parameter $\widetilde{m}$ is then used to locate the QPT point and to test the scaling relation in Eq.(1.2.14) as shown in Fig.1.8.
The discussion about the quantum Ising model will be concluded by the end of the Sec.1.2.2 where we show that it allows for an exact analytical solution [Pfe70, Pfe71] based on the Jordan-Wigner transformation.

1.2.2 Jordan-Wigner transformation

The main observation that underlies the Jordan Wigner technique [Jor28] is that a spin $\frac{1}{2}$ operator behaves as a fermion if we map its *up* $\uparrow$ (*down* $\downarrow$) configuration into an *occupied* (*empty*) state of a fermionic variable. This can be easily done considering the ladder combinations

$$|\uparrow\rangle \equiv \hat{\sigma}^+ \, |\downarrow\rangle \,, \qquad |\downarrow\rangle \equiv \hat{\sigma}^- \, |\uparrow\rangle \tag{1.2.17}$$

where

$$\hat{\sigma}^{+} \equiv \frac{1}{2}(\hat{\sigma}^{x} + i\hat{\sigma}^{y}), \qquad \hat{\sigma}^{-} \equiv \frac{1}{2}(\hat{\sigma}^{x} - i\hat{\sigma}^{y}) \tag{1.2.18}$$

satisfying anticommutation rules $\{\hat{\sigma}^{+}, \hat{\sigma}^{-}\} = 1$. Our aim is to extend such a fermionic description of a single spin $\frac{1}{2}$ to the 1d spin-chain Hamiltonian:

$$\hat{H}_{\text{XY}} = -\frac{J}{2}\sum_{j=1}^{L}\left((1+\kappa)\,\hat{\sigma}_j^{x}\hat{\sigma}_{j+1}^{x} + (1-\kappa)\,\hat{\sigma}_j^{y}\hat{\sigma}_{j+1}^{y}\right) - g\sum_{j=1}^{L}\hat{\sigma}_j^{z}, \tag{1.2.19}$$

where $\hat{\sigma}_j^{k}$ $(k = x, y, z)$ are commuting spin $\frac{1}{2}$ operators at site j, $J > 0$ is the ferromagnetic coupling and g is a transverse magnetic field. The Hamiltonian in Eq.(1.2.19), known as XY model [Lie61], depends on the anisotropy parameter $-1 \leq \kappa \leq 1$ and it reduces to other known models e.g., the Ising spin chain $(\kappa = \pm 1)$ [Pfe70, Pfe71] or the XX isotropic ferromagnet $(\kappa = 0)$ [Tjo70], for some specific choices of κ. The boundary conditions are chosen to be periodic:

$$\hat{\sigma}_{L+1}^{k} \equiv \hat{\sigma}_1^{k}, \qquad k = x, y, z. \tag{1.2.20}$$

Notice that the competition between ferromagnetic order $(\propto J)$ and paramagnetic disorder $(\propto g)$ in the XY model proceeds similarly to the Ising case (see Sec.1.2.1) and leads to the emergence of a QPT. Nevertheless, the phase diagram of the XY model turns out to be much richer than that of the Ising chain due to the anisotropic κ dependence, see Fig.1.9.

To fermionize the spin chain (1.2.19), we first introduce the ladder combinations of spin operators $\hat{\sigma}_j^{\pm}$ at each site j:

$$\hat{\sigma}_j^{+} = \frac{1}{2}(\hat{\sigma}_j^{x} + i\hat{\sigma}_j^{y}) \equiv \hat{b}_j^{\dagger}\,; \tag{1.2.21}$$

$$\hat{\sigma}_j^{-} = \frac{1}{2}(\hat{\sigma}_j^{x} - i\hat{\sigma}_j^{y}) \equiv \hat{b}_j\,; \tag{1.2.22}$$

$$\hat{\sigma}_j^{z} = 2\hat{b}_j^{\dagger}\hat{b}_j - 1 \tag{1.2.23}$$

that fullfil on-site anticommutation rules $\{\hat{b}_j^{\dagger}, \hat{b}_j\} = 1$ but that still satisfy the bosonic algebra for different sites $[\hat{b}_j, \hat{b}_i^{\dagger}] = 0$; this mixed bosonic and fermionic character of the $\hat{b}_j^{\dagger}$, $\hat{b}_j$ operators is due to the symmetric behavior of the spin variables under exchange along the chain (they are bosons).
It follows that $\hat{b}_j^{\dagger}$ $(\hat{b}_j)$ may be viewed as the creation (annihilation) operator of bosonic quasi-particles with a hard core that prevents double occupancy

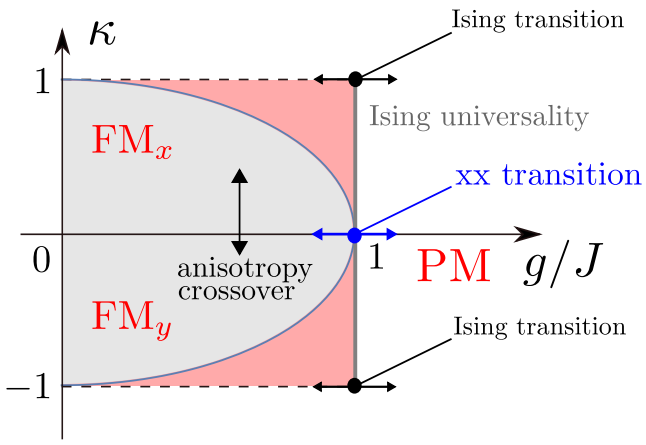

Figure 1.9: **Phase diagram of the XY model.** Illustration of the phase diagram of the XY model in Eq.(1.2.19). The model shows an "Ising-like" QPT arising for $g/J = 1$ where a paramagnetic disordered phase (PM), $g/J \gg 1$, is connected with a ferromagnetically ordered phase (FM), $g/J \ll 1$. Due to the presence of anisotropies κ, the ferromagnetic state can be either x-oriented (FM$_x$) or y-oriented (FM$_y$) depending on the relative strength of the ferromagnetic couplings $J_x = J(1+\kappa)/2$ and $J_y = J(1-\kappa)/2$. A crossover between the two ferromagnetic states is then observed across the isotropy line $\kappa = 0$. The FM phase presents also an oscillatory regime (*light gray region*) for $\kappa^2 + (\frac{g}{J})^2 < 1$. As we will show, for any value of $\kappa \neq 0$, the criticality at $g/J = 1$ belongs to the Ising universality class (i.e., it is governed by the same critical exponents, *dark gray line*). The isotropic transition (XX model, *in blue*) has instead different critical exponents.

of a site. Next, the Jordan-Wigner (JW) transformation allows to get true fermionic operators through the mapping [Jor28]:

$$\hat{c}_j^\dagger \equiv \prod_{i=1}^{j-1}(-\hat{\sigma}_i^z)\,\hat{b}_j^\dagger\,, \qquad \hat{c}_j \equiv (\hat{c}_j^\dagger)^\dagger \tag{1.2.24}$$

where we introduced the JW string

$$\prod_{i=1}^{j-1}(-\hat{\sigma}_i^z) = \exp\left(i\pi \sum_{i<j} \hat{b}_i^\dagger\,\hat{b}_i\right) \tag{1.2.25}$$

that antisymmetrizes the wave function under particle exchange. It is easy to see that the new set of operators satisfies the fermionic algebra

$$\{\hat{c}_i, \hat{c}_j^\dagger\} = \delta_{ij}, \quad \{\hat{c}_i, \hat{c}_j\} = 0 = \{\hat{c}_i^\dagger, \hat{c}_j^\dagger\} \tag{1.2.26}$$

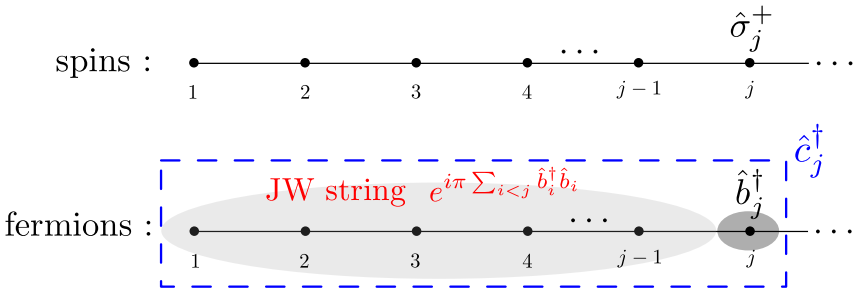

Figure 1.10: **Illustration of the Jordan-Wigner transformation.** Any spin variable $\hat{\sigma}_j^+$ can be written as a product of a hard core boson $\hat{b}_j^\dagger$ (which fermionizes the single spin at the site j) times a JW string that antisymmetrizes the wave function under particle exchange.

and conserves the number operator $\hat{\sigma}_j^z = 2\hat{b}_j^\dagger \hat{b}_j - 1 = 2\hat{c}_j^\dagger \hat{c}_j - 1$; we will refer to these fermionic operators as *lattice fermions*. At this point, inverting the JW transformation in Eq.(1.2.24):

$$\hat{\sigma}_j^+ = \exp\left(-i\pi \sum_{i<j} \hat{b}_i^\dagger \hat{b}_i\right) \hat{c}_j^\dagger, \qquad \hat{\sigma}_j^- = \hat{c}_j \exp\left(i\pi \sum_{i<j} \hat{b}_i^\dagger \hat{b}_i\right) \tag{1.2.27}$$

we can write the various terms entering in the Hamiltonian (1.2.19) as

$$\hat{\sigma}_i^x \hat{\sigma}_j^x = (\hat{c}_i^\dagger - \hat{c}_i)(\hat{c}_j^\dagger + \hat{c}_j) \tag{1.2.28}$$

$$\hat{\sigma}_i^y \hat{\sigma}_j^y = -(\hat{c}_i^\dagger + \hat{c}_i)(\hat{c}_j^\dagger - \hat{c}_j) \tag{1.2.29}$$

$$\hat{\sigma}_j^z = 2\hat{c}_j^\dagger \hat{c}_j - 1. \tag{1.2.30}$$

and thus express the XY model as quadratic form of lattice fermions:

$$\begin{aligned} \hat{H}_{\rm XY} = &- J\Bigg(\sum_{j=1}^{L-1} \left[\hat{c}_j^\dagger \hat{c}_{j+1} + \hat{c}_{j+1}^\dagger \hat{c}_j + \kappa \left(\hat{c}_j^\dagger \hat{c}_{j+1}^\dagger + \hat{c}_{j+1}\hat{c}_j\right)\right] \\ &- e^{i\pi \sum_{j=1}^{L} \hat{c}_j^\dagger \hat{c}_j} \left[\hat{c}_L^\dagger \hat{c}_1 + \hat{c}_1^\dagger \hat{c}_L + \kappa \left(\hat{c}_L^\dagger \hat{c}_1^\dagger + \hat{c}_1 \hat{c}_L\right)\right] \Bigg) - 2g \sum_{j=1}^{L} \hat{c}_j^\dagger \hat{c}_j. \end{aligned} \tag{1.2.31}$$

Since we shall focus on the bulk critical behavior of large-size systems, we can neglect the boundary term in Eq.(1.2.31) and consider

$$\hat{H}_{\rm XY} = -J \sum_{j=1}^{L-1} \left[\hat{c}_j^\dagger \hat{c}_{j+1} + \hat{c}_{j+1}^\dagger \hat{c}_j + \kappa \left(\hat{c}_j^\dagger \hat{c}_{j+1}^\dagger + \hat{c}_{j+1}\hat{c}_j\right)\right] - 2g \sum_{j=1}^{L} \hat{c}_j^\dagger \hat{c}_j. \tag{1.2.32}$$

The latter can be reduced to a free fermionic system by means of a Bogoliubov transformation, as shown in the following for the specific cases $\kappa = 0, 1$. Finally, we notice that the Jordan-Wigner transformation does not provide an exact solution for spin-chain Hamiltonians containing terms of the form e.g.

$$\propto \hat{\sigma}_i^z \hat{\sigma}_j^z \ , \quad \propto \hat{\sigma}_j^x \tag{1.2.33}$$

as the Heisenberg model in Eq.(1.2.4), for which the description in terms of lattice fermions gives rise to non-local interactions.

$\kappa = 0$: XX model

If we set $\kappa = 0$, the Hamiltonian in Eq.(1.2.19) reduces to the isotropic XX model,

$$\hat{H}_{\rm XX} \ = -J \sum_{j=1}^{L-1} \left(\hat{c}_j^\dagger \hat{c}_{j+1} + \text{h.c.} \right) - 2g \sum_{j=1}^{L} \hat{c}_j^\dagger \hat{c}_j \tag{1.2.34}$$

which is known to have a QPT arising for $\tilde{g} \equiv g/J = 1$, as shown in Fig.1.9. Notice that the choice $\kappa = 0$ erases all the terms in Eq.(1.2.32) that violate the conservation of the total number of particles $\hat{N} = \sum_j \hat{c}_j^\dagger \, \hat{c}_j = \sum_j \hat{b}_j^\dagger \, \hat{b}_j$. Hence, a simple Fourier transformation is enough to diagonalize the Hamiltonian. We define:

$$\hat{\eta}_q \equiv \frac{1}{\sqrt{L}} \sum_{j=1}^{L} \hat{c}_j \ e^{-iqr_j} \qquad \hat{\eta}_q \equiv (\hat{\eta}_q^\dagger)^\dagger \tag{1.2.35}$$

with $r_j = a\, j$ (a is the lattice spacing), and we use Eq.(1.2.35) into Eq.(1.2.34) obtaining

$$\hat{H}_{\rm XX} \ = \sum_q 2J \, |\cos(qa) - \tilde{g}| \, \hat{\eta}_q^\dagger \, \hat{\eta}_q \tag{1.2.36}$$

which is nothing but a free fermionic model with energy spectrum

$$\varepsilon_q(g, J) = 2J \, |\cos(qa) - \tilde{g}| \, . \tag{1.2.37}$$

In particular, we can see that the energy scale of the lowest excitations ($q = 0$) vanishes close to the critical point $\tilde{g} = 1$ as

$$\varepsilon_0(g, J) = 2J|1 - \tilde{g}| \tag{1.2.38}$$

from which we read the critical exponent $z\nu = 1$. Moreover, expanding the energy spectrum for $q \to 0$ and close to the critical point $\tilde{g} = 1$, we have

$$\lim_{q \to 0} \ \varepsilon_q(g, J) \Big|_{\tilde{g}=1} \propto q^2 \tag{1.2.39}$$

which fixes the dynamical exponent $z = 2$ and therefore $\nu = 1/2$.

$\kappa = 1$: Ising model

As we have anticipated in Sec.1.2.1, the quantum Ising model is exactly solvable. Indeed, by setting $\kappa = 1$ (or equivalently $\kappa = -1$) the XY spin-chain (1.2.19) reduces to the Ising Hamiltonian (1.2.1) and from Eq.(1.2.32) we have

$$\hat{H}_{\text{Ising}} = -J \sum_{j=1}^{L-1} \left[\hat{c}_j^\dagger \hat{c}_{j+1} + \hat{c}_{j+1}^\dagger \hat{c}_j + \hat{c}_j^\dagger \hat{c}_{j+1}^\dagger + \hat{c}_{j+1} \hat{c}_j \right] - 2g \sum_{j=1}^{L} \hat{c}_j^\dagger \hat{c}_j. \tag{1.2.40}$$

Introducing the operators in Fourier space

$$\hat{\gamma}_q \equiv \frac{1}{\sqrt{L}} \sum_{j=1}^{L} \hat{c}_j \, e^{-iqr_j} \qquad \hat{\gamma}_q \equiv (\hat{\gamma}_q^\dagger)^\dagger \tag{1.2.41}$$

we have

$$\hat{H}_{\text{Ising}} = J \sum_q \left[2 \left(\cos(qa) - \widetilde{g} \right) \hat{\gamma}_q^\dagger \hat{\gamma}_q + i \sin(qa) \left(\hat{\gamma}_{-q}^\dagger \hat{\gamma}_q^\dagger + \hat{\gamma}_{-q} \hat{\gamma}_q \right) \right], \tag{1.2.42}$$

with $\widetilde{g} \equiv g/J$. Notice that for the case $\kappa = 1$ a Fourier description is not enough to remove the terms which violate the fermionic particles conservation. Nevertheless, we can define a unitary transformation (Bogoliubov)

$$\hat{\eta}_q^\dagger = u_q \hat{\gamma}_q^\dagger + i v_q \hat{\gamma}_{-q}, \qquad \hat{\eta}_q = (\hat{\eta}_q^\dagger)^\dagger \tag{1.2.43}$$

with u_q, v_q real numbers satisfying

$$u_q^2 + v_q^2 = 1, \quad u_q = u_{-q}, \quad v_q = -v_{-q} \tag{1.2.44}$$

and choose these parameters in order to remove the unwanted terms in Eq.(1.2.42). It is easy to show that the new operators $\hat{\eta}_q^\dagger$, $\hat{\eta}_q$ are fermionic operators and satisfy canonical anticommutation rules

$$\{\hat{\eta}_q^\dagger, \hat{\eta}_k\} = \delta_{qk} \qquad \{\hat{\eta}_q^\dagger, \hat{\eta}_k^\dagger\} = 0 = \{\hat{\eta}_q, \hat{\eta}_k\}. \tag{1.2.45}$$

Now, inverting the relation (1.2.43),

$$\hat{\gamma}_q^\dagger = u_q \hat{\eta}_q^\dagger - i v_q \hat{\eta}_{-q} \, , \tag{1.2.46}$$

and substituting it into Eq.(1.2.42) we find that the choice:

$$u_q = \cos(\theta_q/2), \quad v_q = \sin(\theta_q/2) \qquad \theta_q \equiv \frac{\sin(qa)}{\widetilde{g} - \cos(qa)} \tag{1.2.47}$$

leads to the final result

$$\hat{H}_{\text{Ising}} = \sum_q \varepsilon_q(g,J)\ \hat{\eta}_q^\dagger\,\hat{\eta}_q \tag{1.2.48}$$

with energy spectrum

$$\varepsilon_q(g,J) = 2J\sqrt{\Big(1+\widetilde{g}^2-2\widetilde{g}\cos(qa)\Big)}\,. \tag{1.2.49}$$

It follows that the energy gap of low-energy modes ($q=0$) vanishes for $\widetilde{g}=1$ as

$$\varepsilon_0(g,J) = 2J\,|1-\widetilde{g}| \tag{1.2.50}$$

and the critical exponent $z\nu=1$. Then, from the low-momentum expansion in the vicinity of the critical point

$$\lim_{q\to 0}\ \varepsilon_q(g,J)\,\Big|_{\widetilde{g}=1} \propto |q|, \tag{1.2.51}$$

we can fix the dynamical exponent $z=1$ and thus the correlation length exponent $\nu=1$.

General case

Finally, we mention that the QPT arising across $\widetilde{g}\equiv g/J=1$ at fixed κ belongs to the Ising universality class for any $\kappa\neq 0$. Indeed, it can be shown [Lie61] that the diagonalization of (1.2.32) in the generic case leads to the energy spectrum

$$\varepsilon_q(g,J,\kappa) = 2J\sqrt{\big(\widetilde{g}-\cos(qa)\big)^2+\kappa^2\sin^2(qa)}. \tag{1.2.52}$$

One can easily verify that Eq.(1.2.52) correctly reproduces the results of the Ising case (1.2.49) ($\kappa=\pm 1$) and of the XX case (1.2.37) ($\kappa=0$). The quasi-energies spectrum satisfies

$$\varepsilon_0(g,J,\kappa) = 2J\ |1-\widetilde{g}|\,; \qquad \Rightarrow\ z\nu=1 \tag{1.2.53}$$

independently on κ, and

$$\lim_{q\to 0}\ \varepsilon_q(g,J,\kappa)\,\Big|_{\widetilde{g}=1} \begin{cases} \propto |q|; & \kappa\neq 0 \quad \Rightarrow\ z=1;\ \nu=1; \\ \propto q^2; & \kappa=0 \quad \Rightarrow\ z=2;\ \nu=1/2; \end{cases} \tag{1.2.54}$$

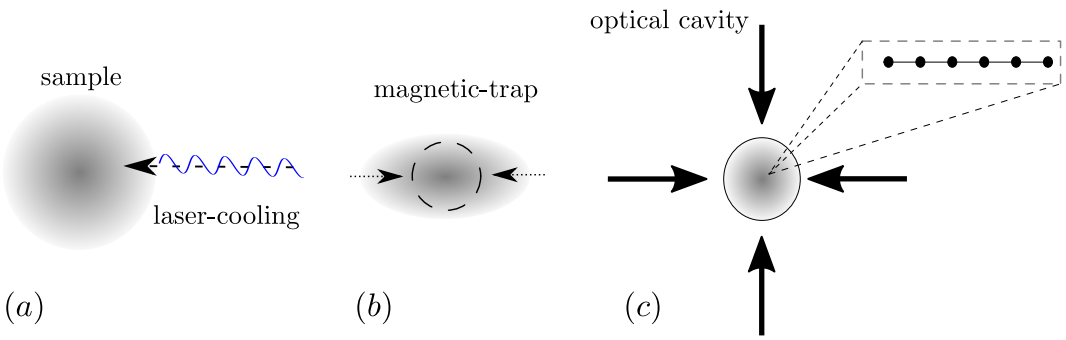

Figure 1.11: **Example of an experimental setup.** (a) A sample of bosonic atoms is laser-cooled in order to create a Bose-Einstein condensate. (b) Magnetic traps are used to reduce thermal fluctuations and then relaxed properly to obtain a 3d condensate with spherical symmetry. (c) Engineered optical cavities generate a lattice structure of the desidered geometry.

which fixes the critical exponents in the Ising universality class for any $\kappa \neq 0$. We remark that this result is valid only in the case in which the transition point $\widetilde{g} = 1$ is crossed with a fixed κ. In general, if we vary the anisotropy parameter across the criticality we observe a multicritical behavior [Kar00, Muk09, Den09, Dzi10].

1.3 Cold atoms

Another paradigmatic model for the study of quantum phase transitions is the Bose-Hubbard model [Fis89] (see also [Caz11]) which is used to describe the properties of cold Bose gases in optical lattice potentials. The emergence of a quantum critical point in such systems can be easily understood as follows. Consider a gas of bosons with repulsive interactions kept at a sufficiently low temperature so that it forms a Bose Einstein condensate. Now, let us imagine that such a gas is subject to a space-periodic potential which induces a lattice structure, where different sites correspond to local minima separated by energy barriers. Clearly, when the external potential is weak enough, the bosonic particles are still able to freely move through the lattice sites (thanks to quantum mechanical hopping processes) and the resulting many body state preserves the properties of a condensate. On the other hand, as soon as the potential is strong enough to suppress the hopping amplitude, the ground state inevitably changes and will be characterized by the bosons occupations on each site. The

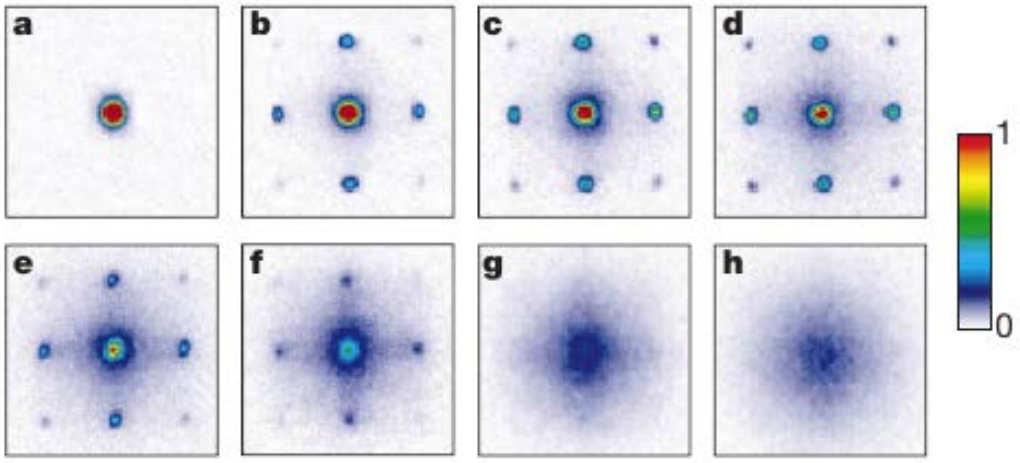

Figure 1.12: **Experimental observation of superfluid-to-insulator QPT** (Reprinted from Ref. [Gre02] with the permission of *Nature*). A 3d sample of ultracold ^{87}Rb atoms is investigated with absorption imagining techniques: the optical potential is suddenly switched off and the gas is let free to expand (for a time window $\sim$ 15ms) and thus to create interference patterns that are recorded. The different panels **a**-**h** correspond to different values of the lattice depth (increasing from **a** to **h**) and show the changes in the interference patterns of the atomic cloud across the superfluid-to-insulator QPT. In particular, in the superfluid regime (where all atoms are delocalized over the lattice with long-range coherence) we obtain high-contrast 3d interference patterns (**a**) whereas, increasing the lattice depth, higher-order interference peaks arise (**b**-**e**) due to the emergent localization effects. Notice that for very deep lattices the interference patterns do not increase and ultimately disappear (**f**-**h**), as expected from a incoherent background.

competition between the delocalizing hopping processes and the localizing effect induced by the external potential results into a superfluid-to-insulator QPT, similar to that observed in liquid helium ^{4}He [Ray64, Ave85, Bew06].

This setup is experimentally accessible [Gre02, Cro09, Lan15, Fol00, Hof07, Li18, Web03a, Hal09, Web03b, Tak14, Hal10, Kin06, Kin04] considering e.g. a dilute sample of rubidium atoms ^{87}Rb that are first laser-cooled below the Bose-Einstein condensation temperature and then transferred into a cigar-shaped magnetic trapping potential. By a proper tuning of the trap frequency,

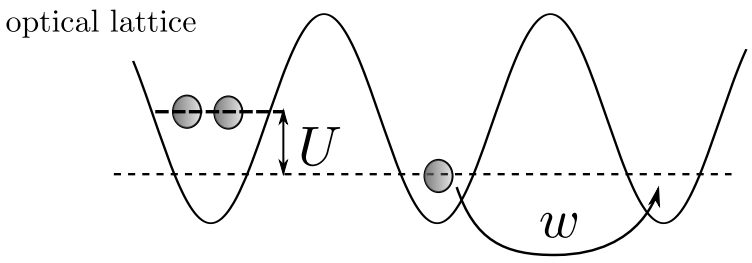

Figure 1.13: **Illustration of the Bose-Hubbard Hamiltonian.** The bosonic particles reside on the local minima of a space-periodic potential created by means of optical cavities. The dynamics of the system is generated by the interplay of a kinetic term $\propto w$ (rooted in the tunneling probability across the energy barriers) with the repulsive on-site interactions $\propto U$ among the bosons. Notice that the ratio w/U can be modified through the lattice depth.

one can create a condensate with up to 10^5 atoms and with no discernible thermal fluctuations. Afterwards, engineered optical standing waves create lattice structures of different geometry, see Fig.1.11. Notice that the lattice depth can be modified through the intensity of the laser beams in the optical cavity allowing the investigation of different regions of the phase diagram. Experimental datas are then obtained with imaging techniques, see Fig.1.3 (figure taken from [Gre02]).

1.3.1 Bose-Hubbard model

The theoretical framework for the investigation of cold atoms on optical lattices is typically the Bose-Hubbard (BH) model [Fis89] (see also [Caz11]), whose Hamiltonian in 1d is given by

$$\hat{H}_{\text{BH}} = -w \sum_{j=1}^{L-1} (\hat{a}_j^\dagger \hat{a}_{j+1} + \text{h.c.}) + \frac{U}{2} \sum_{j=1}^{L} \hat{n}_j(\hat{n}_j - 1) - \mu \sum_{j=1}^{L} \hat{n}_j \tag{1.3.1}$$

where $\hat{a}_j^\dagger$ ($\hat{a}_j$) is the creation (annihilation) operator of a bosonic particle and $\hat{n}_j \equiv \hat{a}_j^\dagger \hat{a}_j$ is the occupation number operator at site j. Here, the first term ($\propto w$) represents hopping magnitude, $U > 0$ is the on-site repulsive interaction and μ is the chemical potential. Of course, by acting on the optical potential allows to modify the energy barriers among the sites and thus the value of the hopping parameter w. It follows that U does only set the energy scale of the problem and that the superfluid-to-insulator transition is driven by the ratio

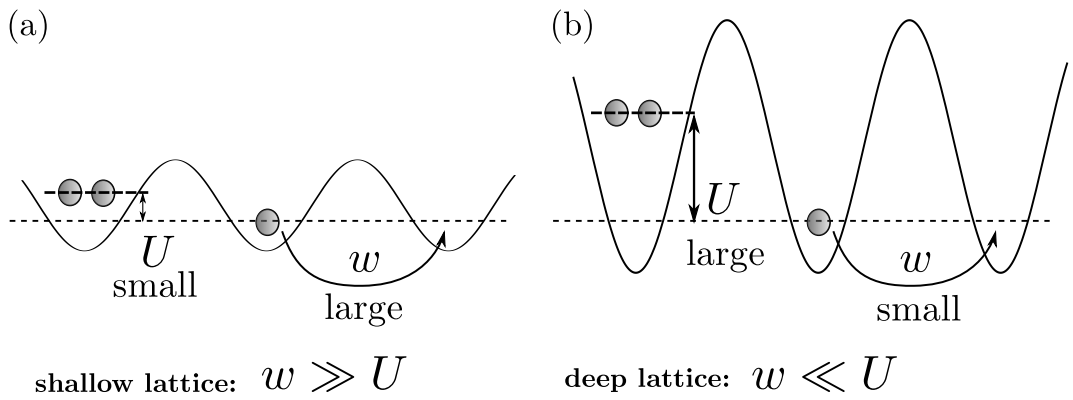

Figure 1.14: **Different regimes of the BH model**. (a) Shallow lattice limit: for weak optical potential the kinetic term ($\propto w$) in (1.3.1) is dominant and we expect a superfluid behavior of the ground state. (b) Deep lattice limit: when the energy barriers among sites are very high the hopping magnitude is suppressed and the on-site interaction is the relevant process. In this regime, we do expect a localized ground state with insulating properties.

w/U. An illustration of the Bose-Hubbard Hamiltonian in Eq.(1.3.1) is given in Fig.1.13.
Notice that the model (1.3.1) possesses a global $U(1)$ symmetry under the phase transformation

$$\hat{a}_j \;\mapsto\; \hat{a}_j\, e^{i\varphi} \tag{1.3.2}$$

that is physically associated with the conservation of the total number of particles

$$\hat{N} = \sum_{j=1}^{L} \hat{n}_j. \tag{1.3.3}$$

The main features of the superfluid (insulating) phase can be analyzed considering the limiting case $w/U \gg 1$ ($w/U \ll 1$) corresponding to a shallow (deep) optical lattice configuration, see Fig.1.14.

Shallow lattice limit

The shallow lattice $w/U \gg 1$ corresponds to weak optical potential where the kinetic term dominates over the on-site repulsive interaction. In this regime, the BH Hamiltonian can be approximated as

$$\hat{H}_{\text{BH}} \simeq -w \sum_{j=1}^{L-1} \left(\hat{a}_j^\dagger \hat{a}_{j+1} + \text{h.c.}\right) - \mu \sum_{j=1}^{L} \hat{n}_j \tag{1.3.4}$$

at the leading order in U/w. The latter is a quadratic form in terms of the bosonic operators $\hat{a}_j^\dagger$, $\hat{a}_j$ and it is readily diagonalized in Fourier space

$$\hat{H}_{\text{BH}} = \sum_q \varepsilon_q(w,\mu)\ \hat{\eta}_q^\dagger \hat{\eta}_q, \qquad w/U \gg 1; \tag{1.3.5}$$

where

$$\hat{\eta}_q^\dagger \equiv \frac{1}{\sqrt{L}} \sum_{j=1}^{L} e^{iqr_j}\ \hat{a}_j^\dagger, \qquad \hat{\eta}_q = (\hat{\eta}_q^\dagger)^\dagger \tag{1.3.6}$$

with $r_j = a\,j$, a is the lattice spacing. The model describes free bosonic excitations with energy spectrum

$$\varepsilon_q(w,\mu) = -(2w\cos(qa) + \mu). \tag{1.3.7}$$

The ground state of the system with a given number of particles N is

$$|\Psi_0\rangle = \left(\hat{\eta}_{q=0}^\dagger\right)^N |0\rangle = \left[\frac{1}{\sqrt{L}} \sum_{j=1}^{L} \hat{a}_j^\dagger\right]^N |0\rangle \tag{1.3.8}$$

where $|0\rangle$ is the zero quasi-particles state (vacuum), $\hat{\eta}_q\,|0\rangle = 0$. Notice that the ground state Ψ_0 is a product state in the Fourier space i.e., it is *localized in momentum space*. We shall refer to this state as *superfluid* (SF) state.

Deep lattice limit

Next, in the deep lattice limit $w/U \ll 1$, we can write at the leading order in w/U:

$$\hat{H}_{\text{BH}} \simeq \sum_{j=1}^{L} \left(-\mu\ \hat{n}_j + \frac{U}{2}\hat{n}_j(\hat{n}_j - 1)\right) \tag{1.3.9}$$

that is, as expected, a pure local operator. The many-body wave function $|\Psi\rangle$ reduces to a product of the single sites wave functions

$$|\Psi\rangle = \prod_{j=1}^{L} |n_j\rangle\,, \tag{1.3.10}$$

which are conveniently described in terms of the occupation eigenstates $\hat{n}_j\,|n_j\rangle = n\,|n_j\rangle$. We can say therefore that in this regime the state of the system is *localized in space*.

The ground state energy of the system in the deep lattice regime follows from the minimization of the quantity

$$-\mu\, n + \frac{U}{2}\, n(n-1) \tag{1.3.11}$$

with respect to the occupation number n and independently on the lattice site j. The resulting state has a uniform particle distribution with sites occupation:

$$n = \begin{cases} 0 & \mu/U < 0 \\ 1 & 0 < \mu/U < 1 \\ 2 & 1 < \mu/U < 2 \\ \text{etc.} \end{cases} \tag{1.3.12}$$

and is called *Mott-Insulator* (MI) state.

Phase diagram

We have seen that the BH model (1.3.1) shows different ground state properties ranging from a SF to a MI state on varying w/U. Therefore, we do expect the existence of a QPT occurring for some finite value of w/U. Unfortunately, the BH model (with finite interaction U) does not allow for an exact analytical solution. Nevertheless, one can have a very accurate estimation of the transition point by means of DMRG numerical simulations, see e.g. [KÖ0, Sch11]. Moreover, a qualitative understanding of the phase boundaries is provided by the mean-field approximation, that we are going to briefly resume.

The mean field (MF) approximation relies on the substitution

$$\hat{a}_i^\dagger\, \hat{a}_j \;\overset{\text{MF}}{\mapsto}\; \hat{a}_i^\dagger\, \langle \hat{a}_j \rangle + \langle \hat{a}_i^\dagger \rangle\, \hat{a}_j - \langle \hat{a}_i^\dagger \rangle \langle \hat{a}_j \rangle \tag{1.3.13}$$

which replaces the effect of the neighbor sites on a site j with a uniform parameter $\phi \equiv \langle \hat{a}_i \rangle$ (called mean field) and that allows for a decoupling of the kinetic term $\propto w$ in Eq.(1.3.1):

$$-w \sum_{j=1}^{L} (\hat{a}_j^\dagger \hat{a}_{j+1} + \text{h.c.}) \;\overset{\text{MF}}{\mapsto}\; -2w \sum_{j=1}^{L} (|\phi|^2 + \phi^*\, \hat{a}_j + \phi\, \hat{a}_j^\dagger). \tag{1.3.14}$$

Under this approximation, the BH model becomes a local Hamiltonian

$$\hat{H}_{\text{BH}} \approx \hat{H}_{\text{BH}}^{\text{MF}} \equiv \sum_{j=1}^{L} \Big[-2w(|\phi|^2 + \phi^*\, \hat{a}_j + \phi\, \hat{a}_j^\dagger) - \mu\, \hat{n}_j + \frac{U}{2}\, \hat{n}_j(\hat{n}_j - 1) \Big]. \tag{1.3.15}$$

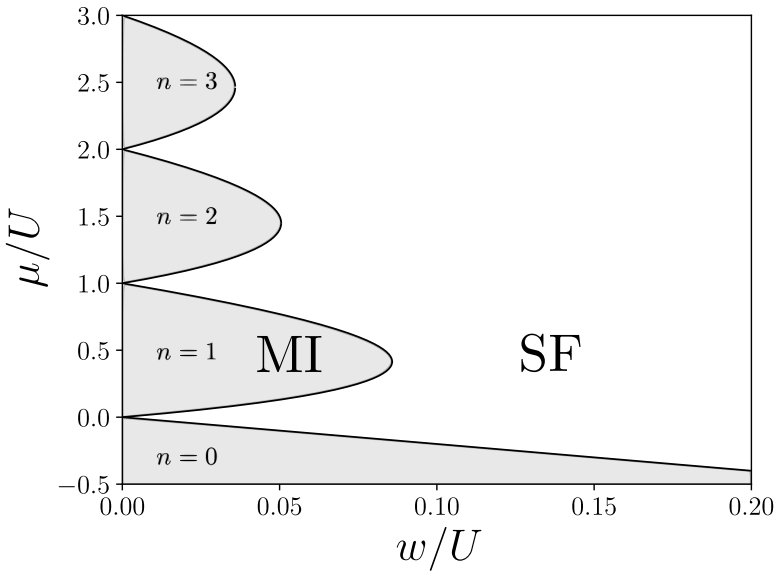

Figure 1.15: **Mean field phase diagram of the Bose-Hubbard model.** Plot of the 1d mean-field phase diagram of the BH model. The *gray lobes* correspond to MI states labeled with the on-site occupation number $n = 0, 1, 2, \ldots$ according to Eq.(1.3.12) for a given μ/U. The *white region* represents the SF phase.

Now, if we start from a nearly-insulating state where w/U is small, we can treat the mean field ϕ as a perturbation over the incoherent background. We proceed by writing the ground state energy in the Landau-Ginzburg form

$$E_0(\phi) = e_0 + e_2 \, |\phi|^2 + e_4 \, |\phi|^4 + \mathcal{O}(|\phi|^6) \tag{1.3.16}$$

with coefficients e_i that are computed with standard perturbation theory. The zeroth order corresponds to the deep lattice case where $\phi = 0$ and the mean-field analysis turns out to be exact. Therefore, we have simply

$$e_0 = E_{\overline{n}} \equiv \mu \, \overline{n} - \frac{U}{2} \overline{n} \, (\overline{n} - 1) \tag{1.3.17}$$

and the occupation number $\overline{n}$ is fixed according to the Eq.(1.3.12). Next, at the second order we obtain

$$E_0(\phi) = e_0 + \left(2w|\phi|^2 + 4w^2 \sum_{n \neq \overline{n}} \frac{| \, \langle \overline{n}| (\phi^* \, \hat{a}_j + \phi \, \hat{a}_j^\dagger) |n\rangle \, |^2}{E_{\overline{n}} - E_n} \right) + \mathcal{O}(|\phi|^4), \tag{1.3.18}$$

where $|n\rangle = \prod_j |n_j\rangle$ are localized states with site occupation n and energy E_n. Recalling that

$$\langle \overline{n}|(\phi^* \hat{a}_j + \phi \hat{a}_j^\dagger)|n\rangle = \begin{cases} \phi^* \sqrt{\overline{n}+1} & n = \overline{n}+1 \\ \phi \sqrt{\overline{n}} & n = \overline{n}-1 \\ 0 & \text{otherwise} \end{cases} \tag{1.3.19}$$

we arrive to the result

$$e_2 = 2w + 4w^2 \Big[\frac{\overline{n}+1}{\mu - U\overline{n}} - \frac{\overline{n}}{\mu - U(\overline{n}-1)} \Big], \tag{1.3.20}$$

that leads to

$$E_0(\phi) = e_0 + 2w|\phi|^2 + 4w^2|\phi|^2 \Big[\frac{\overline{n}+1}{\mu - U\overline{n}} - \frac{\overline{n}}{\mu - U(\overline{n}-1)} \Big] + \mathcal{O}(|\phi|^4). \tag{1.3.21}$$

This expression reminds the free energy of a classical ϕ^4-theory, where the spontaneous symmetry breaking at the transition is associated with the emergence of a mexican-hat shape of the potential. Using the well-known machinery, we conclude that the MI phase is stable as far as the coefficient $e_2 > 0$. Here, the ground state energy is minimized with the choice $\phi = 0$ that corresponds to the results in Eq.(1.3.12). On the other hand, when $e_2 < 0$ quartic terms are needed to minimize the ground state energy and the (degenerate) vacuum will be associated with a non-zero value of ϕ. The phase boundary follows from the condition $e_2 = 0$ in Eq.(1.3.21) which results into the parametric curve

$$\frac{1}{2w} = \frac{\overline{n}}{\mu - U(\overline{n}-1)} - \frac{\overline{n}+1}{\mu - U\overline{n}}\,, \tag{1.3.22}$$

which is shown in Fig.1.15. The solution of Eq.(1.3.22) generates a series of Mott lobes on varying of μ/U where the ground state has a uniform space distribution characterized by different occupation numbers $n = 0, 1, 2, \ldots$ (compare with Eq.(1.3.12)). For large w/U the state is always superfluid as expected. Quite interestingly, the SF phase persists for small w/U when we have incommensurate fillings (i.e., when μ/U is an integer).

Chapter 2

Driven systems

We have presented so far different classes of quantum critical models and discussed the ground state properties in different regions of their phase diagrams. With this background, our focus moves to the analysis of dynamical systems and in particular to the *non-equilibrium* behavior that can emerge during the time evolution of a quantum system. In other words, from now on our aim will be to answer the following questions:

How does a quantum system, prepared in some initial state of interest, evolve when an external parameter is varied in time? How can non-equilibrium behaviors arise in such dynamical systems?

and more importantly, to which kind of interesting phenomena the non-equilibrium physics can lead to. But first, let us mention that

- We do exclude time-independent Hamiltonians. Indeed, for these systems the time evolution consists in the accumulation of dynamical phases in the basis of the eigenstates.

- We shall consider the so-called *driven systems* where one or more parameters of a quantum Hamiltonian are varied in time. If we denote with t_s the typical time scale of the variation of the Hamiltonian, we have the two limiting cases:

    - *adiabatic limit* $t_s \to \infty$, where the system evolves through instantaneous realizations of the ground state. This means that an adiabatic evolution of the ground state is conceptually equivalent to a collection of equilibrium systems for each instant of time.

- *quench limit* $t_s \to 0$, where the Hamiltonian is suddenly modified at a time $t = t_0^+$ and the time evolution for $t > t_0$ results into a relaxation problem with the post-quench Hamiltonian.

Among all the possible kinds of driven systems, a slow driving across a critical point is surely one of the most interesting. In this situation, in fact, the development of large-scale modes leads inevitably to a regime in which the time variation of the parameter cannot be relaxed and out-of-equilibrium behaviors emerge. Moreover, because of a diverging relaxation time (due to the critical slowing down), the system will always perceive the external variations as a sudden change, no matter how slow is the driving. To state this differently, we will cross over from an *adiabatic-to-quench* regime as soon as we get sufficiently close to the criticality. Interestingly, the breakdown of the adiabatic behavior across the transition leads to the development of topological defects in the new phase (reached right after the driving). The presence of topological defects can be desired e.g. in the study of the early cosmological structures arising across high-energy thermal phase transitions, or less wanted, as for instance in the context of quantum information where one typically aims for a full control of quantum states. Nevertheless, the Kibble-Zurek prediction [Kib76, Kib80, Zur85] on the defects density revealed to be an important milestone in the analysis of the non-equilibrium behaviors and opened the road to more recent developments, such as engineered *shortcut-to-adiabaticity*, see e.g. [Che10, dC14, Cam15a, Acc15, Fun17], or the extension to inhomogeneous setups [Pla07, Col09, Dzi10].

2.1 Kibble-Zurek mechanism

Let $\hat{H}(g)$ be a quantum Hamiltonian depending on some adimensional parameter g and let us suppose that the system has an isolated critical point located at g_c. At $t = t_0$ the system is prepared in the ground state of $\hat{H}$ for a certain $g(t_0) > g_c$ and, for later times $t > t_0$, g is varied across the critical point up to a value $g(t_f) < g_c$. For instance, we may consider

$$\delta g(t) = t^\alpha / t_s \,, \qquad t \in [t_0 < 0 \,, t_f > 0]; \tag{2.1.1}$$

where $\delta g(t) \equiv g_c - g(t)$, t_s is the time scale of the driving and $\alpha > 0$ is a positive odd exponent. Here, the time variable t ranges from $t_0 < 0$ to $t_f > 0$ so that g_c is reached at $t = 0$ which is but a convenient choice, see Fig.2.1.

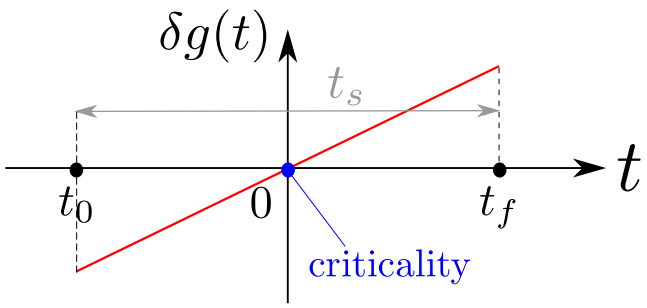

Figure 2.1: **Driving protocol across a QPT.** An illustration of a linear ramp protocol $\delta g(t) = t/t_s$ across the quantum criticality. Notice that in our convention the QPT is reached at $t = 0$.

Notice that Eq.(2.1.1) is quite general because any regular function of time $\delta g(t)$ allows a Taylor expansion for $g \to g_c$:

$$\delta g(t) = \frac{\mathrm{d}^\alpha(\delta g(t))}{\mathrm{d}t^\alpha}\Big|_{t=0} t^\alpha + \mathcal{O}(t^{\alpha+1}) , \qquad \frac{\mathrm{d}^\alpha(\delta g(t))}{\mathrm{d}t^\alpha}\Big|_{t=0} \equiv t_s^{-1} ; \tag{2.1.2}$$

where the α^{th} is the first non-zero derivative of $\delta g(t)$. We can then set $\alpha = 1$ and consider hereafter a linear variation of the control parameter $\delta g(t) = t/t_s$. The extension to non-linear protocols is straightforward, see e.g. [Dzi10].

We remark that the problem is characterized by the presence of two different time scales, namely, the internal time scale $\tau = \xi^z$ (which takes into account the relaxation mechanisms of the system excitations) and the external time scale t_s which has been introduced with the protocol (2.1.1). Clearly, they are self-consistently related since τ is defined (at each instant of time) through the instantaneous energy spectrum of excitations $\varepsilon_q(t)$ which depends on the Hamiltonian parameter $g(t)$ and thus on t_s.
Nevertheless, we can assume that the protocol $\delta g(t)$ is made in such a way to ensure an adiabatic evolution (i.e., $t_s \gg 1$ is large in a sense that will be specified later on) at least during the early stage $t_0 \leq t \lesssim 0$, where τ is exponentially small. The dynamics proceeds therefore through equilibrium states by connecting the instantaneous ground states of the system on varying of g with time.
As soon as $t \to 0$, we do enter in the critical domain where the instantaneous correlation length satisfies (see Eq.(1.1.4))

$$\xi(t) \propto |\delta g(t)|^{-\nu} = |t/t_s|^{-\nu} \tag{2.1.3}$$

leading to the scaling form of the correlations in Eq.(1.1.7). This situation is expected to apply as long as the system can adapt itself to the variations of the control parameter $\delta g(t)$. The impact of the external field's variations on the equilibrium properties of the system can be quantified via the time scale:

$$\tau_{\rm adapt}(t) \equiv \left(\frac{\dot{\xi}(t)}{\xi(t)}\right)^{-1} = \left(\left|\frac{\delta\dot{g}(t)}{\delta g(t)}\right|\right)^{-1} \propto |t|, \tag{2.1.4}$$

and thus compared with the instantaneous relaxation time $\tau(t) = \xi^z(t)$. Indeed, these scales do compete during the driving as the system tries to relax towards a new equilibrium configuration and to follow the protocol simultaneously. As a result, as long as $\tau < \tau_{\rm adapt}$, the system manages to equilibrate the external perturbation and to follow the protocol (2.1.1). On the other hand, when $\tau > \tau_{\rm adapt}$, the system will be unable to adapt to the external changes anymore and it collectively falls out of equilibrium. The crossover time $\tau_{\rm KZ}$ between the two regimes is then given by the self-consistent equation

$$\tau(\tau_{\rm KZ}) = \tau_{\rm adapt}(\tau_{\rm KZ}) \tag{2.1.5}$$

which leads to the *Kibble-Zurek* (KZ) time scale

$$\tau_{\rm KZ} \equiv (t_s)^{z\nu/(1+z\nu)}\,. \tag{2.1.6}$$

In the time window $t \in [-\tau_{\rm KZ}, \tau_{\rm KZ}]$, where the critical slowing down dominates over the external driving, the system is assumed to freeze out and the correlation length remains bounded to the value

$$\ell_{\rm KZ} \equiv \xi(\tau_{\rm KZ}) = (t_s)^{\nu/(1+z\nu)}\,. \tag{2.1.7}$$

The dynamics of the system can be schematically divided into three stages, namely, an early adiabatic regime for $t \in [t_0, -\tau_{\rm KZ}]$, an intermediate quench regime for $t \in [-\tau_{\rm KZ}, \tau_{\rm KZ}]$ and a final adiabatic evolution at times $t \in [\tau_{\rm KZ}, t_f]$ right after the transition. This ansatz goes under the name of Kibble-Zurek approximation [Dzi10, Pol11, dC13] and it is illustrated in Fig.2.2.
Notice that the KZ approximation holds even in the limit of quasi-static driving, where formally $t_s \to \infty$. We conclude therefore that [Dzi10, Pol11, dC13],

Breakdown of adiabaticity - *A driving across a QPT is never performed adiabatically; even if the time scale t_s of the external variations is formally sent to ∞, there will be inevitably a time τ_{KZ} where the adiabatic assumption will fail due to the emergence of large scale fluctuations that cannot be relaxed.*

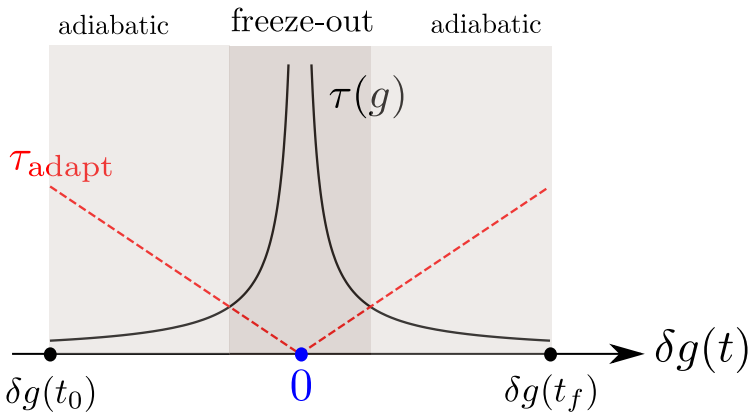

Figure 2.2: **Illustration of the Kibble-Zurek approximation.** We prepare the system initially in the ground state of $\hat{H}(g_0)$ for a certain value $g_0 > g_c$. We then vary the parameter g in time across the phase boundary up to a final value $g_f < g_c$. As long as the relaxation time $\tau < \tau_{\rm adapt}$ the system adapts to the external field variations and adiabatically follows the protocol (*light gray region on the left*). In the vicinity of the transition point, the divergence of τ leads inevitably to a time $\tau_{\rm KZ}$ where $\tau = \tau_{\rm adapt}$ after which the system cannot adjust to the external variations anymore and falls collectively out of equilibrium (*dark gray region*). The system remains frozen in this region until τ decays again in the new phase (*light gray region on the right*).

Notice that a bounded correlation length $\ell_{\rm KZ}$ across criticality leads to the development of topological defects in the quantum phase arising for $g < g_c$. Indeed, at the transition the degrees of freedom of the system are correlated over domains of size $\ell_{\rm KZ}$ and different realizations of the broken phase are developed only in local domains, see Fig.2.3. Equivalently, the defect production can be understood considering the different evolution of the instantaneous ground state and of the actual state of the system. Indeed, right after the transition (i.e., for $t \simeq \tau_{\rm KZ}$) the state of the system is frozen in the ground state $\Psi_0(-\tau_{\rm KZ})$ corresponding to $\hat{H}(-\tau_{\rm KZ})$ which is not anymore the ground state of the instantaneous Hamiltonian $\hat{H}(\tau_{\rm KZ})$. Inevitably, the change of background leads to the development of excitations whose density $\rho_{\rm ex}$ is expected to be

$$\rho_{\rm ex} \propto \ell_{\rm KZ}^{-1} = (t_s)^{-\nu/(1+z\nu)} . \tag{2.1.8}$$

Eq.(2.1.8) follows from the assumption that the number of correlated clusters (i.e., the number of topological defects) corresponds to the number of excitations observed in the new quantum phase.

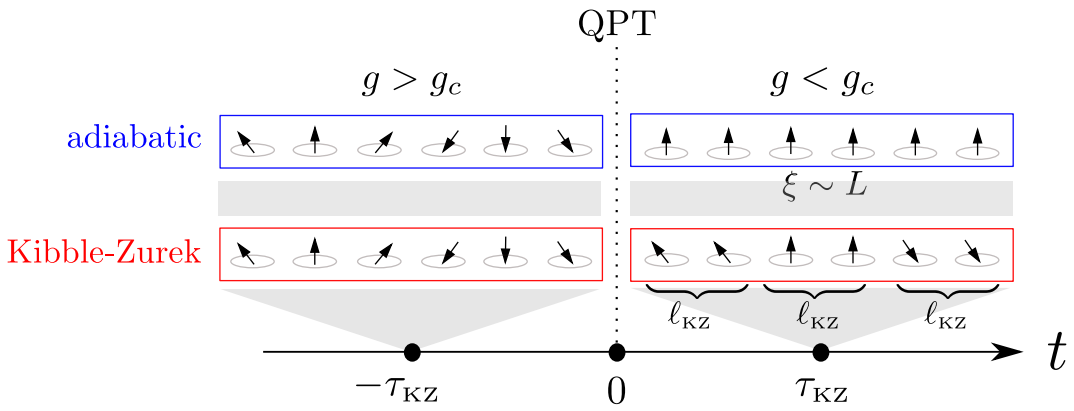

Figure 2.3: **Defects production across a QPT.** Illustration of the Kibble-Zurek mechanism: in the early stage $t \in [t_0, -\tau_{\rm KZ}]$ the system is assumed to evolve adiabatically and the typical lattice configurations are invariant under the full symmetry group of the Hamiltonian (here represented with a disordered configuration, on the left). Right after the transition, i.e., when $t \simeq \tau_{\rm KZ}$ the system is correlated only over domains of size $\ell_{\rm KZ}$ where the local lattice configurations are invariant under a certain realization of the broken symmetry (here represented with an ordered configuration, on the right). Topological defects (corresponding to excitations over the new background) are expected to be of the order of $L/\ell_{\rm KZ}$. Notice that the KZ scenario (*bottom*) is quite different from what we would have expected from an adiabatic guess (*top*) where the system is correlated over the whole chain.

The last result is known as *Kibble-Zurek mechanism* [Kib76, Kib80, Zur85]. It was initially derived by Thomas Kibble [Kib76, Kib80] as explanation of the cosmological structures generated across thermal high-energy phase transitions in the early Universe and then extended by Wojciech H. Zurek in classical [Zur85] and quantum [Zur05] statistical systems.

Scaling limit

We remark that the equilibrium scaling relation of Eq.(1.1.7) is not valid for driven systems. Nevertheless, in the limit of slow driving, the system is still suitable for a scaling description in terms of the KZ scale $\ell_{\rm KZ}$. More precisely, we can define a non-equilibrium scaling as the limit $t \to 0$, $t_s \to \infty$ at fixed $x/\ell_{\rm KZ}$,

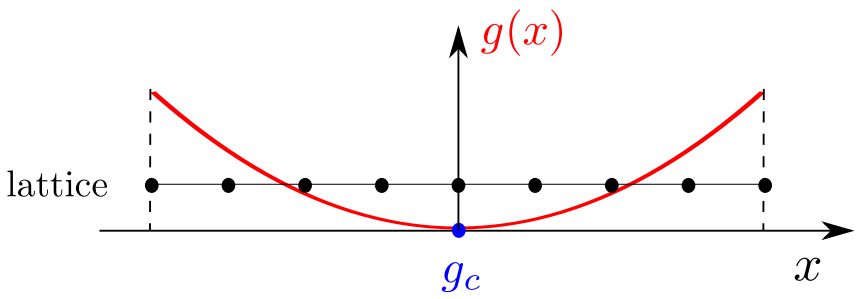

Figure 2.4: **Illustration of an inhomogeneous control parameter.** Consider a quantum system for which the interaction with an external trapping potential induces a bulk critical behavior (*in blue*). Notice that the situation is equivalent to that of a driven system where the instantaneous configurations (associated with a certain $g(t)$) are now replaced with local descriptions of the chain.

$t/\tau_{\rm KZ}$ where equal-time correlations of a local observable $\hat{O}(x,t)$ satisfy [Cha12]

$$\langle\Psi(t)|\hat{O}(x,t)\,\hat{O}(x',t)|\Psi(t)\rangle \propto \ell_{\rm KZ}^{-2d_o}\,\mathcal{G}_{oo}^{\rm KZ}\left(\frac{|x-x'|}{\ell_{\rm KZ}},\frac{t}{\tau_{\rm KZ}}\right) \tag{2.1.9}$$

where $\Psi(t)$ is the actual state of the system and $\mathcal{G}_{oo}^{\rm KZ}$ is a non-equilibrium scaling function. Notice that (by construction) the non-equilibrium scaling relation of Eq.(2.1.9) reduces to Eq.(1.1.7) when $t\to-\tau_{\rm KZ}$ since then $\xi(-\tau_{\rm KZ})=\ell_{\rm KZ}$. Similarly to Eq.(1.1.8), in finite-size systems we define a non-equilibrium FSS as the limit $t\to 0$, $t_s, L\to\infty$ with fixed $x/\ell_{\rm KZ}$, $\tau/\ell_{\rm KZ}$ where

$$\langle\Psi(t)|\hat{O}(x,t)\,\hat{O}(x',t)|\Psi(t)\rangle \propto L^{-2d_o}\,\mathcal{G}_{oo}^{\rm KZ}\left(\frac{|x-x'|}{\ell_{\rm KZ}},\frac{t}{\tau_{\rm KZ}},\frac{\ell_{\rm KZ}}{L}\right). \tag{2.1.10}$$

The extension to n-points correlators is straightforward.

2.1.1 Trap-size scaling

Consider now a time-independent Hamiltonian $\hat{H}(g)$ which depends on an external field $g=g(x)$ with a certain spatial dependence. Notice that this situation is quite common and typically arises due to the presence of an external trapping potential which confines the particles into a finite space region, see e.g. [Min05, Cap07, Cam10b, Cam10a, Rou10, Ber11, Ber12b, Col12b, Col13a, Col13b, Wen13, Dub17, Sco17, Bru17, Col18, Sco18b, Bru18, Rug19]. Suppose also

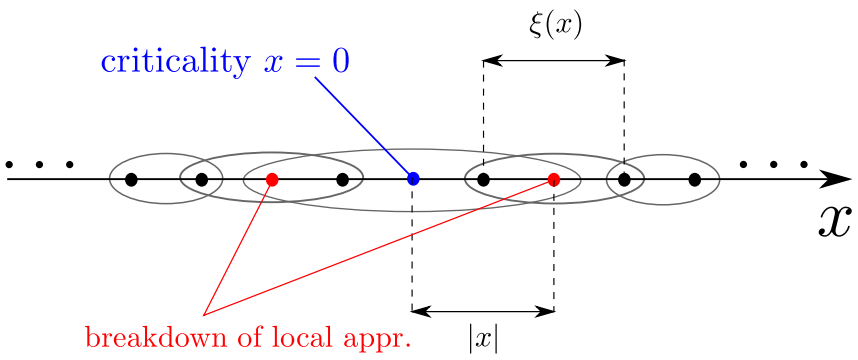

Figure 2.5: **Kibble-Zurek ansatz in space.** Illustration of a trapped system with a bulk critical behavior arising around the spatial point $x = 0$ (*in blue*). Local portions of the system realize local equilibrium configurations as long as the local correlation length $\xi(x)$ (*grey circles*) is smaller than the distance from the criticality $|x|$. In the opposite case the influence of the bulk critical behavior on the local correlations inevitably leads to a breakdown of the local approximation (*in red*).

that g_c is a critical point of the model and that the external field has a space profile[§]

$$\delta g(x) \equiv g(x) - g_c = k\,|x|^{\mathrm{w}} \tag{2.1.11}$$

where $k > 0$ is the trap amplitude and $\mathrm{w} > 0$ is a positive exponent, see Fig.2.4. One can easily understand that this setup is suitable for an analogous KZ description made in terms of the space coordinate [Pla07, Col09, Dzi10].
Indeed, for a sufficiently smooth potential (i.e., $k \ll 1$ in a sense that will made precise later) and away from the critical locus $|x| > 0$, we do expect that the system is locally at equilibrium with a local value $g(x)$ of the external field.

On the other hand, for $|x| \to 0$ we enter in the critical regime where local portions of the lattice around a spatial point x are correlated up to a distance

$$\xi(x) \propto |\delta g(x)|^{-\nu} = (k\,|x|^{\mathrm{w}})^{-\nu} \tag{2.1.12}$$

and satisfy a local approximation only if $\xi(x)$ results smaller than the distance from the criticality $|x|$[¶]. Indeed, when $\xi(x) > |x|$ the influence of the bulk

[§]Without loss of generality we set the criticality at $x = 0$ which is but a convenient choice. Notice that Eq.(2.1.11) is a quite general assumption for the description of the bulk critical behavior. Indeed, any regular function $g(x)$ allows a Taylor expansion in the vicinity of $x = 0$ (compare with Eq.(2.1.2)).

[¶]Notice that this intuitive condition can be derived considering the quantity $|\delta g(x)/\frac{\mathrm{d}}{\mathrm{d}x}\delta g(x)| \propto |x|$ (compare with Eq.(2.1.4).

critical behavior on local correlations leads inevitably to a breakdown of the local approximation, see Fig.2.5. The crossover distance $\ell_{\rm KZ}$ is thus defined by the KZ condition [Pla07, Col10b, Col11]

$$\xi(\ell_{\rm KZ}) = \ell_{\rm KZ} \tag{2.1.13}$$

which leads to the result

$$\ell_{\rm KZ} = |k|^{-\nu/(1+{\rm w}\nu)}. \tag{2.1.14}$$

Notice that the KZ length $\ell_{\rm KZ}$ is consistent with the typical length scale induced by the external trapping potential and thus the exponent

$$\nu_g \equiv \nu/(1+{\rm w}\nu) \tag{2.1.15}$$

is known as *trap-size exponent* [Cam10a, Cam10b]. The length scale $\ell_{\rm KZ}$ induces also an inhomogeneous scaling limit in line with that of Eq.(2.1.9). In particular, we define the trap-size scaling (TSS) limit as the limit $k \to 0$, $|x| \to 0$ at fixed $x/\ell_{\rm KZ}$ and $t/\tau_{\rm KZ}$ (here $\tau_{\rm KZ} \equiv (\ell_{\rm KZ})^z = |k|^{-z\nu_g}$) where equal-time correlations of local observables behave as in Eq.(2.1.9). The extension of the TSS to finite-size systems is made considering $L \to \infty$ and $k, |x| \to 0$ at fixed $x/\ell_{\rm KZ}$, $t/\tau_{\rm KZ}$ such that

$$\langle\Psi_0|\hat{O}(x,t)\,\hat{O}(x',t)|\Psi_0\rangle \propto L^{-2d_o}\,\mathcal{G}^{\rm TSS}_{oo}\left(\frac{|x-x'|}{\ell_{\rm KZ}}, \frac{t}{\tau_{\rm KZ}}, \frac{\ell_{\rm KZ}}{L}\right) \tag{2.1.16}$$

with $\mathcal{G}^{\rm TSS}_{oo}$ a TSS function. Notice that for $L \ll \ell_{\rm KZ}$, it is expected that the scaling relation (2.1.16) matches the ordinary FSS behavior (see Eq.(1.1.8)); whereas for $L \gg \ell_{\rm KZ}$ the system matches the TSS infinite volume behavior where the presence of inhomogeneities becomes manifest.

Chapter 3

Periodic Driving

Another central role in the study of driven systems is played by the investigation of time-periodic external perturbations. In fact, periodically driven systems naturally arise in many experimental setups, as for instance, when materials are irradiated with electromagnetic waves or when one testes the mechanical response to periodic deformations. Typically, when the external driving frequency is much slower than the internal frequency of reference, the system reacts adiabatically and does follow the evolution of the Hamiltonian whereas, in the opposite regime of fast driving, the system feels only a static potential which results from the interplay of the external forcing and of the internal dynamics [Buk15]. Away from these two limiting regimes one finds a very rich scenario where the system can show a broad range of time-evolutions, from the development of breathing modes to the formation of dynamical instabilities. These behaviors have a long history that dates back to the Kapitza pendulum [Kap51, Kap65] or to the kicked-rotor model [Cas79], where several counter-intuitive features of recent interest (such as dynamical localization, see e.g. [Gro91, Bav92, D'A13, Gua14] and integrability-to-chaos crossover [D'A16, Rei13]) are already present.
From the theory side, the analysis of periodically driven systems mainly relies on *Floquet theory* [Buk15, Eck17]. In its general formulation (which is very similar to that of Bloch theory for periodic lattices but made in terms of time), Floquet theory states that it is possible to find a time-periodic unitary transformation which factorizes the dynamics into three stages. In order, an initial kick, a linear phase evolution for a relatively long time and final sudden kick. The way of doing this is not unique and translates into different gauges, which however lead to the same dynamics. The physical interpretation is rather

clear: the linear phase evolution corresponds to a *stroboscopic dynamics*, i.e., to a collection of time instants that proceeds with steps of one period and for which the system allows for a time-independent description. On the other hand, the kick operators are responsible for the so-called *micromotion* occuring inside the periods and carrying the time-dependence of the external forcing.
A focus on the stroboscopic evolution simplifies dramatically the analysis which results completely described in terms of a (time-independent) Floquet Hamiltonian. The knowledge of the Floquet Hamiltonian allows then to study the long-time properties and the possible relaxation of the system towards a cyclic evolution. Unfortunately, the Floquet Hamiltonian is seldom obtainable exactly; more often, approximation schemes are needed.
The recent attention dedicated to Floquet theory (see e.g. [Har99, Rah03a, Rah03b, Cre09, Rus12, Gol14, Laz14, Eck15, Lor17, Ber17, Gri17, Ple17, Kan18, Ler18, Tap18]) has led to the development of Floquet engineered systems, where non-equilibrium states of matter are generated by a proper tuning of the external perturbations, especially using radiation for the coherent manipulation of quantum systems [Eck17].

3.1 Floquet Dynamics

Let us move one step back in order to discuss Floquet theory more precisely. We consider the unitary dynamics generated by the Schrödinger equation

$$i\partial_t \, |\Psi(t)\rangle = \hat{H}(t) \, |\Psi(t)\rangle \, , \tag{3.1.1}$$

in the presence of time-periodic Hamiltonians

$$\hat{H}(t) = \hat{H}(t+\mathcal{T}) = \sum_{k=-\infty}^{\infty} e^{ik\omega t} \hat{H}_k \tag{3.1.2}$$

with driving period $\mathcal{T}$ (and frequency $\omega \equiv 2\pi/\mathcal{T}$) and with Fourier components $\hat{H}_k$. Now, at least formally, we can define a unitary time-periodic map $\hat{W}(t) = \hat{W}(t+\mathcal{T})$ such that the time evolution of the transformed state

$$|\Psi_{\text{eff}}(t)\rangle \equiv \hat{W}(t) \, |\Psi(t)\rangle \tag{3.1.3}$$

is generated by an effective time-independent Hamiltonian

$$\hat{H}_{\text{eff}} \equiv \hat{W}(t) \, \hat{H}(t) \, \hat{W}^\dagger(t) + i \left(\frac{\mathrm{d}}{\mathrm{d}t} \hat{W}(t) \right) \hat{W}^\dagger(t). \tag{3.1.4}$$

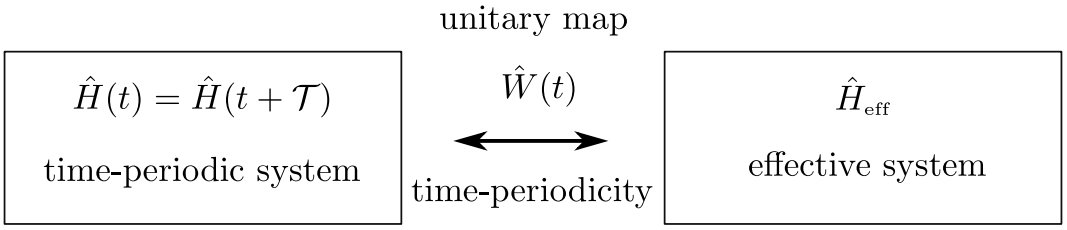

Figure 3.1: **Mapping to effective Hamiltonians**. A time-periodic system can be mapped, by means of a proper unitary transformation $\hat{W}(t)$, to an effective time-independent problem. This observation is the basis of Floquet Theory which turns out to be a very powerful instrument for the analysis of periodically driven quantum systems.

Thus, the time evolution in the effective frame is simply

$$\hat{U}_{\text{eff}}(t,t_0) = \exp\left(-i(t-t_0)\hat{H}_{\text{eff}}\right) \tag{3.1.5}$$

and leads to the formal solution of the time-dependent problem $|\Psi(t)\rangle = \hat{U}(t,t_0)\ |\Psi(t_0)\rangle$ with

$$\hat{U}(t,t_0) = \hat{W}^\dagger(t)\ e^{-i(t-t_0)\hat{H}_{\text{eff}}}\ \hat{W}(t_0). \tag{3.1.6}$$

Here, we see that the time evolution of a Floquet system can be divided into a time-periodic motion generated by a hermitian kick-operator $\hat{\mathcal{K}}$

$$\hat{W}^\dagger(t) \equiv \exp\left(\ i\hat{\mathcal{K}}(t)\ \right) \tag{3.1.7}$$

and by a linear phase evolution generated by the time-independent effective Hamiltonian $\hat{H}_{\text{eff}}$ [Gol14], see Fig.3.2.
The solution of the eigenproblem associated with the effective Hamiltonian

$$\hat{H}_{\text{eff}}\ |u_n\rangle = \varepsilon_n\ |u_n\rangle \tag{3.1.8}$$

allows to define quasi-stationary states of the time-periodic problem called Floquet states [Shi65, Zel67]:

$$|\psi_n(t)\rangle = e^{-it\varepsilon_n}\ |\phi_n(t)\rangle \tag{3.1.9}$$

with $|\phi_n(t)\rangle \equiv \hat{W}^\dagger(t)\ |u_n\rangle$. These states are eigenstates of the time evolution operator $\hat{U}$ over one driving period

$$|\psi_n(t+\mathcal{T})\rangle = \hat{U}(t+\mathcal{T},t)\ |\psi_n(t)\rangle = \exp(i\mathcal{T}\varepsilon_n)\ |\psi_n(t)\rangle\,, \tag{3.1.10}$$

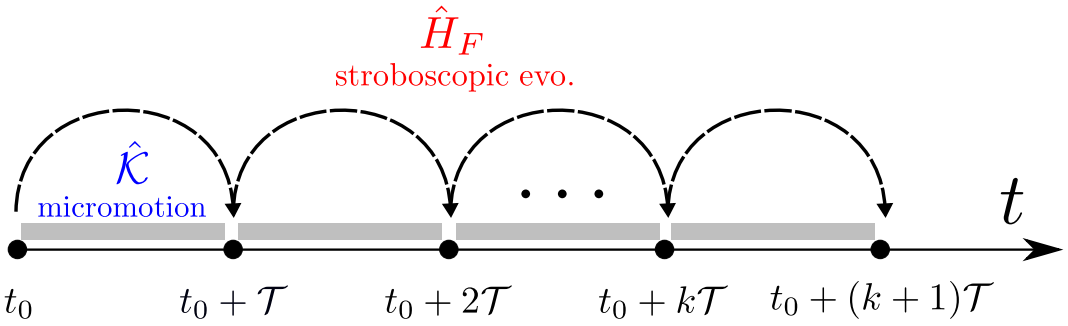

Figure 3.2: **Floquet evolution.** The dynamics of a periodically driven system can be divided into a linear phase evolution, carried by a time independent effective Hamiltonian in Eq.(3.1.4), plus a time-periodic component generated by the micromotion operator in Eq.(3.1.7). We have seen that these quantities are not uniquely defined. However, a nice physical interpretation is given by choosing $\hat{W}$ as in Eq.(3.1.14) that leads to the definition of the Floquet Hamiltonian $\hat{H}_F$ (3.1.17). In this case, the time-independent component of the dynamics (generated by $\hat{H}_F$) is responsible for the stroboscopic evolution among the periods (*dashed line*) whereas the micromotion $\hat{\mathcal{K}}$ generates the time-periodic dynamics inside each period (*gray boxes*).

with deviations from a periodic evolution that are governed by the quasi-energies ε_n. Floquet states also provide a complete and orthogonal basis at any time t. This means that a generic state $|\Psi(t)\rangle$ can be expressed as a superposition of Floquet states

$$|\Psi(t)\rangle = \sum_n c_n \, e^{-it\varepsilon_n} \, |\psi_n(t)\rangle \tag{3.1.11}$$

with overlap coefficients $c_n \equiv e^{it_0\varepsilon_n} \, \langle\psi_n(t_0)|\Psi(t_0)\rangle$. It follows that the spectrum of the operator $\hat{U}(t+\mathcal{T},t)$ (known also as monodromy operator) will play a crucial role in the study of the long-time behavior of the driven system.

We remark that the choice of the effective Hamiltonian is not unique but it does not affect the physical results. For instance, by multiplying the map $\hat{W}$ with a (time-independent) unitary operator $\hat{\mathcal{U}}$,

$$\hat{W}'(t) = \hat{\mathcal{U}} \, \hat{W}(t), \tag{3.1.12}$$

we obtain a conjugated effective Hamiltonian

$$\hat{H}'_{\text{eff}} = \hat{\mathcal{U}} \, \hat{H}_{\text{eff}} \, \hat{\mathcal{U}}^\dagger \tag{3.1.13}$$

with same spectrum of quasi-energies ε_n. However, a convenient choice might be to consider the modified map

$$\hat{W}'(t) = \hat{W}^\dagger(t_0)\, \hat{W}(t) \equiv \hat{W}(t, t_0) \tag{3.1.14}$$

that leads to the effective Hamiltonian

$$\hat{H}_F(t_0) = \hat{W}^\dagger(t_0)\, \hat{H}_{\text{eff}}\, \hat{W}(t_0) \tag{3.1.15}$$

and to the kick operator

$$\hat{W}^\dagger(t)\, \hat{W}(t_0) \equiv \exp\left(i\hat{\mathcal{K}}(t) \right). \tag{3.1.16}$$

With this choice, the time evolution operator in Eq.(3.1.6) becomes

$$\hat{U}(t, t_0) = \exp\left(i\hat{\mathcal{K}}(t) \right)\, \exp\left(-i(t - t_0)\, \hat{H}_F(t_0)\right) \tag{3.1.17}$$

and in particular for $t = t_0 + k\mathcal{T}$, k a positive integer, we have that $\hat{W}^\dagger(t)\, \hat{W}(t_0) = \hat{\mathbb{1}}$ and

$$\hat{U}(t_0 + k\mathcal{T}, t_0) = \exp\left(-ik\mathcal{T}\, \hat{H}_F(t_0)\right). \tag{3.1.18}$$

The effective Hamiltonian $\hat{H}_F$ in Eq.(3.1.15) generates the physical evolution among steps of one period $\mathcal{T}$ and it is called *Floquet Hamiltonian*[§], see Fig.3.2. We also mention that the quasi-energies spectrum is not uniquely defined. Indeed, one can modify the map as

$$\hat{W}'(t, t_0) = \hat{W}(t, t_0)\, \exp\left(im\omega t\ |u_m\rangle \langle u_m|\right), \tag{3.1.19}$$

with m an integer, that does modify the Floquet Hamiltonian as

$$\hat{H}'_F(t_0) = \hat{H}_F(t_0) + m\omega\ |u_m\rangle \langle u_m| \tag{3.1.20}$$

and creates a shift of the quasi-energies

$$\varepsilon_{nm} = \varepsilon_n + m\omega, \qquad |\phi_{nm}(t)\rangle = e^{im\omega t}\ |\phi_n(t)\rangle. \tag{3.1.21}$$

However, the shift of the spectrum does not modify the Floquet states

$$|\psi_n(t)\rangle = e^{-it\varepsilon_n}\ |\phi_n(t)\rangle = e^{-it\varepsilon_{nm}}\ |\phi_{nm}(t)\rangle \tag{3.1.22}$$

[§]There is a certain ambiguity when one refers to Floquet Hamiltonians. Many authors are used to call Floquet Hamiltonian also the effective Hamiltonian in Eq.(3.1.4). Conversely, we will make use of this name only for the Hamiltonian appearing in Eq.(3.1.15).

and it allows to choose the quasi-energies to lie in the same interval of width ω. Therefore, in analogy with Bloch's theorem for periodic lattices, our choice of the quasi-energies (with reference $m = 0$) is equivalent to the choice of the first Brillouin zone for the definition of quasi-momenta.

We have seen that the time evolution of periodically driven quantum systems can be investigated by means of Floquet theory once we provide a map $\hat{W}$ to an effective time-independent description. This in turns implies that we need a procedure to obtain the operator $\hat{W}$ for generic time-periodic Hamiltonians. In the following, we present two possibility of doing so: high-frequency expansions (see Sec.3.1.1), which provide a suitable approximation of the Floquet Hamiltonian in the case of a fast-oscillating forcing, and an exact algebraic method (see Sec.3.1.2) with which the Floquet problem is cast onto a set of coupled first-order differential equations for classical functions whose solution defines the map $\hat{W}$.

3.1.1 High-frequency expansion

Without loss of generality, we search for $\hat{W}(t)$ in an exponential form:

$$\hat{W}(t) \equiv \exp\Big(i\hat{\Phi}(t)\Big), \qquad \hat{\Phi}(t) = \hat{\Phi}(t+\mathcal{T}), \quad \hat{\Phi}(t) = \hat{\Phi}^{\dagger}(t) \tag{3.1.23}$$

with $\hat{\Phi}$ a time-periodic hermitian operator. Next, with the help of Baker-Campbell-Hausdorff (BCH) formulae [Bak02, Cam97a, Cam97b, Hau06] (see also [Hal03]) :

$$e^{\hat{A}}\, e^{\hat{B}} = e^{\hat{C}}, \quad \hat{C} \equiv \hat{A} + \hat{B} + \frac{1}{2}[\hat{A}, \hat{B}] + \ldots; \tag{3.1.24a}$$

$$e^{\hat{A}}\, \hat{B}\, e^{-\hat{A}} = \hat{B} + [\hat{A}, \hat{B}] + \frac{1}{2}[\hat{A}, [\hat{A}, \hat{B}]] + \ldots; \tag{3.1.24b}$$

$$e^{-\hat{A}(x)}\, \Big(\partial_x\, e^{\hat{A}(x)}\Big) = \partial_x\, \hat{A}(x) + \frac{1}{2}[\partial_x\, \hat{A}(x), \hat{A}(x)] + \ldots; \tag{3.1.24c}$$

for generic operators $\hat{A}$ and $\hat{B}$, we can write the formal expansion for the effective Hamiltonian in Eq.(3.1.4):

$$\begin{aligned}\hat{H}_{\text{eff}} &= e^{i\hat{\Phi}(t)}\ \hat{H}(t)\ e^{-i\hat{\Phi}(t)} + i\left(\frac{\mathrm{d}}{\mathrm{d}t}\, e^{i\hat{\Phi}(t)}\right)\ e^{-i\hat{\Phi}(t)} \\ &= \hat{H}(t) + \frac{\mathrm{d}}{\mathrm{d}t}\hat{\Phi}(t) + i[\hat{\Phi}(t), \hat{H}(t)] + \frac{i}{2}[\frac{\mathrm{d}}{\mathrm{d}t}\hat{\Phi}(t), \hat{\Phi}(t)] \\ &- \frac{1}{2}[\hat{\Phi}(t), [\hat{\Phi}(t), \hat{H}(t)]] + \frac{1}{6}[\hat{\Phi}(t), [\hat{\Phi}(t), \frac{\mathrm{d}}{\mathrm{d}t}\hat{\Phi}(t)]] + \dots \end{aligned} \tag{3.1.25}$$

A perturbative approach to the Floquet problem can be employed when the driving frequency $\omega \equiv 2\pi/\mathcal{T}$ is much larger than the typical energy scale defined by the Hamiltonian's matrix elements. In this case, we can write down the high-frequency expansions[§]:

$$\hat{H}_{\text{eff}} = \sum_{a=0}^{\infty} \omega^{-a}\ \hat{H}^{(a)}_{\text{eff}}; \qquad \hat{\Phi}(t) = \sum_{a=1}^{\infty} \omega^{-a}\, \hat{\Phi}^{(a)}(t), \tag{3.1.26}$$

and we solve Eq.(3.1.25) imposing the time-independence of $\hat{H}_{\text{eff}}$ at each order in $1/\omega$. For instance, at the zeroth order we have[¶]:

$$\begin{aligned}\hat{H}^{(0)}_{\text{eff}} &= \frac{\mathrm{d}}{\mathrm{d}t}\hat{\Phi}^{(1)}(t) + \hat{H}(t) \\ &= \frac{\mathrm{d}}{\mathrm{d}t}\hat{\Phi}^{(1)}(t) + \hat{H}_0 + \sum_{k\neq 0} e^{ik\omega t}\hat{H}_k. \end{aligned} \tag{3.1.27}$$

Here, the time-independent part fixes the effective Hamiltonian to $\hat{H}^{(0)}_{\text{eff}} = \hat{H}_0$, while for the map we have

$$\hat{\Phi}^{(1)}(t) = \sum_{k\neq 0} \frac{i}{k\omega}\ e^{ik\omega t}\ \hat{H}_k \tag{3.1.28}$$

so that it cancels the unwanted terms in Eq.(3.1.27). The physical interpretation is rather clear. At the zeroth order the effective time-independent frame consists simply in the time-averaged system while the time-periodic contribution is

[§]Without loss of generality we considered a map $\hat{\Phi}$ having zero mean. Indeed, any constant term can be absorbed in definition of the time-averaged system Hamiltonian $\hat{H}_0$.

[¶]Notice that $\hat{\Phi}^{(a)}$ is time-periodic and so it does have an expansion in Fourier modes. It follows that $\mathrm{d}\hat{\Phi}^{(a)}/\mathrm{d}t$ contributes to the order $(a-1)$ of the high-frequency expansion.

carried by the effect of the other Fourier modes. This procedure can be iterated to higher orders obtaining [Rah03a, Rah03b, Gol14, Eck17]

$$\hat{H}_{\text{eff}} = \hat{H}_0 + \sum_{k\neq 0} \frac{[\hat{H}_k, \hat{H}_{-k}]}{2\omega k} + \sum_{k\neq 0} \frac{[[\hat{H}_k, \hat{H}_0], \hat{H}_{-k}]}{2\omega^2 k^2} + \sum_{k,q\neq 0} \frac{[\hat{H}_k, [\hat{H}_q, \hat{H}_{-k-q}]]}{3\omega^2 k\, q} + \mathcal{O}(\omega^{-3}); \tag{3.1.29}$$

with the associated map

$$\hat{\Phi}(t) = \sum_{k\neq 0} \frac{i}{k\omega}\, e^{ik\omega t}\, \hat{H}_k - \frac{i}{\omega^2} \sum_{k\neq 0} \left[\frac{e^{ik\omega t}\, [\hat{H}_0, \hat{H}_k]}{k^2} + \sum_{q\neq -k} \frac{e^{i(k+q)\omega t}\, [\hat{H}_k, \hat{H}_q]}{2k(k+q)} \right] + \mathcal{O}(\omega^{-3}). \tag{3.1.30}$$

The Floquet Hamiltonian $\hat{H}_F$ follows from Eq.(3.1.15) (together with the BCH formula (3.1.24b)):

$$\hat{H}_F(t_0) = e^{-i\hat{\Phi}(t_0)}\, \hat{H}_{\text{eff}}\, e^{i\hat{\Phi}(t_0)} = \hat{H}_{\text{eff}} - i[\hat{\Phi}(t_0), \hat{H}_{\text{eff}}] - \frac{1}{2}[\hat{\Phi}(t_0), [\hat{\Phi}(t_0), \hat{H}_{\text{eff}}]] + \dots, \tag{3.1.31}$$

which gives in high-frequency expansion

$$\begin{aligned} \hat{H}_F(t_0) = \hat{H}_0 &+ \sum_{k\neq 0} \frac{\frac{1}{2}[\hat{H}_k, \hat{H}_{-k}] + e^{ik\omega t_0}[\hat{H}_k, \hat{H}_0]}{\omega k} + \sum_{k,q\neq 0} \frac{[\hat{H}_k, [\hat{H}_q, \hat{H}_{-k-q}]]}{3kq\omega^2} \\ &+ \sum_{k,q\neq 0} \frac{e^{i(k+q)\omega t_0}([[\hat{H}_k, \hat{H}_{q-k}], \hat{H}_0] + [\hat{H}_k, [\hat{H}_q, \hat{H}_0]]) - e^{ik\omega t_0}[\hat{H}_k, [\hat{H}_q, \hat{H}_{-q}]]}{2kq\omega^2} \\ &+ \sum_{k\neq 0} \frac{\frac{1}{2}[[\hat{H}_k, \hat{H}_0], \hat{H}_{-k}] + e^{ik\omega t_0}[[\hat{H}_0, \hat{H}_k], \hat{H}_0]}{\omega^2 k^2} + \mathcal{O}(\omega^{-3}). \end{aligned} \tag{3.1.32}$$

Similar results can be derived for the micromotion operator $\exp(i\hat{\mathcal{K}}(t)) = \exp(-i\hat{\Phi}(t))\exp(i\hat{\Phi}(t_0))$ in Eq.(3.1.16) with the help of (3.1.24a).

High-frequency expansions provide a very powerful instrument for the analysis of Floquet systems. Indeed, with the knowledge of the Fourier modes of a given Hamiltonian (that can be ultimately computed with fast Fourier numerical routines) the lowest terms of the Floquet Hamiltonian are read in Eq.(3.1.31). The main limitations of these perturbative expansions rely on the convergence of the Magnus expansions in Eq.(3.1.26) which is not

guaranteed. In particular, it was proven [Cas01] that in many-body quantum systems (where the energy spectrum ranges up to macroscopically large values), high-frequency expansions reveal to be not accurate and the re-summation is typically not convergent. Nevertheless, high-frequency expansions are widely used, e.g. [Rah03b, Gol14, Eck15, Gol15, Iti15, Mik16], and give good qualitative results in engineered Floquet systems where the target state of the time evolution is well approximated with the lowest terms of the Magnus expansion [Eck17].

3.1.2 Exact algebraic approach

Consider the Hamiltonian of a single spin $\frac{1}{2}$ coupled to a time-dependent magnetic field $\Omega(t)$ that oscillates in the plane xy with a certain frequency ω:

$$\hat{H}(t) = -\vec{\Omega}(t)\cdot\vec{\sigma}, \quad \vec{\Omega} \equiv (\Omega_1\cos(\omega t), \Omega_1\sin(\omega t), \Omega_0)\,; \quad \vec{\sigma} \equiv (\hat{\sigma}^x, \hat{\sigma}^y, \hat{\sigma}^z)\,, \tag{3.1.33}$$

which is one of the simplest exactly solvable Floquet systems.
Indeed, from first courses in quantum mechanics, we know that the transformation $\hat{W}(t) = \exp(i\omega t\,\hat{\sigma}^z)$ generates a time-independent effective Hamiltonian

$$\hat{H}_{\text{eff}} = \frac{(\Omega_0-\omega)}{2}\,\hat{\sigma}^z + \frac{\Omega_1}{2}\,\hat{\sigma}^x \tag{3.1.34}$$

in terms of which the dynamics is readly solved. The latter follows by noticing that the two dimensional Hilbert space of a single spin $\frac{1}{2}$ can be expressed in terms of the operatorial basis of quaternions, namely the three Pauli operators $(\hat{\sigma}^x, \hat{\sigma}^y, \hat{\sigma}^z)$ plus the normalised identity $\hat{\mathbb{1}}/2$ satisfying a $\mathfrak{su}(2)$ algebra, for which it is known that

$$\exp\left(i\vec{\sigma}\cdot\vec{a}\right) = \cos(|\vec{a}|)\,\hat{\mathbb{1}} + \frac{\vec{a}\cdot\vec{\sigma}}{|\vec{a}|}\sin(|\vec{a}|) \tag{3.1.35}$$

with $\vec{a}$ a generic vector of three-components. Then, making the ansatz for the Floquet map:

$$\hat{W}(t) = \exp\left(i f_z(t)\,\hat{\sigma}^z + i f_x(t)\,\hat{\sigma}^x + i f_y(t)\,\hat{\sigma}^y\right) \tag{3.1.36}$$

and substituting it into Eq.(3.1.4), one is able to fix the value of the functions $(f_z(t), f_x(t), f_y(t))$ by imposing the time-independence of $\hat{H}_{\text{eff}}$.
This perhaps trivial example teaches us the main features of a possible exact algebraic approach to generic Floquet systems. In fact, we learn that

- An operatorial basis $\{\hat{F}_k\}$ for the generator of the time evolution $\hat{H}(t)$ satisfying a closed algebra allows us to write a generic time-dependent transformation $\hat{W}(t)$ acting on the system as the exponential of a linear combination of the basis elements, i.e.,

$$\hat{W}(t) = \exp(i \sum_k f_k(t)\, \hat{F}_k). \tag{3.1.37}$$

  The reason behind this is due to the closure of the Lie algebra of $\{\hat{F}_k\}$ that constrains $\hat{W}(t)$ to live in the associated Lie group. Equivalently, $\hat{W}(t)$ can be expressed as[§]

$$\hat{W}(t) = \prod_k \exp\left(i\, g_k(t)\, \hat{F}_k\right) \tag{3.1.38}$$

  with a different set of functions $g_k(t)$.

- Having a closed algebra allows, at least formally, to re-sum the BCH expansions of nested commutators (3.1.24) and to derive effective Hamiltonians without the use of high-frequency expansions.

With this in mind, we can now consider a generic time-periodic Hamiltonian $\hat{H}(t) = \hat{H}(t+\mathcal{T})$ describing the time evolution of a quantum system living in a finite Hilbert space of dimension n. For such a system, it is always possible to design an operatorial basis $\{\hat{F}_k\}$, $k = 0, \ldots, n^2-1$ having a closed algebraic structure (for instance, the generators of $\mathfrak{su}(n)$ together with the identity provide a basis of this kind). By construction, the Hamiltonian has a decomposition

$$\hat{H}(t) = \sum_{j=0}^{n^2-1} h_j(t)\, \hat{F}_j \tag{3.1.39}$$

with time-periodic parameters $h_j(t) \equiv \mathrm{tr}(\hat{H}(t)\, \hat{F}_j)$, and writing the map $\hat{W}(t)$ as in Eq.(3.1.38) for some unknown time-periodic functions $g_k(t)$, we arrive to the effective Hamiltonian

$$\begin{aligned}\hat{H}_{\text{eff}} = &\sum_{j=0}^{n^2-1} \left(\prod_{k=0}^{n^2-1} e^{i\, g_k(t) \hat{F}_k}\right) h_j(t)\, \hat{F}_j \left(\prod_{k=n^2-1}^{0} e^{-i\, g_k(t) \hat{F}_k}\right) \\ &- \sum_{j=0}^{n^2-1} \left(\prod_{k=0}^{j-1} e^{i\, g_k(t)}\right) \frac{\mathrm{d}}{\mathrm{d}t} g_j(t)\, \hat{F}_j \left(\prod_{k=n^2-1}^{j+1} e^{-i\, g_k(t)}\right).\end{aligned} \tag{3.1.40}$$

[§]The two parametrizations of $\hat{W}$ are related via BCH formulae (3.1.24).

It is easy to see from Eq.(3.1.24b) that the effective Hamiltonian (3.1.40) can be represented with the closed expression

$$\hat{H}_{\text{eff}} = \sum_{j=0}^{n^2-1} h_j^{\text{eff}}\, \hat{F}_j \tag{3.1.41}$$

with a set of time-independent effective parameters h_j^{eff} defined consistently from

$$\begin{aligned}\sum_{j=0}^{n^2-1} h_j^{\text{eff}}\, \hat{F}_j = \sum_{j=0}^{n^2-1} \left(\prod_{k=0}^{n^2-1} e^{i\, g_k(t) \hat{F}_k}\right)\, h_j(t)\, \hat{F}_j\, \left(\prod_{k=n^2-1}^{0} e^{-i\, g_k(t) \hat{F}_k}\right) \\ - \sum_{j=0}^{n^2-1} \left(\prod_{k=0}^{j-1} e^{i\, g_k(t)}\right)\, \frac{\mathrm{d}}{\mathrm{d}t} g_j(t)\, \hat{F}_j\, \left(\prod_{k=n^2-1}^{j+1} e^{-i\, g_k(t)}\right)\end{aligned} \tag{3.1.42}$$

as a certain combination involving $h_j(t)$, $g_k(t)$ and $\dot{g}_k(t)$.
Moreover, if we fix the values of the effective parameters h_j^{eff}, Eq.(3.1.42) translates into a set of coupled first-order differential equations for $g_k(t)$ whose solution allows to specify the map $\hat{W}(t)$.

This point is remarkable: instead of deriving the effective Hamiltonian from a given map $\hat{W}(t)$, we can impose the desired effective description (specifying the parameters h_j^{eff}) and then get the transformation $\hat{W}(t)$ that connects $\hat{H}_{\text{eff}}$ to the Floquet system as solution of the equations (3.1.42).
The derivation of the Floquet Hamiltonian follows from Eq.(3.1.15):

$$\begin{aligned}\hat{H}_F(t_0) &= \sum_{j=0}^{n^2-1} \left(\prod_{k=n^2-1}^{0} e^{-i\, g_k(t_0)}\right)\, h_j^{\text{eff}}\, \hat{F}_j\, \left(\prod_{k=0}^{n^2-1} e^{i\, g_k(t_0)}\right) \\ &= \sum_{j=0}^{n^2-1} h_j^F(t_0)\, \hat{F}_j,\end{aligned} \tag{3.1.43}$$

which also admits a closed expression in terms of the basis of $\{\hat{F}_k\}$. In the following, we shall refer to the set of parameters $h_j^F(t_0)$ as *Floquet parameters*.
Similarly, one can write down a closed expression for the micromotion operator $\exp(i\hat{\mathcal{K}}(t)) = \hat{W}^\dagger(t)\, \hat{W}(t_0)$ with the help of (3.1.24a).

Notice that this procedure easily extends to generic time-dependent systems. In fact, writing the time-dependent Hamiltonian $\hat{H}(t)$ as in Eq.(3.1.39) and considering the parametrization of the time evolution operator:

$$\hat{U}(t, t_0) = \prod_k \exp\left(i\, \lambda_k(t, t_0)\, \hat{F}_k\right) \tag{3.1.44}$$

for some unknown functions $\lambda_k(t)$, one easily derives from the Schrödinger equation $(i\partial_t \hat{U}(t,t_0))\,\hat{U}^\dagger(t,t_0) = \hat{H}(t)$:

$$\left(\frac{\mathrm{d}}{\mathrm{d}t}\prod_{k=0}^{n^2-1}\exp\left(i\,\lambda_k(t,t_0)\,\hat{F}_k\right)\right)\prod_{k=n^2-1}^{0}\exp\left(-i\,\lambda_k(t,t_0)\,\hat{F}_k\right) = \sum_{j=0}^{n^2-1} h_j(t)\;\hat{F}_j \tag{3.1.45}$$

which translates into a set of coupled first-order differential equations for $\lambda_k(t)$.

Clearly, the main limitation of this method consists in the derivation and the solution of the system of differential equations, especially in Floquet systems where one requires the time-periodicity of the solution. Nevertheless, with a proper numerical implementation, one can solve for the dynamics of a large variety of time-dependent quantum systems with numerically exact precision and without the use of uncontrolled approximations.

3.2 About Floquet's Theorem

The main idea and the standard terminology behind Floquet theory comes from an old well-known mathematical theorem [Flo83], derived in the late XIX century by Gaston Floquet[§]. In his work, Floquet investigated the space of solutions of first-order differential equations with time-periodic coefficients (see Eq.(3.2.1) below) and he proved the existence of quasi-periodic solutions called Floquet modes. The connection with the dynamics generated by the Schrödinger equation (3.1.1) is then obvious. For completeness and for later purposes, we shall briefly review the content of the Floquet theorem and its main consequences.

Let us consider the following first-order differential equation

$$\frac{\mathrm{d}}{\mathrm{d}t}\vec{x}(t) = \mathbb{A}(t)\;\vec{x}(t) \tag{3.2.1}$$

where $\vec{x}$ is a n-vector and $\mathbb{A}(t) = \mathbb{A}(t+\mathcal{T})$ is a $n\times n$ time-periodic matrix with period $\mathcal{T}$. The time periodicity of the problem implies that for each known solution, let us say, $\vec{x}(t)$, the vector $\vec{x}(t+\mathcal{T})$ is also a solution.
Now, let $\mathbb{X}(t)$ be the $n\times n$ fundamental solution matrix of the Eq.(3.2.1). By definition, each of its columns contains an independent solution of Eq.(3.2.1)

$$\mathbb{X}(t) = \left[\;\vec{x}_1(t)\;\middle|\;\ldots\;\middle|\;\vec{x}_n(t)\;\right] \tag{3.2.2}$$

[§]A. M. Gaston Floquet was a french mathematician and professor in Nancy.

that we can choose, without loss of generality, with initial conditions $[\vec{x}_i(t_0)]_j = \delta_{ij}$. Indeed, a different choice of the solutions in $\mathbb{X}(t)$ will lead to a different fundamental solution matrix $\mathbb{Q}(t)$ related to the first one by a non-singular $n \times n$ matrix $\mathbb{M}$

$$\mathbb{Q}(t) = \mathbb{X}(t)\,\mathbb{M}\,, \tag{3.2.3}$$

because of the linear independence of the solutions. It follows that

$$\mathbb{X}(t+\mathcal{T}) = \mathbb{X}(t)\,\mathbb{M} \tag{3.2.4}$$

and setting $t = t_0$ we have $\mathbb{X}(t_0) = \hat{\mathbb{1}}$ that leads to

$$\mathbb{M} = \mathbb{X}(t_0+\mathcal{T})\,. \tag{3.2.5}$$

We shall refer to $\mathbb{M}$ as the *monodromy matrix* of the Floquet problem. Now, let $\mathbb{Y}(t)$ be another (unknown) fundamental solution:

$$\mathbb{Y}(t) = \mathbb{X}(t)\;\mathbb{K} \tag{3.2.6}$$

with $\mathbb{K}$ a non singular $n \times n$ matrix. If we evaluate $\mathbb{Y}(t)$ after one period

$$\mathbb{Y}(t+\mathcal{T}) = \mathbb{Y}(t)\;\;\mathbb{K}^{-1}\mathbb{M}\,\mathbb{K}, \tag{3.2.7}$$

we notice that different fundamental solutions lead to conjugated monodromy matrices preserving the trace. For sake of simplicity, we assume that $\mathbb{M}$ has n eigenvectors even though this hypothesis can be relaxed, see e.g. [Ces71]. Then, by choosing the matrix $\mathbb{K}$ properly we can have

$$\mathbb{K}^{-1}\;\mathbb{M}\;\mathbb{K} = \mathrm{diag}\,(\lambda_1, \ldots, \lambda_n) \tag{3.2.8}$$

which implies from Eq.(3.2.7) that $\mathbb{Y}(t)$ has also a diagonal structure. In other words, the solutions $\vec{y}(t)$ satisfy the relation

$$y_i(t) = \delta_{ij}\mathbb{Y}_{ij}(t), \qquad y_i(t+\mathcal{T}) = \lambda_i\; y_i(t)\,. \tag{3.2.9}$$

With the ansatz,

$$y_i(t) = \lambda_i^{kt}\; p_i(t) \tag{3.2.10}$$

we can easily see that the conditions in Eq.(3.2.9) are satisfied if and only if $k = 1/\mathcal{T}$ and $p_i(t) = p_i(t+\mathcal{T})$. Notice also that the eigenvalues of the monodromy matrix dictate the stability of the Floquet solution:

- if there exists at least one $|\lambda_i| > 1$ then $y_i(t \to \infty) \to \infty$ and the solution is *unstable*;

- if all $|\lambda_i| \leq 1$ then $y_i(t \to \infty)$ remains bounded and the solution is *stable*.

From these results, we finally arrive to:

Floquet's Theorem. *Any solution of the first-order differential equation in (3.2.1) can be written in the form*

$$\vec{x}(t) = \mathrm{diag}\left(\lambda_1^{t/\mathcal{T}}, \ldots, \lambda_n^{t/\mathcal{T}}\right) \vec{p}(t) \tag{3.2.11}$$

where $\vec{p}(t) = \vec{p}(t+\mathcal{T})$ is a time-periodic function, and its stability is dictated by the eigenvalues λ_i of the associated monodromy matrix.

3.2.1 Stability intervals of the Hill equation

For later purposes, we mention the application of Floquet theory to the study of the *Hill equation* [Mag66]:

$$\left(\partial_t^2 + \omega^2(t)\right) y(t) = 0\,, \tag{3.2.12}$$

with $\omega(t) = \omega(t+\mathcal{T})$ a time-periodic function. Despite its simplicity, the Hill equation is able to describe in rather simple terms a broad class of interesting phenomena which range from engineering to physics, including astronomy, electric circuits, the theory of metals conductance and even cyclothron physics and quantum optics. It is named after George W. Hill, who made remarkable progresses in the theory of such equation during his studies about the lunar perigee [Hil86]. However, the appearance of the Hill equation probably dates further back in the past. The interest for Hill equation for stability problems was instead established by Aleksandr M. Ljapunov [Lja07].

The stability of the solutions of the Hill equation can be probed by using Floquet theory. Defining $x_1(t) \equiv y(t)$, $x_2(t) \equiv \partial_t\, y(t)$, we cast the Hill equation in the Floquet form:

$$\partial_t \begin{bmatrix} x_1 \\ x_2 \end{bmatrix} = \begin{bmatrix} 0 & 1 \\ -\omega(t) & 0 \end{bmatrix} \begin{bmatrix} x_1 \\ x_2 \end{bmatrix} \tag{3.2.13}$$

and we consider the fundamental matrix solution

$$\mathbb{X}(t) = \begin{bmatrix} y_1(t) & y_2(t) \\ \\ \partial_t\, y_1(t) & \partial_t\, y_2(t) \end{bmatrix} \tag{3.2.14}$$

where the two independent solutions satisfy $y_1(t_0) = 1$, $\partial_t y_1(t_0) = 0$ and $y_2(t_0) = 0$, $\partial_t y_2(t_0) = 1$ i.e., $\mathbb{X}(t_0) = \hat{\mathbb{1}}$ as before. The stability of the solutions can be investigated by solving the eigenproblem associated with the monodromy matrix $\mathbb{M} \equiv \mathbb{X}(t_0 + \mathcal{T})$ that leads to the secular equation

$$\lambda^2 - \mathrm{tr}(\mathbb{M})\lambda + \det(\mathbb{M}) = 0. \tag{3.2.15}$$

It is easy to show that $\det(\mathbb{M})$ is equal to one. Indeed, from the wronskian

$$\mathbb{W}(t) \equiv y_1(t)\, \partial_t y_2(t) - y_2(t)\, \partial_t y_1(t) \tag{3.2.16}$$

we can see that $\partial_t \mathbb{W}(t) = 0$ and so $\mathbb{W}(t) = \mathbb{W}(t_0) = 1$. From this we conclude that $\mathbb{W}(t_0 + \mathcal{T}) = \det(\mathbb{M}) = 1$. At this point, we are able to find the roots of Eq.(3.2.15):

$$\lambda_{1,2} = \frac{1}{2}\left(\mathrm{tr}(\mathbb{M}) \pm \sqrt{\mathrm{tr}(\mathbb{M})^2 - 4}\right), \tag{3.2.17}$$

that satisfy $\lambda_1 \lambda_2 = 1$. Depending on the value of the trace of the monodromy matrix we have the following scenarios:

- if $|\mathrm{tr}(\mathbb{M})| < 2$ there are two complex conjugate roots lying on the unit circle i.e., $\lambda_{1,2} = e^{\pm i\varphi}$. The solutions are bounded and the system is *stable*.

- if $|\mathrm{tr}(\mathbb{M})| > 2$ then $\lambda_{1,2}$ are real roots. Since their product is equal to one, they must be of the form $|\lambda_1| > 1$ and $|\lambda_2| < 1$ or viceversa. The system is *unstable* and the solutions have an exponential growth.

- if $|\mathrm{tr}(\mathbb{M})| = 2$ we have two possibilities : (i) $\lambda_1 = 1 = \lambda_2$ and the solution is fully periodic $y(t) = y(t + \mathcal{T})$; (ii) $\lambda_1 = -1 = \lambda_2$ and the solution $y(t) = y(t + 2\mathcal{T})$ has periodicity $2\mathcal{T}$, as follows from Floquet's theorem.

We conclude that the space of Hill operators can be classified into conjugacy classes of the monodromy matrix associated with stable or unstable evolution and eventually a boundary case where one has fully periodic solutions of period $\mathcal{T}$ or $2\mathcal{T}$.

3.2.2 Kirillov's criterion

From a second perspective, the classification of the Hill operators can be perfomed considering the orbit method of Alexandre A. Kirillov [Kir82]. The latter does not only reproduces the results obtained by standard Floquet

theory (i.e., the classification of the Hill operators into conjugacy classes of monodromy), but it also allows a further classification where the Hill operators within each of the monodromy classes are grouped into different orbits. The proof of the Kirillov's results is somewhat complicated and it goes beyond the scope of this introduction. Therefore, we limit ourselves to a short summary of the results that will be necessary for later discussions. Technical aspects and further information are then found in the Ref. [Kir82, Unt10].

Let us consider the so-called stabilizer group [Unt10]:

$$\mathrm{stab}(\omega) \equiv \left\{ \varphi(t) \in \mathrm{diff}_+ \left(\mathbb{R}/2\pi\mathbb{Z}\right) \,:\, \varphi^* \left(\partial_t^2 + \omega^2\right) = \partial_t^2 + \omega^2 \right\} \tag{3.2.18}$$

consisting of all the time reparametrizations $t \mapsto \varphi(t)$ whose action leaves the Hill operator invariant. Notice that here we have set for simplicity the period $\mathcal{T} = 2\pi$ which is a convenient but not restrictive choice.

A function $s(t) \in C^\infty(\mathbb{R}/2\pi\mathbb{Z})$ belongs to the Lie algebra associated with the stabilizer group if and only if it satisfies the following equation:

$$\frac{1}{2}\dddot{s} + 2\omega^2 \dot{s} + 2\omega\,\dot{\omega}\, s = 0 \quad \Leftrightarrow \quad s(t) \in \mathrm{Lie}(\mathrm{stab}(\omega)) \tag{3.2.19}$$

and the quantity $I(s) = \ddot{s}\, s - \frac{1}{2}(\dot{s})^2 + 2\omega^2 s^2$ is a constant of motion. Generically, $\mathrm{Lie}(\mathrm{stab}(\omega))$ is one dimensional, so the function $s(t)$ is fixed up to a multiplicative constant, and the sign of $I(s)$ is therefore unambiguous. As follows from Kirillov's work, the stability of the Hill problem is given by the sign of this constant (assuming s to be a real function): $I(s) > 0$ is a stable regime, $I(s) < 0$ is an unstable regime while $I(s) = 0$ corresponds to the boundary situation where one has pure periodic solutions.
As shown in Ref. [Khe09, Unt10], these two perspectives are actually equivalent even though the Kirillov's method provides a further classification of the Hill operators in the same conjugacy class. More precisely, it was proven [Kir82] that within each conjugacy class, the Hill operators can be grouped into different orbits that are connected by a (orientation preserving) time reparametrization $t \mapsto t' \equiv \varphi(t) \in \mathrm{diff}_+ \left(\mathbb{R}/2\pi\mathbb{Z}\right)$. The results (excluding the boundary regime $I(s) = 0$) can be summarized as follows [Unt10]:

Case 1. The function $s(t) \in \mathrm{Lie}(\mathrm{stab}(\omega)$ is conjugated by a time reparametrization $t \mapsto \varphi(t)$, to a (non-zero) constant $a\,\partial_t$ ($a \neq 0$) which stabilizes the operator $\partial^2 + \alpha$, for a certain $\alpha > 0$. The invariant $I(s) = 2\alpha a^2$ is positive and $\frac{1}{2\pi}\int_0^{2\pi} \frac{\mathrm{d}t}{s(t)} = 1/a$. From these defining relations one easily obtains the parameter of the orbit, α, from the knowledge of $s(t)$.

Case 2. The function $s(t)$ is conjugated to $a\sin(n\,t)(1+\alpha\,\sin(nt))\partial_t$, $n=1,2,\ldots,$ $0\leq\alpha\leq 1$, which stabilizes the operator $\partial^2+v_{n,\alpha}$, where

$$v_{n,\alpha}=\frac{n^2}{4}\left(\frac{1+6\alpha\sin(nt)+4\alpha^2\sin^2(nt)}{(1+\alpha\sin(nt))^2}\right). \tag{3.2.20}$$

The invariant takes the values $I(s)=-2a^2n^2<0$ and the integral of $1/s$ over a period reads[§]: p.v. $\int_{\gamma_{[0,2\pi]}}\frac{\mathrm{d}t}{s(t)}=\frac{2\pi\alpha}{a\sqrt{1-\alpha^2}}$. Knowing $s(t)$ (hence $I(s)$), it is easy to determine the parameters n, α of the orbit of ω. Namely, the number of zeros of the function s on a period is equal to $2n$ while the defining relations for $I(s)$ and the integral of $1/s$ over a period yield to a and then α.

[§]Here the notation p.v. stands for Cauchy principal value; $\gamma_{[0,2\pi]}$ denotes a complex deformation of the interval $[0,2\pi]$ which avoids singularities.

Part II

Analysis of driven systems

Chapter 4

Non-equilibrium dynamics in trapped Bose gases

Abstract

In this chapter, we investigate the non-equilibrium dynamics of a low-density 1d Tonks-Girardeau gas subject to time-dependent harmonic potentials. This study was initially motivated by noticing that the typical setup of cold atoms experiments is characterized by the presence of a trap (with quasi-harmonic spatial profile) and thus by asking about the consequences on the system's evolution arising from the time variation of such a potential.
With the aim of shedding light on this scenario, we first consider a slow trap-release experiment that corresponds to an inhomogeneous time-dependent driving across the XX critical line, see Sec.4.1. Here, the interplay between time and space dependences of the driving protocol does not allow for a standard Kibble-Zurek description of the non-equilibrium behavior. Therefore, we consider a perturbative approach where inhomogeneities are accounted with trap-size scaling arguments while the time-dependence is considered with a quasi-adiabatic perturbation theory, see Sec.4.2 and 4.3. With this procedure, we are able to write corrections to the standard local-density approximation results for the density profile and to provide a suitable approximation of the non-equilibrium dynamics for slow time variations of the trap.
Next, in Sec.4.5 we derive an exact solution based on the identification of Ermakov-Lewis dynamical invariants in terms of which the time-evolved density reveals to be just a dynamical rescaling of the initial profile. The application of this result for the special case of an Efimov expansion is also commented.

The second part of the chapter focus on the case of a time-periodic driving, see Sec.4.7. With the help of Floquet Theory together with the Ermakov-Lewis invariants, we show that the time evolution of the Tonks-Girardeau gas undergoes two main scenarios depending on the kind of external forcing, namely a stable regime and an unstable one. The former is related to elliptic values of the monodromy matrix and corresponds to the physical scenario in which the periodic forcing leads to the emergence of breathing modes in the cloud. The latter is instead related to hyperbolic monodromies where the forcing increases the internal energy of the cloud and causes its rapid spread favouring the equilibrium zero-density Mott-insulator configuration. Both scenarios are suitable for a scaling description as we explicitly pointed out.

4.1 Tonks Girardeau limit

The dynamics of trapped cold atoms on optical lattices can be described by means of the BH model (1.3.1) by adding a term of the form $\sum_j V(j,t)\,\hat{n}_j$, where V is a time-dependent trap potential. More precisely, we consider the following Hamiltonian:

$$\begin{aligned}\hat{H}(t) &= \hat{H}_{\text{BH}} + \sum_{j=1}^{L} V(j,t)\,\hat{n}_j \\ &= -w \sum_{j=-L/2}^{L/2-1} (\hat{a}_j^\dagger \hat{a}_{j+1} + \text{h.c.}) + \frac{U}{2} \sum_{j=-L/2}^{L/2} \hat{n}_j(\hat{n}_j - 1) + \sum_{j=-L/2}^{L/2} (V(j,t) - \mu)\hat{n}_j\end{aligned} \tag{4.1.1}$$

where we recall $\hat{a}_j^\dagger$ ($\hat{a}_j$) is the standard creation (annihilation) operator satisfying the usual canonical bosonic algebra $[\hat{a}_i, \hat{a}_j^\dagger] = \delta_{ij}$, $[\hat{a}_i, \hat{a}_j] = [\hat{a}_i^\dagger, \hat{a}_j^\dagger] = 0$ and where $\hat{n}_j = \hat{a}_j^\dagger \hat{a}_j$ stands for the occupation number at site j. Notice that the presence of the potential V is equivalent to a time-dependent inhomogeneous chemical potential. It is therefore convenient to set

$$\mu_{\text{eff}}(j,t) \equiv \mu - V(j,t). \tag{4.1.2}$$

We shall investigate the trapped BH model in the limit of strong repulsive interactions, where formally $U/w \to \infty$. In this limit, the bosons behave as if they possess a hard core preventing a double occupancy of a given site and the

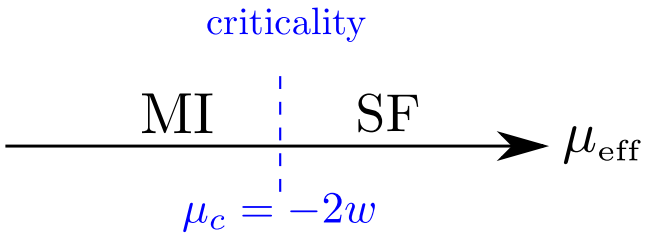

Figure 4.1: **XX criticality for trapped TG gas.** We investigate the Bose-Hubbard model in the limit of strong repulsive interactions where formally $U/w \to \infty$. In this limit, the BH model reduces to a XX spin-chain and it shows a QPT driven by the chemical potential at $\mu_c = -2w$ that separates a SF regime ($|\mu| < 2w$) from a zero-density MI state ($\mu < -2w$). In the case of a trapped system, μ is simply replaced by $\mu_{\rm eff}$, see Eq.(4.1.2).

Hamiltonian (4.1.1) reduces to

$$\hat{H}_{\rm TG}(t) = -w \sum_{j=-L/2}^{L/2-1} (\hat{b}_{j+1}^\dagger \hat{b}_j + \text{h.c.}) - \sum_{j=-L/2}^{L/2} \mu_{\rm eff}(j,t)\, \hat{n}_j \tag{4.1.3}$$

with a new set of operators $\hat{b}_j^\dagger$, $\hat{b}_j$ satisfying the bosonic algebra for different sites but that fulfills on-site anticommutation rules (the occupation operator is $\hat{n}_j = \hat{b}_j^\dagger \hat{b}_j$), see Sec.1.2.2. We shall refer to the Hamiltonian in Eq.(4.1.3) as *Tonks Girardeau* (TG) gas [Pet00, Gir60, Gir65] or as the *hard-core* limit of a Bose-Hubbard model.
Tonks-Girardeau gases are experimentally realized already for moderately large values of the ratio U/w, see [Kin04], providing a good effective description of the atomic cloud in the regime of low-densities[§].
Notice that the TG limit is very different from the deep lattice limit (see Sec.1.3), where we have considered $w \simeq 0$ resulting in a MI ground state. In fact, as we have seen in Sec.1.2.2, the Hamiltonian (4.1.3) reduces under a Jordan-Wigner transformation to a spinless tight-binding Fermi system:

$$\hat{H}_{\rm TG}(t) = \sum_{i,j=-L/2}^{L/2} \hat{c}_i^\dagger\, A_{ij}(t)\, \hat{c}_j \tag{4.1.4}$$

where we introduced the matrix $A(t)$ with components

$$A_{ij}(t) \equiv -\mu_{\rm eff}(j,t)\, \delta_{ij} - w\, (\delta_{i,j+1} + \delta_{i+1,j})\,, \tag{4.1.5}$$

[§]Clearly, at higher densities the bosonic nature of the gas will manifest and the lattice sites will inevitably be occupied by more particles.

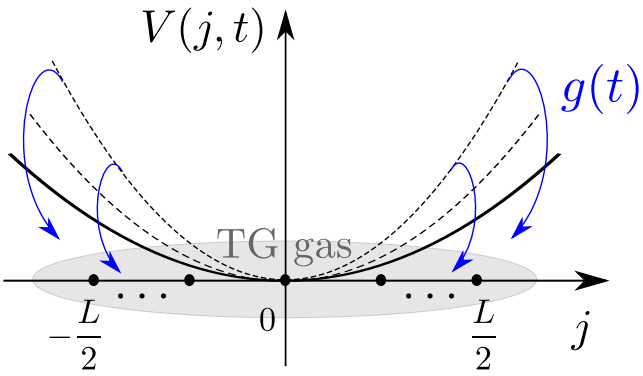

Figure 4.2: **A trap release experiment.** A TG gas is first prepared at equilibrium and then transferred into a harmonic trapping potential. At $t = t_0$, the local portion around the site $j = 0$ is in the critical domain (compare with TSS arguments of Sec.2.1). At later times $t > t_0$, the trap is gradually opened causing the driving of local domains (with different driving rates) towards the critical regime; when $t \to 0$ (and so $g(t) \to 0$), the whole becomes critical. Notice that the interplay between time-dependence and inhomogeneity leads to a demanding analysis which cannot be investigated with simple KZ arguments.

and where $\hat{c}_j^\dagger$, $\hat{c}_j$ are the lattice fermions of Sec.1.2.2. It is easy to see that the Hamiltonian in Eq.(4.1.4) is equivalent to that of a XX model (see Eq.(1.2.34)) where the transverse magnetic field is now replaced by the effect of the inhomogeneous chemical potential. It follows that the TG model shows a QPT for $\mu_{\text{eff}}(j,t) = \pm 2w$ separating a MI regime ($|\mu_{\text{eff}}(j,t)| > 2w$) from the SF phase ($|\mu_{\text{eff}}(j,t)| < 2w$), see Fig.4.1. Since we are interested in a low-density regime, we set $\mu = -2w$ (which corresponds to a zero-density MI absolute ground state in the absence of the trap) from hereafter and thus $\mu_{\text{eff}} = -2w - V(j,t)$.

In what follows, we will consider a harmonic spatial profile of the trapping potential

$$V(j,t) = g(t)\,|j|^2 \tag{4.1.6}$$

where $g(t) \geq 0$ is a generic function of time.
Notice that a *trap release* protocol (where $g(t) \to 0$ as $t \to 0$) corresponds to an inhomogeneous driving across the critical point $\mu_c = -2w$ (recall $\mu_{\text{eff}}(j,t) \equiv -2w - V(j,t) \to \mu_c$), see Fig.4.2. Clearly, since μ_{eff} has a non-trivial time and space dependence, local portions of the system are driven with different rates towards the critical point. Moreover, the interplay between the time and the space dependence does not allow for a standard KZ description

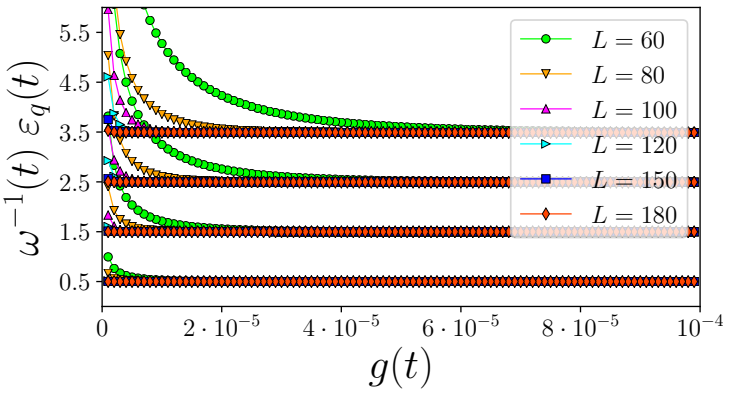

Figure 4.3: **Instantaneous spectrum of quasi-energies.** The plot shows the rescaled lowest ($q = 0, 1, 2, 3$) single-particle quasi-energies $\omega^{-1}(t)\,\varepsilon_q(t)$ with $\omega(t) \equiv \sqrt{2|g(t)|}$ and $w = 1/2$. The latter are numerically obtained from the exact diagonalization of the matrix $A(t)$ as a function of $g(t)$ and for different system sizes.

of the non-equilibrium behavior.

4.2 Adiabatic evolution

4.2.1 Instantaneous diagonalization

At a given time t the quadratic form in Eq.(4.1.4) is readily diagonalized through a unitary transformation and it casts into a free fermionic theory:

$$\hat{H}(t) = \sum_{q=0}^{L} \varepsilon_q(t)\,\hat{\eta}_q^\dagger(t)\,\hat{\eta}_q(t) \tag{4.2.1}$$

where $\varepsilon_q(t)$ are the quasi-energies of the fermionic excitations created (destroyed) by the operators $\hat{\eta}_q^\dagger$ ($\hat{\eta}_q$) which are defined through

$$\hat{\eta}_q^\dagger(t) \equiv -\sum_{j=-L/2}^{L/2} \psi_q(j,t)\,\hat{c}_j^\dagger\,, \qquad \hat{\eta}_q(t) = (\hat{\eta}_q^\dagger(t))^\dagger. \tag{4.2.2}$$

Here, $\psi_q(j,t)$ are the Bogoliubov coefficients associated with the unitary transformation, satisfying the orthonormality condition $\sum_j \psi_q^*(j,t)\,\psi_k(j,t) = \delta_{qk}$

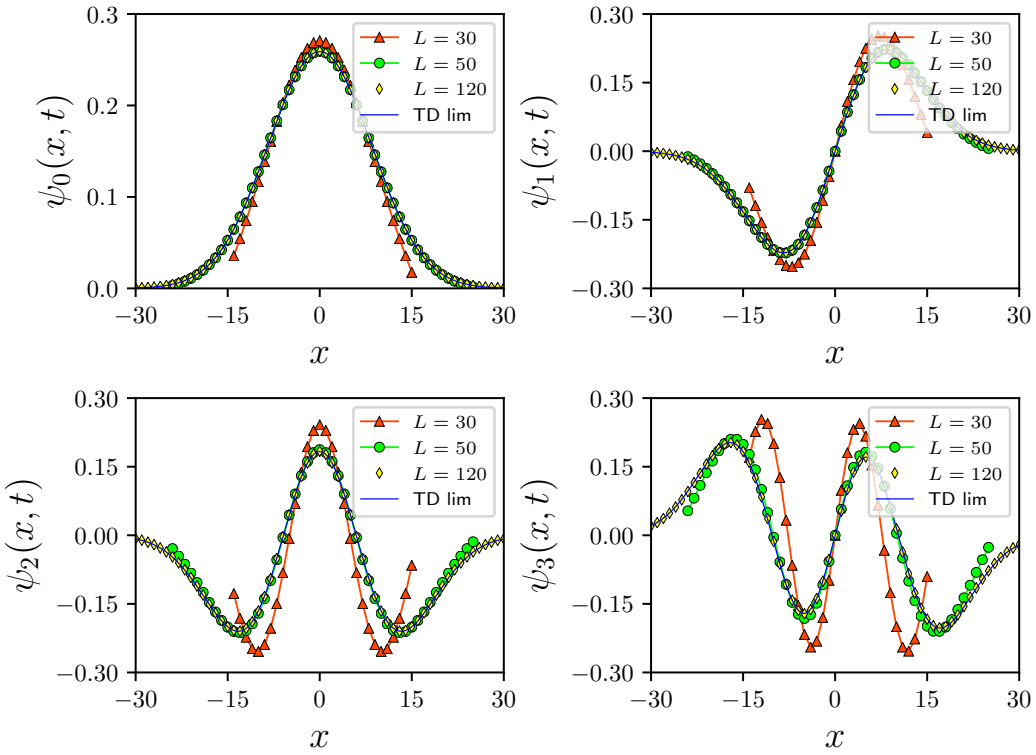

Figure 4.4: **Instantaneous eigenstates.** The $q = 0, 1, 2, 3$ eigenvectors obtained from the exact numerical diagonalization of the matrix $A(t)$ at $g(t) = 10^{-4}$ for different system sizes are compared with the TD expectation in Eq.(4.2.7).

which in turn implies the canonical anticommutation algebra $\{\hat{\eta}_q^\dagger, \hat{\eta}_k\} = \delta_{qk}$, $\{\hat{\eta}_q^\dagger, \hat{\eta}_k^\dagger\} = 0 = \{\hat{\eta}_q, \hat{\eta}_k\}$; the minus sign in Eq.(4.2.2) is irrelevant and set for further conveniences.
Such instantaneous transformation is derived through the diagonalization of the matrix $A(t)$ in Eq.(4.1.4) (considering t just as a parameter):

$$A(t)\,\psi_q(t) = \varepsilon_q(t)\,\psi_q(t) \tag{4.2.3}$$

where $\psi_q(t)$ is a vector having components $\psi_q(j,t)$. The presence of inhomogeneities does not allow to follow the analytical computation of Sec.1.2.2, but a numerical exact diagonalization can be easily perfomed for this problem (see Fig.4.3). However, in the thermodynamic (TD) limit $L \to \infty$ in which the lattice site j is replaced by a continuous variable $x = aj$ (a is the lattice

spacing), we can expand

$$\psi_q(x_0 \pm a, t) \simeq \psi_q(x_0, t) \pm a\partial_x \psi_q(x_0, t) + \frac{a^2}{2}\partial_x^2 \psi_q(x_0, t) \tag{4.2.4}$$

and reduce the eigenproblem in Eq.(4.2.3) to

$$w\, \partial_x^2 \psi_q(x, t) + \Big(\varepsilon_q(t) - V(x, t)\Big)\psi_q(x, t) = 0 \tag{4.2.5}$$

where $V(x, t) = g(t)x^2$ is the continuum version of the lattice potential in Eq.(4.1.6). Without loss of generality, the choice $w = 1/2$ leads to the stationary Schrödinger equation for the 1d Harmonic Oscillator (HO) :

$$\frac{1}{2}\left(-\partial_x^2 + \omega^2(t)\, x^2\right)\psi_q(x, t) = \varepsilon_q(t)\, \psi_q(x, t), \qquad \omega(t) \equiv \sqrt{2g(t)} \tag{4.2.6}$$

with energies ε_q and corresponding eigenfunctions ψ_q. Explicitly the solution is

$$\psi_q(x, t) = \sqrt{\frac{\sqrt{\omega(t)}}{2^q\, q!\sqrt{\pi}}}\, e^{-\frac{1}{2}\omega(t)\, x^2}\, \mathrm{He}_q(x\sqrt{\omega(t)}), \qquad \varepsilon_q(t) = \omega(t)\left(q + \frac{1}{2}\right) \tag{4.2.7}$$

where $q \in \mathbb{N}$ and He_q denotes the q^{th} Hermite polynomial [Abr64] with physical normalization implied from the normalization of the single-particle wave functions $\psi_q(x, t)$. In Fig.4.3 we show the exact low-lying single-particle rescaled energies as a function of the trap amplitude $|g(t)|$ and we compare them to the continuum limit expectations given above. As the system size increases, the agreement gets better and better. The associated lowest eigenvectors are shown in Fig.4.4.

The trap frequency $\omega(t)$ defines an instantaneous length scale in the problem $\ell_{\mathrm{KZ}}(t) \equiv 1/\sqrt{\omega(t)}$ in terms of which the solution reads

$$\psi_q(x, t) = \ell_{\mathrm{KZ}}^{-1/2}\, \chi_q(\frac{x}{\ell_{\mathrm{KZ}}}), \qquad \chi_q(u) = \frac{1}{\sqrt{2^q\, q!\, \sqrt{\pi}}}\, e^{-\frac{1}{2}u^2}\, \mathrm{He}_q(u) \tag{4.2.8}$$

for the eigenstates, and

$$\varepsilon_q(t) = \ell_{\mathrm{KZ}}^{-2}\, (q + \frac{1}{2}) \tag{4.2.9}$$

for the energy spectrum, where ℓ_{KZ} is a shorthand notation of $\ell_{\mathrm{KZ}}(t)$. These scaling forms are in agreement with general time-dependent trap-size scaling

(TSS) arguments, see Sec.2.4. Indeed, we can notice that the lenght scale $\ell_{\rm KZ}(t)$ satisfies the relation in Eq.(2.1.14)

$$\ell_{\rm KZ}(t) \propto |g(t)|^{-\nu_g}, \qquad \nu_g = \frac{\nu}{1+\nu \mathrm{w}} = \frac{1}{4} \tag{4.2.10}$$

with w= 2 and provided the critical exponent $\nu = 1/2$ at the XX criticality (see Sec.(1.2.2), Eq.(1.2.54)).
As shown in Sec.2.4, for $L \gg \ell_{\rm KZ}(t)$ finite-size corrections can be neglected and the TSS matches its infinite volume behavior. Therefore, we will consider the TD limit as $L \to \infty$, $g(t) \to 0$ at fixed $L/\ell^2_{\rm KZ}$ (or equivalently $L^2\, g(t)$) where we do expect that the analytical TD results agree with exact diagonalization numerical data.

4.2.2 Adiabatic evolution of the density profile

At the initial time t_0 the system is prepared in the N-particle ground state of the TG gas in Eq.(4.1.3) which is

$$|\Psi_0(t_0)\rangle = \prod_{q=0}^{N-1} \hat{\eta}^\dagger_q(t_0)\ |0\rangle \tag{4.2.11}$$

where $|0\rangle$ is the vacuum state such that $\hat{\eta}_q(t_0)\ |0\rangle = 0\ \forall q$, since all the quasi-energies are positive. The energy associated to the initial state $\Psi_0(t_0)$ is thus simply given by

$$E_0(t_0) = \sum_{q=0}^{N-1} \varepsilon_q(t_0). \tag{4.2.12}$$

For very slow time-variations of the confining potential, we may employ at first an adiabatic approximation so that the state of the system remains at later times $t > t_0$ in the instantaneous ground state $|\Psi_0(t)\rangle = \prod_{q=0}^{N-1} \hat{\eta}^\dagger_q(t)\ |0\rangle$. The evolution of the particle density is thus expected to be given by the adiabatic density profile:

$$\begin{aligned}
\rho^{\rm ad}(j,t) &= \langle \Psi_0(t)|\hat{c}^\dagger_j\, \hat{c}_j|\Psi_0(t)\rangle \\
&= \prod_{k,k'=0}^{N-1} \sum_{q,q'=0}^{L} \psi^*_q(j,t)\, \psi_{q'}(j,t)\ \langle 0|\hat{\eta}_k(t)\, \hat{\eta}^\dagger_q(t)\, \hat{\eta}_{q'}(t)\, \hat{\eta}^\dagger_{k'}(t)|0\rangle \\
&= \sum_{k=0}^{N-1} |\psi_k(j,t)|^2,
\end{aligned} \tag{4.2.13}$$

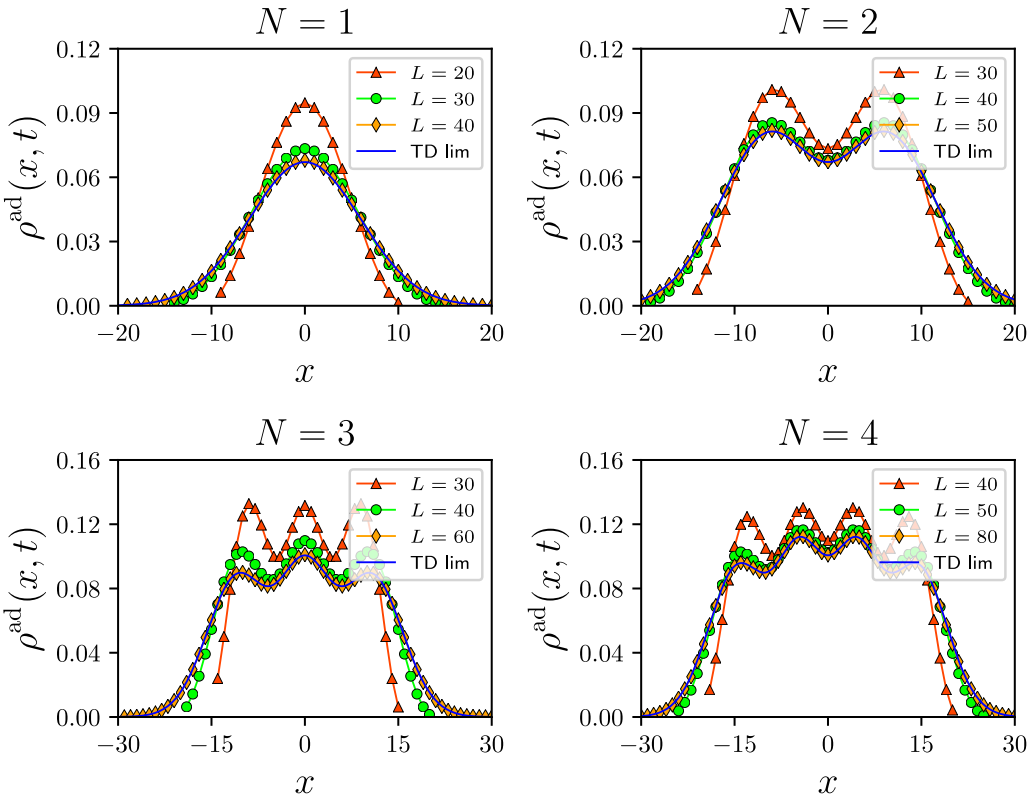

Figure 4.5: **Adiabatic evolution of the density profile.** The density profile for an adiabatic evolution is shown for a different number of particles $N = 1, 2, 3, 4$ at a time $g(t) = 10^{-4}$. Numerical results are compared with the TD analytical expectation for different lattice sizes. In the large-size limit, exact numerical results perfectly match the analytical results. On the other hand, finite-size corrections are visible for smaller sizes and lead to quite a discrepancy between the TD limit expectation and the actual finite-size density profile.

or in the TD limit by the scaling form

$$\rho^{\mathrm{ad}}(x,t) = \ell_{\mathrm{KZ}}^{-1} f^{\mathrm{ad}}\left(\frac{x}{\ell_{\mathrm{KZ}}}\right), \qquad f^{\mathrm{ad}}(u) = \sum_{q=0}^{N-1} |\chi_q(u)|^2, \tag{4.2.14}$$

where the functions χ_q are defined in Eq.(4.2.8). In Fig.4.5, we show the convergence of the adiabatic density profile obtained from exact numerical diagonalization toward the TD limit expression for a small number of particles N. Notice that the agreement with the TD results is also dictated by the value

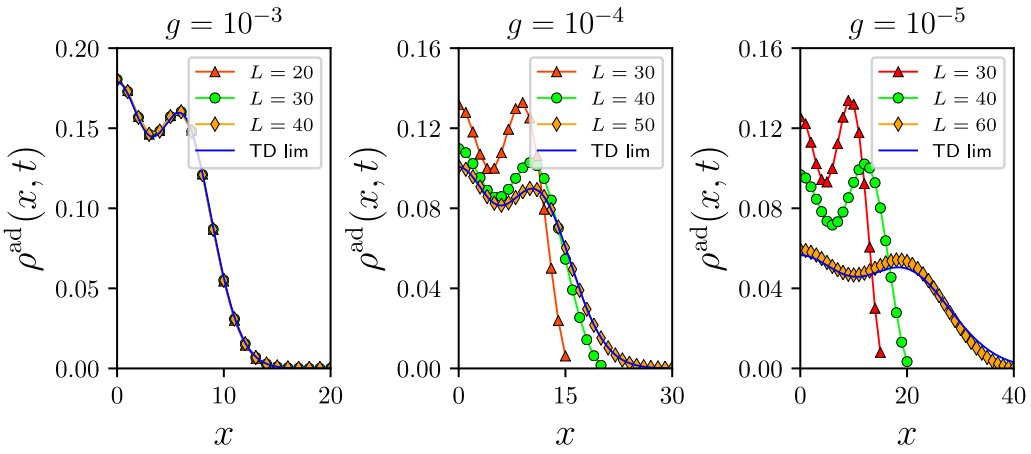

Figure 4.6: **Adiabatic evolution for different $g(t)$.** The density profile obtained from an adiabatic approximation is shown for different values of the trap amplitude: $g(t) = 10^{-3}, 10^{-4}, 10^{-5}$. Numerical results for $N = 3$ and for different lattice sizes are compared with the TD analytical results. As expected, the bigger the amplitude is, the smaller the system size is needed to achieve the TD limit.

of $g(t)$[§], as we can see in Fig.4.6.

For a large number of bosons the adiabatic density profile matches its *local density approximation* (LDA) limit. The LDA is obtained assuming that, for each instant of time t and around each (coarse-grained) point x, there is a local flat band of excitations with dispersion

$$\varepsilon(x) = -(\cos q_F(x) + \mu_{\mathrm{eff}}(x,t)) \tag{4.2.15}$$

where $q_F(x)$ is the local Fermi surface. Locally, the single-particle band is filled up to the global Fermi level, given here by $\varepsilon_F = \varepsilon_{N-1}(t)$, and the LDA density profile is deduced from the associated Fermi momentum $q_F(x) = \pi\rho^{\mathrm{LDA}}(x)$

[§]Recall that the TD limit is taken as $L \to \infty$, $g(t) \to 0$ at fixed $L^2 g(t)$ where we do expect small finite-size corrections.

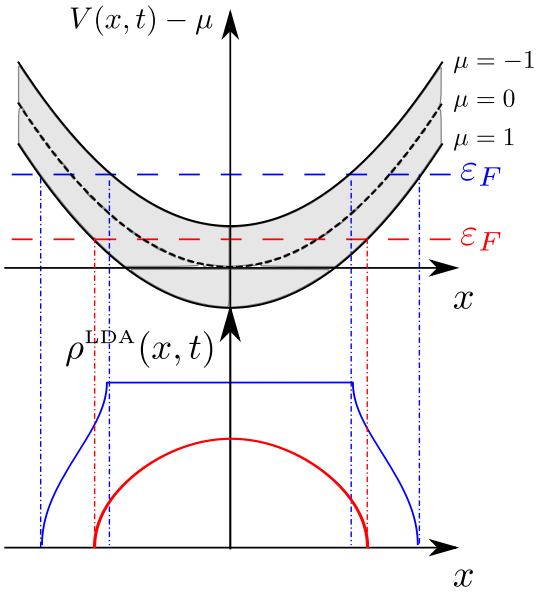

Figure 4.7: **LDA density profile.** Illustration of the LDA density for a trapped TG gas. At a given time t, all the quasi-particles with energies $\varepsilon(x,t) = -(\cos q_F(x) + \mu_{\rm eff}(x,t)) < \varepsilon_F(t)$ below the Fermi level are added to the ground state. Thus, at fixed number of particles N (where $\varepsilon_F = \varepsilon_{N-1}$) and on varying the chemical potential, the LDA density is given by Eq.(4.2.16). Notice that the system is locally in the SF regime for points x such that $V(x,t) - 1 < \varepsilon_{N-1} < V(x,t) + 1$ (*grey strip*). Conversely, when $\varepsilon_{N-1} < V(x,t) - 1$ ($> V(x,t) + 1$), we observe a local $n = 0$ ($n = 1$) MI state.

leading to [Wen13, Cam10a, Col12b]

$$\rho^{\rm LDA}(x,t) = \begin{cases} 0, & V(x,t) - \varepsilon_{N-1}(t) > 1; \\ \frac{1}{\pi}\mathrm{acos}(V(x,t) - \mu - \varepsilon_{N-1}(t)), & |V(x,t) - \varepsilon_{N-1}(t)| < 1; \\ 1, & V(x,t) - \varepsilon_{N-1}(t) < -1; \end{cases} \tag{4.2.16}$$

as shown in Fig.4.7. Hence, setting $\mu = -1$ and considering $N \gg 1$ such that $N/\ell_{\rm KZ}^2 \ll 1$[§], we have

$$V(x,t) - \varepsilon_{N-1}(t) = \frac{1}{\ell_{\rm KZ}^2(t)}\left(1 + \frac{1}{2}\left(\frac{x}{\ell_{\rm KZ}}\right)^2 - 2N\right) > -1, \tag{4.2.17}$$

[§]This assumption is compatible with a low-density regime.

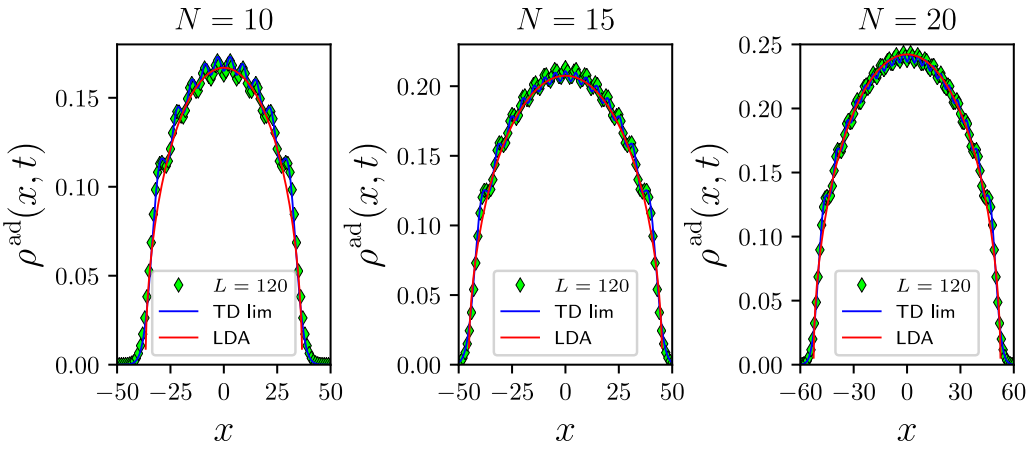

Figure 4.8: **LDA adiabatic evolution.** The adiabatic density profile at $g(t) = 10^{-4}$ for a large number N of bosons. The panels show the numerical results compared with the TD expectation and with the LDA approximation value.

which leads to

$$\rho^{\rm LDA}(x,t) = \frac{1}{\pi}\mathrm{acos}\Big(1 + V(x,t) - \varepsilon_{N-1}(t)\Big). \tag{4.2.18}$$

This is shown in Fig.4.8 for three different values of N. The exact numerical profile, as obtained from numerical exact diagonalization, is compared to the TD limit in Eq.(4.2.14) and to the LDA results. Notice that one can recover the scaling form (4.2.14) from Eq.(4.2.18) in the limit $N \ll \ell_{\rm KZ}^2$. Indeed, from the definition $\ell_{\rm KZ} = 1/\sqrt{\omega(t)} = (2|g(t)|)^{-1/4}$ and with the expression of the potential $V(x,t) = |g(t)|\,x^2$ one has

$$\rho^{\rm LDA}(x,t) = \frac{1}{\pi}\mathrm{acos}\left(1 - \frac{1}{2\ell_{\rm KZ}^2}\left[2N - 1 - \left(\frac{x}{\ell_{\rm KZ}}\right)^2\right]\right). \tag{4.2.19}$$

For $N/\ell_{\rm KZ}^2 \ll 1$, expanding the acos function to the leading order in $\sqrt{N}$, one obtains a *semi-circle law*

$$\rho^{\rm LDA}(x,t) \simeq \frac{1}{\pi\,\ell_{\rm KZ}}\left(2N - 1 - \left(\frac{x}{\ell_{\rm KZ}}\right)^2\right)^{1/2} \overset{N\gg 1}{\simeq} \frac{\sqrt{2N}}{\pi\,\ell_{\rm KZ}}\left(1 - \frac{1}{2}\left(\frac{x}{\ell_{\rm KZ}\sqrt{N}}\right)^2\right)^{1/2} \tag{4.2.20}$$

in agreement with the scaling form in Eq.(4.2.14). The space region over which the adiabatic density profile spreads is in $[-\ell_N, \ell_N]$ with

$$\ell_N(t) \equiv \ell_{\rm KZ}(t)\,\sqrt{2N-1} \overset{N\gg 1}{\simeq} \ell_{\rm KZ}(t)\,\sqrt{2N}. \tag{4.2.21}$$

In terms of such a length scale ℓ_N, the adiabatic density profile takes the scaling form

$$\rho^{\rm LDA}(x,t) \simeq \frac{N}{\ell_N} f^{\rm LDA}\left(\frac{x}{\ell_N}\right), \qquad f^{\rm LDA}(u) = \frac{2}{\pi}\sqrt{1-u^2}. \tag{4.2.22}$$

Some remarks.

From general KZ arguments (see Sec.2.1), we expect that the adiabatic approximation ultimately fails when we drive the system close to criticality. Notice that the breakdown of adiabaticity at the critical point is strictly connected with the validity of a local density approximation for this setup.
We can conclude therefore that the adiabatic results provide a reliable approximation of the time evolution only for slowly-varying protocols $g(t)$ that are sufficiently far from criticality[§].

In the following section, we shall consider the leading perturbative corrections over the adiabatic background that will lead to non-equilibrium corrections of the LDA result.

4.3 Quasi-adiabatic perturbation theory

A first analysis of the non-equilibrium effects emerging over the adiabatic background of Sec.4.2 can be obtained considering the leading perturbative corrections to the adiabatic evolution of the initial ground state $\Psi_0(t_0)$.
As shown in the appendix 4.A, the quasi-adiabatic (QAD) state $\Psi(t)$ evolved from the initial N-particle ground state (4.2.11) is given by

$$|\Psi(t)\rangle \simeq e^{-i\int_{t_0}^{t} ds\, E_0(s)} \left(|\Psi_0(t)\rangle + \sum_{p=N}^{L} \sum_{k=0}^{N-1} a_{pk}(t)\ |\Psi_0[p,\underline{k}](t)\rangle \right) \tag{4.3.1}$$

where $|\Psi_0[p,\underline{k}](t)\rangle \equiv \hat{\eta}_p^\dagger(t)\hat{\eta}_k(t)\,|\Psi_0(t)\rangle$ is the instantaneous ground state in which a particle has been promoted from the lowest levels $k = 0,\dots,N-1$ ($\underline{k}$ denotes a vacancy in the position k) towards higher ones $p = N,\dots,L$ (recall that the particles have a fermionic nature and so double occupancies are forbidden). The transition amplitude $a_{pk}(t)$ is given by

$$a_{pk}(t) = \int_{t_0}^{t} dt'\, \frac{\partial_{t'} K_{pk}(t')}{\varepsilon_p(t') - \varepsilon_k(t')} \exp\left(-i\int_{t'}^{t} dt''\,[\varepsilon_p(t'') - \varepsilon_k(t'')]\right) \tag{4.3.2}$$

[§]The range of validity of the adiabatic approximation will be defined more precisely in Sec.4.3 where it will correspond to the zeroth order of the quasi-adiabatic expansion, see Eq.(4.3.6).

where

$$K_{pk}(t) \equiv -\sum_{j=-L/2}^{L/2} \psi_p^*(j,t)\, \mu_{\text{eff}}(j,t)\, \psi_k(j,t) \tag{4.3.3}$$

is the instantaneous transition amplitude of the perturbation

$$\delta\hat{H}(t) \equiv -\sum_{j=-L/2}^{L/2} \mu_{\text{eff}}(j,t)\, \hat{n}_j = \sum_{p,k=0}^{L} K_{pk}(t)\, \hat{\eta}_p^\dagger\, \hat{\eta}_k(t). \tag{4.3.4}$$

In the TSS limit $g \to 0$, $L \to \infty$, the amplitude $a_{pk}(t)$ can be analytically computed using the TD limit expressions (4.2.8) and (4.2.9). After a straightforward computation one obtains:

$$a_{pk}(t) = C_{pk}\, \delta_{p-2,k}\, \log\left(\frac{\ell_{\text{KZ}}(t)}{\ell_{\text{KZ}}(t_0)}\right), \qquad C_{pk} = \frac{\sqrt{p(k+1)}}{k-p}. \tag{4.3.5}$$

Starting from the initial N-particle ground state $\Psi_0(t_0)$, at leading order in QAD perturbation theory only the lowest energy levels are activated: $(p,k) = (N+1, N-1)$ and for $N > 1$, $(p,k) = (N, N-2)$. A crude approximation $p \simeq k \simeq N \gg 1$ shows then that the transition amplitude is of order $N \log(\ell_{\text{KZ}}(t)/\ell_{\text{KZ}}(t_0))$. Consequently, the one-jump expansion approximation of Eq.(4.3.1) is compatible with a QAD perturbation theory at the first order in

$$\epsilon \equiv \mathcal{O}\left(N \log\left(\frac{\ell_{\text{KZ}}(t)}{\ell_{\text{KZ}}(t_0)}\right)\right) = \mathcal{O}\left(N\, \nu_g \log\left(\frac{g(t)}{g(t_0)}\right)\right). \tag{4.3.6}$$

Recall that $\ell_{\text{KZ}}(t > t_0) > \ell_{\text{KZ}}(t_0)$ and so the parameter ϵ increases with time. The range of validity of the adiabatic approximation is associated with the zeroth order of the QAD expansion and corresponds to modest trap-size variations $\ell_{\text{KZ}}(t)/\ell_{\text{KZ}}(t_0) \simeq 1$ for which $\epsilon \simeq 0$.

4.3.1 Quasi-adiabatic density profile

The particle density at a given site j and time t is given by

$$\rho(j,t) = \sum_{q,q'=0}^{L} \psi_q^*(j,t)\, \langle\Psi(t)|\hat{\eta}_q^\dagger(t)\, \hat{\eta}_{q'}(t)|\Psi(t)\rangle\, \psi_{q'}(j,t). \tag{4.3.7}$$

With the QAD expansion in Eq.(4.3.1) at the leading order in ϵ, the two-point function is

$$\langle\Psi(t)|\hat{\eta}_q^\dagger(t)\,\hat{\eta}_{q'}(t)|\Psi(t)\rangle = \sum_{k=0}^{N-1}\delta_{qk}\,\delta_{q'k} + \sum_{p=N}^{L}\sum_{k=0}^{N-1}\Big(a^*_{pk}(t)\,\delta_{q'k}\,\delta_{qp} + a_{pk}(t)\,\delta_{q'p}\,\delta_{qk}\Big) + \mathcal{O}(\epsilon^2). \tag{4.3.8}$$

Here, the first term gives the adiabatic contribution (4.2.13) whereas the leading deviations from adiabaticity are

$$\delta\rho(j,t) \equiv \rho(j,t) - \rho^{\rm ad}(j,t) = \left(\sum_{q=N}^{L}\sum_{q'=0}^{N-1} a^*_{qq'}(t)\,\psi^*(j,t)\,\psi_{q'}(j,t) + \text{c.c.}\right) + \mathcal{O}(\epsilon^2). \tag{4.3.9}$$

In the TSS limit $g \to 0$, $L \to \infty$, using the expressions in Eq.(4.2.8) and (4.2.9), we obtain

$$\delta\rho(x,t) = \frac{2}{\ell_{\rm KZ}(t)}\log\left(\frac{\ell_{\rm KZ}(t)}{\ell_{\rm KZ}(t_0)}\right)\Big[C_{N,N-2}\,\chi_N\left(\frac{x}{\ell_{\rm KZ}(t)}\right)\chi_{N-2}\left(\frac{x}{\ell_{\rm KZ}(t)}\right) + C_{N+1,N-1}\,\chi_{N+1}\left(\frac{x}{\ell_{\rm KZ}(t)}\right)\chi_{N-1}\left(\frac{x}{\ell_{\rm KZ}(t)}\right)\Big] \tag{4.3.10}$$

with $C_{1,-1} = 0$ by convention. Using the recursion relations of the Hermite polynomials, the density deviation $\delta\rho(x,t)$ can be rewritten as

$$\delta\rho(x,t) = \frac{1}{2\ell_{\rm KZ}(t)}\log\left(\frac{\ell_{\rm KZ}(t)}{\ell_{\rm KZ}(t_0)}\right)\left[F_N\left(\frac{x}{\ell_{\rm KZ}(t)}\right) + F_{N-1}\left(\frac{x}{\ell_{\rm KZ}(t)}\right)\right] \tag{4.3.11}$$

where

$$F_q(u) \equiv \big(\chi_q'(u)\big)^2 - u^2\,\chi_q^2(u). \tag{4.3.12}$$

A plot of the QAD density profile for low values of N is shown in Fig.4.9.

At large particle number $N \gg 1$, the Hilbert-Hermite functions $\chi_N(u)$ take significant values only in the region $|u| < \sqrt{2N}$ where the zeros of the Hermite polynomials are located. Outside that region the Hilbert-Hermite functions decay exponentially fast. In the limit $N \gg 1$, it has been shown [Dom07]

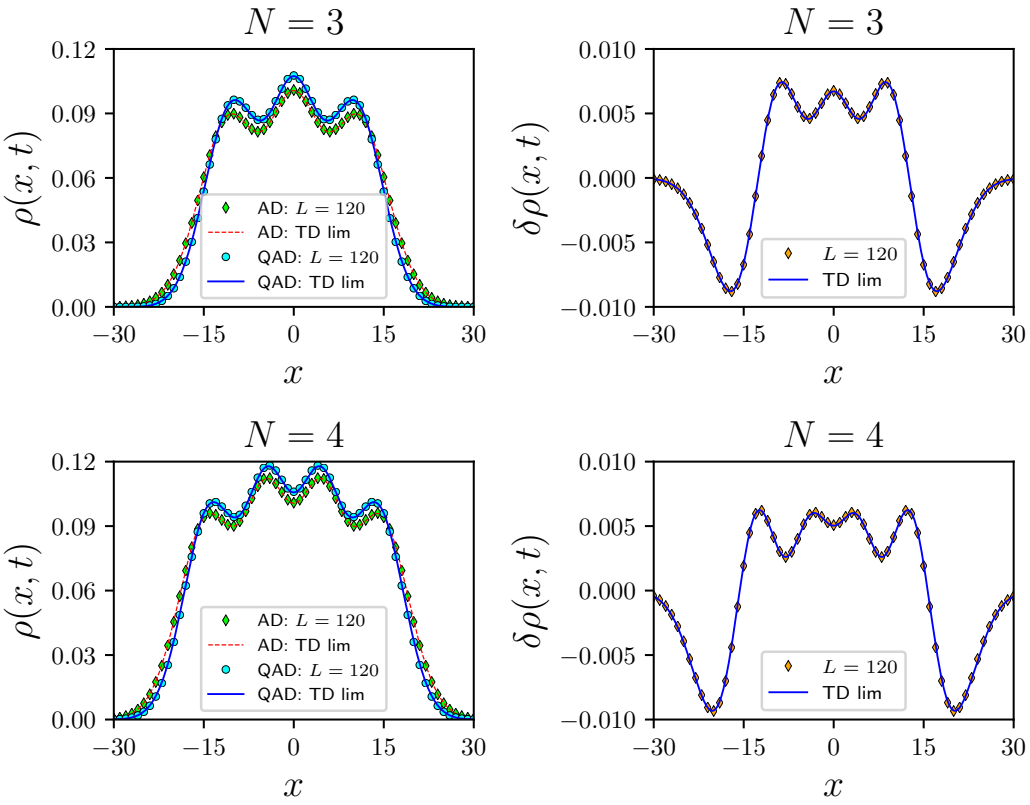

Figure 4.9: **Quasi adiabatic evolution of the density profile.** *Left panel.* The density profile at first-order in QAD perturbation theory is compared with the adiabatic result for $N = 3, 4$. *Right panel.* Leading deviations from the adiabatic density profile $\delta\rho$ for $N = 3, 4$. The plots are made with $g(t_0) = 10^{-4}$ and fixing $\epsilon = 0.2$.

that the Hermite polynomials have the asymptotic representation for $\theta \in (-\pi/2, \pi/2)$:

$$\mathrm{He}_N(\sqrt{2N}\sin\theta) \sim \left(\frac{2N}{e}\right)^{N/2} \sqrt{\frac{2}{\cos\theta}}\, e^{N\sin^2\theta}\, \cos(\varphi_N(\theta)) \tag{4.3.13}$$

with the phase

$$\varphi_N(\theta) = N\left[\frac{1}{2}\sin(2\theta) + \theta - \frac{\pi}{2}\right] + \frac{\theta}{2}. \tag{4.3.14}$$

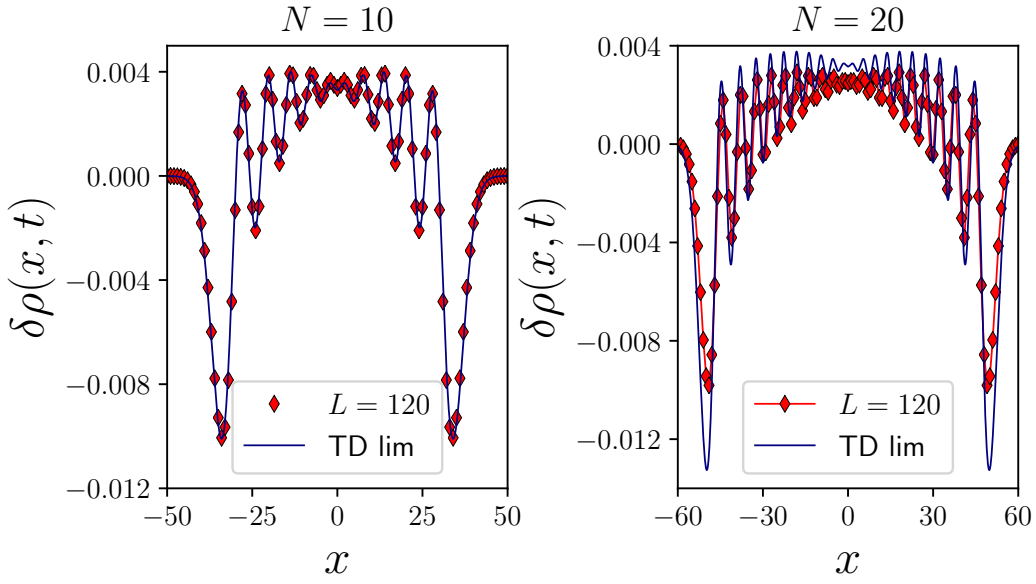

Figure 4.10: **Deviations from adiabaticity at large** N**.** Leading QAD deviations from the density profile for a large number of bosons N. The plot is made considering $\epsilon = 0.2$ and $g(t_0) = 10^{-4}$.

With Stirling formula $N! \simeq \sqrt{2\pi N}\,(\frac{N}{e})^N$ and with the asymptotic representation given above, the Hilbert-Hermite functions take the asymptotic form

$$\chi_N(\sqrt{2N}\sin\theta) \sim \frac{1}{(2N)^{1/4}}\sqrt{\frac{2}{\pi\cos\theta}}\cos(\varphi_N(\theta)). \tag{4.3.15}$$

Using this, one has from Eq.(4.3.12) the asymptotic expression for large N

$$F_N(u) \sim -\frac{2}{\pi}(2N)^{1/2}\frac{1}{\sqrt{1-\frac{u^2}{2N}}}\left[\frac{u^2}{2N} - \sin^2(\varphi_N(u))\right]. \tag{4.3.16}$$

Here, the $\sin^2(\varphi_N)$ gives a widely oscillating term and taking its average, $\sin^2(\varphi_N) \sim 1/2$, one finally obtains a scaling form for the deviation $\delta\rho(x,t)$ as a function of the scaling variable x/ℓ_N:

$$\delta\rho(x,t) \sim \frac{\epsilon}{\ell_N} f^{\delta\rho}\left(\frac{x}{\ell_N}\right), \qquad f^{\delta\rho}(u) = \frac{4}{\pi}\frac{1/2-u^2}{\sqrt{1-u^2}}, \tag{4.3.17}$$

where we have set the parameter ϵ associated with the QAD expansion to

$$\epsilon = N\log\left(\frac{\ell_N(t)}{\ell_N(t_0)}\right). \tag{4.3.18}$$

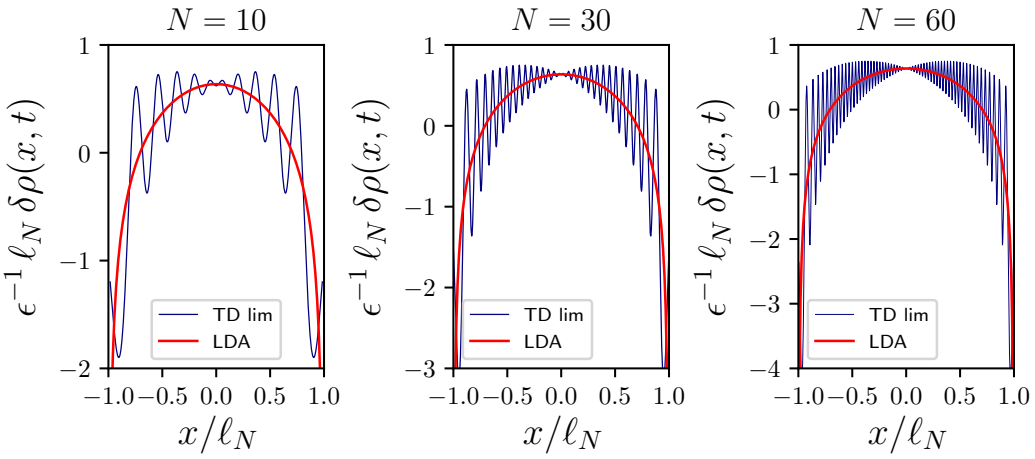

Figure 4.11: **Quasi adiabatic evolution at large N.** The asymptotic behavior of the leading QAD corrections to the density profile (4.3.17) for a different number N of bosons is compared with the result in Eq.(4.3.11).

This behavior is shown in Fig.4.10 and Fig.4.11 for the associated scaling function at large N. Notice that using the asymptotic expansion in Eq.(4.3.15) one has after averaging the $\cos^2$ term

$$\chi^2_{q\gg 1}(u) \sim \frac{1}{\pi}\,\frac{1}{\sqrt{2q-u^2}}\,\Theta(q-\frac{u^2}{2}) \tag{4.3.19}$$

where $\Theta(q)$ is the Heaviside step function. It follows that the adiabatic density is

$$\rho^{\rm ad}(x,t) = \frac{1}{\ell_{\rm KZ}(t)}\sum_{q=0}^{N-1}\chi^2_q(u) \sim \frac{1}{\pi\ell_{\rm KZ}(t)}\int_{u^2/2}^{N}\frac{dq}{2q-u^2} \sim \frac{N}{\ell_N(t)}\,\frac{2}{\pi}\sqrt{1-\frac{u^2}{2N}} \tag{4.3.20}$$

which is nothing but the LDA semi-circle law of Eq.(4.2.22).

4.4 Ermakov-Lewis approach

Let us consider the single-particle Schrödinger equation

$$(i\partial_t - \hat{H}(t))\phi(x,t) = 0; \qquad \hat{H}(t) \equiv -\frac{1}{2}\left(\partial_x^2 - \omega^2(t)\,x^2\right), \tag{4.4.1}$$

governing the time evolution of the initial kth eigenstate $\phi_k(x,t_0)=\psi(x,t_0)$. A convenient way that leads to exact solutions of (4.4.1) for a given protocol $\omega(t)$ is to consider the theory of dynamical invariants. For our purposes, we can summarize the dynamical invariants approach as follows, leaving the details to the appendices 4.C, 4.D.

Dynamical invariants – *For a given time-dependent Hamiltonian $\hat{H}(t)$, let us suppose to know a dynamical invariant $\hat{\mathscr{I}}$ i.e., a hermitian time-dependent operator that satisfies*

$$\frac{\mathrm{d}}{\mathrm{d}t}\hat{\mathscr{I}}(t)=-i[\hat{\mathscr{I}}(t),\hat{H}(t)]+\partial_t\hat{\mathscr{I}}(t)=0 \tag{4.4.2}$$

at any instant of time. Then any solution of the Schrödinger equation $(i\partial_t-\hat{H}(t))\phi=0$ can be written as

$$|\phi(t)\rangle=\sum_{n\in spec(\hat{\mathscr{I}})}\exp(i\alpha_n(t))\ \langle\mathfrak{h}_n(t_0)|\phi(t_0)\rangle\ |\mathfrak{h}_n(t)\rangle \tag{4.4.3}$$

where $\mathfrak{h}_n(t)$ are the instantaneous eigenvectors of the dynamical invariant $(\hat{\mathscr{I}}(t)\,\mathfrak{h}_n(t)=\lambda_n\,\mathfrak{h}_n(t))$ and α_n is the Lewis phase, defined as the solution of the differential equation

$$\frac{\mathrm{d}}{\mathrm{d}t}\alpha_n(t)=\langle\mathfrak{h}_n(t)|i\partial_t-\hat{H}(t)|\mathfrak{h}_n(t)\rangle\,;\qquad \alpha_n(t_0)=0. \tag{4.4.4}$$

At this point, we want to apply the general theory of dynamical invariants for the solution of the single-particle Schrödinger equation (4.4.1).
To do so, we construct an operator $\hat{\mathscr{I}}$ that satisfies (4.4.2) for the time-dependent HO Hamiltonian using the ansatz:

$$\hat{\mathscr{I}}(t)=\frac{1}{2}\left(a(t)x^2-b(t)\partial_x^2-ic(t)[x\,\partial_x+\partial_x\,x]\right) \tag{4.4.5}$$

where a, b and c are unknown functions of time. Then, by imposing the time independence of $\hat{\mathscr{I}}$ as in Eq.(4.4.2), we obtain the following conditions on the parameters:

$$\dot{a}(t)=2\omega^2(t)\,c(t); \tag{4.4.6a}$$

$$\dot{b}(t)=-2c(t); \tag{4.4.6b}$$

$$\dot{c}(t)=-a(t)+\omega^2(t)\,b(t); \tag{4.4.6c}$$

which cast into one differential equation

$$\frac{1}{2}\dddot{b}(t) + 2\omega^2(t)\,\dot{b}(t) + 2\dot{\omega}(t)\,\omega(t)\,b(t) = 0 \tag{4.4.7}$$

by setting $a = \omega^2\, b + \ddot{b}/2$ and $c = -\dot{b}/2$. Moreover, it is easy to show that the quantity

$$I(b) \equiv b\,\ddot{b} - \frac{1}{2}\left(\dot{b}\right)^2 + 2\omega^2\, b^2 = 2\omega_0^2, \tag{4.4.8}$$

with $\omega_0 \equiv \omega(t_0)$, is a constant of motion of the Eq.(4.4.7). Therefore, without loss of generality, we can integrate Eq.(4.4.7) obtaining

$$\ddot{\zeta}(t) + \omega^2(t)\,\zeta(t) = \omega_0^2\zeta^{-3}(t) \tag{4.4.9}$$

in terms of the variable $\zeta^2 \equiv b$, that is called *Ermakov-Pinney* equation [Pin50]. Inserting the constraint about the dynamical invariance in the Eq.(4.4.5) we obtain the so-called *Ermakov-Lewis* (EL) invariants [Unt10, Sco17, Sco18b]:

$$\hat{\mathscr{I}}_{\text{EL}}(\zeta(t)) \equiv \frac{1}{2}\left[\frac{\omega_0^2\, x^2}{\zeta^2} - \left(\zeta\,\partial_x - i\dot{\zeta}\,x\right)^2\right] \tag{4.4.10}$$

with ζ satisfying the Ermakov-Pinney equation (4.4.9) for a given value of $\omega(t)$. Notice that the operator in Eq.(4.4.10) provides a class of invariants since the dynamical invariance constraint in Eq.(4.4.9) is satisfied for a generic choice of the initial conditions on $\zeta(t_0)$ and $\dot{\zeta}(t_0)$. However, a convenient choice is to fix the initial conditions in Eq.(4.4.9) as

$$\zeta(t_0) = 1 \qquad \dot{\zeta}(t_0) = 0 \tag{4.4.11}$$

so that the resulting EL invariant $\hat{\mathscr{I}}_{\text{EL}}(t_0) \equiv \hat{H}(t_0)$ coincides with the system Hamiltonian at the initial time.

EL eigenvectors

Next, we define $\hat{x}_\zeta \equiv x/\zeta$ and $\hat{p}_\zeta \equiv -i\left(\zeta\,\partial_x - i\dot{\zeta}\,x\right)$ satisfying canonical commutation rules $[\hat{x}_\zeta, \hat{p}_\zeta] = i$, so that the operators

$$\hat{a}_\zeta \equiv \sqrt{\frac{\omega_0}{2}}\left(\hat{x}_\zeta + \frac{i}{\omega_0}\hat{p}_\zeta\right) = \sqrt{\frac{\omega_0}{2}}\left[\frac{x}{\zeta} + \frac{1}{\omega_0}\left(\zeta\,\partial_x - i\dot{\zeta}\,x\right)\right]; \tag{4.4.12}$$

$$\hat{a}_\zeta^\dagger \equiv \sqrt{\frac{\omega_0}{2}}\left(\hat{x}_\zeta - \frac{i}{\omega_0}\hat{p}_\zeta\right) = \sqrt{\frac{\omega_0}{2}}\left[\frac{x}{\zeta} - \frac{1}{\omega_0}\left(\zeta\,\partial_x - i\dot{\zeta}\,x\right)\right], \tag{4.4.13}$$

cast the EL invariant in the form of a harmonic oscillator

$$\hat{\mathscr{I}}_{\rm EL}(t) = \omega_0 \left(\hat{a}^\dagger_\zeta(t)\, \hat{a}_\zeta(t) + \frac{1}{2} \right). \tag{4.4.14}$$

This means that for any instant of time t, the operator $\hat{a}^\dagger_\zeta$ ($\hat{a}_\zeta$) plays the role of a creation (annihilation) operator for the HO in Eq.(4.4.14).
The normalized ground state can be computed from the condition $\hat{a}_\zeta\ |\mathfrak{h}_0\rangle = 0$ which gives at a given time t

$$\begin{aligned} |\mathfrak{h}_0(t)\rangle &= \frac{\omega_0^{1/4}}{\sqrt{\sqrt{\pi}\,\zeta(t)}}\ \exp\left(i\frac{\dot{\zeta}(t)}{2\zeta(t)}\, x^2 - \frac{\omega_0\, x^2}{2\zeta^2(t)} \right) \\ &= \frac{\omega_0^{1/4}}{\sqrt{\zeta(t)}}\ \exp\left(i\frac{\dot{\zeta}(t)}{2\zeta(t)}\, x^2 \right)\ \chi_0\left(\frac{\sqrt{\omega_0}\, x}{\zeta(t)} \right) \end{aligned} \tag{4.4.15}$$

where $\chi_q(u)$ are the Hilbert-Hermite functions introduced in Eq.(4.2.8). From the ground state, the tower of eigenstates is built with the usual relation $|\mathfrak{h}_n\rangle = \left(\hat{a}^\dagger_\zeta\right)^n\ |\mathfrak{h}_0\rangle\,/\sqrt{N!}$ and reads

$$|\mathfrak{h}_n(t)\rangle = \frac{\omega_0^{1/4}}{\sqrt{\zeta(t)}}\ \exp\left(i\frac{\dot{\zeta}(t)}{2\zeta(t)}\, x^2 \right)\ \chi_n\left(\frac{\sqrt{\omega_0}\, x}{\zeta(t)} \right). \tag{4.4.16}$$

Lewis phase

Finally, the set of eigenstates $\mathfrak{h}_n$ leads to the Lewis phase (4.4.4) [Unt10]:

$$\alpha_n(t) = -\omega_0 \left(n + \frac{1}{2} \right) \int_{t_0}^{t} \frac{\mathrm{d}t'}{\zeta^2(t')} \tag{4.4.17}$$

that defines the natural time scale of the problem (at a given time t) to be $\int^t \mathrm{d}t' \zeta^{-2}(t')$ instead of $(\ell_{\rm KZ}(t))^z$ obtained from the TSS arguments.

We conclude that the time-evolved single-particle wave function associated with the Schrödinger equation (4.4.1) is:

$$\phi_k(x,t) = \frac{1}{\sqrt{\zeta(t)}} \exp\left[i\frac{\dot{\zeta}(t)}{2\zeta(t)}\, x^2 - i\omega_0(k+\frac{1}{2}) \int_{t_0}^{t} \frac{\mathrm{d}t'}{\zeta^2(t')} \right] \psi_k\left(\frac{x}{\zeta(t)}, t_0 \right) \tag{4.4.18}$$

as follows from Eqs.(4.4.3), (4.4.16), (4.4.17) and provided the initial conditions (4.4.11) for $\hat{\mathscr{I}}_{\rm EL}$.

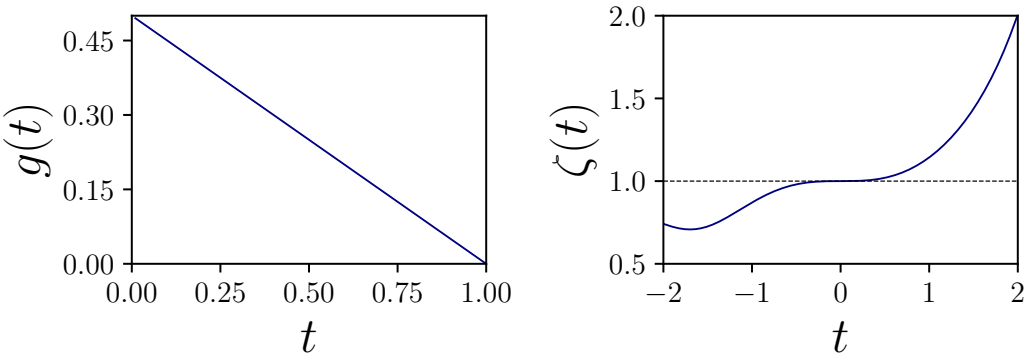

Figure 4.12: **Solution for a linear ramp.** We show (*left*) the linear ramp protocol in Eq.(4.5.3) with $\omega_0 = 1$,$\alpha = 1$ and (*right*) the associated solution ζ of the Ermakov-Pinney Eq.(4.4.9) with initial conditions $\zeta(t_0) = 1$, $\dot{\zeta}(t_0) = 0$.

4.5 Exact dynamics during a trap release

Consider again the single-particle Schrödinger equation:

$$i\partial_t \phi_q(x,t) = \frac{1}{2}\left(-\partial_x^2 + \omega^2(t)\, x^2\right) \phi_q(x,t) \tag{4.5.1}$$

where $\omega(t) = \sqrt{2|g(t)|}$ and suppose that at $t = t_0$, $\phi_q(x,t_0) = \psi_q(x,t_0)$ is an eigenstate of the harmonic oscillator with initial frequency ω_0. According to the dynamical invariant approach [Lew67, Lew68, Lew69, Lew82, Kag96], the time-evolved single-particle wave function $\phi_q(x,t)$ can be expressed as [Min05, Cam10a, Cam10b, Sco17]

$$\phi_q(x,t) = \frac{1}{\sqrt{\zeta(t)}} \exp\left[i\frac{\dot{\zeta}(t)\, x^2}{2\zeta(t)} - i\omega_0(q+\frac{1}{2})\int_{t_0}^{t} \frac{\mathrm{d}t'}{\zeta^2(t')}\right] \psi_q\left(\frac{x}{\zeta(t)}, t_0\right), \tag{4.5.2}$$

where ζ is a real solution of the Eq.(4.4.9) with initial conditions $\zeta(t_0) = 1$, $\dot{\zeta}(t_0) = 0$. The problem is thus reduced to solving this differential equation given the time-dependent protocol $g(t)$. For instance, setting a linear ramp

$$g(t) = g_0(1 - \alpha t), \qquad t \leq 1,\, t_0 = 0 \tag{4.5.3}$$

with time scale $1/\alpha$, a solution for ζ is explicitly known in terms of Airy functions, see [Cam10a], and is plotted in Fig.4.12 as an illustration.

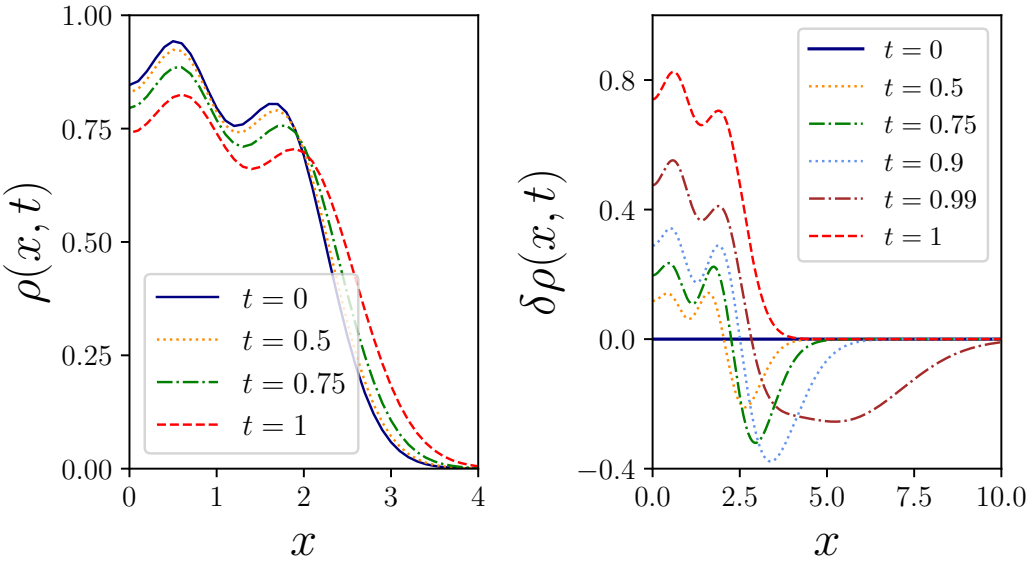

Figure 4.13: **Exact evolution of the density profile.** *Left panel.* The exact non-equilibrium density evolution in Eq.(4.5.4) for a cloud of $N = 4$ particles subject to a linear ramp protocol (4.5.3). *Right panel.* The associated departure from adiabaticity $\delta\rho = \rho - \rho^{\text{ad}}$ of the density profile at various instants of time. Notice that at $t = 1$ the trapping potential has been completely removed but we see a non-flat density profile (that we would expect from a naive adiabatic guess). This is a clear example of KZ freezing across a QPT.

From the knowledge of the single-particle wave functions (4.5.2) we can write down the N-particles density (see appendix 4.B):

$$\rho(x,t) = \frac{1}{\zeta(t)} \sum_{k=0}^{N-1} \left| \psi_k \left(\frac{x}{\zeta(t)}, t_0 \right) \right|^2 = \frac{1}{\zeta(t)\,\ell_{\text{KZ}}(t_0)} \sum_{k=0}^{N-1} \left| \chi_k \left(\frac{x}{\zeta(t)\ell_{\text{KZ}}(t_0)} \right) \right|^2 . \tag{4.5.4}$$

Quite remarkably, we notice that Eq.(4.5.4) is an exact scaling form meaning that the dynamics of the system can be completely absorbed with the definition of a non-trivial length scale $\ell(t) \equiv \ell_{\text{KZ}}(t_0)\,\zeta(t)$. The adiabatic limit is then recovered when $t \to t_0$ for which $\lim_{t\to t_0} \zeta(t) = 1$ and thus $\ell(t_0) = \ell_{\text{KZ}}(t_0)$. The exact time evolution of the density profile for the linear ramp protocol (4.5.3) is shown in Fig.4.13.

Comparison with the quasi-adiabatic case

The knowledge of an exact solution for the dynamics of the trapped TG gas allows us to test whether if first-order QAD perturbative results give already a suitable approximation of the non-equilibrium evolution or not. In fact, QAD expansions provide a general machinery for the study of inhomogeneous time-dependent systems whereas the dynamical invariant approach tends to be model-dependent.

To do so, let us consider the linear ramp in Eq.(4.5.3) in the quasi-adiabatic regime, i.e., when the driving rate $\alpha \to 0$. With the formal expansions of $\zeta(t)$ and of $\omega^2(t)$,

$$\zeta(t) = \zeta_0(t) + \alpha\,\zeta_1(t) + \mathcal{O}(\alpha^2); \qquad \omega^2(t) = \omega_0^2\left(1 - \frac{1}{2}\alpha t + \mathcal{O}(\alpha^2)\right); \quad (4.5.5)$$

we can solve the Eq.(4.4.9) iteratively at each order in perturbation theory. At the zeroth order we have

$$\ddot{\zeta}_0(t) + \omega_0^2\,\zeta_0(t) = \omega_0^2\,\zeta^{-3}(t) \quad (4.5.6)$$

having the trivial solution $\zeta_0 = 1$, which is necessary for the continuity at t_0. Notice that the zeroth order is nothing but the adiabatic approximation. Next, the first-order equation is

$$\ddot{\zeta}_1(t) + 4\omega_0^2\,\zeta_1(t) - \frac{1}{2}\omega_0^2\,t = 0 \quad (4.5.7)$$

with initial conditions $\zeta_1(0) = 0$, $\dot{\zeta}_1(0) = 0$ whose solution is

$$\zeta_1(t) = \frac{1}{8}\left(t - \frac{\sin(2\omega_0 t)}{2\omega_0}\right). \quad (4.5.8)$$

In the TSS limit we considered so far (where $g_0 \sim L^{-2}$ and so $\omega_0 \sim L^{-1} \ll 1$) the function $\zeta(t)$, at leading order in α, shows a cubic growth in time:

$$\zeta(t) \simeq 1 + \frac{\alpha}{12}\omega_0^2\,t^3. \quad (4.5.9)$$

The QAD limit of the exact density profile (4.5.4) can be expressed as a dynamical scaling form characterized by the QAD length scale

$$\ell_{\mathrm{QAD}}(t) \equiv \ell_{\mathrm{KZ}}(0)\left(1 + \frac{\alpha}{12}\omega_0^2\,t^3\right) = \ell_{\mathrm{KZ}}(0)\left(1 + \frac{\alpha}{6}g_0\,t^3\right). \quad (4.5.10)$$

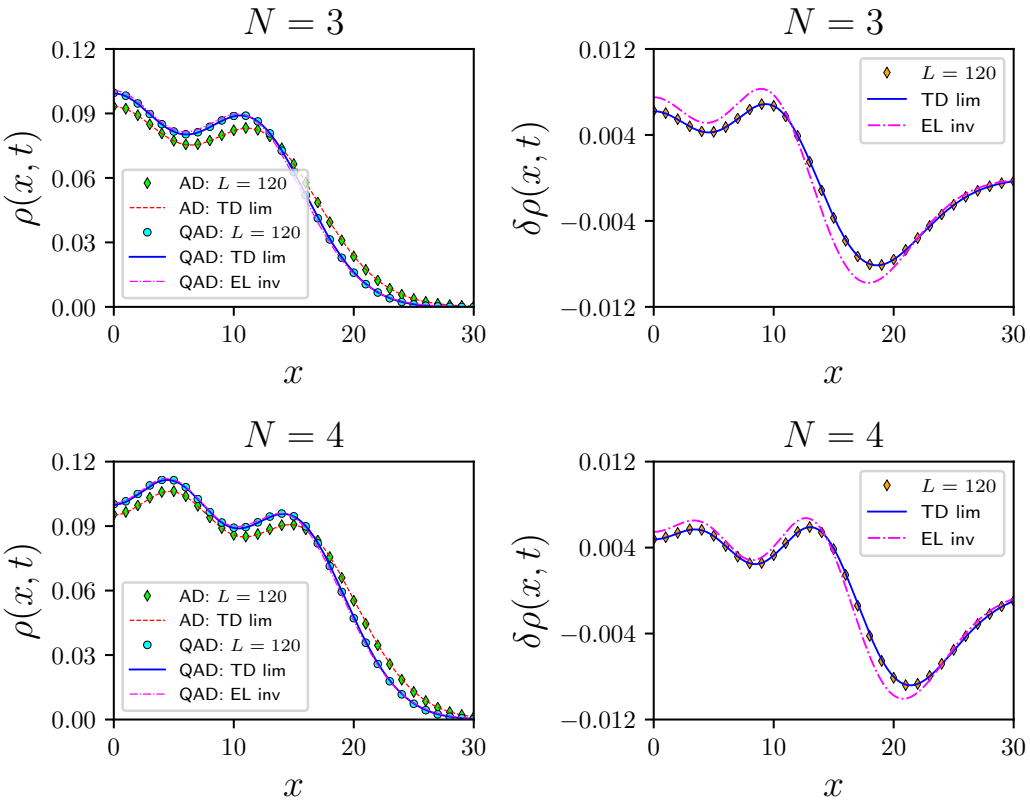

Figure 4.14: **Comparison of the QAD pertubative expansions.** *Left.* The density profile in the QAD limit for $N = 3, 4$. *Right.* Associated deviation from adiabaticity during the trap release. Numerical exact diagonalization, TD analytical results (4.3.10) and the QAD density profile (4.5.4)-(4.5.10) obtained with the use of dynamical invariants are compared. The plots are made fixing $\epsilon = 0.2$ and $t = 4/N$.

Notice that, in the perturbative regime considered here, the QAD length scale is always smaller than the adiabatic one:[§]

$$\ell_{\rm QAD}(t) \ll \ell_{\rm KZ}(t), \qquad \ell_{\rm KZ} = (2g(t))^{-1/4} \simeq \ell_{\rm KZ}(0)\,(1+\alpha t/4) \tag{4.5.11}$$

and thus the expansion (contraction) of the cloud is always slower than what would have been expected from a naive adiabatic guess. This feature is related to the freezing out of the dynamics close to the critical point with the consequent

[§]One can easily see that, at small times ($t \ll 1$), $g_0\, t^3/6 \ll t/4$.

breakdown of the adiabatic behavior. In Fig.4.14, we show a comparison between the QAD density profile obtained with this EL approach and the result developed previously with QAD time-dependent perturbation theory. The comparison is made using $\epsilon = \nu_g\, N\, \alpha t$, which follows from (4.3.6) and (4.5.3).

4.6 Efimov expansion

An interesting situation is found when the harmonic trap frequency decreases as the inverse of time

$$\omega(t) = \frac{\lambda}{t} \tag{4.6.1}$$

from an initial time $t_0 = 1$ set to one in the following such that the initial frequency is $\omega_0 \equiv \omega(t_0) = \lambda$. This time dependence is generated by the ramp

$$g(t) = \frac{\lambda^2}{2\, t^2}. \tag{4.6.2}$$

As argued below, when the initial frequency λ is larger than a threshold value, the release of the TG gas confined within a harmonic trap with this type of $1/t$ dependence leads to the appearance of a sequence of plateaus P_n, i.e., of times where the expansion of the cloud surprisingly stops, despite of the continuous decreasing of the trap frequency. Moreover, the location of these plateaus obeys a geometric scaling relation.

To explain this intriguing dynamics, we consider the Ermakov-Pinney equation with frequency (4.6.1),

$$\frac{1}{\lambda^2}\,\ddot{\zeta}(t) + \frac{1}{t^2}\,\zeta(t) = \zeta^{-3}(t), \tag{4.6.3}$$

and with initial conditions $\zeta(1) = 1$, $\dot{\zeta}(1) = 0$. Next, defining

$$\zeta(t) \equiv \sqrt{t}\, r\left(\lambda\, \log(t)\right), \tag{4.6.4}$$

one can derive an equivalent Ermakov-Pinney equation with a time-independent frequency:

$$r''(u) + \left(1 - \frac{1}{4\lambda^2}\right) r(u) = r^{-3}(u) \tag{4.6.5}$$

$u \equiv \lambda \log(t)$, having boundary conditions

$$r(0) = 1, \qquad r'(0) = -\frac{1}{2\lambda}. \tag{4.6.6}$$

At this point, with the substitution $f(u) \equiv r^2(u)$, we obtain from Eq.(4.6.5)

$$\frac{1}{2} f(u)\, f''(u) - \frac{1}{4} \left(f'(u)\right)^2 + \left(1 - \frac{1}{4\lambda^2}\right) f^2(u) = 1 \tag{4.6.7}$$

that is nothing but the EL invariant $I(f)$ of Eq.(4.4.8). Hence, with a time derivative and excluding trivial solutions ($f(u) \neq 0$), one arrives to:

$$f'''(u) + 4\left(1 - \frac{1}{4\lambda^2}\right) f'(u) = 0, \tag{4.6.8}$$

with boundary conditions $f(0) = 1$, $f'(0) = -1/\lambda$ and $I(f) = 1$.
Notice that Eq.(4.6.8) has two distinct regimes, namely, one with a high initial frequency $\omega_0 = \lambda > 1/2$ for which

$$s^2 \equiv 1 - \frac{1}{4\lambda^2} > 0 \tag{4.6.9}$$

and another one at low initial frequencies, $\omega_0 = \lambda < 1/2$, for which

$$-\kappa^2 \equiv 1 - \frac{1}{4\lambda^2} < 0. \tag{4.6.10}$$

In the former case, $\lambda > 1/2$, one finds an oscillatory solution of the form

$$f'(u) = A \sin\left(2su + \varphi\right) \tag{4.6.11}$$

which leads to the final result

$$r(u) = \frac{1}{s}\left[1 - \sqrt{1 - s^2}\, \sin\left(2su + \operatorname{asin}\sqrt{1 - s^2}\right)\right]^{1/2}; \qquad \lambda > 1/2. \tag{4.6.12}$$

On the other hand, when $\lambda < 1/2$, Eq.(4.6.8) is solved by

$$f'(u) = A \cosh\left(2\kappa u + \varphi\right), \tag{4.6.13}$$

which then gives

$$r(u) = \frac{1}{\kappa}\left[-1 + \sqrt{1 + \kappa^2}\, \cosh\left(2\kappa u - \operatorname{acosh}\sqrt{1 + \kappa^2}\right)\right]^{1/2}; \qquad \lambda < 1/2. \tag{4.6.14}$$

It is easy to check that (4.6.12), (4.6.14) are solutions of Eq.(4.6.5) with boundary conditions (4.6.6) for the high/low initial frequency regimes respectively.
The typical size of the bosonic cloud $2\ell_N(t) = 2\sqrt{2N}\,\ell(t)$ is extracted from the

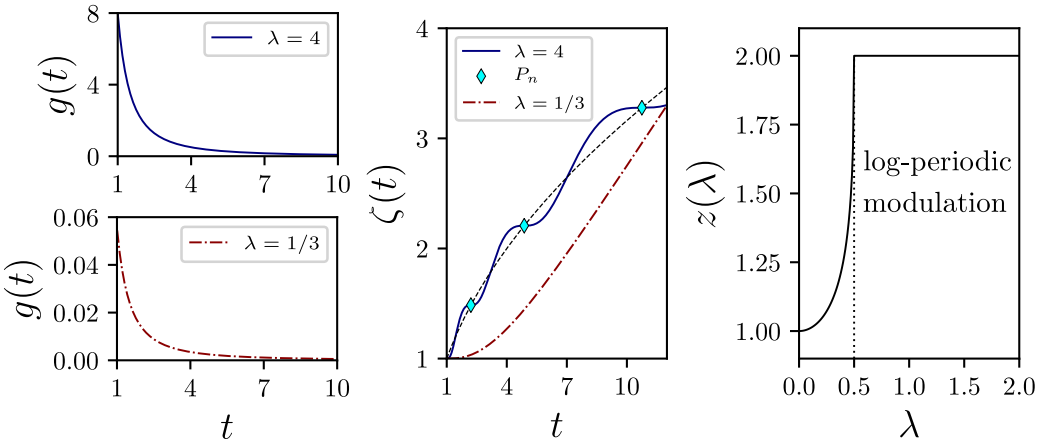

Figure 4.15: **Efimov expansion.** *Left panels*: The $1/t$-protocol of Eq.(4.6.2) and the associated solutions $\zeta(t)$ of the Ermakov-Pinney Eq.(4.6.3) in the two regimes of high $\lambda = 4$ (*blue, full line*) and low $\lambda = 1/3$ (*red, dashed dotted line*) initial frequency. Notice that the solution for $\lambda = 4$ exhibits a square root dependence in time (*black, dashed line*) with log-periodic modulations. In particular, the solution exhibits a series of plateaus (*diamonds*) located at times $P_n = \exp(2\pi\, n/\sqrt{4\lambda^2 - 1})$. *Right panel*: The behavior of the dynamical exponent $z(\lambda)$ as function of the initial frequency: for $0 \leq \lambda \leq 1/2$ it varies continuously from a ballistic value $z = 1$ to a diffusive one $z = 2$ while for $\lambda > 1/2$ it remains constant and log-periodic modulations are developed.

exact density profile (4.5.4) and it is given through

$$\ell(t) = \ell_{\mathrm{KZ}}(t_0)\, \zeta(t) = \sqrt{\frac{t}{\lambda}}\, r\left(\lambda \log(t)\right). \tag{4.6.15}$$

We can see in the high initial frequency case, that is for $\lambda > 1/2$, a square root expansion with a typical log-periodic modulation. In fact, the zeros of the solution (4.6.11), $u_n = n\pi/s$ $(n = 1, 2, \dots)$, for which $r(\frac{n\pi}{s}) = 1$, define a discrete scaling symmetry in time:

$$t_0 \mapsto P_n\, t_0 : \qquad \frac{\ell(P_n\, t_0)}{\ell(t_0)} = \sqrt{P_n} \tag{4.6.16}$$

with the geometric sequence

$$P_n = \exp\left(2\pi\, n/\sqrt{4\lambda^2 - 1}\right). \tag{4.6.17}$$

Around these points, the expansion of the cloud is strongly suppressed due to vanishing first and second-order derivatives and

$$\left.\frac{\mathrm{d}^m \ell(t)}{\mathrm{d}t^m}\right|_{t_2=e^{\frac{2\pi}{\sqrt{4\lambda^2-1}}}t_1} = e^{\frac{-\pi(2m-1)}{\sqrt{4\lambda^2-1}}} \left.\frac{\mathrm{d}^m \ell(t)}{\mathrm{d}t^m}\right|_{t_1}, \tag{4.6.18}$$

for any $m > 2$. On the contrary, at lower initial frequencies $\lambda < 1/2$, the expansion of the cloud at long times is governed by a pure power-law

$$\ell(t) \sim t^{x(\lambda)} \qquad t \gg 1 \tag{4.6.19}$$

with a dynamical exponent $z(\lambda) \equiv 1/x(\lambda)$ that varies continuously with the initial frequency λ and which is given through

$$x(\lambda) = \frac{1}{2} + \kappa(\lambda)\,\lambda = \frac{1}{2}\left(1 + \sqrt{1-4\lambda^2}\right). \tag{4.6.20}$$

Such a behavior is reminiscent of marginal perturbations, such as the Hilhorst-van Leeuwen ones [Hil81, Ber90, Igl93, Kar00], affecting the equilibrium critical exponents at a second order phase transition continuously. Notice that the log-periodic modulation can be seen as the emergence of a complex exponent $x(\lambda)$. Indeed, in the high initial frequency regime, the parameter $\kappa(\lambda > 1/2) = is(\lambda)$ and the power law behavior in Eq.(4.6.20) is

$$t^{\frac{1}{2}+\kappa(\lambda)\,\lambda} = t^{\frac{1}{2}(1+2is(\lambda)\,\lambda)}. \tag{4.6.21}$$

Taking its real part gives the log-periodic modulation:

$$\zeta(t) \sim \sqrt{\mathrm{Re}\left(t^{\frac{1}{2}(1+2is(\lambda)\,\lambda)}\right)} \sim \sqrt{t\,\cos\left(2s(\lambda)\,\lambda\log(t)\right)}. \tag{4.6.22}$$

In Fig.4.15, we report the solutions (4.6.12), (4.6.14) and the behavior of the dynamical exponent (4.6.20) as a function of λ.

The emergence of a discrete scaling symmetry in time for TG gases in $1/t$-dependent harmonic traps is known as *Efimov effect* [Efi70, Bra06, Nai17]. Efimov effect was born with the study of the zero-energy Schrödinger equation for three identical bosons, where one finds an effective $1/x^2$-potential in hyperspherical coordinates:

$$-\frac{\partial^2}{\partial x^2}\psi(x) - \frac{s_0^2+1/4}{x^2}\psi(x) = 0\,. \tag{4.6.23}$$

Efimov expansion	
Equation:	Dynamics of the TG cloud length scale (4.6.3)
short-range boundaries:	Equilibrium at t_0
solution:	$\ell(t)$ is log-periodic
threshold:	controlled by the initial frequency λ
Efimov states (see [Efi70, Bra06, Nai17])	
Equation:	zero-energy Schrödinger eq. (4.6.23)
short-range boundaries:	Short-range cutoff $x = x_0$ for spherical sol.
solution:	$\psi(x)$ is log-periodic
threshold:	controlled by the mass ratio s_0

Table 4.1: **Analogy between Efimov effects.** Comparison between the expansion of a TG gas in harmonic trap with frequency $\omega = \lambda/t$ and the quantum three-body problem in hyperspherical coordinates.

The analogy is established by noticing that the derivative of the Ermakov-Pinney equation (4.4.7) for the $1/t$-protocol (4.6.2),

$$\dddot{b}(t) + \frac{4\lambda^2}{t^2}\,\dot{b}(t) - \frac{4\lambda^2}{t^3}\,b(t) = 0, \qquad (b \equiv \zeta^2) \tag{4.6.24}$$

allows solutions of the form $b = c_1\,\psi_1^2 + c_{12}\,\psi_1\,\psi_2 + c_2\,\psi_2^2$, with $\psi_{1,2}$ two linearly independent solutions of

$$\frac{\mathrm{d}^2\psi(t)}{\mathrm{d}t^2} + \frac{1}{\lambda^2\,t^2}\,\psi(t) = 0, \tag{4.6.25}$$

as explicitly shown in Ref. [Den16]. Quite remarkably, on one hand the Efimov effect predicts an infinite series of three-bosons states (*Efimov trimers* [Kra06, Zac09, Kno09]) whose energies display a geometric progression; on the other, it is responsible for the emergence of a discrete scaling symmetry in time during the expansion of a scale-invariant Fermi gas, see Table 4.1. Efimov expansions have been experimentally observed and reported in the recent work [Den16] where the size of the expanding Fermi gas grows through a sequence of plateaus which are distributed log-periodically.

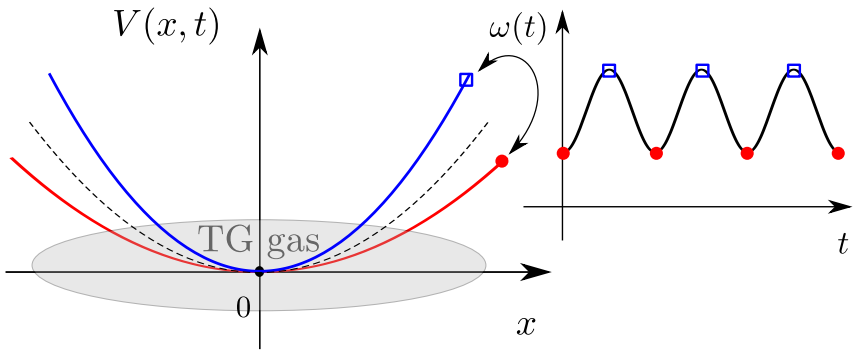

Figure 4.16: **Floquet dynamics of trapped TG gas.** A 1d Tonks-Girardeau gas at low-densities is loaded on a harmonic trap potential with varying frequency $\omega(t)$. The time-variations are now supposed to be periodic $\omega(t) = \omega(t + \mathcal{T})$ so that the potential oscillates in time between a stronger (*squares*) and a weaker (*circles*) configuration. Notice that this setup allows for investigations with Floquet theory, see Sec.3.1.

4.7 Periodic driving in trapped Tonks-Girardeau gases

We now turn to the case of a Floquet driving for this setup. In other words, we shall consider a one-dimensional TG gas (4.1.3) at low densities, loaded on a harmonic trap potential with a generic time-periodic dependence, see Fig.4.16. Recall also that the single-particle Hamiltonian for such a system can be reduced in the TD limit to a time-periodic HO with Schrödinger operator

$$\hat{\mathcal{S}}(\omega) \equiv i\partial_t - \frac{1}{2}\left(-\partial_x^2 + \omega^2(t)x^2\right), \qquad \omega(t) = \omega(t+\mathcal{T}) \tag{4.7.1}$$

and, without loss of generality, we shall set the driving period $\mathcal{T} \equiv 2\pi$ from hereafter.

4.7.1 Classification of Schrödinger operators

Consider first the Hill problem $(\partial_t^2 + \omega^2)\, y(t) = 0$ associated in the semi-classical limit to the Schrödinger operator $\hat{\mathcal{S}}$ (4.7.1)[§]. As we have argued in

[§]Consider the Hamiltonian function: $H = \frac{1}{2}(p^2 + \omega^2(t)\, x^2)$ of a (classical) HO; the motion in the phase space is governed by the equations: $\dot{x} = p$, $\dot{p} = -\omega^2(t)\, x$, which are then equivalent to the Hill's equation $\ddot{x} + \omega^2(t)\, x = 0$. See [Unt10] for further information.

Sec.3.2.1, its monodromy matrix $\mathbb{M}(\omega) \in \mathrm{sl}(2,\mathbb{R})$ is defined as

$$\mathbb{M}(\omega)\, Y(t) = Y(t+2\pi); \qquad Y(t) \equiv \begin{bmatrix} y_1(t) \\ y_2(t) \end{bmatrix} \tag{4.7.2}$$

where y_1, y_2 are a pair of linearly independent solutions of the Hill's equation $\ddot{y}_{1,2}(t) + \omega^2(t)\, y_{1,2}(t) = 0$. Recall that a different choice of bases leads to a conjugated monodromy matrix having the same trace. In particular, from Floquet's theorem we have concluded that the Hill operator is stable (unstable) if $|\mathrm{tr}(\mathbb{M}(\omega))| < 2$ (> 2), see Sec.3.2.1. Notice that in the following we shall equivalently refer to these regimes as *elliptic* (*hyperbolic*) monodromy class which is but a historical notation[§]. Same conclusions may be derived from the orbit theory of $\mathrm{sl}(2,\mathbb{R})$, see the appendix 4.D. Equivalently, the information about the conjugacy classes of monodromy can be investigated using the Kirillov's method where from the solutions of the Eq.(3.2.19):

$$\frac{1}{2}\dddot{b}(t) + 2\dot{\omega}(t)\,\omega(t)\,b(t) + 2\omega^2(t)\,\dot{b}(t) = 0, \tag{4.7.3}$$

the sign of the invariant $I(b) = b\,\ddot{b} - \frac{1}{2}(\dot{b})^2 + 2\omega^2\, b^2$ dictates the stability of the problem being positive (negative) in the stable (unstable) regime. Quite remarkably, the equation (3.2.19) is nothing but the derivative of the Ermakov-Pinney equation (4.4.7) that we have encountered in Sec.4.4. This allows us to quantize the monodromy matrix (associated to the Hill problem) into a monodromy operator (see Sec.3.1) characterizing the stroboscopic evolution of wave functions associated with the Schrödinger operator $\hat{\mathcal{S}}$. Notice that in Sec.4.4 we have set $I(b) \equiv 2\omega_0^2 > 0$ which leads us to choose $b(t)$ to be a purely imaginary function in the unstable regime. We conclude that the information about monodromy classes of $\hat{\mathcal{S}}(\omega)$ is preserved in the semi-classical limit and thus one can equivalently look at the associated Hill operator $(\partial_t^2 + \omega^2)$ instead of $\hat{\mathcal{S}}(\omega)$.

Moreover, one of the main advantages of this classification lies in the fact that Schrödinger operators belonging to a specific class are grouped into orbits which are connected by a simple (orientation preserving) time reparametrization $t \;\mapsto\; t' = \varphi(t)$, $\varphi \in \mathrm{diff}_+(\mathbb{R}/2\pi\mathbb{Z})$. It follows that one needs to know only a single representative to understand the behavior of the full orbit. The essential

[§]If we interpret the half-trace of the monodromy matrix as the eccentricity of a conic section $e = \frac{1}{2}|\mathrm{tr}(\mathbb{M})|$, then the stable (unstable) regime corresponds to ellipses (hyperbolas). Similarly, the boundary regime $e = 0$ is called also *parabolic class*.

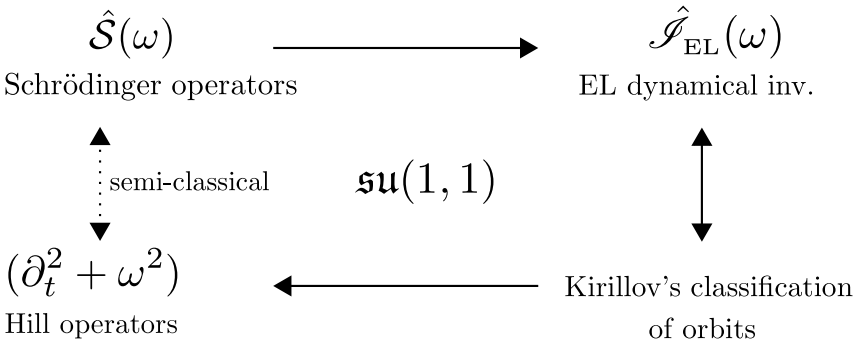

Figure 4.17: **Classification of Schrödinger operators.** The space of time-periodic harmonic Schrödinger operators can be classified into conjugacy classes of different monodromies by looking at the associated Hill problem. Indeed, even though the dynamics of the system in the semi-classical limit is very different from that of the quantum case, the information about the monodromy is preserved since it is related to the underlying $\mathfrak{su}(1,1)$ algebraic structure. This connection is made even more explicitly if one constructs the EL invariants which are naturally connected with the Kirillov's classification of orbits.

remark here [Unt10] is that time-reparametrization orbits of the space of time-periodic HO are in one-to-one correspondence with the time-reparametrization orbits of the space of Hill opertors, a problem which was widely studied and fully solved by Kirillov [Kir82], see Sec.3.2.1. The explanation behind this remarkable fact is due to a underlying $\mathfrak{su}(1,1)$ algebraic structure, as mentioned in the appendix 4.D, see Fig.4.17.

Monodromy classes & time-reparametrization orbits

Let us make the previous discussion about time-reparametrization orbits more concrete. Consider the Schrödinger operator (4.7.1) with a certain time-periodic frequency $\omega(t)=\omega(t+2\pi)$. We construct the EL dynamical invariant $\hat{\mathscr{I}}_{\mathrm{EL}}(t)$ with the usual machinery of the Ermakov-Pinney equation (4.4.9) (see Sec.4.4):

$$\begin{aligned}&\dddot{\zeta}(t)+\omega^2(t)\zeta(t)=\omega_0^2\,\zeta^{-3}(t),\\&\zeta(t+2\pi)=\zeta(t);\quad \dot{\zeta}(t+2\pi)=\dot{\zeta}(t)\end{aligned}\tag{4.7.4}$$

where we considered periodic boundary conditions that ensure the existence of a solution for ζ[¶]. Afterwards, we classify the operator $\hat{\mathcal{S}}(\omega)$ into a specific monodromy class through the sign of the invariant $I(b \equiv \zeta^2)$ and thus extract the orbital parameters as explained in Sec.3.2.2.

Now, let be ω' another choice of the frequency for which the Schrödinger operators $\hat{\mathcal{S}}(\omega)$ and $\hat{\mathcal{S}}(\omega')$ belong to the same orbit. Then, the time-evolved single-particle wave functions $\phi^{[\omega]}$, $\phi^{[\omega']}$ associated with the two frequencies ω, ω' are related by [Unt10]

$$\phi^{[\omega']}(x,t) = \frac{1}{(\dot{\varphi})^{1/4}} \exp\left(\frac{i}{4}\frac{\ddot{\varphi}}{\dot{\varphi}}\, x^2\right) \phi^{[\omega]}\left(x\,(\dot{\varphi})^{-1/2}, \varphi\right) \tag{4.7.5}$$

while the EL invariants $\zeta^{[\omega]}$, $\zeta^{[\omega']}$ satisfy

$$\left(\zeta^{[\omega']}(t)\right)^2 = (\dot{\varphi})^{-1} \left(\zeta^{[\omega]}(\varphi^{-1})\right)^2 \tag{4.7.6}$$

with $\varphi(t)$ a reparametrization of the time coordinate. Notice that Eq.(4.7.6) can be used as a definition for φ if we provide the solutions $\zeta^{[\omega]}$, $\zeta^{[\omega']}$ from the associated Ermakov-Pinney equations (4.7.4).

An example: square wave modulation of ω

The conjugacy classes of different monodromy can be generated by the simple situation where the system is subject to a time periodic ramp whose frequency is varied as a square wave:

$$\omega(t) = \omega(t+2\pi) = \begin{cases} \omega_1 & \text{if } 0 < t < \tau \\ \omega_2 & \text{if } \tau < t < 2\pi \end{cases} \tag{4.7.7}$$

where ω_1, $\omega_2 > 0$ are constants. For this setting, the Eq.(4.7.4) becomes in terms of the variable $b \equiv \zeta^2$

$$\ddot{b}(t)\, b(t) - \frac{1}{2}\left(\dot{b}(t)\right)^2 + 2\omega^2(t)\, b^2(t) = 2\omega_1^2. \tag{4.7.8}$$

Away from the discontinuities, $t \neq 0^{\pm}$, $\tau^{\pm}$, we can differentiate the last equation obtaining

$$\dddot{b}(t) + 4\omega_{1,2}^2(t)\, \dot{b}(t) = 0 \tag{4.7.9}$$

[¶]It was proven in Ref. [Kir82] that the Eq.(4.4.9) with time-periodic ω has always a periodic solution.

which can be readily integrated

$$b(t) = \begin{cases} b_1(t) = \alpha_1\, e^{i2\omega_1 t} + \gamma_1 + \beta_1\, e^{-2i\omega_1 t} & \text{if } 0 < t < \tau \\ b_2(t) = \alpha_2\, e^{i2\omega_2 t} + \gamma_2 + \beta_2\, e^{-2i\omega_2 t} & \text{if } \tau < t < 2\pi \end{cases} \tag{4.7.10}$$

with $\alpha_{1,2}$, $\beta_{1,2}$, $\gamma_{1,2}$ constants that have to be fixed imposing continuity conditions at $t = 0$ and at $t = \tau$. To do so, we can relate the unknown constants to the function $b(t)$ and its derivates with the notation:

$$\vec{b}(t) = \begin{bmatrix} b(t) \\ \dot{b}(t) \\ \ddot{b}(t) \end{bmatrix} = \mathbf{Q}(t) \begin{bmatrix} \alpha_{1,2} \\ \gamma_{1,2} \\ \beta_{1,2} \end{bmatrix} \tag{4.7.11}$$

where

$$\mathbf{Q}(t) \equiv \begin{bmatrix} e^{i2\omega(t)t} & 1 & e^{-i2\omega(t)t} \\ i2\omega(t)\, e^{i2\omega(t)t} & 0 & -i2\omega(t)\, e^{-i2\omega(t)t} \\ -4\omega^2(t)\, e^{i2\omega(t)t} & 0 & -4\omega^2(t)\, e^{i2\omega(t)t} \end{bmatrix}, \qquad t \in (0,\tau) \wedge (\tau, 2\pi). \tag{4.7.12}$$

Imposing the continuity of the function $b(t)$ and of its first derivative at $t = 0,\ \tau$ we have the conditions:

$$\vec{b}(\tau^+) = \mathbf{B}_{[\tau^+ \leftarrow \tau^-]}\, \vec{b}(\tau^-), \qquad \mathbf{B}_{[\tau^+ \leftarrow \tau^-]} \equiv \begin{bmatrix} 1 & 0 & 0 \\ 0 & 1 & 0 \\ -2(\omega_2^2 - \omega_1^2) & 0 & 1 \end{bmatrix} \tag{4.7.13a}$$

$$\vec{b}(0^+) = \mathbf{B}_{[0^+ \leftarrow 2\pi^-]}\, \vec{b}(2\pi^-), \qquad \mathbf{B}_{[0^+ \leftarrow 2\pi^-]} \equiv \begin{bmatrix} 1 & 0 & 0 \\ 0 & 1 & 0 \\ -2(\omega_1^2 - \omega_2^2) & 0 & 1 \end{bmatrix} \tag{4.7.13b}$$

The set of conditions (4.7.13) together with Eq.(4.7.11) yields

$$\begin{bmatrix} \alpha_2 \\ \gamma_2 \\ \beta_2 \end{bmatrix} = \underbrace{\mathbf{Q}^{-1}(\tau^+)\, \mathbf{B}_{[\tau^+ \leftarrow \tau^-]}\, \mathbf{Q}(\tau^-)}_{\equiv \mathbf{T}_1} \begin{bmatrix} \alpha_1 \\ \gamma_1 \\ \beta_1 \end{bmatrix}; \tag{4.7.14a}$$

$$\begin{bmatrix} \alpha_1 \\ \gamma_1 \\ \beta_1 \end{bmatrix} = \underbrace{\mathbf{Q}^{-1}(0^+)\, \mathbf{B}_{[0^+ \leftarrow 2\pi^-]}\, \mathbf{Q}(2\pi^-)}_{\equiv \mathbf{T}_2} \begin{bmatrix} \alpha_2 \\ \gamma_2 \\ \beta_2 \end{bmatrix}; \tag{4.7.14b}$$

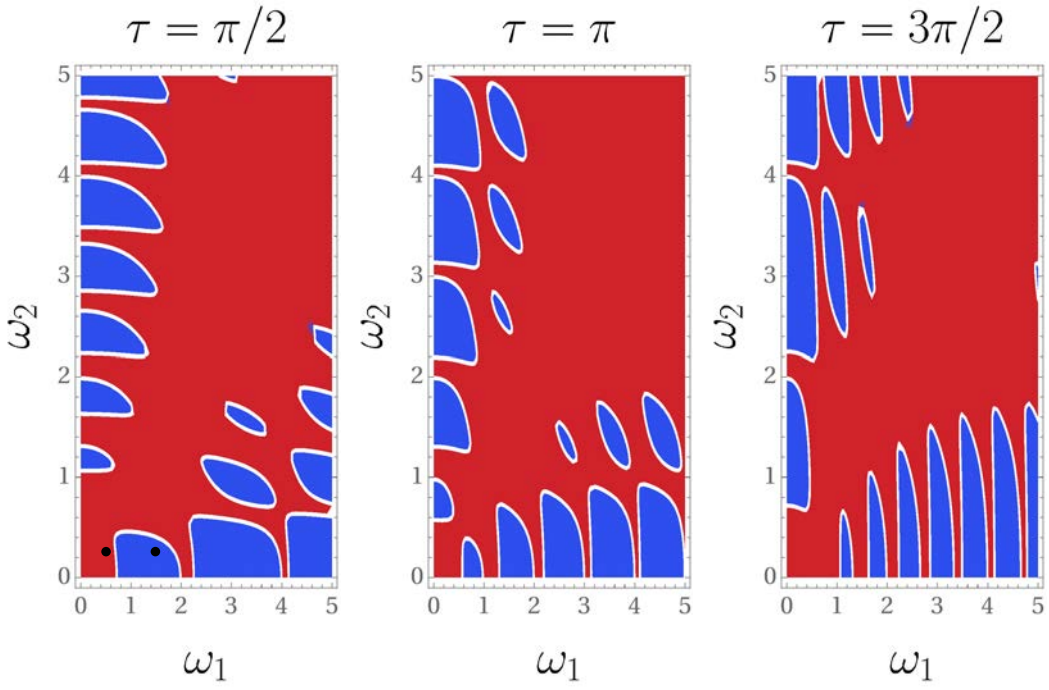

Figure 4.18: **Monodromy plot.** The two different classes, elliptic (in *blue*) and hyperbolic (in *red*) separated by a parabolic regime (in *white*) as obtained from the half-trace of the monodromy matrix in Eq.(4.7.16) as a function of ω_1 and ω_2 and for three values of $\tau = \pi/2, \pi, 3\pi/2$. The black dots (on the left panel) represent the values $(\omega_1, \omega_2, \tau) = (\frac{1}{2}, \frac{1}{4}, \frac{\pi}{2})$ and $(\omega_1, \omega_2, \tau) = (\frac{3}{2}, \frac{1}{4}, \frac{\pi}{2})$ considered explicitly below in the computation of physical quantities.

Thus,

$$\begin{bmatrix} \alpha_1 \\ \gamma_1 \\ \beta_1 \end{bmatrix} = \mathbf{T}_2 \, \mathbf{T}_1 \begin{bmatrix} \alpha_1 \\ \gamma_1 \\ \beta_1 \end{bmatrix} \tag{4.7.15}$$

is the eigenvector of $\mathbf{T}_2 \, \mathbf{T}_1$ associated to the eigenvalue 1. From the first set of coefficients in the region $t \in [0, \tau]$, we can extract then the second set using the first relation in Eq.(4.7.14a).
The classification of monodromy is obtained from the trace of the monodromy

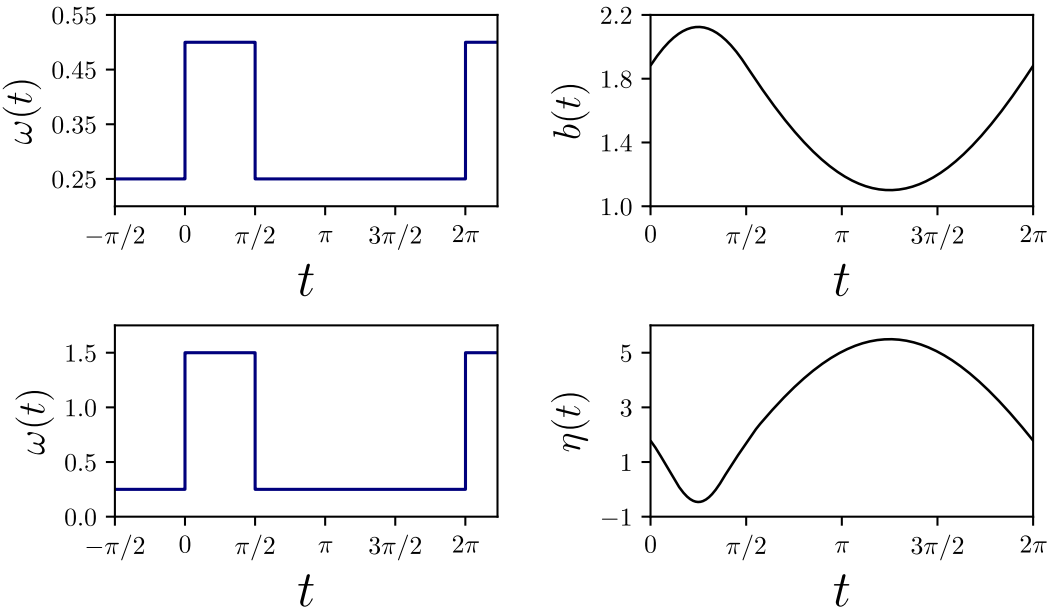

Figure 4.19: **Elliptic vs hyperbolic evolution.** The square-wave frequency protocol (4.7.7) (*left*) and the associated solution of Eq.(4.7.4) (*right*) for different values of the parameters: (*top*) elliptic case with $(\omega_1, \omega_2, \tau) = (\frac{1}{2}, \frac{1}{4}, \frac{\pi}{2})$; (*bottom*) hyperbolic case with $(\omega_1, \omega_2, \tau) = (\frac{3}{2}, \frac{1}{4}, \frac{\pi}{2})$ where the associated solution is purely imaginary ($b(t) \equiv i\eta(t)$).

matrix $\mathbb{M}(\omega)$ of the associated Hill problem (see the appendix 4.F):

$$\begin{aligned}\frac{1}{2}\mathrm{tr}\left(\mathbb{M}(\omega_1, \omega_2, \tau)\right) = \cos(\omega_1\tau)\,\cos(\omega_2(2\pi-\tau)) \\ -\frac{1}{2}\left(\frac{\omega_1}{\omega_2}+\frac{\omega_2}{\omega_1}\right)\sin(\omega_1\tau)\sin(\omega_2(2\pi-\tau)).\end{aligned} \tag{4.7.16}$$

The elliptic (hyperbolic) situation arises for a set of parameters $(\omega_1, \omega_2, \tau)$ for which $\frac{1}{2}|\mathrm{tr}(\mathbb{M})| < 1$ (> 1). In Fig.4.18 we show the elliptic and hyperbolic domains for a given value of τ. Note in particular that if $\omega_1 = \omega_2 \equiv \omega$, $|\mathrm{tr}(\mathbb{M})| = |2\cos(\omega)| \leq 2$ as expected. In Fig.4.19, we show the solutions for $b(t)$ for two different points of the monodromy phase diagram, $(\omega_1, \omega_2, \tau) = (\frac{1}{2}, \frac{1}{4}, \frac{\pi}{2})$ and $(\omega_1, \omega_2, \tau) = (\frac{3}{2}, \frac{1}{4}, \frac{\pi}{2})$ corresponding respectively to the elliptic and hyperbolic case. As we can see, the solution $b(t)$ is a positive real function in the elliptic situation whereas it takes purely imaginary values $b \equiv i\eta$ in the hyperbolic regime (with a number of zeros that defines the orbital parameter n, see Sec.3.2.2).

4.7.2 Non-equilibrium dynamics in the elliptic class

Consider a choice of ω for which the system belongs to an orbit of elliptic monodromy. In this case the EL operator (4.4.10) takes the form of a harmonic oscillator. Its eigenfunctions $\mathfrak{h}_\lambda$ are given by (see Eq.(4.4.16))

$$\mathfrak{h}_\lambda(x,t) = \frac{1}{\sqrt{\zeta(t)}} \exp\left(i\frac{\dot{\zeta}(t)}{2\zeta(t)}\,x^2\right) \psi_\lambda\left(\frac{x}{\zeta(t)}, t_0\right) \tag{4.7.17}$$

and the spectrum is $\omega_0(\lambda+1/2)$ with $\lambda = 1, 2, \ldots$ an integer. The Lewis phase acquired by the eigenvectors is (see Eq.(4.4.17)):

$$\alpha_\lambda = -\omega_0(\lambda+\frac{1}{2})\int_0^t \frac{\mathrm{d}t'}{\zeta^2(t')}. \tag{4.7.18}$$

All the information about the choice of the periodic frequency function $\omega(t)$ is thus contained in the 2π-periodic function $\zeta(t)$, which is a periodic solution of the Eq.(4.7.4). Notice that the constant frequency $\omega(t) = \omega_0$ situation, for which a solution of Eq.(4.7.4) is given by the constant $\zeta \equiv 1$, also belongs to the elliptic case; we will refer to this situation as the equilibrium limit.

Stroboscopic evolution of the one-particle wave function

The stroboscopic dynamics of the one-particle wave function is obtained by considering time-steps of one period $\Delta t = 2\pi$ starting from the initial time $t_0 = 0$. From Eq.(4.4.3) we obtain after $n \in \mathbb{N}$ periods:

$$\phi_k(x, 2\pi n) = \sum_{\lambda=0}^{\infty} \int_{\mathbb{R}} \mathrm{d}y\, \mathfrak{h}_\lambda^*(y,0)\, \psi_k(y)\, e^{-inT(\lambda+\frac{1}{2})}\, e^{i\frac{\dot{\zeta}_0}{2\zeta_0}x^2}\, \frac{1}{\sqrt{\zeta_0}}\, \psi_\lambda\left(\frac{x}{\zeta_0}\right) \tag{4.7.19}$$

with the notations $\zeta_0 \equiv \zeta(0)$, $\dot{\zeta}_0 \equiv \dot{\zeta}(0)$ and $\psi_q(x) \equiv \psi_q(x,0)$ and where we have defined

$$T \equiv \omega_0 \int_0^{2\pi} \frac{\mathrm{d}t}{\zeta^2(t)}. \tag{4.7.20}$$

Using the definition of the Mehler kernel K_e (see the appendix 4.E), the expression (4.7.19) can be written in the form

$$\phi_k(x, 2\pi n) = \int_{\mathbb{R}} \mathrm{d}y\, \exp\left(i\frac{\dot{\zeta}_0}{2\zeta_0}\,(x^2-y^2)\right) \psi_k(y)\, \mathrm{K}_e\left(\overline{x}, \overline{y}\,|\, inT\right), \tag{4.7.21}$$

where the kernel is explicitly given by

$$\mathrm{K}_e\left(\overline{x},\overline{y}\,|\,inT\right) \equiv \frac{\sqrt{\omega_0}}{\zeta_0}\,\frac{\exp\left(\frac{i}{2}(\overline{x}^2+\overline{y}^2)\cot(nT)-\overline{x}\,\overline{y}/\sin(nT)\right)}{\sqrt{2\pi i\,\sin(nT)}} \tag{4.7.22}$$

and with the shorthand notations $\overline{x}\equiv x\sqrt{\omega_0}/\zeta_0$, $\overline{y}\equiv y\sqrt{\omega_0}/\zeta_0$.

Stroboscopic evolution of the energy spectrum

We want to understand how the energy spectrum of the HO Hamiltonian in Eq.(4.7.1) evolves in time when the system is subjected to a periodic variation of the harmonic trap. In particular, exploiting the 2π-periodicity of the Hamiltonian in Eq.(4.7.1) and of the result (4.7.21), we look at the energy of the kth level of the initial Hamiltonian after n periods:

$$\begin{aligned}\varepsilon_k(2\pi n) &\equiv \langle\phi_k(2\pi n)|\hat{H}(0)|\phi_k(2\pi n)\rangle\\ &= \langle\phi_k(2\pi n)|-\frac{\partial_x^2}{2}|\phi_k(2\pi n)\rangle+\langle\phi_k(2\pi n)|\frac{\omega_0^2\,x^2}{2}|\phi_k(2\pi n)\rangle\\ &=\varepsilon_k^{(1)}(2\pi n)+\varepsilon_k^{(2)}(2\pi n)\end{aligned} \tag{4.7.23}$$

where we have divided the expectation value into the kinetic part ($\varepsilon_k^{(1)}$) and the potential ($\varepsilon_k^{(2)}$). The expectation value of the potential is given by the expression

$$\varepsilon_k^{(2)}(2\pi n)=\int_{\mathbb{R}}\mathrm{d}y\,\int_{\mathbb{R}}\mathrm{d}y'\,e^{i\frac{\dot{\zeta}_0}{2\zeta_0}(y^2-y'^2)}\,\psi_k(y)\,\psi_k(y')\,\mathcal{I}_2\left(y,y'\,|\,nT\right) \tag{4.7.24}$$

where

$$\mathcal{I}_2\left(y,y'\,|\,nT\right)\equiv\frac{\omega_0^2}{2}\int_{\mathbb{R}}\mathrm{d}x\,\mathrm{K}_e^*\left(\overline{x},\overline{y}\,|\,inT\right)\,x^2\,\mathrm{K}_e\left(\overline{x},\overline{y}'\,|\,inT\right). \tag{4.7.25}$$

Performing the integration over x of the kernel $\mathcal{I}_2$ and inserting the expression in Eq.(4.7.24) we obtain:

$$\begin{aligned}\varepsilon_k^{(2)}(2\pi n) = -\frac{1}{2}\zeta_0^4\,\sin^2(nT)\,\int_{\mathbb{R}}\mathrm{d}y\,\int_{\mathbb{R}}\mathrm{d}y'\,\delta(y-y')\,\times\\ \frac{1}{2}\left(\partial_y^2+\partial_{y'}^2\right)\left[\psi_k(y)\,\psi_k(y')\,\exp\left(\frac{i\omega_0}{2\zeta_0^2}(-\cot(nT)+\frac{\dot{\zeta}_0\zeta_0}{\omega_0})(y^2-y'^2)\right)\right].\end{aligned} \tag{4.7.26}$$

The action of the derivative and the integral can be easily computed using the recursion properties of Hilbert-Hermite functions ψ_q [Abr64]. The result is

$$\varepsilon_k^{(2)}(2\pi n) = \frac{1}{2}\Big[\zeta_0^4 \sin^2(nT) + \Big(\cos(nT) - \frac{\dot{\zeta}_0\zeta_0}{\omega_0}\sin(nT)\Big)^2\Big]\,\omega_0\,\Big(k+\frac{1}{2}\Big)\,. \tag{4.7.27}$$

With the same procedure we also compute the expectation value of the kinetic term:

$$\varepsilon_k^{(1)}(2\pi n) = \int_{\mathbb{R}} \mathrm{d}y \int_{\mathbb{R}} \mathrm{d}y'\, e^{i\frac{\dot{\zeta}_0}{2\zeta_0}(y^2-y'^2)}\,\psi_k(y)\,\psi_k(y')\,\mathcal{I}_1\,(y,y'\,|\,nT) \tag{4.7.28}$$

where $\mathcal{I}_1\,(y,y'\,|\,nT)$ is defined to be

$$\mathcal{I}_1\,(y,y'\,|\,nT) \equiv -\frac{1}{2}\int_{\mathbb{R}} \mathrm{d}x\, e^{-i\frac{\dot{\zeta}_0}{2\zeta_0}x^2}\,\mathrm{K}_e^*\,(\overline{x},\overline{y}\,|\,inT)\;\partial_x^2\, e^{i\frac{\dot{\zeta}_0}{2\zeta_0}x^2}\,\mathrm{K}_e\,(\overline{x},\overline{y}'\,|\,inT)\,. \tag{4.7.29}$$

Performing the integration over x of the kernel $\mathcal{I}_1$, the expression (4.7.28) becomes

$$\begin{aligned}\varepsilon_k^{(1)}(2\pi n) =& \frac{\omega_0}{2\zeta_0^2}\int_{\mathbb{R}} \mathrm{d}y \int_{\mathbb{R}} \mathrm{d}y'\,\delta(y-y')\Big[\frac{\zeta_0^2}{\omega}\Big(\cos(nT)+\frac{\dot{\zeta}_0\zeta_0}{\omega_0}\sin(nT)\Big)^2\,\partial_y\,\partial_{y'} \\ &- i\Big(\cot(nT)+\frac{\dot{\zeta}_0\zeta_0}{\omega_0}\Big)\,(\partial_y\,y' - y\,\partial_{y'}) + \frac{\omega_0}{\zeta_0^2}\,\frac{y\,y'}{\sin^2(nT)}\Big]\;\times \\ &\Big[\psi_k(y)\,\psi_k(y'\,\exp\Big(\frac{i\omega_0}{2\zeta_0^2}(-\cot(nT)+\frac{\dot{\zeta}_0\zeta_0}{\omega_0})(y-y'^2)\Big)\Big],\end{aligned} \tag{4.7.30}$$

which finally leads to

$$\begin{aligned}\varepsilon_k^{(1)}(2\pi n) =& \frac{1}{2}\Big[\Big(\cos(nT)+\frac{\dot{\zeta}_0\zeta_0}{\omega_0}\sin(nT)\Big)^2 \\ &+ \frac{1}{\zeta_0^4}\sin^2(nT)\Big(1+\Big(\frac{\dot{\zeta}_0\zeta_0}{\omega_0}\Big)^2\Big)^2\Big]\,\omega_0\,\Big(k+\frac{1}{2}\Big)\,.\end{aligned} \tag{4.7.31}$$

The stroboscopic evolution of the energy ε_k is given by the sum of the kinetic part (4.7.31) and of the potential (4.7.27):

$$\begin{aligned}\varepsilon_k(2\pi n) =& \omega_0\,\Big(k+\frac{1}{2}\Big)\,\Big[\cos^2(nT)+\Big(\frac{\dot{\zeta}_0\zeta_0}{\omega_0}\Big)^2\sin^2(nT) \\ &+ \frac{1}{2}\sin^2(nT)\Big(\zeta_0^4+\frac{1}{\zeta_0^4}\Big(1+\Big(\frac{\dot{\zeta}_0\zeta_0}{\omega_0}\Big)^2\Big)^2\Big)\Big].\end{aligned} \tag{4.7.32}$$

Notice that for $n = 0$ we recover the initial value of the energy $\varepsilon_k(0) = \omega_0(k+\frac{1}{2})$. Furthermore, setting $\zeta_0 = 1$ the equilibrium value of the energy is recovered at any instant of time. It is interesting to consider a time average $\langle\,\cdot\,\rangle_{\mathbf{t}}$ of the energy that can be defined as follows

$$\langle\varepsilon_k\rangle_{\mathbf{t}} \equiv \lim_{m\to\infty}\frac{1}{m}\sum_{n=0}^{m}\varepsilon_k(2\pi n) = \int_0^{2\pi}\frac{d\theta}{2\pi}\,\varepsilon_k(\theta) \tag{4.7.33}$$

where the identity above holds not only in $\mathbb{L}^1$ as follows from standard ergodic theory argument, see e.g. [Da 10], but also in a stronger sense, implying in particular pointwise convergence [Kui74]. The averaged energy is thus

$$\langle\varepsilon_k\rangle_{\mathbf{t}} = \frac{1}{2}\Big[1+\left(\frac{\dot\zeta_0\zeta_0}{\omega_0}\right)^2+\frac{1}{2}\Big(\zeta_0^4+\frac{1}{\zeta_0^4}\Big(1+\left(\frac{\dot\zeta_0\zeta_0}{\omega_0}\right)^2\Big)^2\Big)\Big]\,\omega_0\,(k+\frac{1}{2}). \tag{4.7.34}$$

In the special case where $\dot\zeta_0 = 0$, the system exhibits a sort of equipartition between the expectation values of the kinetic part and the potential part

$$\langle\varepsilon_k^{(1)}\rangle_{\mathbf{t}} = \zeta_0^4\;\langle\varepsilon_k^{(2)}\rangle_{\mathbf{t}} \tag{4.7.35}$$

where the factor ζ_0^4 can be explained by the different scaling of the kinetic part of the HO Hamiltonian in terms of the variable $\overline{x} = x\sqrt{\omega_0}/\zeta_0$, $\hat H(0) = \frac{\omega_0\zeta_0^2}{2}(-\frac{1}{\zeta_0^4}\,\partial_{\overline{x}}^2+\overline{x}^2)$. The stroboscopic evolution of the energy for the elliptic point $(\omega_1,\omega_2,\tau) = (\frac{1}{2},\frac{1}{4},\frac{\pi}{2})$ of the protocol (4.7.7) is shown in Fig.4.20.

Stroboscopic evolution of the N-particle density

In this section we derive the stroboscopic evolution of the particle density for a system composed of N hard-core bosons initially prepared in the ground state Ψ_0 (4.2.11). The N-particle density is given by (see the appendix 4.B):

$$\rho(x,2\pi n) = \sum_{k=0}^{N-1}|\phi_k(x,2\pi n)|^2 \tag{4.7.36}$$

and, using the result (4.7.21) for the stroboscopic evolution of the single-particle wave function we have

$$\rho(x,2\pi n) = \int_{\mathbb{R}}\mathrm{d}y\int_{\mathbb{R}}\mathrm{d}y' e^{i\frac{\dot\zeta_0}{2\zeta_0}(y^2-y'^2)}\mathrm{K}_e^*\left(\overline{x},\overline{y}\,|\,inT\right)\;\mathrm{K}_e\left(\overline{x},\overline{y}'\,|\,inT\right)\;\mathcal{K}_N\left(y,y'\right) \tag{4.7.37}$$

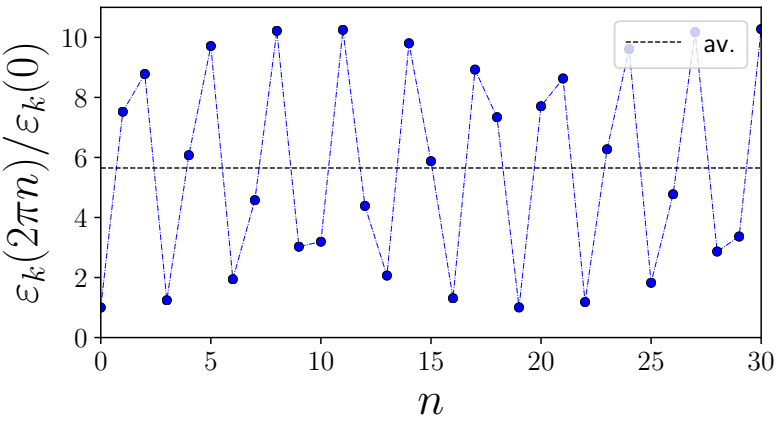

Figure 4.20: **Elliptic energy evolution.** The stroboscopic evolution of the single-particle quasi-energy $\varepsilon_k(2\pi n)/\varepsilon_k(0)$ associated with the elliptic point $(\omega_1, \omega_2, \tau) = (\frac{1}{2}, \frac{1}{4}, \frac{\pi}{2})$ of the square-wave protocol in Eq.(4.7.7). The dashed line represents the average value of Eq.(4.7.35).

where we have introduced the Christoffel-Darboux kernel [Abr64]

$$\mathcal{K}_N(y, y') \equiv \sum_{k=0}^{N-1} \psi_k(y)\, \psi_k(y') = \sqrt{2N} \left(\frac{\psi_N(y')\, \psi_{N-1}(y) - \psi_N(y)\, \psi_{N-1}(y')}{2\sqrt{\omega_0}(y' - y)} \right). \tag{4.7.38}$$

If we consider a large number of bosons $N \gg 1$, the Hilbert-Hermite functions $\psi_N(x)$ take significant values only in the region $|x| \leq \sqrt{2N/\omega_0}$ where the zeros the Hermite polynomials are located. Outside that region the Hilbert-Hermite functions decay exponentially fast. In this limit they can be represented by the asymptotic expansion (see [Sze39] p.201)

$$\psi_{N-\frac{1}{2}\pm\frac{1}{2}}(x) \overset{N\to\infty}{\simeq} \omega_0^{1/4}\, (2N)^{-1/4} \sqrt{\frac{2}{\pi}}\, (\sin\theta)^{-1/2}\, \sin\left[\frac{N}{2}(\sin(2\theta) - 2\theta) \mp \frac{\theta}{2} + \frac{3}{4}\pi \right] \tag{4.7.39}$$

where $x = \sqrt{(2N/\omega_0)}\cos\theta$ and $\theta \in [0, \pi]$. The Christoffel-Darboux kernel (4.7.38) can be handled using the asymptotic expression in Eq.(4.7.39) and becomes

$$\mathcal{K}_N(y, y') \overset{N\to\infty}{\simeq} \sqrt{\omega_0}\, \frac{(2N)^{-1/2}}{\pi\, (\cos\theta' - \cos\theta)}\, (\sin\theta\, \sin\theta')^{-1/2}\, F(\theta, \theta'), \tag{4.7.40}$$

where $y = \sqrt{(2N/\omega_0)}\,\cos(\theta)$, $y' = \sqrt{(2N/\omega_0)}\,\cos\theta'$ and

$$F(\theta,\theta') \equiv \sin\left[\frac{N}{2}(s(\theta')-s(\theta))\right]\,\sin\left(\frac{\theta+\theta'}{2}\right)+\cos\left[\frac{N}{2}(s(\theta')+s(\theta)\right]\,\sin\left(\frac{\theta'-\theta}{2}\right) \tag{4.7.41}$$

with $s(\theta) \equiv \sin(2\theta) - 2\theta$. Using this and computing explicitly the product of the two Mehler kernels in Eq.(4.7.37), the N-particle density in the limit $N \gg 1$ is given by

$$\rho(x,2\pi n) \overset{N\to\infty}{\simeq} \frac{\sqrt{2N\omega_0}\,\zeta_0^{-2}}{2\pi^2\,|\sin(nT)|}\int_0^\pi \mathrm{d}\theta\int_0^\pi \mathrm{d}\theta\,\frac{\sqrt{\sin\theta\,\sin\theta'}}{\cos\theta'-\cos\theta}\,F(\theta,\theta')\,\times$$

$$\exp\left[i2N\left(\frac{-\cot(nT)+\frac{\dot\zeta_0\zeta_0}{\omega_0}}{2\zeta_0^2}(\cos^2\theta-\cos^2\theta')+\frac{\tilde x}{\zeta_0^2\,\sin(nT)}\,(\cos\theta-\cos\theta')\right)\right] \tag{4.7.42}$$

where $\tilde x \equiv x/\sqrt{(2N/\omega_0)}$ and with the conditions $|y|,\ |y'| \le |x|$. The last expression is a double oscillatory integral. Applying the stationary phase method, we conclude that the phase factor contributes with subleading terms $\sim \mathcal{O}(N^{-1/2})$ while the leading contribution $\sim \mathcal{O}(\sqrt{N})$ comes from the region in which $\theta' \simeq \theta$. By Taylor expanding the functions around $\theta' = \theta + \delta$, $\delta \ll 1$, we obtain

$$\rho(x,2\pi n) \overset{N\to\infty}{\simeq} \frac{\sqrt{2N\omega_0}\,\zeta_0^{-2}}{2\pi^2\,|\sin(nT)|}\int_0^\pi \mathrm{d}\theta\int_{\theta-\delta}^{\theta+\delta}\frac{\mathrm{d}\theta}{\theta'-\theta}\,\times$$

$$\left(\sin[N(\cos(2\theta)-1)(\theta'-\theta)]\,\sin\theta+\cos[N\,s(\theta)]\,\sin\left(\frac{\theta'-\theta}{2}\right)\right)\,\times$$

$$\exp\left[i2N\left(\frac{-\cot(nT)+\frac{\dot\zeta_0\zeta_0}{\omega_0}}{2\zeta_0^2}\sin(2\theta)\,(\theta'-\theta)+\frac{\tilde x}{\zeta_0^2\,\sin(nT)}\,\sin\theta\,(\theta-\theta')\right)\right]. \tag{4.7.43}$$

The estimation of the integral

$$\int_{|\gamma|>\delta}\mathrm{d}\gamma\,\frac{\sin(N\gamma)}{\gamma} \sim \mathcal{O}(N^{-1}\,\delta^{-1}) \to 0, \qquad \delta \gg N^{-1} \tag{4.7.44}$$

allows us to integrate the expression in Eq.(4.7.43) over θ' using the well-known integral $\int_{\mathbb{R}}\mathrm{d}x\,\sin(qx)/x = \pi\,\mathrm{sgn}(q)$, $q \in \mathbb{R}$, obtaining

$$\rho(x,2\pi n) \overset{N\to\infty}{\simeq} \frac{\sqrt{2N\omega_0}\zeta_0^{-2}}{4\pi|\sin(nT)|}\int_0^\pi \mathrm{d}\theta\,\sin\theta\,\left(\mathrm{sgn}(\Phi_+)+\mathrm{sgn}(\Phi_-)\right), \tag{4.7.45}$$

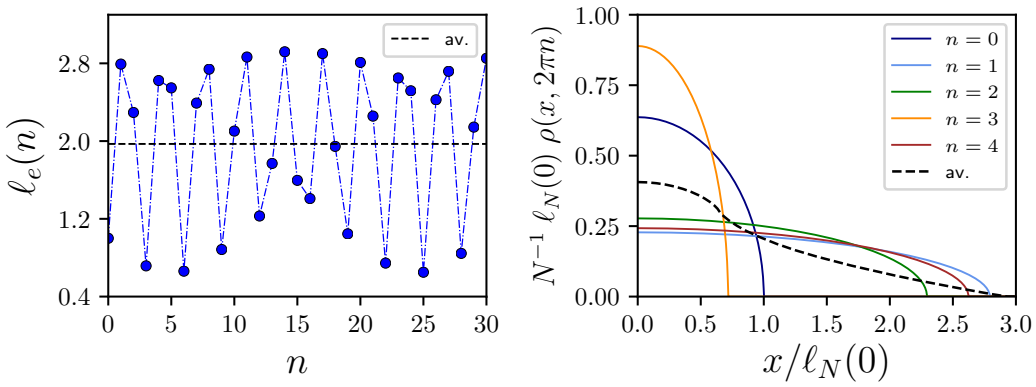

Figure 4.21: **Elliptic density evolution.** *Left:* The support $\ell_e(n)$ of equation (4.7.47) for the elliptic point $(\omega_1,\omega_2,\tau)=(\frac{1}{2},\frac{1}{4},\frac{\pi}{2})$ of the square-wave protocol in Eq.(4.7.7) as function of $n\in\mathbb{N}$. *Right:* The associated stroboscopic evolution of the rescaled N-particle density $\ell_N(0)\,\rho(x,2\pi n)/N$ (4.7.48) as function of $\tilde{x}=x/\ell_N(0)$. The dashed line shows the time averaged density of (4.7.49) computed numerically with $m=10^3$.

where

$$\Phi_\pm(\theta)\equiv\sqrt{1+a^2}\,\sin\left[\theta\mp\operatorname{asin}\left(\frac{a}{\sqrt{1+a^2}}\right)\right]\mp b,\qquad\begin{cases}a\equiv(-\cot(nT)+\frac{\dot{\zeta}_0\zeta_0}{\omega_0})/\zeta_0^2;\\ b\equiv\tilde{x}/(\zeta_0^2\sin(nT)).\end{cases}\tag{4.7.46}$$

Notice that the functions $\Phi_\pm$ have roots only if the condition

$$|\tilde{x}|\le\ell_e(n)\equiv\sqrt{\zeta_0^4\,\sin^2(nT)+\left(\frac{\dot{\zeta}_0\zeta_0}{\omega_0}\,\sin(nT)-\cos(nT)\right)^2}\tag{4.7.47}$$

is satisfied. Otherwise the functions $\Phi_\pm$ have opposite signs and there are no contributions for the N-particle density. Inside the support $|\tilde{x}|\le\ell_e(n)$, the study of the sign of the functions $\Phi_\pm$ leads to the result:

$$\rho(x,2\pi n)\overset{N\to\infty}{\simeq}\frac{2}{\pi}\,\frac{N}{\ell_N(0)\,\ell_e(n)}\,\sqrt{1-\left(\frac{\tilde{x}}{\ell_e(n)}\right)^2}\tag{4.7.48}$$

where we recall $\ell_N(0)=\sqrt{2N/\omega_0}$ is the typical length scale of the system at the equilibrium. Indeed, setting $\zeta\equiv1$ the well-known semi-circle law is

recovered. The stroboscopic evoultion of the N-particle density for the case $(\omega_1, \omega_2, \tau) = (\frac{1}{2}, \frac{1}{4}, \frac{\pi}{2})$ of the square-wave example (4.7.7) is shown in Fig.4.21. The time averaged density is given by

$$\langle \rho(x) \rangle_{\mathbf{t}} \overset{N\to\infty}{\simeq} \lim_{m\to\infty} \frac{2}{\pi} \frac{N}{\ell_N(0) m} \sum_{n=0}^{m} \frac{1}{\ell_e(n)} \sqrt{1 - \left(\frac{\tilde{x}}{\ell_e(n)}\right)^2} \tag{4.7.49}$$

and can be easily computed numerically. As one can see in Fig.4.21, it deviates significantly from a simple semi-circle law.

4.7.3 Non-equilibrium dynamics in the hyperbolic class

Consider now the EL operator in Eq.(4.4.10) in terms of the variable $b \equiv \zeta^2$,

$$\hat{\mathscr{I}}_{\text{EL}}(t) = \frac{1}{2b(t)} \left(\omega_0^2 x^2 + (ib(t)\,\partial_x + \frac{1}{2}\,\dot{b}(t)\,x)^2\right). \tag{4.7.50}$$

If we set the frequency $\omega(t)$ in such a way to have hyperbolic monodromy, the function $b(t) \in i\mathbb{R}$ and the EL operator can be conveniently written in terms of the real variable $\eta(t) \equiv -ib(t)$:

$$\hat{\mathscr{I}}_{\text{EL}}(t) = -\frac{i}{2\eta(t)}\left[\eta^2(t)\,\partial_x^2 + \omega_0^2\left(1 - \frac{\dot{\eta}^2(t)}{4\omega_0^2}\right) x^2 + \frac{1}{2}\,\dot{\eta}(t)\,\eta(t)\,(i\partial_x + ix\,\partial_x)\right], \tag{4.7.51}$$

which can be reduced to a harmonic repulsor, i.e., a harmonic oscillator with imaginary frequency, through a unitary transformation $\hat{U} = \exp\left(-i\dot{\eta}x^2/4\eta\right)$:

$$\hat{U}\,\hat{\mathscr{I}}_{\text{EL}}(t)\,\hat{U}^\dagger = -\frac{i\eta(t)}{2}\left(\partial_x^2 + \frac{\omega_0^2\,x^2}{\eta^2(t)}\right). \tag{4.7.52}$$

From this observation, the eigenfunctions of the EL operator can be easily derived:

$$\mathfrak{h}_\lambda^\pm(x,t) = \left(\frac{\omega_0}{\eta(t)}\right)^{-1/4} \exp\left[\frac{i\dot{\eta}(t)}{4\eta(t)}\,x^2\right] \chi_{i\lambda}^\pm\left(x\sqrt{\frac{\omega_0}{\eta(t)}}\right) \tag{4.7.53}$$

where $\chi_q^\pm$ are the eigenfunctions of a unit frequency harmonic repulsor (see the appendix 4.E). The spectrum of the EL operator in this case is the whole real line $\lambda \in \mathbb{R}$. The value of the Lewis phase (4.4.4) in the hyperbolic regime is [Unt10]:

$$i\alpha(t) = -\omega_0\lambda \int_0^t \frac{\mathrm{d}t'}{\eta(t')}. \tag{4.7.54}$$

In the following, for a given ω in the hyperbolic domain and provided a solution of the associated Eq.(4.7.4) in terms of η, we derive the stroboscopic behavior of the TG gas.

Stroboscopic evolution of the one-particle wave function

The stroboscopic evolution of the single-particle wave function in the case of hyperbolic monodromy can be deduced by plugging into the general expression (4.4.3) the Lewis phase and the eigenfunctions $\mathfrak{h}_\lambda$ given above:

$$\phi_k(x, 2\pi n) = \int_{\mathbb{R}} \mathrm{d}\lambda \int_{\mathbb{R}} \mathrm{d}y\, \mathfrak{h}^*_\lambda(y, 0)\, \psi_k(y)\, e^{-nT}\, \mathfrak{h}_\lambda(x, 0) \tag{4.7.55}$$

where we have defined

$$T \equiv \omega_0 \int_{\gamma[0,2\pi]} \frac{\mathrm{d}t}{\eta(t)} \tag{4.7.56}$$

and $\gamma[0, 2\pi]$ is the complex deformation of the real interval $[0, 2\pi]$ which avoids the singularities, as explained in [Unt10]. Using the definition of the hyperbolic Mehler kernel (see the appendix 4.E) we can write Eq.(4.7.55) as

$$\phi_k(x, 2\pi n) = \int_{\mathbb{R}} \exp\left(\frac{i\dot{\eta}_0}{4\eta_0}(x^2 - y^2)\right) \psi_k(y)\, \mathrm{K}_h\left(\overline{x}, \overline{y}\,|\, nT\right), \tag{4.7.57}$$

with the notations $\eta_0 \equiv \eta(0)$, $\dot{\eta}_0 \equiv \dot{\eta}(0)$, $\overline{x} \equiv x\sqrt{\omega_0/\eta_0}$, $\overline{y} \equiv y\sqrt{\omega_0/\eta_0}$ and where the hyperbolic kernel is explicitly given by

$$\mathrm{K}_h\left(\overline{x}, \overline{y}\,|\, nT\right) = \sqrt{\frac{\omega_0}{\eta_0}}\, \frac{\exp\left[-\frac{i}{2}\left(\overline{x}^2 + \overline{y}^2\right)\coth(nT) + i\overline{x}\,\overline{y}/\sinh(nT)\right]}{\sqrt{2\pi\,\sinh(nT)}}. \tag{4.7.58}$$

Stroboscopic evolution of the energy spectrum

Following the procedure used in the Sec.4.7.2, we compute the stroboscopic evolution of the energy spectrum in the case of hyperbolic monodromy. Using the expression of the single-particle wave function in Eq.(4.7.57), the computation of the expectation value (4.7.23) gives

$$\varepsilon^{(2)}_k(2\pi n) = \frac{1}{2}\left[\left(\cosh(nT) + \frac{\dot{\eta}}{2\omega_0}\sinh(nT)\right)^2 + \eta_0^2 \sinh^2(nT)\right]\omega_0\,\left(k + \frac{1}{2}\right) \tag{4.7.59}$$

for the contribution of the potential and

$$\begin{aligned}\varepsilon^{(1)}_k(2\pi n) =& \frac{1}{2\eta_0^2}\left[\left(\cosh(nT) - \frac{\dot{\eta}_0}{2\omega_0}\,\sinh(nT)\right)^2\right. \\ &\left. + \frac{1}{\eta_0^2}\,\sinh^2(nT)\left(1 - \frac{\dot{\eta}_0^2}{4\omega_0^2}\right)\right]\omega_0\,\left(k + \frac{1}{2}\right)\end{aligned} \tag{4.7.60}$$

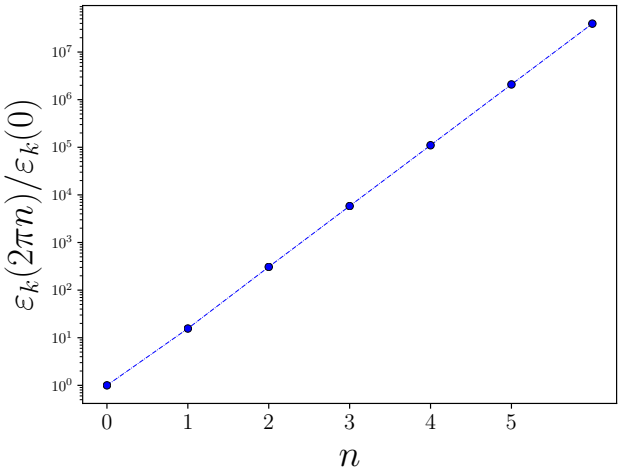

Figure 4.22: **Hyperbolic energy evolution.** The stroboscopic evolution of the energy spectrum $\varepsilon_k(2\pi n)/\varepsilon_k(0)$ as a function of $n \in \mathbb{N}$ shows an exponential growth (here in logarithmic scale). The plot corresponds to the hyperbolic point $(\omega_1, \omega_2, \tau) = (\frac{3}{2}, \frac{1}{4}, \frac{\pi}{2})$ for the square-wave protocol (4.7.7).

for the kinetic term. Hence, the result for the stroboscopic evolution of the energy spectrum is given by

$$\varepsilon_k(2\pi n) = \Big[\cosh^2(nT) + \frac{\dot{\eta}_0^2}{4\omega_0^2} \sinh^2(nT) + \frac{1}{2} \sinh^2(nT) \Big((\eta_0^2 + \frac{1}{\eta_0^2} \Big(1 - \frac{\dot{\eta}_0^2}{4\omega_0^2} \Big) \Big) \Big] \omega_0 \Big(k + \frac{1}{2} \Big). \quad (4.7.61)$$

Notice first that the initial value of the energy $\varepsilon_k(0) = \omega_0(k + \frac{1}{2})$ is recovered for $n = 0$. The frequencies $\omega(t)$ in the hyperbolic monodromy class vary in time in such a way to pump energy into the system at each cycle and the energy grows exponentially in time. The physical scenario can be placed in analogy with a seesaw: depending on the behavior of the periodic forcing, the amplitude of the oscillations can either increase or remain bounded after each cycle. In Fig.4.22 the stroboscopic evolution of the energy spectrum is showed for the hyperbolic point $(\omega_1, \omega_2, \tau) = (\frac{3}{2}, \frac{1}{4}, \frac{\pi}{2})$ of the square wave frequency (4.7.7).

Large N particle density stroboscopic evolution

The stroboscopic evolution of the N-particle density for a system initially prepared in the ground state Ψ_0 (4.2.11) can be derived similarly to Sec.4.7.2

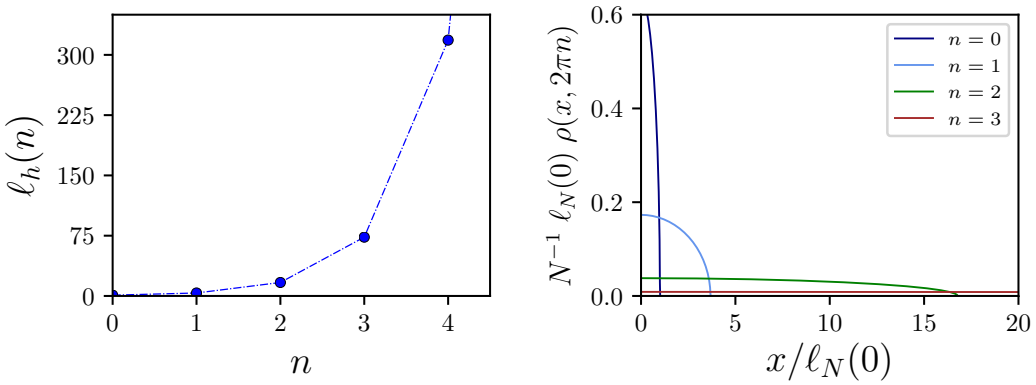

Figure 4.23: **Hyperbolic density evolution.** *Left:* The support $\ell_h(n)$ of equation (4.7.64) for the hyperbolic point $(\omega_1, \omega_2, \tau) = (\frac{3}{2}, \frac{1}{4}, \frac{\pi}{2})$ of the protocol (4.7.7) is shown as function of $n \in \mathbb{N}$. *Right:* The associated stroboscopic evolution of the rescaled N-particle density $\ell_N(0)\,\rho(x, 2\pi n)/N$ in Eq.(4.7.63) as function of $\tilde{x} = x/\ell_N(0)$.

for the hyperbolic case. From the general expression (4.7.36) and using the result in Eq.(4.7.57), we arrive at

$$\rho(x, 2\pi n) = \int_{\mathbb{R}} \mathrm{d}y \int_{\mathbb{R}} \mathrm{d}y'\, e^{i\frac{\dot{\eta}_0}{4\eta_0}(y^2 - y'^2)}\; \mathrm{K}_h^*\left(\overline{x}, \overline{y}\,|\,nT\right)\; \mathrm{K}_h\left(\overline{x}, \overline{y}'\,|\,nT\right)\; \mathcal{K}_N(y, y'). \tag{4.7.62}$$

The hyperbolic case is exactly similar to the elliptic one, up to the replacement of the kernel K_e with K_h and the change of notation for the phase. Therefore, in the limit of large number of particles $N \gg 1$, the same kind of asymptotic expansions as in Sec.4.7.2 leads to the final result

$$\rho(x, 2\pi n) \overset{N\to\infty}{\simeq} \frac{2}{\pi} \frac{N}{\ell_N(0)\,\ell_h(n)} \sqrt{1 - \left(\frac{\tilde{x}}{\ell_h(n)}\right)^2}, \tag{4.7.63}$$

where the dynamical support $\ell_h(n)$, given by

$$\ell_h(n) \equiv \sqrt{\eta_0^2\, \sinh^2(nT) + \left(\cosh(nT) + \frac{\dot{\eta}_0}{2\omega_0}\, \sinh(nT)\right)^2}, \tag{4.7.64}$$

is growing exponentially in time. As a consequence, the N-particle density spreads more and more in space after each period and approaches the zero-density MI configuration of the untrapped TG gas. Indeed, the external forcing

gives the system more and more energy making the effect of the trap gradually negligible. The plot of the N-particle density and of the support (4.7.64) for the hyperbolic point $(\omega_1, \omega_2, \tau) = (\frac{3}{2}, \frac{1}{4}, \frac{\pi}{2})$ of the protocol (4.7.7) are shown in Fig.4.23.

Some remarks.

We have investigated the time-evolution of a TG gas subject to a time-periodic harmonic trap potential and we have derived exact scaling solutions for the stroboscopic evolution of the particle density. In particular, in the limit of large number of particles $N \gg 1$, the density profile shows a semi-circle shape, governed in time by a characteristic support that depends on the type of periodic forcing. Quite remarkably, the final result depends only on the monodromy class of the perturbation giving rise to breathing modes or to dynamical instabilities in the elliptic/hyperbolic case respectively. The details of the external perturbation enter in the expression of the density profile only through the periodic solution ζ of the Ermakov-Pinney equation (4.7.4). Different kinds of forcing belonging to the same orbit are then connected via time-reparametrizations, as explained in Sec.4.7.1.

Appendix

4.A Quasi-adiabatic perturbation theory

Let us consider the wave function $\Psi(t)$ evolved from the initial ground state $\Psi_0(t_0)$:

$$|\Psi(t)\rangle = \hat{U}(t, t_0)\ |\Psi_0(t_0)\rangle\,. \tag{4.A.1}$$

We may employ a Trotter discretization of the time coordinate so that the time-evolution operator $\hat{U}(t, t_0)$ becomes

$$\hat{U}(t, t_0) = \lim_{N\to\infty} \prod_{j=0}^{N} e^{-i\hat{H}_j\, \mathrm{d}t} \tag{4.A.2}$$

where $\hat{H}_j \equiv \hat{H}(t_j)$, $t_j \equiv t_0 + j/N(t - t_0)$ and $\mathrm{d}t \equiv (t - t_0)/N$. It follows that the time-evolved wave function can be written as

$$|\Psi(t)\rangle = \lim_{N\to\infty} e^{-iE_0(t_0)\,\mathrm{d}t} \prod_{j=1}^{N} e^{-i\hat{H}_j\, \mathrm{d}t}\ |\Psi_0(t_0)\rangle\,. \tag{4.A.3}$$

Clearly, the initial ground state of the system is no more an eigenstate of the instantaneous Hamiltonians $\hat{H}_j$ for $j \geq 1$. Therefore, we are in need of a *quasi-adiabatic* (QAD) approximation [Col11, Col12a], where one replaces

$$|\Psi_0(t_{j-1})\rangle \simeq |\Psi_0(t_j)\rangle + \mathrm{d}t \sum_{n\neq 0} \frac{\langle n(t_j)|\mathrm{d}\hat{H}_j|\Psi_0(t_j)\rangle}{E_n(t_j) - E_0(t_j)} \tag{4.A.4}$$

with $\mathrm{d}\hat{H}_j \equiv (\hat{H}_j - \hat{H}_{j-1})/\mathrm{d}t$ and $\hat{H}_j\ |n(t_j)\rangle = E_n(t_j)\ |n(t_j)\rangle$. Here, the first term reproduces the adiabatic limit whereas the second term accounts for the one-jump processes where a single quasi-particle is promoted from the lowest levels towards higher excited states. Employing such a QAD approximation, from Eq.(4.A.3) we obtain [Col11, Col12a]

$$|\Psi(t)\rangle \simeq \lim_{N\to\infty} \Bigg[e^{-i\sum_{j=0}^{N-1} E_0(t_j)\,\mathrm{d}t}\ |\Psi_0(t)\rangle \tag{4.A.5}$$

$$+ \sum_{n\neq 0} \Bigg(\sum_{j=1}^{N} \mathrm{d}t\ e^{-i\sum_{k=j}^{N-1} E_n(t_k)\,\mathrm{d}t}\ \frac{\langle n(t_j)|\mathrm{d}\hat{H}_j|\Psi_0(t_j)\rangle}{E_n(t_j) - E_0(t_j)}\ e^{-i\sum_{k=0}^{j-1} E_0(t_k)\,\mathrm{d}t} \Bigg)\ |n(t)\rangle \Bigg] \tag{4.A.6}$$

which becomes in the limit $N \to \infty$ where $\mathrm{d}t \to 0$

$$|\Psi(t)\rangle \simeq e^{-i\int_{t_0}^{t} \mathrm{d}t'\, E_0(t')}\ |\Psi_0(t)\rangle \tag{4.A.7}$$

$$+ \sum_{n\neq 0} \int_{t_0}^{t} \mathrm{d}t'\, e^{-i\int_{t'}^{t} \mathrm{d}s\, E_n(s)}\ \frac{\langle n(t')|\partial_{t'}\hat{H}(t')|\Psi_0(t')\rangle}{E_n(t') - E_0(t')}\ e^{-i\int_{t_0}^{t'} \mathrm{d}s\, E_n(s)}. \tag{4.A.8}$$

4.B N-particle density

We compute the wave function of N hard-core bosons initially prepared in the ground state Ψ_0 (4.2.11) of the Hamiltonian (4.1.3) at $t = t_0$:

$$\Psi_N(\vec{x}, t) = \frac{\Delta(\vec{x})}{|\Delta(\vec{x})|} \frac{1}{\sqrt{N!}} \det_{j,k=0}^{N-1} \phi_k(x_j, t) \tag{4.B.1}$$

where $\vec{x} \equiv (x_0, \ldots, x_{N-1})$ and

$$\Delta(\vec{x}) \equiv \prod_{0\leq i<j\leq N-1} \mathrm{sgn}\,(x_i - x_j) \tag{4.B.2}$$

is the Vandermonde determinant which symmetrizes the Slater determinant under particle exchanges. The N-particle density can be computed starting from the definition:

$$\rho(x,t) \equiv \int_{\mathbb{R}^N} \mathrm{d}\vec{x}\ \ \Psi_N^*(\vec{x},t)\,\Psi_N(\vec{x},t)\ \sum_{j=0}^{N-1}\delta(x-x_j); \tag{4.B.3}$$

It is possible to write the particle density as a functional derivative of a generating functional $\mathcal{Z}[a]$:

$$\rho(x,t) = \frac{\delta}{\delta a(x)}\bigg|_{a\equiv 1}\mathcal{Z}[a], \tag{4.B.4}$$

where

$$\mathcal{Z}[a] \equiv \frac{1}{N!}\int_{\mathbb{R}^N}\mathrm{d}\vec{x}\ \prod_{j=0}^{N-1}a(x_j)\ \det_{j,k=0}^{N-1}\phi_k^*(x_j,t)\ \det_{j',k'=0}^{N-1}\phi_{k'}(x_{j'},t). \tag{4.B.5}$$

The Andrejeff's relation [And09] allows us to rewrite the generating functional as:

$$\mathcal{Z}[a] = \det_{k,k'=0}^{N-1}\left(\int_{\mathbb{R}}\mathrm{d}x\,a(x)\,\phi_k^*(x,t)\ \phi_{k'}(x,t)\right), \tag{4.B.6}$$

hence, the expression (4.B.4) becomes

$$\rho(x,t) = \frac{\delta}{\delta a(x)}\bigg|_{a\equiv 1}\mathcal{Z}[a] = \det_{k,k'=0}^{N-1}B_{k,k'}[1]\ \ \mathrm{tr}\left[(B_{k,k'}[1])^{-1}\,\frac{\delta B_{k,k'}[a]}{\delta a(x)}\bigg|_{a\equiv 1}\right], \tag{4.B.7}$$

where we have introduced the definition

$$B_{k,k'}[a] \equiv \int_{\mathbb{R}}\mathrm{d}x\,a(x)\,\phi_k^*(x,t)\,\phi_{k'}(x,t). \tag{4.B.8}$$

Using the result (4.4.18) for the one-particle wave function we can compute the matrix elements $B_{k,k'}[a]$ explicitly. The results are

$$B_{k,k'}[1] = \int_{\mathbb{R}}\mathrm{d}x\,\phi_k^*(x,t)\,\phi_{k'}(x,t) = \delta_{k,k'}; \tag{4.B.9}$$

$$\frac{\delta B_{k,k'}[a]}{\delta a(x)}\bigg|_{a\equiv 1} = \phi_k^*(x,t)\,\phi_{k'}(x,t). \tag{4.B.10}$$

Inserting the last two results into (4.B.7) we obtain

$$\rho(x,t) = \sum_{k=0}^{N-1}|\phi_k(x,t)|^2 \tag{4.B.11}$$

which is a well-known result [Min05, Cam10a, Sco17, Sco18b].

4.C Dynamical invariants

We call *dynamical invariant* a hermitian time-dependent operator $\hat{\mathscr{I}}$ that is a conserved charge of the system at any instant of time i.e.,

$$\frac{\mathrm{d}}{\mathrm{d}t}\,\hat{\mathscr{I}}(t) = -i[\hat{\mathscr{I}}(t), \hat{H}(t)] + \partial_t\,\hat{\mathscr{I}}(t) = 0, \quad \forall\, t. \tag{4.C.1}$$

Let us denote with $\mathfrak{h}_n$ the eigenvectors of the dynamical invariant, $\hat{\mathscr{I}}(t)\ |\mathfrak{h}_n\rangle = \lambda_n(t)\ |\mathfrak{h}_n(t)\rangle$. It is easy to show that the associated eigenvalues λ_n do not depend on time [Unt10]. Indeed, applying the invariance property (4.C.1) to the eigenstate $\mathfrak{h}_n(t)$ yields

$$\partial_t\,\hat{\mathscr{I}}(t)\ |\mathfrak{h}_n(t)\rangle - i\left(\hat{\mathscr{I}}(t) - \lambda_n(t)\right)\hat{H}(t)\,|\mathfrak{h}_n(t)\rangle = 0 \tag{4.C.2}$$

and projecting on $\langle\mathfrak{h}_m(t)|$ gives a first equation

$$\langle\mathfrak{h}_m(t)|\partial_t\,\hat{\mathscr{I}}(t)|\mathfrak{h}_n(t)\rangle - i\,(\lambda_m - \lambda_n)\,\langle\mathfrak{h}_m(t)|\hat{H}(t)|\mathfrak{h}_n(t)\rangle = 0. \tag{4.C.3}$$

Next, from the eigenproblem $\hat{\mathscr{I}}(t)\ |\mathfrak{h}_n\rangle = \lambda_n(t)\ |\mathfrak{h}_n(t)\rangle$, we obtain after differentiation

$$\partial_t\,\hat{\mathscr{I}}(t)\ |\mathfrak{h}_n(t)\rangle + \left(\hat{\mathscr{I}}(t) - \lambda_n(t)\right)|\dot{\mathfrak{h}}_n\rangle = \dot{\lambda}_n\ |\mathfrak{h}_n(t)\rangle\,. \tag{4.C.4}$$

Combining the Eq.(4.C.3) with the Eq.(4.C.4) for $n = m$ we read that $\dot{\lambda}_n = 0$. Moreover, for $n \neq m$ the latter gives the relation

$$\langle\mathfrak{h}_m(t)|i\partial_t - \hat{H}(t)|\mathfrak{h}_n(t)\rangle = 0. \tag{4.C.5}$$

It follows that one may choose the eigenvectors $\mathfrak{h}_n$ by multiplying them with an appropriate time-dependent phase so that they satisfy the associated Schrödinger equation $(i\partial_t - \hat{H}(t))\phi = 0$ [Unt10].

In particular, if we define for each n the *Lewis phase* α_n as the solution of the equation

$$\dot{\alpha}_n(t) = \langle\mathfrak{h}_n(t)|i\partial_t - \hat{H}(t)|\mathfrak{h}_n(t)\rangle\,, \qquad \alpha_n(t_0) = 0 \tag{4.C.6}$$

then, the gauge transformed eigenvectors

$$|\mathfrak{h}_n(t)\rangle \ \mapsto\ e^{i\alpha_n(t)}\ |\mathfrak{h}_n(t)\rangle \equiv |\tilde{\mathfrak{h}}_n(t)\rangle \tag{4.C.7}$$

are solutions of the Schrödinger equation $(i\partial_t - \hat{H}(t))\tilde{\mathfrak{h}}_n = 0$. In other words, a generic solution of the time-dependent Schrödinger equation is given by

$$|\phi(t)\rangle = \sum_{n\in\mathrm{spec}(\hat{\mathscr{I}}_{\mathrm{EL}})} \langle\mathfrak{h}_n(t_0)|\phi(t_0)\rangle\ e^{i\alpha_n(t)}\ |\mathfrak{h}_n(t)\rangle\,. \tag{4.C.8}$$

4.D The group su$(1,1)$

Let us address the question about dynamical invariants of harmonic Hamiltonians from an algebraic point of view. To do so, let us consider a generic time-dependent harmonic Hamiltonian

$$\hat{H}(t) = \omega(t)\,\left(\hat{a}^\dagger\hat{a} + \frac{1}{2}\right) \tag{4.D.1}$$

written in terms of the standard creation (annihilation) operators

$$\hat{a} = \frac{1}{\sqrt{2}}\,(x + \partial_x)\,, \qquad \hat{a}^\dagger = \frac{1}{\sqrt{2}}\,(x - \partial_x)\,. \tag{4.D.2}$$

Clearly, the time evolved single particle state of the system satisfying $(i\partial_t - \hat{H}(t))\phi = 0$ is somewhat complicated and can be formally expressed as

$$|\phi(t)\rangle = \hat{U}(t,t_0)\;|\phi(t_0)\rangle \qquad \hat{U}(t,t_0) \equiv \mathbf{T}\exp\left(-i\int_{t_0}^{t}\mathrm{d}t'\,\hat{H}(t')\right), \tag{4.D.3}$$

with $\mathbf{T}$ denoting the time-ordered product. However, if we consider the following extension of the Hamiltonian:

$$\hat{H}(t) = \omega(t)\,\left(\hat{a}^\dagger\hat{a} + \frac{1}{2}\right) \;\mapsto\; \hat{\mathscr{I}}(t) = a(t)\hat{H}(t) + b(t)\hat{a}\,\hat{a} + c(t)\,\hat{a}^\dagger\,\hat{a}^\dagger \tag{4.D.4}$$

for some fictitious parameters a, b, c and if we introduce the combinations

$$\hat{\kappa}_0 \equiv \frac{1}{2}\left(\hat{a}^\dagger\,\hat{a} + \frac{1}{2}\right); \quad \hat{\kappa}_- \equiv \frac{1}{2}\,\hat{a}\,\hat{a}; \quad \hat{\kappa}_+ \equiv \frac{1}{2}\,\hat{a}^\dagger\,\hat{a}^\dagger, \tag{4.D.5}$$

we can notice that $\hat{\mathscr{I}}$ has a closed algebraic structure defined through

$$[\hat{\kappa}_0, \hat{\kappa}_\pm] = \pm\hat{\kappa}_\pm, \qquad [\hat{\kappa}_+, \hat{\kappa}_-] = -2\hat{\kappa}_0 \tag{4.D.6}$$

which is known as $\mathfrak{su}(1,1)$ Lie algebra. It follows that the time evolution generated by $\hat{\mathscr{I}}(t)$ consists in a transformation belonging to the Lie group su$(1,1)$. Notice also that su$(1,1)$ provides the maximal symmetry group of a quantum harmonic oscillator since the time evolution operator $\hat{U}(t,t_0)$ generated by $\hat{H}(t)$ satisfies

$$\mathrm{span}\left(\left\{\hat{U}(s,t_0)\right\}_{s=t_0}^{t}\right) \subseteq \mathrm{su}(1,1). \tag{4.D.7}$$

For later purposes, it is worth to briefly review the properties of the group su$(1,1)$, see e.g. [Kis12, Ino13]. We define the Lie group su$(1,1)$ as

$$\mathrm{su}(1,1) \equiv \left\{\hat{g}\;:\;\det(\hat{g}) = 1, \quad \hat{g}^\dagger\,\hat{\sigma}^z\,\hat{g} = \hat{\sigma}^z\right\} \tag{4.D.8}$$

where $\hat{\sigma}^z$ is the diagonal Pauli operator. It follows that any $\hat{g} \in \mathrm{su}(1,1)$ allows a representation

$$\hat{g} = \begin{bmatrix} \alpha & \beta \\ \beta^* & \alpha^* \end{bmatrix} \tag{4.D.9}$$

with α, $\beta \in \mathbb{C}$ satisfying $|\alpha^2| - |\beta^2| = 1$. Moreover, for any $\hat{g} \in \mathrm{su}(1,1)$ there exists $\hat{h} \in \mathrm{sl}(2,\mathbb{R})$ such that

$$\hat{g} = c\,\hat{h}\,c^\dagger, \qquad c = \frac{1}{\sqrt{2}} \begin{bmatrix} 1 & -i \\ 1 & +i \end{bmatrix} \tag{4.D.10}$$

i.e., the group $\mathrm{su}(1,1)$ is isomorphic to a two-dimensional Minkowski space described through the group $\mathrm{sl}(2,\mathbb{R})$. Next, it is well-known that any element $\hat{h} \in \mathrm{sl}(2,\mathbb{R})$ admits a representation

$$\hat{h} = \hat{h}_\theta\,\hat{h}_\eta\,\hat{h}_k \tag{4.D.11}$$

as a product of three one-parameter subsets where

$$\hat{h}_\theta = \begin{bmatrix} \cos(\theta/2) & \sin(\theta/2) \\ -\sin(\theta/2) & \cos(\theta/2) \end{bmatrix} \tag{4.D.12a}$$

generates a rotation associated to the compact subgroup $\mathrm{su}(2)$,

$$\hat{h}_\eta = \begin{bmatrix} e^{\eta/2} & 0 \\ 0 & e^{-\eta/2} \end{bmatrix} \tag{4.D.12b}$$

is a Lorentz boost and

$$\hat{h}_k = \begin{bmatrix} 1 & k \\ 0 & 1 \end{bmatrix} \tag{4.D.12c}$$

is a unipotent subset generating shear transformations. It is well-known that the elements $\hat{h}$ of the group $\mathrm{sl}(2,\mathbb{R})$ have eigenvalues λ satisfying the secular equation

$$\lambda^2 - \mathrm{tr}(\hat{h})\,\lambda + 1 = 0 \tag{4.D.13}$$

which gives $\lambda_{1,2} = [\mathrm{tr}(\hat{h}) \pm \sqrt{\mathrm{tr}(\hat{h})^2 - 4}]/2$. It follows that the elements $\hat{h} \in \mathrm{sl}(2,\mathbb{R})$ can be classified via their action on a 2d space:

1. an *elliptic subset* with $|\mathrm{tr}(\hat{h})| < 2$ for which $\hat{h}$ is conjugated to a rotation;

2. a *hyperbolic subset* with $|\mathrm{tr}(\hat{h})| > 2$ for which $\hat{h}$ is conjugated to a squeeze mapping;

3. a *parabolic subset* with $|\mathrm{tr}(\hat{h})| = 2$ for which $\hat{h}$ is conjugated to a shear transformation.

The name of these subsets is rooted in a historical classification based on the half trace $|\mathrm{tr}(\hat{h})|/2$ which gives nothing but the eccentricity of a conic section being equal to ellipses, hyperbolas or parabolas in the three cases respectively. Clearly, the representation (4.D.11) implies for any $\hat{g} \in \mathrm{su}(1,1)$ that

$$\hat{g} = \hat{g}_\theta \, \hat{g}_\eta \, \hat{g}_k \tag{4.D.14}$$

where

$$\hat{g}_\theta \equiv c \, \hat{h}_\theta \, c^\dagger = \begin{bmatrix} e^{i\theta/2} & 0 \\ 0 & e^{-i\theta/2} \end{bmatrix} \tag{4.D.15a}$$

is called *elliptic class*,

$$\hat{g}_\eta \equiv c \, \hat{h}_\eta \, c^\dagger = \begin{bmatrix} \cosh(\eta/2) & \sinh(\eta/2) \\ \sinh(\eta/2) & \cosh(\eta/2) \end{bmatrix} \tag{4.D.15b}$$

is the *hyperbolic class* whereas

$$\hat{g}_k \equiv c \, \hat{h}_k \, c^\dagger = \begin{bmatrix} 1 + ik/2 & -ik/2 \\ ik/2 & 1 - ik/2 \end{bmatrix} \tag{4.D.15c}$$

is the *parabolic class*. Notice that the conjugacy classes of $\mathrm{sl}(2,\mathbb{R})$ correspond to different physical evolutions generated by the time-periodic HO Hamilotian in Eq.(4.7.1). Indeed, if we consider the time evolution operator after one driving period $\hat{U}(t_0 + \mathcal{T}, t_0) \in \mathrm{su}(1,1)$, we do expect that:

1. if $\hat{U}(t_0 + \mathcal{T}, t_0)$ belongs to the elliptic conjugacy class then the time evolution of the system is stable

2. if $\hat{U}(t_0+\mathcal{T}, t_0)$ belongs to the hyperbolic conjugacy class then the evolution of the system is unstable

and the latter are separated by an intermediate unstable regime associated with the parabolic subset.

4.E Mehler kernels

We recall the general definition of the Mehler kernel:

$$\mathrm{K}_e(x,y|\tau) \equiv \sum_{n=0}^{\infty} \psi_n(x)\,\psi_n(y)\,e^{-(n+\frac{1}{2})\tau} = \frac{e^{-\frac{y^2}{2}+\frac{x^2}{2}}\; e^{-\frac{\tau}{2}}\; e^{-\frac{(x-ye^{-\tau})^2}{1-e^{-2\tau}}}}{\sqrt{\pi(1-e^{-2\tau})}} \tag{4.E.1}$$

where ψ_n are the eigenstates of an harmonic oscillator with unit frequency. In the case of imaginary time $\tau = it$, $t \in \mathbb{R}$, the kernel can be written in the form:

$$\mathrm{K}_e(x,y|it) = \frac{\exp(\frac{i}{2}(x^2+y^2)\cot(t) - i\,xy/\sin(t))}{\sqrt{2\pi i\,\sin(t)}} \tag{4.E.2}$$

and it is the Green's function of an harmonic oscillator of unit frequency, namely, $(\partial_t \pm (-\partial_x^2 + x^2))\mathrm{K}_e = 0$, see e.g. [Ber04] (pg. 153-4).
The Green kernel in the hyperbolic case is by definition

$$\mathrm{K}_h(x,y|\tau) = \int_{\mathbb{R}} \mathrm{d}q\;\chi_q^{+*}(x)\,\chi_q^{+}(y)\;e^{iq\tau} + \;(+ \leftrightarrow -), \tag{4.E.3}$$

where $\chi_q^{\pm}$ are the eigenfunctions of the unit frequency harmonic repulsor $-\frac{i}{2}(\partial_x^2 + x^2)\,\chi_q^{\pm}(x) = -iq\,\chi_q^{\pm}(x)$ [Unt12]:

$$\begin{aligned}\chi_q^{\pm}(x) = \frac{e^{-q\pi/4-3i\pi/8}}{\sqrt{\pi}}\,2^{-iq/2}\,e^{-ix^2/2}\Big[&\Gamma[\tfrac{1}{2}(\tfrac{1}{2}-iq)]\;{}_1F_1[\tfrac{1}{4}-i\tfrac{q}{2};\tfrac{1}{2};ix^2]\\ &\pm 2x\,e^{i\pi/4}\,\Gamma[\tfrac{1}{2}(\tfrac{3}{2}-iq)]\;{}_1F_1[\tfrac{3}{4}-i\tfrac{q}{2};\tfrac{3}{2};ix^2]\Big]\end{aligned} \tag{4.E.4}$$

in which ${}_1F_1$ are the Kummer's Hypergeometric functions. By construction,

$$\int_{\mathbb{R}} \mathrm{d}y\;\mathrm{K}_h(x,y|\tau)\;\mathrm{K}_h(y,z|\tau') = \mathrm{K}_h(x,z|\tau+\tau')\,, \tag{4.E.5}$$

i.e. K_h is a propagator,

$$(\partial_\tau + \frac{i}{2}(\partial_x^2 + x^2))\,\mathrm{K}_h(x,y|\tau) = 0, \tag{4.E.6}$$

and

$$\lim_{\tau\to 0}\mathrm{K}_h(x,y|\tau) = \delta(x-y). \tag{4.E.7}$$

Performing a complex rotation $(x, y) \mapsto (x\, e^{i\pi/4}, y\, e^{i\pi/4})$ on the space coordinates of the real-time Mehler kernel, one sees that

$$\mathrm{K}_e(e^{i\pi/4}x\,,\, e^{i\pi/4}y\,|t) = \frac{\exp(-\frac{i}{2}(x^2+y^2)\coth(t) + i\,xy/\sinh(t))}{\sqrt{2\pi\,\sinh(t)}} \tag{4.E.8}$$

satisfies the same equation (4.E.6) as K_h and the same initial condition (4.E.7). Thus, the kernel (4.E.8) coincides with K_h.

4.F Monodromy matrix for a square-wave frequency

We investigate the monodromy matrix of a harmonic Hamiltonian in (4.7.1) with square wave frequency (4.7.7) by considering the associated Hill's equation:

$$\ddot{y}(t) + \omega^2(t)\, y(t) = 0\,, \tag{4.F.1}$$

with initial conditions $y(0)$ and $\dot{y}(0)$. In the interval $0 \le t \le \tau$, where $\omega(t) = \omega_1$, a set of independent solutions is given by

$$Y(t) \equiv \begin{bmatrix} y(t) \\ \dot{y}(t) \end{bmatrix} = \begin{bmatrix} \cos(\omega_1 t) & \sin(\omega_1 t)/\omega_1 \\ -\omega_1 \sin(\omega_1 t) & \cos(\omega_1 t) \end{bmatrix} \begin{bmatrix} y(0) \\ \dot{y}(0) \end{bmatrix}. \tag{4.F.2}$$

For times $\tau \le t \le 2\pi$, we can proceed in the same way updating the initial conditions to $Y(\tau)$. The solution now reads

$$Y(t) = \begin{bmatrix} \cos(\omega_2(t-\tau)) & \sin(\omega_2(t-\tau))/\omega_2 \\ -\omega_2 \sin(\omega_2(t-\tau)) & \cos(\omega_2(t-\tau)) \end{bmatrix} Y(\tau). \tag{4.F.3}$$

From the definition of Eq.(4.7.2) and using the last results we obtain:

$$\begin{aligned} \mathbb{M}(\omega) = &\begin{bmatrix} \cos(\omega_2(2\pi-\tau)) & \sin(\omega_2(2\pi-\tau))/\omega_2 \\ -\omega_2 \sin(\omega_2(2\pi-\tau)) & \cos(\omega_2(2\pi-\tau)) \end{bmatrix} \\ &\times \begin{bmatrix} \cos(\omega_1 t) & \sin(\omega_1\tau)/\omega_1 \\ -\omega_1 \sin(\omega_1\tau) & \cos(\omega_1\tau) \end{bmatrix} \end{aligned} \tag{4.F.4}$$

with trace given by [Mag66][§]

$$\mathrm{tr}(\mathbb{M}(\omega)) = 2\cos(\omega_1\tau)\cos(\omega_2(2\pi-\tau)) - \left(\frac{\omega_1}{\omega_2} + \frac{\omega_2}{\omega_1}\right)\sin(\omega_1\tau)\sin(\omega_2(2\pi-\tau)). \tag{4.F.5}$$

[§]Notice that a factor 1/2 is missing in the second term of this expression in [Mag66] pg.114.

Chapter 5

Non-equilibrium dynamics in open quantum systems

Abstract

In this chapter, we move to the description of the non-equilibrium behaviors arising in open quantum systems i.e., in quantum systems that exchange information with an environment, see Sec.5.1. In particular, our focus will be to driven markovian open quantum systems which are suitably described in terms of time-dependent Lindblad master equations. In Sec.5.2, we introduce a vectorization procedure that casts the Lindblad master equation into a "Schrödinger-like" equation which has but a non-unitary character due to the dissapation mechanisms.
Next, in Sec.5.3 we construct a time-independent (super) operator basis for a generic time-dependent Liouvillean generator whose elements form a closed algebraic structure. Notice that the decomposition of the Liouvillean in terms of the elements of this basis moves the model and the time dependences in a set of classical functions leading to a great computational advantage. Moreover, having a closed algebra allows us to extend the algebraic approach of Sec.3.1.2 to the case of open quantum systems and to write down formal exact solutions to generic time-dependent Lindblad equations (see Sec.5.4).
In Sec.5.5, we focus on the case of a periodic driving with the aim of extending standard Floquet theory (see Sec.3.1) to the Floquet-Lindblad framework. In this context, we show how a generalized rotating frame transformation can lead to an exact Floquet description of the open system, reproducing high-frequency perturbative results which have been previously derived [Dai16, Dai17].

We also provide an application of the Floquet-Lindblad approach to the analysis of the finite-time operation of quantum heat-engines, see Sec.5.7 and Sec.5.8.2. The analysis of these quantum devices relies in fact on the existence of a stroboscopic steady-state for the reduced density matrix which can be conviently investigated through the analysis of the spectrum of the Floquet Liouvillean.

5.1 Introduction to open quantum systems

With the name of open quantum system we refer to a quantum system of interest $\mathcal{S}$ that interacts with an external environment $\mathcal{R}$ which is typically inaccessible due to its large number of degrees of freedom. As a consequence, one is not able to investigate the unitary dynamics that takes place in the entire Hilbert space $\mathscr{H}_{\rm tot} = \mathscr{H}_{\mathcal{S}} \otimes \mathscr{H}_{\mathcal{R}}$ and therefore opts for an effective description in $\mathscr{H}_{\mathcal{S}}$ where the degrees of freedom of $\mathcal{R}$ are traced out.
In many cases, the correlations between the system $\mathcal{S}$ and environment $\mathcal{R}$ can be neglected and this effective dynamics is conveniently described in terms of an appropriate equation of motion for the reduced density matrix $\hat{\rho}$ in $\mathcal{S}$ of the form

$$\frac{\mathrm{d}}{\mathrm{d}t}\hat{\rho}(t) = -i[\hat{H}, \hat{\rho}(t)] + \check{\mathcal{D}}\,\hat{\rho}(t) \tag{5.1.1}$$

where the first term reproduces the standard unitary evolution generated by an effective Hamiltonian $\hat{H}$ whereas $\check{\mathcal{D}}$ accounts for the dissipative contribution arising from the interaction with the environment.
Notice that Eq.(5.1.1) has the form of a master equation. In fact, if we interpret $\hat{\rho}$ as a quantum probability distribution of states, the effect of $\check{\mathcal{D}}$ can be viewed as a gain (and loss) source that affects the time-evolution of $\hat{\rho}$.
Clearly, there must be some constraints on the general structure of Eq.(5.1.1) due to the unitary character of the global evolution. Moreover, a physical evolution must preserve the general properties of a density matrix. As we shall see in the following section, these conditions are summarized in the so-called *complete-positive-trace-preserving* (CPTP) property of the dynamical map which evolves the state $\hat{\rho}$ according to Eq.(5.1.1).

5.1.1 Dynamical maps

The general conditions on the effective dynamics of an open quantum system $\mathcal{S}$ can be investigated through the analysis of the global unitary problem. Indeed, at any instant of time, the time-evolved state $\hat{\rho}(t)$ in $\mathcal{S}$ is obtained from the

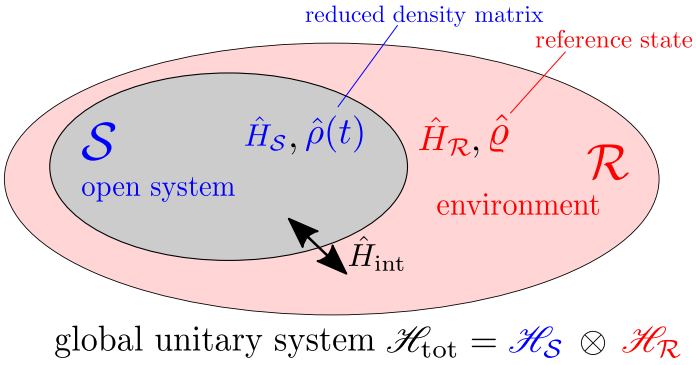

Figure 5.1: **Illustration of open quantum systems.** Consider a bipartition of a generic quantum system into a system of interest $\mathcal{S}$ (*gray region*) and the remaining degrees of fredoom that we call environment $\mathcal{R}$ (*light red region*). The subsystems evolve according to their internal dynamics ($\hat{H}_{\mathcal{S}}$ and $\hat{H}_{\mathcal{R}}$ respectively) and have some interactions $\hat{H}_{\rm int}$. Clearly, if we consider the global system, the time evolution is unitary and it is generated by the total Hamiltonian $\hat{H}_{\rm tot} = \hat{H}_{\mathcal{S}} + \hat{H}_{\mathcal{R}} + \hat{H}_{\rm int}$. On the other hand, if we focus only on the subsystem $\mathcal{S}$ the reduced dynamics shows some non-unitary effects due to the interactions with the environment.

density matrix of the global system $\hat{\rho}_{\rm tot}(t)$ with a partial trace operation over the degrees of freedom of $\mathcal{R}$

$$\hat{\rho}(t) \equiv {\rm tr}_{\mathcal{R}}(\hat{\rho}_{\rm tot}(t)) = \sum_{\nu} \langle \varphi_\nu | \hat{\rho}_{\rm tot}(t) | \varphi_\nu \rangle \ , \tag{5.1.2}$$

where $\{|\varphi_\nu\rangle\}$ is a reference basis of $\mathscr{H}_{\mathcal{R}}$. The global unitary problem has the formal solution

$$\hat{\rho}_{\rm tot}(t) = \hat{U}(t,t_0)\ \hat{\rho}_{\rm tot}(t_0)\ \hat{U}^\dagger(t,t_0) \tag{5.1.3}$$

in terms of the unitary time-evolution operator

$$\hat{U}(t,t_0) \equiv \mathbf{T}\ \exp\left(-i \int_{t_0}^{t} \hat{H}_{\rm tot}(t')\, {\rm d}t'\right), \tag{5.1.4}$$

with $\mathbf{T}$ denoting the time-ordered product. Here, the Hamiltonian $\hat{H}_{\rm tot} = \hat{H}_{\mathcal{S}} + \hat{H}_{\mathcal{R}} + \hat{H}_{\rm int}$ is made of the sum of the internal dynamics of the subsystems $\mathcal{S}$ and $\mathcal{R}$ and of the interactions $\hat{H}_{\rm int}$ between them, see Fig.5.1. It is also important to assume that the system and the environment are initially uncorrelated i.e.,

$$\hat{\rho}_{\rm tot}(t_0) = \hat{\rho}(t_0) \otimes \hat{\varrho} \tag{5.1.5}$$

where $\hat{\varrho}$ is a reference state of $\mathcal{R}$. In this way one can prepare at $t = t_0$ the system in the desired state $\hat{\rho}(t_0)$ considering the influence of the external environment only at later times $t > t_0$.
Next, from Eq.(5.1.3) and Eq.(5.1.5), using completeness relations

$$\sum_{\alpha} |\alpha\rangle \langle\alpha| = \hat{\mathbb{1}} \tag{5.1.6}$$

for $\{|\alpha\rangle\}$ an orthonormal basis of $\mathscr{H}_{\rm tot}$, we obtain[§]

$$\hat{\rho}_{\rm tot}(t) = \hat{U}\ \hat{\rho}_{\rm tot}(t_0)\ \hat{U}^\dagger = \sum_{\alpha,\gamma,\delta,\beta} |\alpha\rangle \langle\alpha|\hat{U}|\gamma\rangle \langle\gamma|\hat{\rho}(t_0)\otimes\hat{\varrho}|\delta\rangle \langle\delta|\hat{U}^\dagger|\beta\rangle \langle\beta| \tag{5.1.7}$$

that is,

$$\hat{\rho}_{\rm tot}(t) = \sum_{\alpha,\gamma,\delta,\beta} |\alpha\rangle\, U_{\alpha\gamma}\ \left(\hat{\rho}(t_0)\otimes\hat{\varrho}\,\right)_{\gamma\delta}\ U^*_{\delta\beta}\,\langle\beta|\ , \tag{5.1.8}$$

with the shorthand notation $U_{\alpha,\beta} \equiv \langle\alpha|\hat{U}|\beta\rangle$. With a proper choice of the basis, we can express the elements $|\alpha\rangle \in \mathscr{H}_{\rm tot}$ as tensor products $|\alpha\rangle = |n\rangle \otimes |\mu\rangle \equiv |n\otimes\mu\rangle$, with $|n\rangle \in \mathscr{H}_{\mathcal{S}}$ and $|\mu\rangle \in \mathscr{H}_{\mathcal{R}}$. Doing so, Eq.(5.1.8) becomes[¶]

$$\hat{\rho}_{\rm tot}(t) = \sum_{n,k,l,m}^{[\mathcal{S}]} \sum_{\mu,\nu,\lambda,\eta}^{[\mathcal{R}]} |n\otimes\mu\rangle\, U_{nk\,;\,\mu\nu}\ \left(\hat{\rho}(t_0)\right)_{kl} \otimes \left(\hat{\varrho}\right)_{\nu\lambda}\ U^*_{lm\,;\,\lambda\eta}\,\langle m\otimes\eta|\,, \tag{5.1.9}$$

where now $U_{nk\,;\,\mu\nu} \equiv \langle n\otimes\mu|\hat{U}|k\otimes\nu\rangle$. Hence, we use the spectral decomposition in order to write the reference state $\hat{\varrho}$ as

$$\hat{\varrho} = \sum_{\nu}^{[\mathcal{R}]} \lambda_\nu\ |\nu\rangle \langle\nu|\,, \quad (\lambda_\nu \geq 0; \quad \sum_{\nu} \lambda_\nu = 1) \tag{5.1.10}$$

which then leads to

$$\hat{\rho}_{\rm tot}(t) = \sum_{n,k,l,m}^{[\mathcal{S}]} \sum_{\mu,\nu,\eta}^{[\mathcal{R}]} \lambda_\nu\ |n\otimes\mu\rangle\, U_{nk\,;\,\mu\nu}\ \left(\hat{\rho}(t_0)\right)_{kl}\ U^*_{lm\,;\,\nu\eta}\,\langle m\otimes\eta|\,. \tag{5.1.11}$$

Finally, after a partial trace over $\mathcal{R}$ (that fixes $\mu = \eta$), we get

$$\hat{\rho}(t) = {\rm tr}_{\mathcal{R}}\left(\hat{\rho}_{\rm tot}(t)\right) = \sum_{n,k,l,m}^{[\mathcal{S}]} \sum_{\mu,\nu}^{[\mathcal{R}]} \lambda_\nu\ |n\otimes\mu\rangle\, U_{nk\,;\,\mu\nu}\,\left(\hat{\rho}(t_0)\right)_{kl}\ U^*_{lm\,;\,\nu\mu}\,\langle m\otimes\mu| \tag{5.1.12}$$

[§]For a better typography, we drop out the time-indices of $\hat{U}(t,t_0)$.

[¶]The notations $[\mathcal{S}]$ (system), $[\mathcal{R}]$ (reservoir) on top of the sums have been inserted to help the reader in understanding the nature of the indices. They do not have any other particular meaning.

or equivalently,

$$\hat{\rho}(t) = \mathrm{tr}_{\mathcal{R}}\left(\hat{\rho}_{\mathrm{tot}}(t)\right) = \sum_{\mu,\nu}^{[\mathcal{R}]} \lambda_\nu \, \langle\mu|\hat{U}(t,t_0)|\nu\rangle \, \hat{\rho}(t_0) \, \langle\nu|\hat{U}^\dagger(t,t_0)|\mu\rangle \, . \tag{5.1.13}$$

We conclude that the effective dynamics in $\mathcal{S}$ has the generic form [Kra71]

$$\hat{\rho}(t) \equiv \sum_{\alpha=(\mu,\nu)}^{[\mathcal{R}]} \hat{W}_\alpha(t,t_0) \, \hat{\rho}(t_0) \, \hat{W}_\alpha^\dagger(t,t_0) \tag{5.1.14}$$

with a set of operators $\hat{W}_\alpha \in \mathrm{end}(\mathscr{H}_{\mathcal{S}})$, $\alpha \equiv (\mu,\nu)$, defined as

$$\hat{W}_\alpha(t,t_0) \equiv \sqrt{\lambda_\nu} \, \langle\mu|\hat{U}(t,t_0)|\nu\rangle \, . \tag{5.1.15}$$

Here, we notice that the decomposition (5.1.14) implies that the reduced dynamics of $\hat{\rho}$ is made out of the sum of several elementary processes $\hat{W}_\alpha$ that implement consistently the effective role of the internal dynamics and of the interactions with environment (notice that α is an index of $\mathcal{R}$). Notice also that, by construction, the operators $\hat{W}_\alpha$ satisfy a completeness condition:

$$\sum_\alpha \hat{W}_\alpha \, \hat{W}_\alpha^\dagger = \hat{\mathbb{1}} \tag{5.1.16}$$

and that the trace of $\hat{\rho}$ is preserved

$$\mathrm{tr}(\hat{\rho}(t)) = \mathrm{tr}(\hat{\rho}(t_0)) = 1, \tag{5.1.17}$$

as follows simply from (5.1.16) using the cyclicity property of the trace.

We now introduce the dynamical map $\check{\Lambda}$:

$$\hat{\rho}(t) \equiv \check{\Lambda}(t,t_0) \, \hat{\rho}(t_0) = \mathrm{tr}_{\mathcal{R}}\left(\hat{\rho}_{\mathrm{tot}}(t)\right), \tag{5.1.18}$$

that implements a (non-unitary) reduced dynamics in $\mathcal{S}$ and that formally solves the Eq.(5.1.1), see Fig.5.2. Notice that the notation $\check{\Lambda}$ stands for a *super-operator*

$$\hat{\rho}' = \mathrm{F}_\Lambda(\hat{\rho}) \equiv \check{\Lambda} \, \hat{\rho} \tag{5.1.19}$$

i.e., an object $\mathrm{F}_\Lambda(\cdot)$ that acts on an operator $\hat{\rho}$ and that produces a new operator $\hat{\rho}'$. We shall keep this notation in the following.

From the analysis of the global unitary evolution, we are able to state the following conditions on the dynamical map:

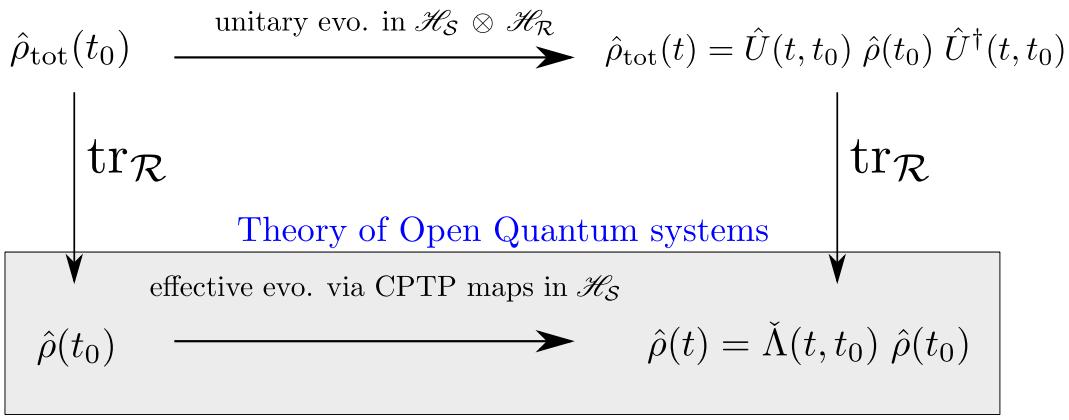

Figure 5.2: **Reduced dynamics in open systems.** We describe the reduced dynamics of an open system $\mathcal{S}$ with the help of a dynamical map $\check{\Lambda}$ that acts on the reduced density matrix $\hat{\rho}$ providing its time evolution (*gray box*). The latter must satisfy some CPTP conditions that can be derived by a formal looking into the global unitary problem. The global unitary problem and the reduced dynamics are then connected at any instant of time with a partial trace operation over the degrees of freedom of the environment.

- It always has a decomposition (5.1.14):

$$\check{\Lambda}(t,t_0)\,\bullet \equiv \sum_\alpha \hat{W}_\alpha(t,t_0)\,\bullet\,\hat{W}_\alpha^\dagger(t,t_0) \tag{5.1.20}$$

  with a set of elementary processes $\hat{W}_\alpha \in \mathrm{end}(\mathscr{H}_\mathcal{S})$. This relation is known as *Kraus decomposition* of a dynamical map.

- It satisfies a completeness relation

$$\check{\Lambda}\,\hat{\mathbb{1}} = \hat{\mathbb{1}} \tag{5.1.21}$$

  as follows from (5.1.16); this automatically implies a trace preservation property.

- It is a positive-definite map since it maps density matrices into density matrices. More precisely, a stronger condition called *complete posivity* is satisfied, see e.g. [Ali87, Bre07]. Complete positivity condition can be understood as follows.
  Consider a positive linear map ϕ so that $\forall\, a \geq 0$ its image $\phi(a) \geq 0$. Any linear map $\phi : A \to B$ allows then to define an extended map

$\hat{\mathbb{1}} \otimes \phi : \mathbb{C}^n \otimes A \to \mathbb{C}^n \otimes B$, which acts trivially on the first space. If the map $\hat{\mathbb{1}} \otimes \phi$ is a positive map, then we will say that ϕ is n-positive. If this condition holds for any $n = 1, 2, \ldots$ then ϕ is said to be complete positive.
Now, suppose that your open system is made of a subsystem $\mathcal{S}$ plus a n-level system with which $\mathcal{S}$ does not interact. Moreover, let us suppose that the n-level system evolves with a trivial Hamiltonian $\hat{H}_n = 0$. For an observer focused on $\mathcal{S}$, we cannot distinguish the situations in which the n-level system is present or not. The joined dynamical map is then $\check{\Lambda}_n = \hat{\mathbb{1}} \otimes \check{\Lambda}$ and it acts on $\mathrm{end}(\mathbb{C}^n \otimes \mathscr{H}_{\mathcal{S}})$. Since $\check{\Lambda}_n$ is a dynamical map, we have to require positivity for any n. This then implies complete positivity of the dynamical (sub) map $\check{\Lambda}$ acting on $\mathcal{S}$.

Heisenberg picture

The expectation value of any observable $\hat{O} \in \mathrm{end}(\mathscr{H}_{\mathcal{S}})$ can be computed as

$$\langle \hat{O} \rangle \equiv \mathrm{tr}(\hat{\rho}(t)\, \hat{O}) \tag{5.1.22}$$

where the time evolution is carried by the state $\hat{\rho}(t)$. In this sense, Eq.(5.1.22) represents the Schrödinger picture of the reduced time evolution. Equivalently, we can consider an Heisenberg picture using the *duality relation*:

$$\mathrm{tr}(\hat{\rho}(t)\, \hat{O}) = \mathrm{tr}(\check{\Lambda}(t, t_0)\, \rho(t_0)\, \hat{O}) = \mathrm{tr}(\rho(t_0)\, \check{\Lambda}^{\star}(t, t_0)\, \hat{O}) = \mathrm{tr}(\rho(t_0)\, \hat{O}(t)) \tag{5.1.23}$$

where the dual-map $\check{\Lambda}^{\star}$, responsible for the time evolution of the operator $\hat{O}$, has the Kraus decomposition:

$$\check{\Lambda}^{\star}(t, t_0)\, \hat{O} = \sum_{\alpha} \hat{W}_{\alpha}^{\dagger}(t, t_0)\, \hat{O}\, \hat{W}_{\alpha}(t, t_0)\,, \qquad \sum_{\alpha} \hat{W}_{\alpha}^{\dagger}(t, t_0)\, \hat{W}_{\alpha}(t, t_0) = \hat{\mathbb{1}}; \tag{5.1.24}$$

as follows from (5.1.14), (5.1.16) and (5.1.23).

5.1.2 Lindblad master equation

In this section, we would like to derive the general structure of a quantum master equation (5.1.1) that generates the reduced time evolution in $\mathcal{S}$.
One can easily see that a generic form of a quantum master equation is

$$\frac{\mathrm{d}}{\mathrm{d}t}\hat{\rho}(t) = \check{\mathscr{L}}(t)\, \hat{\rho}(t) + \int_{t_0}^{t} \mathrm{d}t'\, \check{\kappa}(t')\, \hat{\rho}(t - t') \tag{5.1.25}$$

where $\check{\mathscr{L}}$ is a markovian generator whereas $\check{\kappa}$ represents a memory kernel. In fact, in general, the typical relaxation times of the environment can be much larger than those of the open system and thus the reduced dynamics in $\mathcal{S}$ will be inevitably affected also by the previous configurations of the system, see e.g. [Kho14, Har15, Bre16, Ara19].
Nevertheless, when the environment is large and weakly-coupled to the open system, one can reasonably assume that the decay of the environment's excitations is exponentially fast and thus that a markovian approximation holds. Notice that a large variety of physical systems proved to be well-described in the markovian approximation, see e.g. [Spo80, Pro08, Kos11, Pro11a, Kar13, Pop13, Bcv14, Wal16, Mon17a, Mon17b, Bau17, Bcv17, Kos17, Wal18, Sco18a, Bau19, Rib19, Sco19].
Markov approximation in turn implies for the dynamical map $\check{\Lambda}$ a semi-group property i.e.,

$$\check{\Lambda}(t,s)\,\check{\Lambda}(s,t_0) = \check{\Lambda}(t,t_0); \quad \forall\, t \geq s \geq t_0 \tag{5.1.26}$$

and allows to write a generator of the reduced time evolution as

$$\frac{\mathrm{d}}{\mathrm{d}t}\hat{\rho}(t) = \check{\mathscr{L}}(t)\,\hat{\rho}(t); \tag{5.1.27}$$

$$\frac{\mathrm{d}}{\mathrm{d}t}\,\hat{O}(t) = \frac{\partial}{\partial t}\hat{O}(t) + \check{\mathscr{L}}^{\star}(t)\,\hat{O}(t); \tag{5.1.28}$$

for the Schrödinger and Heisenberg picture respectively. We will refer to the generator $\check{\mathscr{L}}$ as *Liouvillean*. Clearly, the Liouvillean is related to the dynamical map through the formal solution

$$\check{\Lambda}(t,t_0) \equiv \mathbf{T}\exp\left(\int_{t_0}^{t}\check{\mathscr{L}}(t')\,\mathrm{d}t'\right) \tag{5.1.29}$$

and similarly for the dual-generator $\check{\mathscr{L}}^{\star}$.

The general structure of a markovian generator for an open system of finite Hilbert-space dimension $\dim(\mathscr{H}_{\mathcal{S}}) = n$ can be easily derived considering the differential action of the dynamical map close to the identity. First, we introduce a traceless orthonormal set of operators $\{\hat{F}_k\}$, $k = 1, \ldots, n^2-1$

$$\mathrm{tr}(\hat{F}_k^{\dagger}\,\hat{F}_l) = \delta_{kl}\,, \quad \mathrm{tr}(\hat{F}_k) = 0\,,\ \forall\, k,l \tag{5.1.30}$$

and we add to this set the normalized identity $\hat{F}_0 = \hat{\mathbb{1}}/n$. In this basis, the dynamical map reads

$$\check{\Lambda}(t,s)\,\hat{\rho}(s) = \sum_{k,l=0}^{n^2-1} C_{kl}(t,s)\,\hat{F}_k\,\hat{\rho}(s)\,\hat{F}_l^{\dagger} \tag{5.1.31}$$

where $C_{kl}(t,s)$ is a semi-positive hermitian matrix. Then, by construction

$$\begin{aligned}\check{\mathscr{L}}(t)\,\hat{\rho} &= \lim_{\epsilon\to 0}\frac{\check{\Lambda}(t+\epsilon,t)\,\hat{\rho}-\hat{\rho}}{\epsilon}\\ &= \lim_{\epsilon\to 0}\Big(\frac{C_{00}(t+\epsilon,t)-n^2}{n^2\,\epsilon}\;\hat{\rho}+\sum_{k=1}^{n^2-1}\frac{C_{0k}(t+\epsilon,t)}{n\,\epsilon}\;\hat{F}_k\,\hat{\rho}\\ &+\sum_{k=1}^{n^2-1}\frac{C^*_{0k}(t+\epsilon,t)}{n\,\epsilon}\;\hat{\rho}\,\hat{F}_k^\dagger+\sum_{k,l=1}^{n^2-1}\frac{C_{kl}(t+\epsilon,t)}{\epsilon}\;\hat{F}_k\,\hat{\rho}\,\hat{F}_l^\dagger\Big),\end{aligned}\tag{5.1.32}$$

where we used the shorthand $\hat{\rho}=\hat{\rho}(t)$. Now, if we define

$G(t)\equiv\lim_{\epsilon\to0}\frac{1}{2n^2\,\epsilon}\;(C_{00}(t+\epsilon,t)-n^2)$ a real function;

$\hat{K}(t)\equiv\sum_{k=1}^{n^2-1}\lim_{\epsilon\to0}\frac{1}{n\,\epsilon}\,C_{0k}(t+\epsilon,t)\,\hat{F}_k$;

$\hat{A}(t)\equiv\hat{K}(t)+G(t)$;

$\gamma_{kl}(t)\equiv\lim_{\epsilon\to0}\frac{1}{\epsilon}\,C_{kl}(t+\varepsilon,t)$ a semi-positive hermitian matrix,

we obtain

$$\check{\mathscr{L}}(t)\,\hat{\rho}=\hat{A}(t)\,\hat{\rho}+\hat{\rho}\,\hat{A}^\dagger(t)+\sum_{k,l=1}^{n^2-1}\gamma_{kl}(t)\,\hat{F}_k\,\hat{\rho}\,\hat{F}_l^\dagger\tag{5.1.33}$$

and using the trace preservation property ($\mathrm{tr}(\check{\mathscr{L}}(t)\,\hat{\rho})=0$)

$$\hat{A}(t)+\hat{A}^\dagger(t)=-\sum_{k,l=1}^{n^2-1}\gamma_{kl}(t)\hat{F}_l^\dagger\,\hat{F}_k\,.\tag{5.1.34}$$

Writing then $\hat{A}(t)\,\hat{\rho}+\hat{\rho}\,\hat{A}^\dagger(t)=[\frac{\hat{A}(t)-\hat{A}^\dagger(t)}{2},\hat{\rho}]+\{\frac{\hat{A}(t)+\hat{A}^\dagger(t)}{2},\hat{\rho}\}$ and introducing the quantity

$$\hat{H}(t)\equiv\frac{\hat{A}^\dagger(t)-\hat{A}(t)}{2i},\tag{5.1.35}$$

which is hermitian $\hat{H}(t)=\hat{H}^\dagger(t)$ by construction, we finally obtain

$$\check{\mathscr{L}}(t)\,\rho=-\,i[\hat{H}(t),\hat{\rho}]+\sum_{k,l=1}^{n^2-1}\gamma_{kl}(t)\,\Big(\hat{F}_k\,\hat{\rho}\,\hat{F}_l^\dagger-\frac{1}{2}\left\{\hat{F}_l^\dagger\,\hat{F}_k,\hat{\rho}\right\}\Big)\,.\tag{5.1.36}$$

Moreover, since $\gamma_{kl}(t)$ is semi-positive definite, there always exists a suitable linear combination $\hat{L}_\alpha \in \mathrm{end}(\mathscr{H}_\mathcal{S})$ of the operators $\{\hat{F}_k\}$ in terms of which the generator assumes a diagonal structure:

$$\check{\mathscr{L}}(t)\,\hat{\rho} = -i[\hat{H}(t),\hat{\rho}] + \sum_{\alpha=1}^{n^2-1} \Gamma_\alpha(t)\,\left(\hat{L}_\alpha\,\hat{\rho}\,\hat{L}_\alpha^\dagger - \frac{1}{2}\{\hat{L}_\alpha^\dagger\,\hat{L}_\alpha,\hat{\rho}\}\right); \quad \Gamma_\alpha(t) \geq 0\,. \tag{5.1.37}$$

This result is known as *Lindblad master equation* [Lin75, Lin76, Gor76] and it was proven to be the most general markovian generator for the reduced dynamics of a finite-dimensional open system. However, for a large class of unbounded operators, an expression similar to Eq. (5.1.36) can be written and defines rigorously a quantum dynamical semi-group (5.1.26). Notice that in Eq.(5.1.36) the operator $\hat{H} = \hat{H}^\dagger$ can be interpreted as an effective Hamiltonian for $\mathcal{S}$ that includes the internal dynamics and other possible effects due to the surroundings whereas the set of operators $\hat{L}_\alpha \in \mathrm{end}(\mathscr{H}_\mathcal{S})$, called *jump operators*, accounts for elementary dissipative processes. The matrix $\mathrm{diag}(\Gamma_\alpha)$ is called *relaxation matrix* and it contains the relevant physical information about the dissipation, as obtained from phenomenological considerations. Its elements can be interpreted therefore as e.g. lifetimes or as relaxation times associated with a specific dissipative mechanism $\hat{L}_\alpha$.

Notice that it is possible to write a Lindblad equation also for the dual-space. In fact, from Eq.(5.1.23), taking a time derivative, we obtain

$$\frac{\mathrm{d}}{\mathrm{d}t}\,\mathrm{tr}(\hat{\rho}(t)\,\hat{O}) = \mathrm{tr}((\check{\mathscr{L}}(t)\,\hat{\rho}(t))\,\hat{O}) = \mathrm{tr}(\hat{\rho}(t_0)\,(\check{\mathscr{L}}^\star(t)\,\hat{O}(t))) \tag{5.1.38}$$

that leads to the Heisenberg Lindblad generator

$$\check{\mathscr{L}}^\star(t)\,\hat{O} = i[\hat{H}(t),\hat{O}] + \sum_{k,l=1}^{n^2-1} \gamma_{kl}(t)\,\left(\hat{F}_l^\dagger\,\hat{O}\,\hat{F}_k - \frac{1}{2}\left\{\hat{F}_l^\dagger\,\hat{F}_k,\hat{O}\right\}\right). \tag{5.1.39}$$

For future convenience, we can finally write the Lindblad equation (5.1.36) as

$$\check{\mathscr{L}}(t)\,\hat{\rho} = \check{\mathcal{H}}(t)\,\hat{\rho} + \check{\mathcal{D}}(t)\,\hat{\rho} \tag{5.1.40}$$

where we have introduced the Hamiltonian (or unitary) generator:

$$\check{\mathcal{H}}(t)\,\bullet \equiv -i[\hat{H}(t),\bullet] \tag{5.1.41}$$

and the non-Hamiltonian (or non-unitary) generator

$$\check{\mathcal{D}}(t)\,\bullet \equiv \check{\mathscr{L}}(t)\,\bullet - \check{\mathcal{H}}(t)\,\bullet. \tag{5.1.42}$$

5.1.3 How to build a markovian master equation?

In principle, the master equation (5.1.36) should be derived from the Hamiltonian of the global unitary system using markovian approximation. However, this easily runs into difficulties due to the large number of degrees of freedom in question and it becomes very often practically impossible.
An alternative approach is thus to consider only the effective role of the environment acting on the open system with the help of some phenomenological hints. To do so, let us consider first a classical balance equation of the form [Ali87]:

$$\frac{\mathrm{d}}{\mathrm{d}t}\, p_k(t) = \sum_{l=1}^{n} a_{kl}\, p_l(t) - a_{lk}\, p_k(t)\,, \quad k = 1, \ldots, n \tag{5.1.43}$$

where p_k is a probability associated to a state k and a_{kl} are transition amplitudes with which we take into account gains and losses of the state. We may associate to the matrix a_{kl} the transition map

$$(M\, x)_k = \sum_{l=1}^{n} a_{kl}\, x_l \tag{5.1.44}$$

and its dual

$$(M^\star x)_k = \sum_{l=1}^{n} a_{lk}\, x_l\,. \tag{5.1.45}$$

These are positive maps in the sense that they transform probabilities into probabilities. Writing the classical equation in an operatorial form we have

$$\frac{\mathrm{d}}{\mathrm{d}t}\, \vec{p}(t) = M\, \vec{p}(t) - \left(M^\star\, \vec{I}\right) \cdot \vec{p}(t) \tag{5.1.46}$$

where we introduced a probability distribution

$$\vec{p} \equiv \begin{bmatrix} p_1 \\ \ldots \\ p_n \end{bmatrix}, \tag{5.1.47}$$

with

$$\vec{I} \equiv \begin{bmatrix} 1 \\ \ldots \\ 1 \end{bmatrix} \tag{5.1.48}$$

a n-vector of units and the composition rule of two vectors reads

$$\vec{x} \cdot \vec{y} \equiv \begin{bmatrix} x_1\, y_1 \\ \ldots \\ x_n\, y_n \end{bmatrix}. \tag{5.1.49}$$

For the quantization of this classical master equation we have to replace [Ali87]:

1. the probability distribution $\vec{p}$ with a density matrix $\hat{\rho}$
2. the positive transition map M (and its dual) with a complete positive quantum transition map $\check{\Phi}$
3. the composition rule $x \cdot y$ of classical functions with a composition rule for operators $X \cdot Y \equiv \frac{1}{2}\{X, Y\}$

Thus, after making the replacements 1-3 and by adding the Hamiltonian part (that is absent in the classical equation), we obtain the formal writing for a quantum master equation

$$\frac{\mathrm{d}}{\mathrm{d}t}\,\hat{\rho} = -i[\hat{H}, \hat{\rho}] + \check{\Phi}\,\hat{\rho} - \frac{1}{2}\{\check{\Phi}^{\star}\hat{\mathbb{1}}, \hat{\rho}\}, \tag{5.1.50}$$

in terms of the quantum transition map $\check{\Phi}$.
Notice that these maps admit a Kraus decomposition (5.1.14): $\check{\Phi}\,\hat{\rho} = \sum_\alpha \hat{W}_\alpha\,\hat{\rho}\,\hat{W}_\alpha^{\dagger}$[§] and so they can be thought as the sum of independent elementary processes $\hat{W}_\alpha\,\hat{\rho}\,\hat{W}_\alpha^{\dagger}$. Using the phenomenological information about the nature of the open system $\mathcal{S}$ and of the environment $\mathcal{R}$, we can thus understand the dominant processes and guess a relevant form for the quantum transition map $\check{\Phi}$.

Two standard examples

Two simple examples of the phenomenological derivation of markovian master equations are briefly discussed in the following. First, let us consider the Hamiltonian of a quantum HO: $\hat{H} = \omega\,(\hat{a}^{\dagger}\,\hat{a} + \frac{1}{2})$, where $\hat{a}^{\dagger}$ ($\hat{a}$) is the standard creation (annihilation) operator satisfying $[\hat{a}, \hat{a}^{\dagger}] = 1$. The eigenstates of $\hat{H}$ are n-phonon states $|n\rangle$ with $\hat{a}^{\dagger}\,\hat{a}\,|n\rangle = n\,|n\rangle$ for $n = 1, 2$, etc.
We assume now that this oscillator interacts with an environment. The effects of the interaction can be, for instance, a friction force which decreases the energy of the oscillator and a pumping Langevin force which, on the other hand, increases the internal energy. In terms of phonons, we can consider the simplest case in which these processes correspond to the creation (annihilation) of a single-phonon excitation. So, we are looking for two quantum transition

[§]It is also easy to see that Eq.(5.1.50) reproduces the Lindblad master equation (5.1.36) if we insert the Kraus decomposition of the quantum transition map.

maps such that:

$$\begin{aligned} \check{\Phi}_1 \, |n\rangle \langle n| &= c_1^{(n)} \, |n+1\rangle \langle n+1| \\ \check{\Phi}_0 \, |n\rangle \langle n| &= c_0^{(n)} \, |n-1\rangle \langle n-1| \end{aligned} \tag{5.1.51}$$

with $c_{1,0}^{(n)}$ some constants. The simplest candidates for the maps above are

$$\begin{aligned} \check{\Phi}_1 \, \hat{\rho} &= \gamma_1 \, \hat{a}^\dagger \, \hat{\rho} \, \hat{a} \, , \qquad \gamma_1 \geq 0 \\ \check{\Phi}_0 \, \hat{\rho} &= \gamma_0 \, \hat{a} \, \hat{\rho} \, \hat{a}^\dagger \, , \qquad \gamma_0 \geq 0 \end{aligned} \tag{5.1.52}$$

which lead to a markovian master equation for the damped-pumped HO:

$$\begin{aligned} \frac{\mathrm{d}}{\mathrm{d}t} \, \hat{\rho} = &- i[\omega(\hat{a}^\dagger \, \hat{a} + \frac{1}{2}), \hat{\rho}] + \frac{\gamma_1}{2} \left(2 \, \hat{a}^\dagger \, \hat{\rho} \, \hat{a} - \{ \hat{a} \, \hat{a}^\dagger, \hat{\rho} \} \right) \\ &+ \frac{\gamma_0}{2} \left(2 \, \hat{a} \, \hat{\rho} \, \hat{a}^\dagger - \{ \hat{a}^\dagger \, \hat{a}, \hat{\rho} \} \right) . \end{aligned} \tag{5.1.53}$$

Next, consider a generic two-level system described by the Hamiltonian $\hat{H} = \sum_{k=x,y,z} h_k \, \hat{\sigma}^k$, where $\hat{\sigma}^k$ are Pauli operators. The eigenstates of the system are denoted with $|\uparrow\rangle$ and $|\downarrow\rangle$. Now suppose to insert the system in an optical cavity where the presence of some lasers can promote either absorption or emission processes. The latter correspond to the quantum maps:

$$\begin{aligned} \check{\Phi}_1 \, |\downarrow\rangle \langle\downarrow| &= c_1 \, |\uparrow\rangle \langle\uparrow| \\ \check{\Phi}_0 \, |\uparrow\rangle \langle\uparrow| &= c_0 \, |\downarrow\rangle \langle\downarrow| \end{aligned} \tag{5.1.54}$$

which are simply implemented in terms of ladder operators $\hat{\sigma}^\pm$ as

$$\begin{aligned} \check{\Phi}_1 \, \hat{\rho} &= \gamma_1 \, \hat{\sigma}^+ \, \hat{\rho} \, \hat{\sigma}^- \, , \qquad \gamma_1 \geq 0 \, , \\ \check{\Phi}_0 \, \hat{\rho} &= \gamma_0 \, \hat{\sigma}^- \, \hat{\rho} \, \hat{\sigma}^+ \, , \qquad \gamma_0 \geq 0 \, . \end{aligned} \tag{5.1.55}$$

The markovian master equation takes therefore the form

$$\begin{aligned} \frac{\mathrm{d}}{\mathrm{d}t} \, \hat{\rho} = &- i \sum_{k=x,y,z} h_k \, [\hat{\sigma}^k \, \hat{\rho}] + \frac{\gamma_1}{2} \left(2 \, \hat{\sigma}^+ \, \hat{\rho} \, \hat{\sigma}^- - \{ \hat{\sigma}^- \, \hat{\sigma}^+, \hat{\rho} \} \right) \\ &+ \frac{\gamma_0}{2} \left(2 \, \hat{\sigma}^- \, \hat{\rho} \, \hat{\sigma}^+ - \{ \hat{\sigma}^+ \, \hat{\sigma}^-, \hat{\rho} \} \right) . \end{aligned} \tag{5.1.56}$$

5.2 Vectorization procedure

We introduce a vectorization procedure that maps the space end($\mathscr{H}_{\mathcal{S}}$) of an open system $\mathcal{S}$ with $\dim(\mathscr{H}_{\mathcal{S}}) = n$, onto an isomorphic and isometric vector space $\mathfrak{K} \sim \mathbb{C}^{n^2}$ such that:

$$|\psi\rangle\langle\phi| \;\mapsto\; |\phi \otimes \psi\rangle \equiv |\phi\rangle \otimes |\psi\rangle \tag{5.2.1}$$

for any $|\psi\rangle$, $|\phi\rangle \in \mathscr{H}_{\mathcal{S}}$ and with $|\phi \otimes \psi\rangle \in \mathfrak{K}$. The vectorization procedure has the following properties:

1. There exists an identity vector $|\hat{\mathbb{1}}\rangle \in \mathfrak{K}$ defined as

$$\hat{\mathbb{1}} = \sum_k |\phi_k\rangle\langle\phi_k| \;\mapsto\; |\hat{\mathbb{1}}\rangle \equiv \sum_k |\phi_k \otimes \phi_k\rangle \tag{5.2.2}$$

   where $\{|\phi_k\rangle\}$ is a basis on $\mathscr{H}_{\mathcal{S}}$.

2. Any operator $\hat{A} \in \text{end}(\mathscr{H}_{\mathcal{S}})$ can be represented as

$$|\hat{A}\rangle = (\hat{\mathbb{1}} \otimes \hat{A})\,|\hat{\mathbb{1}}\rangle = (\hat{A}^{\mathrm{T}} \otimes \hat{\mathbb{1}})\,|\hat{\mathbb{1}}\rangle\,, \tag{5.2.3}$$

   with $|\hat{A}\rangle \in \mathfrak{K}$. This relation is very easy to prove:

$$\begin{aligned}(\hat{\mathbb{1}} \otimes \hat{A})\,|\hat{\mathbb{1}}\rangle &= \sum_k |\phi_k\rangle \otimes |\hat{A}\,\phi_k\rangle = \sum_{k,l} |\phi_k\rangle \otimes |\phi_l\rangle\langle\phi_l|\,\hat{A}\,|\phi_k\rangle \\ &= \sum_{k,l} A_{lk}\;|\phi_k \otimes \phi_l\rangle = |\hat{A}\rangle\end{aligned} \tag{5.2.4}$$

   and similarly for the other.

3. The product of two operators $\hat{A}$, $\hat{B} \in \text{end}(\mathscr{H}_{\mathcal{S}})$ can be vectorized as

$$|\hat{B}\,\hat{A}\rangle = (\hat{\mathbb{1}} \otimes \hat{B}\,\hat{A})\,|\hat{\mathbb{1}}\rangle = (\hat{\mathbb{1}} \otimes \hat{B})(\hat{\mathbb{1}} \otimes \hat{A})\,|\hat{\mathbb{1}}\rangle\,, \tag{5.2.5}$$

   but also as

$$\begin{aligned}|\hat{B}\,\hat{A}\rangle &= ((\hat{B}\,\hat{A})^{\mathrm{T}} \otimes \hat{\mathbb{1}})\,|\hat{\mathbb{1}}\rangle = (\hat{A}^{\mathrm{T}} \otimes \hat{\mathbb{1}})(\hat{B}^{\mathrm{T}} \otimes \hat{\mathbb{1}})\,|\hat{\mathbb{1}}\rangle \\ &= (\hat{A}^{\mathrm{T}} \otimes \hat{\mathbb{1}})(\hat{\mathbb{1}} \otimes \hat{B})\,|\hat{\mathbb{1}}\rangle = (\hat{A}^{\mathrm{T}} \otimes \hat{B})\,|\hat{\mathbb{1}}\rangle\,.\end{aligned} \tag{5.2.6}$$

4. The product of three operators $\hat{A}$, $\hat{B}$, $\hat{C}$ $\in \text{end}(\mathscr{H}_{\mathcal{S}})$ is given by

$$|\hat{A}\,\hat{C}\,\hat{B}\rangle = (\hat{B}^{\mathrm{T}} \otimes \hat{A})\;|\hat{C}\rangle \tag{5.2.7}$$

   as it follows from the previous properties.

5. A dual-space $\mathfrak{K}^\star$ can be defined as follows. For any $\hat{A} \in \text{end}(\mathscr{H}_\mathcal{S})$ we may write

$$\hat{A} = \sum_{k,l} A_{lk} \, |\phi_l\rangle \langle\phi_k| \;\mapsto\; |\hat{A}\rangle = \sum_{k,l} A_{lk} \, |\phi_k \otimes \phi_l\rangle \in \mathfrak{K} \tag{5.2.8}$$

then the adjoint vector $\langle\hat{A}| \in \mathfrak{K}^\star$ is

$$\langle\hat{A}| = \sum_{k,l} A^*_{kl} \, \langle\phi_k \otimes \phi_l| \,. \tag{5.2.9}$$

6. For any $|\hat{A}\rangle \, , |\hat{B}\rangle \in \mathfrak{K}$ a scalar product is defined as

$$\langle\hat{A}|\hat{B}\rangle \equiv \text{tr}(\hat{A}^\dagger \, \hat{B}). \tag{5.2.10}$$

The main advantage of using a vectorized space $\mathfrak{K}$ relies on the fact that the super-operators acting on $\text{end}(\mathscr{H}_\mathcal{S})$ here become just operators on $\mathfrak{K}$[§]. This allows to write the Lindblad master equation (5.1.36) in a vectorized form

$$\begin{aligned} \frac{\mathrm{d}}{\mathrm{d}t} \, |\hat{\rho}(t)\rangle &= \check{\mathscr{L}}(t) \, |\hat{\rho}(t)\rangle \\ &= \Big(\check{\mathcal{H}}(t) + \check{\mathcal{D}}(t)\Big) \, |\hat{\rho}(t)\rangle \end{aligned} \tag{5.2.11}$$

where it turns out to be very similar to a standard Schrödinger equation (despite from its non-unitary character). In particular, from the properties 1-4 of the vectorization procedure it is easy to show that the unitary generator (5.1.41) is

$$\check{\mathcal{H}}(t) \equiv -i\Big[\hat{\mathbb{1}} \otimes \hat{H}(t) - (\hat{H}(t))^{\mathrm{T}} \otimes \hat{\mathbb{1}}\Big] \tag{5.2.12}$$

while the non-unitary generator (5.1.42) reads

$$\check{\mathcal{D}}(t) \equiv \sum_{k,l=1}^{n^2-1} \gamma_{kl}(t) \left[\hat{F}^*_l \otimes \hat{F}_k - \frac{1}{2}\hat{\mathbb{1}} \otimes \hat{F}^\dagger_l \, \hat{F}_k - \frac{1}{2}(\hat{F}^\dagger_l \, \hat{F}_k)^{\mathrm{T}} \otimes \hat{\mathbb{1}}\right]. \tag{5.2.13}$$

From the Kraus decomposition (5.1.14), we can also write the vectorized form of a dynamical map $\check{\Lambda}$ as

$$|\hat{\rho}(t)\rangle = \check{\Lambda}(t,t_0) \, |\hat{\rho}(t_0)\rangle \,, \quad \check{\Lambda}(t,t_0) \equiv \sum_\alpha \hat{W}^*_\alpha(t,t_0) \otimes \hat{W}_\alpha(t,t_0). \tag{5.2.14}$$

Similar results are easily obtained in the Heisenberg picture for the vectorized versions of $\check{\mathscr{L}}^\star$ and $\check{\Lambda}^\star$.

[§]Nevertheless, we shall keep the notation $\check{\Lambda}$ for these operators (instead of $\hat{\Lambda}$) in order to avoid confusion.

5.3 A closed algebra for Liouvilleans

Notice that the non-Hamiltonian generator $\check{\mathcal{D}}$ in Eq.(5.1.36),

$$\check{\mathcal{D}}(t)\,\hat{\rho} = \sum_{k,l=1}^{n^2-1} \gamma_{kl}(t)\,\left(\hat{F}_k\,\hat{\rho}\,\hat{F}_l^\dagger - \frac{1}{2}\left\{\hat{F}_l^\dagger\,\hat{F}_k, \hat{\rho}\right\}\right), \tag{5.3.1}$$

is a quadratic form and thus it is independent of the chosen representation for the $\{\hat{F}_k\}$. However, it is convenient to express a generic Liouvillean $\check{\mathscr{L}}$ in terms of a traceless orthnormal set

$$\mathrm{tr}(\hat{F}_k) = 0\,, \quad \mathrm{tr}(\hat{F}_k\,\hat{F}_l^\dagger) = \delta_{kl}\,, \qquad \forall\, k\,, l\,, \tag{5.3.2}$$

as we did so far. In particular, for an open quantum system $\mathcal{S}$ with $\dim(\mathscr{H}_\mathcal{S}) = n$, the set of the generators of the Lie algebra $\mathfrak{su}(n)$ together with the identity provides a basis of this kind. Moreover, we can always choose these generators to be hermitian $\hat{F}_k \equiv \hat{F}_k^\dagger$. In the following, we will therefore refer with the notation

$$\left\{\ \hat{F}_k\ \right\}_{k=0}^{n^2-1} \tag{5.3.3}$$

to the ensemble of the $\mathfrak{su}(n)$ generators ($\hat{F}_k \equiv \hat{F}_k^\dagger$ with $k = 1, \ldots, n^2-1$) together with the normalized identity $F_0 \equiv \hat{\mathbb{1}}/n$. A general construction of the complete orthonormal set of $\{\hat{F}_k\}_{k=0}^{n^2-1}$ is reported in the appendix 5.A.

Having defined a preferred basis $\{\hat{F}_k\}_{k=0}^{n^2-1}$ for $\mathrm{end}(\mathscr{H}_\mathcal{S})$ allows then to have a preferred super-operator basis in $\mathfrak{K}$. In fact, by writing

$$\hat{H}(t) = \sum_{j=0}^{n^2-1} h_j(t)\,\hat{F}_j \tag{5.3.4}$$

with $h_j(t) \equiv \mathrm{tr}(\hat{H}(t)\,\hat{F}_j)$ and using Eqs.(5.2.12), (5.2.13), it is easy to see that a generic Liouvillean $\check{\mathscr{L}}$ admits a decomposition [Sco19]

$$\check{\mathscr{L}}(t) = \sum_{j=1}^{n^2-1} h_j(t)\,\check{\mathcal{H}}_j + \sum_{k,l=1}^{n^2-1} \gamma_{kl}(t)\,\check{\mathcal{D}}_{kl} \tag{5.3.5}$$

with the definition of the super-operator basis:

$$\check{\mathcal{H}}_j \equiv -i\left(\hat{\mathbb{1}} \otimes \hat{F}_j - \hat{F}_j^* \otimes \hat{\mathbb{1}}\right), \quad j = 1, \ldots, n^2-1; \tag{5.3.6a}$$

$$\check{\mathcal{D}}_{kl} \equiv \left[\hat{F}_l^* \otimes \hat{F}_k - \frac{1}{2}\hat{\mathbb{1}} \otimes \hat{F}_l\,\hat{F}_k - \frac{1}{2}\hat{F}_k^*\,\hat{F}_l^* \otimes \hat{\mathbb{1}}\right], \quad k, l = 1, \ldots, n^2-1. \tag{5.3.6b}$$

The crucial remark here is that the set of super-operators $\{\{\check{\mathcal{H}}_j\}_{j=1}^{n^2-1};\ \{\check{\mathcal{D}}_{kl}\}_{k,l=1}^{n^2-1}\}$ generates a closed Lie algebra [Sco19]. The derivation is cumbersome but uses only well-known properties of $\mathfrak{su}(n)$ (see the appendix 5.A). The result is:

$$[\check{\mathcal{H}}_n, \check{\mathcal{H}}_m] = \sum_{k=1}^{n^2-1} \mathrm{f}_{nmk}\, \check{\mathcal{H}}_k; \tag{5.3.7a}$$

$$[\check{\mathcal{H}}_j, \check{\mathcal{D}}_{kl}] = \sum_{s=1}^{n^2-1} (\mathrm{f}_{jks}\, \check{\mathcal{D}}_{sl} + \mathrm{f}_{jls}\, \check{\mathcal{D}}_{ks}); \tag{5.3.7b}$$

$$\begin{aligned}[\check{\mathcal{D}}_{kl}, \check{\mathcal{D}}_{qm}] = \frac{1}{16} \sum_{s,p,r=1}^{n^2-1} \mathrm{z}_{lks}\, \mathrm{z}_{mqp}\, \mathrm{f}_{spr}\, \check{\mathcal{H}}_r + \frac{1}{4} \sum_{s,p=1}^{n^2-1} (\mathrm{z}_{mqs}(\mathrm{f}_{ksp}\, \check{\mathcal{D}}_{pl} + \mathrm{f}_{slp}\, \check{\mathcal{D}}_{kp}) \\ + \mathrm{z}_{lks}(\mathrm{f}_{sqp}\, \check{\mathcal{D}}_{pm} + \mathrm{f}_{msp}\, \check{\mathcal{D}}_{qp})) + \frac{1}{4} \sum_{s,p=1}^{n^2-1} (\mathrm{z}_{qks}\, \mathrm{z}_{lmp} - \mathrm{z}_{kqs}\, \mathrm{z}_{mlp}) \check{\mathcal{D}}_{sp} \\ + \frac{1}{2n} \sum_{s=1}^{n^2-1} (\delta_{qk}\, \mathrm{f}_{mls} - \delta_{lm}\, \mathrm{f}_{kqs}) \check{\mathcal{H}}_s;\end{aligned} \tag{5.3.7c}$$

where $\mathrm{f}_{abc} \equiv -i\mathrm{tr}([\hat{F}_a, \hat{F}_b]\hat{F}_c)$ and $\mathrm{z}_{abc} = (\mathrm{f}_{abc} - i\mathrm{d}_{abc})$ with $\mathrm{d}_{abc} \equiv \mathrm{tr}(\{\hat{F}_a, \hat{F}_b\}\hat{F}_c)$. Notice that the unitary set (5.3.6a) generates a closed subalgebra (5.3.7a) which is nothing but $\mathfrak{su}(n)$. It follows that our formalism does correctly reproduce the case of a closed unitary evolution when we detach the system from the external environment (compare with the results of Sec.3.1.2).
Despite the complexity of this algebraic structure, we will see that it can be greatly simplified considering specific examples.

5.4 Exact solution of Lindblad equations

Having defined a super-operator basis (5.3.6) with closed algebra (5.3.7) allows a natural extension of the exact algebraic method of Sec.3.1.2 to the case of a Lindblad evolution. Let us denote the dynamical map which solves Eq.(5.2.11) as

$$|\hat{\rho}(t)\rangle = \check{\Lambda}(t, t_0)\ |\hat{\rho}(t_0)\rangle\,, \tag{5.4.1}$$

and let us parametrize the map $\check{\Lambda}(t, t_0)$ as an element of the Lie group associated to the algebra (5.3.7) of the generators (compare with Eq.(3.1.44))

$$\check{\Lambda}(t, t_0) = \prod_{j=1}^{n^2-1} \exp(\lambda_j(t)\, \check{\mathcal{H}}_j) \prod_{k,l=1}^{n^2-1} \exp(\pi_{kl}(t)\, \check{\mathcal{D}}_{kl}) \tag{5.4.2}$$

with a set of time-dependent functions $\lambda_j(t)$, $\pi_{kl}(t)$. The main point now, is that the time dependence is entirely shifted to the set of functions $\lambda_j(t)$, $\pi_{kl}(t)$ which are obtained through the solution of a system of coupled differential equations. To see this more specifically, we may use the Lindblad equation (5.2.11) to write

$$\left(\frac{\mathrm{d}}{\mathrm{d}t}\check{\Lambda}(t,t_0)\right)\left(\check{\Lambda}(t,t_0)\right)^{-1} = \check{\mathscr{L}}(t) \tag{5.4.3}$$

that is (compare with Eq.(3.1.45))

$$\begin{aligned}\frac{\mathrm{d}}{\mathrm{d}t}\Big(\prod_{j=1}^{n^2-1} e^{\lambda_j(t)\,\check{\mathcal{H}}_j}\prod_{k,l=1}^{n^2-1} e^{\pi_{kl}(t)\,\check{\mathcal{D}}_{kl}}\Big)\Big(\prod_{k,l=n^2-1}^{1} e^{-\pi_{kl}(t)\,\check{\mathcal{D}}_{kl}}\prod_{j=n^2-1}^{1} e^{-\lambda_j(t)\,\check{\mathcal{H}}_j}\Big)\\ = \sum_{j=1}^{n^2-1} h_j(t)\,\check{\mathcal{H}}_j + \sum_{k,l=1}^{n^2-1}\gamma_{kl}(t)\,\check{\mathcal{D}}_{kl}\ .\end{aligned} \tag{5.4.4}$$

Using then BCH relations (3.1.24) on the l.h.s., together with the linear independence of the super-operators, will then yield a set of coupled first-order differential equations for the functions $\lambda_j(t)$, $\pi_{kl}(t)$.
In general, these equations are too complex to be solved explicitly. However, as shown below, they become manageable in some specific examples.

5.4.1 Geometrical picture of irreversibility

At a first glance, one may wonder by looking at the exponential form of the dynamical map in Eq.(3.1.44), due to the fact that it is always invertible. Indeed, one expects that the reduced dynamics in $\mathcal{S}$ describes an irreversible process, accompained with a loss of information about the initial state. This means that, at time $t > t_0$, the state $\hat{\rho}(t)$ can result from different initial states $\hat{\rho}(t_0)$, provided the same Liouvillean generator $\check{\mathscr{L}}(t)$.
However, we argue that this method is actually consistent with the irreversibility of the time evolution. To see this simply, we first report a matrix formulation of the Lindblad master equation (5.1.36) [Ali87, Rau02, Rau03, Rau05]. The basic idea of the method is to encode all the information about the reduced density matrix

$$\hat{\rho}(t) = \hat{F}_0 + \sum_{k=1}^{n^2-1} v_k(t)\,\hat{F}_k \tag{5.4.5}$$

in a (n^2-1)-vector:

$$\vec{v}(t) = \begin{bmatrix} v_1(t) \\ \dots \\ v_{n^2-1}(t) \end{bmatrix} \in \mathbb{R}^{n^2-1} \tag{5.4.6}$$

where $v_k(t) \equiv \mathrm{tr}(\hat{\rho}(t)\,\hat{F}_k)$. Notice that the coefficient of $\hat{F}_0$ is always equal to one (since $\mathrm{tr}\hat{\rho} = 1$) and that this constraint has been automatically implemented in the definition of $\vec{v}$. In terms of this vector, the Lindblad equation becomes a sort of Bloch equation in $\mathbb{R}^{n^2-1}$:

$$\frac{\mathrm{d}}{\mathrm{d}t}\hat{\rho}(t) = \check{\mathscr{L}}(t)\,\hat{\rho}(t) \;\mapsto\; \frac{\mathrm{d}}{\mathrm{d}t}\vec{v}(t) = (\mathbf{Q}(t) + \mathbf{R}(t))\;\vec{v}(t) + \vec{k}(t)\,. \tag{5.4.7}$$

To write down the various terms of the Bloch equation appearing on the right, we proceed by separating the Hamiltonian and the non-Hamiltonian contributions of the Lindblad evolution i.e.,

$$\check{\mathcal{H}}(t)\hat{\rho} \;\mapsto \mathbf{Q}(t)\,\vec{v}(t); \qquad \check{\mathcal{D}}(t)\hat{\rho} \;\mapsto \mathbf{R}(t)\,\vec{v}(t) + \vec{k}(t), \tag{5.4.8}$$

and we treat the two parts separately. In the case of a unitary evolution ($\check{\mathcal{D}} = 0$) the dynamics is generated by

$$\frac{\mathrm{d}}{\mathrm{d}t}\hat{\rho} = -i[\hat{H}(t), \hat{\rho}], \tag{5.4.9}$$

which gives

$$\sum_{k=1}^{n^2-1} \frac{\mathrm{d}}{\mathrm{d}t}\,v_k(t) = \sum_{k=1}^{n^2-1} \mathrm{tr}\left(\frac{\mathrm{d}}{\mathrm{d}t}\,\hat{\rho}(t)\,\hat{F}_k\right) = \sum_{k=1}^{n^2-1} -i\mathrm{tr}\left([\hat{H}(t), \hat{\rho}(t)]\,\hat{F}_k\right). \tag{5.4.10}$$

Using then the Hamiltonian decomposition $\hat{H}(t) = \sum_j h_j(t)\,\hat{F}_j$ with $h_j \equiv \mathrm{tr}(\hat{H}(t)\,\hat{F}_j)$, we obtain

$$\frac{\mathrm{d}}{\mathrm{d}t}\,v_k(t) = \sum_{j,l=1}^{n^2-1} -i\mathrm{tr}\left([\hat{F}_j, \hat{F}_l]\,h_j(t)\,v_l(t)\,\hat{F}_k\right) \tag{5.4.11}$$

$$= \sum_{j,l,s=1}^{n^2-1} \mathrm{tr}\left(\mathrm{f}_{jls}\,h_j(t)\,v_l(t)\,\hat{F}_s\hat{F}_k\right) = \sum_{j,l=1}^{n^2-1} \mathrm{f}_{jlk}\,h_j(t)\,v_l(t). \tag{5.4.12}$$

Thus, we identify the (real) matrix $\mathbf{Q}(t)$ with

$$[\mathbf{Q}(t)]_{kl} = \sum_{j=1}^{n^2-1} \mathrm{f}_{jlk}\,h_j(t), \tag{5.4.13}$$

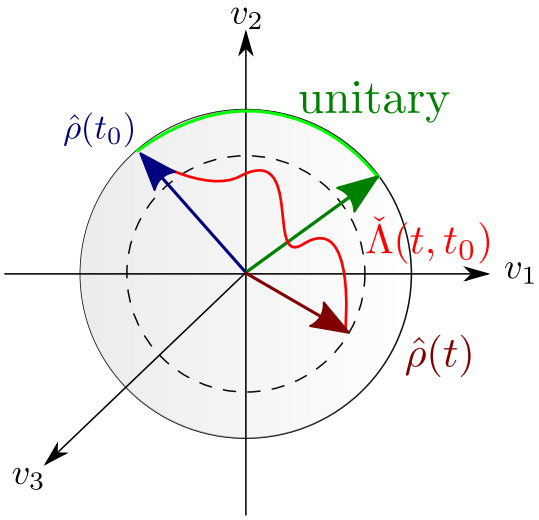

Figure 5.1: **Geometrical interpretation of the time-evolution**. Qualitative drawing of the time-evolution in $\mathbb{R}^{n^2-1}$ (here $n=2$) for a Lindblad evolution written in the matrix form of Eq.(5.4.7). In this formulation, a unitary dynamics corresponds to a motion on the sphere surface with a constant vector length (*green*). In the presence of dissipations, the vector length can change (*red*). The path drawn by the coherence vector $\vec{v}(t)$ from the initial state $\hat{\rho}(t_0)$ (*dark blue*) to $\hat{\rho}(t)$ (*dark red*) is encoded in the dynamical map $\check{\Lambda}$.

responsible for the unitary evolution. Notice that the unitarity of the time-evolution is reflected in the conservation of the vector norm

$$\frac{\mathrm{d}}{\mathrm{d}t}\left\|\vec{v}(t)\right\|^2 = \vec{v}(t)^{\mathrm{T}}\left(\mathbf{Q}(t)^{\mathrm{T}}+\mathbf{Q}(t)\right)\vec{v}(t)=0\,, \tag{5.4.14}$$

following from the skew symmetry $\mathbf{Q}(t)=-\mathbf{Q}(t)^{\mathrm{T}}$of the matrix in Eq.(5.4.13) (due to the antisymmetry of f_{jlk}). Next, we consider the purely dissipative case ($\check{\mathcal{H}}=0$):

$$\frac{\mathrm{d}}{\mathrm{d}t}\hat{\rho}=\check{\mathcal{D}}(t)\hat{\rho}. \tag{5.4.15}$$

A similar procedure shows that the purely dissipative contribution of the Lindblad evolution is instead represented through the matrix

$$\left[\mathbf{R}(t)\right]_{qs}=-\frac{1}{4}\sum_{i,k,l=1}^{N^2-1}\gamma_{ik}(t)(\mathrm{z}^*_{ilq}\mathrm{f}_{kls}+\mathrm{z}_{klq}\mathrm{f}_{ils}) \tag{5.4.16}$$

and the vector

$$\left[\vec{k}(t)\right]_s = \frac{i}{n}\sum_{i,k=1}^{N^2-1}\gamma_{ik}(t)\,\mathrm{f}_{iks}\,, \tag{5.4.17}$$

both real quantities, as shown in [Ali87].
From a geometrical point of view, the time evolution in Eq.(5.4.7) is a kind of rotation in $\mathbb{R}^{n^2-1}$ with a varying vector length: even though rotations are generated by Hamiltonian and non-Hamiltonian terms, the variations of the vector length are due to dissipative effects only. In other words, unitarity constrains the motion of the vector $\vec{v}(t)$ on the hyper-sphere surface whereas the non-unitary terms lift such constraint (with respect to CPTP properties), see Fig.5.1.
In this geometrical interpretation, the dynamical map $\check{\Lambda}$ generates the motion of $\vec{v}$ in $\mathbb{R}^{n^2-1}$. The information about the specific path from $\hat{\rho}(t_0)$ to $\hat{\rho}(t)$ is contained in the set of coordinates λ_j, π_{kl} which allow thus to invert the time-evolution without violating the irreversible nature of the effective dynamics.
In conclusion, a careful analysis about the irreversibility of the time-evolution requires the use of entropy measures and cannot be guessed by only looking at the structure of the dynamical map.

5.4.2 Rotating frame transformation

We introduce a complementary approach for the solution of time-dependent Lindblad equations (5.2.11) based on the idea of a generalized rotating frame. Consider a time-dependent invertible map $\check{W}(t)$ that connects our open system $\mathcal{S}$ to an auxiliary frame $\mathcal{S}_{\text{aux}}$:

$$|\hat{\rho}(t)\rangle \;\mapsto\; |\hat{\rho}_{\text{aux}}(t)\rangle = \check{W}(t)\,|\hat{\rho}(t)\rangle\,. \tag{5.4.18}$$

The evolution in $\mathcal{S}_{\text{aux}}$ is then governed by

$$\frac{\mathrm{d}}{\mathrm{d}t}\,|\hat{\rho}_{\text{aux}}(t)\rangle = \check{\mathscr{L}}_{\text{aux}}\,|\widetilde{\rho}_t\rangle \tag{5.4.19}$$

where

$$\check{\mathscr{L}}_{\text{aux}} = \check{W}(t)\,\check{\mathscr{L}}(t)\,\check{W}(t)^{-1} + \left(\frac{\mathrm{d}}{\mathrm{d}t}\check{W}(t)\right)\check{W}(t)^{-1}\,. \tag{5.4.20}$$

Now, If we can design $\check{W}(t)$ in such a way that $\check{\mathscr{L}}_{\text{aux}}$ is time independent, then the dynamics in the auxiliary frame $\mathcal{S}_{\text{aux}}$ will simply be given by

$$|\hat{\rho}_{\text{aux}}(t)\rangle = \exp\left(\check{\mathscr{L}}_{\text{aux}}\,(t-t_0)\right)\,|\hat{\rho}_{\text{aux}}(t_0)\rangle \tag{5.4.21}$$

and, moving back to the original frame $\mathcal{S}$, we conclude that:

$$\check{\Lambda}(t,t_0) = \check{W}(t)^{-1}\,\exp\left(\check{\mathscr{L}}_{\rm aux}\,(t-t_0)\right)\,\check{W}(t_0). \tag{5.4.22}$$

From general algebraic considerations, we can parametrize $\check{W}(t)$ in the form

$$\check{W}(t) = \prod_{j=1}^{n^2-1}\exp(f_j(t)\,\check{\mathcal{H}}_j)\prod_{k,l=1}^{n^2-1}\exp(g_{kl}(t)\,\check{\mathcal{D}}_{kl})\,, \tag{5.4.23}$$

with coordinates $f_j(t)$, $g_{kl}(t)$. This leads (together with (5.3.5)) to the auxiliary generator:

$$\begin{aligned}\check{\mathscr{L}}_{\rm aux} = &\prod_{j=1}^{n^2-1} e^{f_j(t)\check{\mathcal{H}}_j}\prod_{k,l=1}^{n^2-1} e^{g_{kl}(t)\check{\mathcal{D}}_{kl}}\left(\sum_{i=1}^{n^2-1}h_i(t)\,\check{\mathcal{H}}_i+\sum_{p,q=1}^{n^2-1}\gamma_{pq}(t)\,\check{\mathcal{D}}_{pq}\right)\times\\
&\prod_{k,l=n^2-1}^{1} e^{-g_{kl}(t)\check{\mathcal{D}}_{kl}}\prod_{j=n^2-1}^{1} e^{-f_j(t)\check{\mathcal{H}}_j}+\sum_{i=1}^{n^2-1}\prod_{j=1}^{i-1}e^{f_j(t)\check{\mathcal{H}}_j}\frac{\mathrm{d}}{\mathrm{d}t}f_i\,\check{\mathcal{H}}_i\prod_{j=n^2-1}^{i+1}e^{-f_j(t)\check{\mathcal{H}}_j}\\
&+\sum_{p,q=1}^{n^2-1}\prod_{j=1}^{n^2-1}e^{f_j(t)\check{\mathcal{H}}_j}\prod_{k=1}^{p-1}\prod_{l=1}^{q-1}e^{g_{kl}\check{\mathcal{D}}_{kl}}\frac{\mathrm{d}}{\mathrm{d}t}g_{pq}\,\check{\mathcal{D}}_{pq}\prod_{k=n^2-1}^{p+1}\prod_{l=n^2-1}^{q+1}e^{-g_{kl}(t)\check{\mathcal{D}}_{kl}}\prod_{j=n^2-1}^{1}e^{-f_j(t)\check{\mathcal{H}}_j}.\end{aligned} \tag{5.4.24}$$

Despite the complexity of its nested structure, it is easy to see that the generic expression for $\check{\mathscr{L}}_{\rm aux}$ is made of the blocks:

$$\begin{aligned}&\left[e^{f_j(t)\,\check{\mathcal{H}}_j}\right]\,\check{\mathcal{H}}_i\,\left[e^{-f_j(t)\,\check{\mathcal{H}}_j}\right];\qquad\left[e^{g_{kl}(t)\,\check{\mathcal{D}}_{kl}}\right]\,\check{\mathcal{H}}_j\,\left[e^{-g_{kl}(t)\,\check{\mathcal{D}}_{kl}}\right];\\
&\left[e^{f_j(t)\,\check{\mathcal{H}}_j}\right]\,\check{\mathcal{D}}_{kl}\,\left[e^{-f_j(t)\,\check{\mathcal{H}}_j}\right];\qquad\left[e^{g_{kl}(t)\,\check{\mathcal{D}}_{kl}}\right]\,\check{\mathcal{D}}_{pq}\,\left[e^{-g_{kl}(t)\,\check{\mathcal{D}}_{kl}}\right],\end{aligned} \tag{5.4.25}$$

which can be exactly computed with the help of BCH relations (3.1.24) and of the commutators in (5.3.7). It follows that the auxiliary generator $\check{\mathscr{L}}_{\rm aux}$ admits the closed expression (compare with Eq.(3.1.41))

$$\check{\mathscr{L}}_{\rm aux} = \sum_{j=1}^{n^2-1}h_j^{\rm aux}\,\check{\mathcal{H}}_j+\sum_{k,l=1}^{n^2-1}\gamma_{kl}^{\rm aux}\,\check{\mathcal{D}}_{kl} \tag{5.4.26}$$

in the basis of super-operators (5.3.6). Hence, imposing $h_j^{\rm aux}$, $\gamma_{kl}^{\rm aux}$ to be time-independent, from Eq.(5.4.24) we end up with a set of coupled first-order differential equations that determines the coordinates $f_j(t)$, $g_{kl}(t)$.

Since the choice of the auxiliary frame $\mathcal{S}_{\rm aux}$ is arbitrary (and generally dictated by having a simplified set of differential equations), it may lead to an unphysical auxiliary generator, i.e., to an object $\check{\mathscr{L}}_{\rm aux}$ which does not generate a CPTP dynamics. If this is the case, we have to interpret the auxiliary quantities as some mathematical objects that allow for the solution of the CPTP dynamics observed in $\mathcal{S}$, excluding any physical implication. Conversely, when $\check{\mathscr{L}}_{\rm aux}$ is chosen to be a physical Liouvillean, then Eq.(5.4.22) describes an effective time-independent CPTP evolution resulting from a rotating frame transformation. The rotating frame technique can be viewed as an alternative to other techniques such as the coherence vector formalism [Ali87, Rau02, Rau03, Rau05] where the time-dependent Lindblad equation is cast in the form of a Bloch equation (5.4.7). In the following section, we shall consider the rotating frame technique applied to a periodic driving where it will coincide with the Floquet framework of Sec.3.1.2. For Floquet systems, the method leads to exact results that go beyond those obtained by means of other known techniques.

5.5 Lindblad-Floquet framework

Let us discuss in more detail the case in which the reduced dynamics is generated by a time-periodic Liouvillean $\check{\mathscr{L}}(t) = \check{\mathscr{L}}(t+\mathcal{T})$ with a driving period $\mathcal{T}$. This problem has been analysed in many recent works, see e.g. [Har17, Mag18, Bas18, Don18, Iwa16, Rei18, Ali12, Bar18, Kam11, Pro11b], with the aim of extending the Floquet theory (see Sec.3.1), to the case of periodically driven open quantum systems. The dedicated literature mainly focus on the case of high-frequency driving where one may face the problem perturbatively [Dai16, Dai17] with the use of the Magnus expansion, see e.g. [Bla08]. Here, we show that within the rotating frame technique, one is able to derive an exact Floquet description of the Lindblad evolution (5.2.11), avoiding problems of convergence [Cas01, Moa08] and of lack of CPTP properties [Had15] related to the Magnus expansion. Nonetheless, we will show in Sec.5.5.1 that high-frequency perturbative results can be obtained within our framework and they generalize those of Sec.3.1.1 to the open system's case.

To begin with, we consider again the map $\check{W}(t)$ in Eq.(5.4.23) to the auxiliary frame:

$$|\hat{\rho}_{\rm aux}(t)\rangle = \check{W}(t)\,|\hat{\rho}(t)\rangle\,; \quad \check{W}(t) = \check{W}(t+\mathcal{T}), \tag{5.5.1}$$

requiring its time-periodicity. From Eq.(5.4.23), the time-periodicity of $\check{W}(t)$ implies then that the coordinates $f_j(t) = f_j(t+\mathcal{T})$ and $g_{kl}(t) = g_{kl}(t+\mathcal{T})$ are

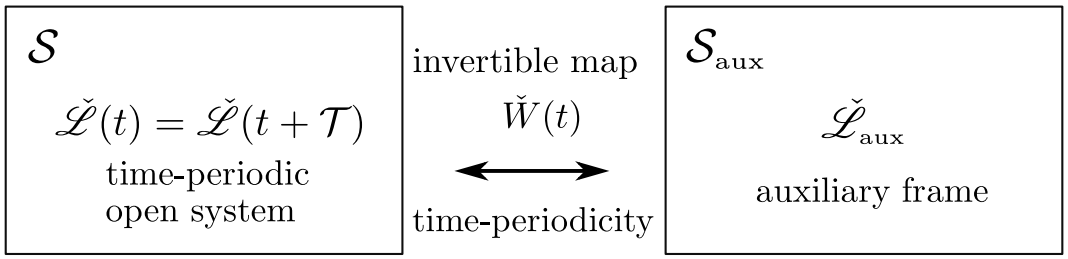

Figure 5.1: **Rotating frame transformation**. A time-periodic open system can be mapped, by means of a proper invertible time-periodic map $\check{W}(t)$, to an auxiliary time-independent problem. In this way, the rotating frame technique of Sec.5.4.2 will coincide with the Floquet framework of Sec.3.1 (compare with Fig.3.1).

now chosen as time-periodic functions, see Fig.5.1.
Next, by evaluating the dynamical map in Eq.(5.4.22) at times $t = t_0 + m\mathcal{T}$, for integer m, we obtain

$$\check{\Lambda}(t,t_0)\Big|_{t=t_0+m\mathcal{T}} = \check{W}(t_0)^{-1}\,\exp\left(\check{\mathscr{L}}_{\rm aux}\, m\mathcal{T}\right)\,\check{W}(t_0) \equiv \exp\left(\check{\mathscr{L}}_F(t_0)\, m\mathcal{T}\right) \tag{5.5.2}$$

where we have introduced the Floquet generator

$$\check{\mathscr{L}}_F(t_0) \equiv \check{W}(t_0)^{-1}\,\check{\mathscr{L}}_{\rm aux}\,\check{W}(t_0). \tag{5.5.3}$$

The dynamical map in Eq.(5.5.2) describes a stroboscopic evolution whereas, introducing the micromotion operator

$$\check{W}(t,t_0) \equiv \check{W}(t)^{-1}\,\check{W}(t_0)\,, \tag{5.5.4}$$

one is able to analyse the evolution at any times $t \geq t_0$. We specify that the Floquet-Liouvillean $\check{\mathscr{L}}_F$ in Eq.(5.5.3) is not unique and depends on the choice of the auxiliary frame. However, one can set the auxiliary parameters $h_j^{\rm aux}$, $\gamma_{kl}^{\rm aux}$ (5.4.26) to be equal to the time averages of the $\mathcal{S}$ parameters in Eq.(5.3.5):

$$h_j^{\rm aux} = \langle h_j \rangle_{\mathbf{t}} \equiv \overline{h}_j\,, \quad \gamma_{kl}^{\rm aux} = \langle \gamma_{kl} \rangle_{\mathbf{t}} \equiv \overline{\gamma}_{kl} \tag{5.5.5}$$

with $\overline{\mathrm{w}} \equiv \langle \mathrm{w} \rangle_{\mathbf{t}} = \mathcal{T}^{-1}\int_0^{\mathcal{T}} \mathrm{d}t\, \mathrm{w}(t)$ for a generic function of time $\mathrm{w}(t)$.

Requiring (5.5.5), we fix the auxiliary frame $\mathcal{S}_{\rm aux}$ and consequently $\check{\mathscr{L}}_F$. Notice that the generator (5.4.20) and $\check{\mathscr{L}}_F$ are related through a similarity transformation (5.5.3) and so they share the same spectrum. This means that requiring

(5.5.5) we are guaranteed that $\check{\mathscr{L}}_F$ is a physical object.
As a consequence of the algebraic structure, the Floquet generator in Eq.(5.5.3) admits a decomposition:

$$\check{\mathscr{L}}_F(t_0) = \sum_{j=1}^{n^2-1} h_j^F(t_0)\,\check{\mathcal{H}}_j + \sum_{k,l=1}^{n^2-1} \gamma_{kl}^F(t_0)\,\check{\mathcal{D}}_{kl}\,, \tag{5.5.6}$$

in the super-operator basis (5.3.6). Here, the set of Floquet parameters $h_j^F(t_0)$, $\gamma_{kl}^F(t_0)$ is defined through the BCH expansion of the r.h.s. of Eq.(5.5.3).

About the existence of a Floquet-Liouvillean

Notice that it is not always possible to find a periodic solution to the set of non-linear first-order differential equations defining $\check{W}(t)$ [Li03]. This means that a periodic Liouvillean $\check{\mathscr{L}}(t)$ cannot be always expressed in terms of a Floquet theory. The reason is rather clear: if we consider an open quantum system which can be described in the markovian approximation with a Liouvillean generator, we are not guaranteed that the stroboscopic evolution preserves markovianity. In other words, the one-period dynamical map

$$\check{\Lambda}(t_0+\mathcal{T},t_0) = \mathbf{T}\exp\left(\int_{t_0}^{t_0+\mathcal{T}} \mathrm{d}t'\;\check{\mathscr{L}}(t')\right), \tag{5.5.7}$$

not necessarily allows a logarithmic operator of the Lindblad form.
We shall not investigate the connection between the existence of periodic solutions for $\check{W}(t)$ and the markovianity of the Floquet evolution, leaving it to further developments. For our purposes, we assume the existence of a periodic solution and we provide a general method to build an exact Floquet-Liouvillean $\check{\mathscr{L}}_F$. We address the reader to Ref. [Sch18b] where the existence of $\check{\mathscr{L}}_F$ is discussed and some markovianity tests are proposed (see also [Wol08, Cub12]).

5.5.1 High-frequency expansion

For large enough driving frequencies $\omega \equiv 2\pi/\mathcal{T} \gg 1$, the rotating frame method of Sec.5.4.2 can be used to derive approximate results in agreement with those obtained by means of high-frequency expansions [Dai16, Dai17] (see also Sec.3.1.1 for the unitary case).

First, we write the Fourier series of the time-periodic Liouvillean as

$$\check{\mathscr{L}}(t) = \check{\mathscr{L}}_0 + \sum_{k\neq 0} e^{ik\omega t}\,\check{V}_k. \tag{5.5.8}$$

Next, we parametrize the map $\check{W}(t)$ to the auxiliary frame $\mathcal{S}_{\text{aux}}$ as

$$\check{W}(t) = \exp\left(\check{\Phi}(t)\right) \tag{5.5.9}$$

with $\check{\Phi}(t) = \check{\Phi}(t+\mathcal{T})$ a linear combination of the super-operators in (5.3.6). At this point, we consider the Magnus expansions in powers of ω^{-1}:

$$\check{\Phi}(t) = \sum_{a=1}^{\infty} \omega^{-a}\, \check{\Phi}^{(a)}(t)\,, \quad \check{\mathscr{L}}_{\text{aux}} = \sum_{a=0}^{\infty} \omega^{-a}\, \check{\mathscr{L}}^{(a)}_{\text{aux}}. \tag{5.5.10}$$

According to Eq.(5.4.20), we then obtain

$$\begin{aligned} \check{\mathscr{L}}_{\text{aux}} =& e^{\check{\Phi}(t)}\, \check{\mathscr{L}}(t)\, e^{-\check{\Phi}(t)} + (\frac{\mathrm{d}}{\mathrm{d}t} e^{\check{\Phi}(t)})\, e^{-\check{\Phi}(t)} \\ =& \check{\mathscr{L}}(t) + \frac{\mathrm{d}}{\mathrm{d}t}\check{\Phi}(t) + [\check{\Phi}(t), \check{\mathscr{L}}(t)] + \frac{1}{2}[\check{\Phi}(t), [\check{\Phi}(t), \check{\mathscr{L}}(t)]] + \dots \end{aligned} \tag{5.5.11}$$

which can be solved in high-frequency expansion (5.5.10) imposing the time independence of $\check{\mathscr{L}}_{\text{aux}}$ order by order. The results read at the second order:

$$\begin{aligned} \check{\mathscr{L}}_{\text{aux}} =& \check{\mathscr{L}}_0 + \frac{1}{\omega}\sum_{k\neq 0} \frac{i}{2k}[\check{V}_k, \check{V}_{-k}] - \frac{1}{\omega^2}\sum_{k\neq 0}\frac{1}{2k^2}[[\check{V}_k, \check{\mathscr{L}}_0], \check{V}_{-k}] \\ & - \frac{1}{\omega^2}\sum_{k,q\neq 0}\frac{1}{3kq}[\check{V}_k, [\check{V}_q, \check{V}_{-k-q}]] + \mathcal{O}(\omega^{-3}) \end{aligned} \tag{5.5.12}$$

and

$$\check{\Phi}(t) = \frac{i}{\omega}\sum_{k\neq 0}\frac{e^{ik\omega t}}{k}\check{V}_k - \frac{1}{\omega^2}\sum_{k\neq 0}\sum_{q\neq -k}\frac{e^{i(k+q)\omega t}}{2k(k+q)}[\check{V}_k, \check{V}_q] + \mathcal{O}(\omega^{-3})\,. \tag{5.5.13}$$

For what concerns the Floquet generator $\check{\mathscr{L}}_F$ in Eq.(5.5.3), we have

$$\begin{aligned} \check{\mathscr{L}}_F(t_0) &= e^{-\check{\Phi}(t_0)}\, \check{\mathscr{L}}_{\text{aux}}\, e^{\check{\Phi}(t_0)} \\ &= \check{\mathscr{L}}_{\text{aux}} + [\check{\Phi}(t_0), \check{\mathscr{L}}_{\text{aux}}] + \frac{1}{2}[\check{\Phi}(t_0), [\Phi(t_0), \check{\mathscr{L}}_{\text{aux}}]] + \dots \end{aligned} \tag{5.5.14}$$

and similarly for the micromotion in Eq.(5.5.4)

$$\begin{aligned} \check{W}(t, t_0) &= \exp\left(-\check{\Phi}(t)\right)\, \exp\left(\check{\Phi}(t_0)\right) \equiv \exp\left(\check{\mathcal{K}}(t, t_0)\right) \\ &= \exp(-\check{\Phi}(t) + \check{\Phi}(t_0) - \frac{1}{2}[\check{\Phi}(t), \check{\Phi}(t_0)] + \dots)\,. \end{aligned} \tag{5.5.15}$$

For sake of simplicity we set $t_0 = 0$. The results in high-frequency expansion (5.5.10) are:

$$\begin{aligned}\check{\mathscr{L}}_F(0) =& \check{\mathscr{L}}_0 + \frac{i}{\omega}\sum_{k\neq 0}\frac{\frac{1}{2}[\check{V}_k, \check{V}_{-k}] - [\check{V}_k, \check{\mathscr{L}}_0]}{k} \\ &+ \frac{1}{\omega^2}\sum_{k,q\neq 0}\frac{\frac{1}{2}[\check{V}_k, [\check{V}_q, \check{\mathscr{L}}_0]] - \frac{1}{2}[\check{V}_k, [\check{V}_q, \check{V}_{-q}]]}{kq} \\ &+ \frac{1}{\omega^2}\sum_{k,q\neq 0}\frac{\frac{1}{3}[\check{V}_k, [\check{V}_q, \check{V}_{-k-q}]] - \frac{1}{2}[[\check{V}_k, \check{V}_{q-k}], \check{\mathscr{L}}_0]}{kq} \\ &- \frac{1}{\omega^2}\sum_{k\neq 0}\frac{\frac{1}{2}[[\check{V}_k, \check{\mathscr{L}}_0], \check{V}_{-k}] - [[\check{V}_k, \check{\mathscr{L}}_0], \check{\mathscr{L}}_0]}{k} + \mathcal{O}(\omega^{-3}); \end{aligned} \tag{5.5.16}$$

and

$$\begin{aligned}\check{\mathcal{K}}(t,0) =& \frac{i}{\omega}\sum_{k\neq 0}\frac{(1-e^{ik\omega t})}{k}\check{V}_k - \frac{1}{\omega^2}\sum_{k\neq 0}\frac{(1-e^{ik\omega t})}{k^2}[\check{V}_k, \check{\mathscr{L}}_0] \\ &- \frac{1}{\omega^2}\sum_{k,q\neq 0}\frac{(1-e^{iq\omega t})[\check{V}_k, \hat{V}_{q-k}] - e^{ik\omega t}\,[\check{V}_k, \check{V}_q]}{2kq} + \mathcal{O}(\omega^{-3}) \end{aligned} \tag{5.5.17}$$

which extend the results of Sec.3.1.1 to the dissipative case.

5.6 Single qubit example

For concreteness, we shall focus now on the case $n = 2$ of a single qubit system. We assume that the system is described by a time-dependent Hamiltonian of the form:

$$\hat{H}(t) = -\frac{1}{2}\Omega(t)\,\hat{\sigma}^z, \tag{5.6.1}$$

describing a two-level system with a time-dependent energy gap $\Omega(t)$, see Fig.5.1a. Next, we add three elementary dissipative processes described by the jump operators (see Sec.5.1.3):

$$\hat{L}_+ = \hat{\sigma}^+\,, \quad \hat{L}_- = \hat{\sigma}^-\,, \quad \hat{L}_z = \hat{\sigma}^z \tag{5.6.2}$$

with time-dependent couplings $\Gamma_j(t) \geq 0$, $\forall t > t_0$ $(j = \pm, z)$. The first two jump operators represent amplitude damping processes due to the presence of

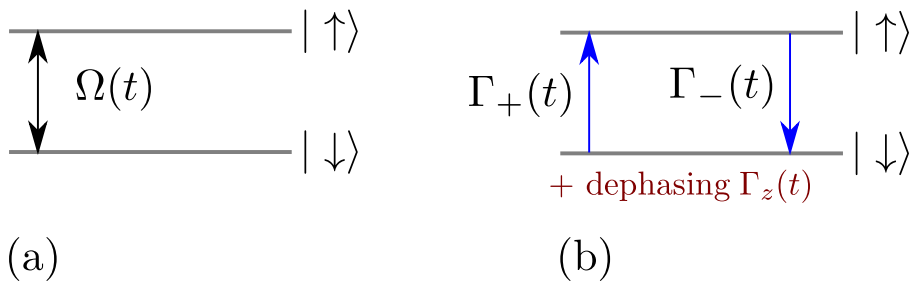

Figure 5.1: **Single qubit example**. (a) We consider a two-level system with time-dependent energy gap $\Omega(t)$. (b) To this model, we add three dissipative processes (5.6.2) corresponding to amplitude damping processes due to the presence of laser polarizers plus a dephasing noise in the $\hat{\sigma}^z$ basis.

laser polarizers whereas the last one represents a dephasing in the $\hat{\sigma}^z$ basis, see Fig.5.1b. In fact, if we consider the Lindblad dissipator associated with $\hat{L}_+$, that is

$$\check{\mathcal{D}}_\uparrow \hat{\rho} = \hat{\sigma}^+ \hat{\rho} \hat{\sigma}^- - \frac{1}{2}\{\hat{\sigma}^-\hat{\sigma}^+, \hat{\rho}\}, \tag{5.6.3}$$

it is easy to see that its target state is given by

$$\check{\mathcal{D}}_\uparrow \hat{\rho} = 0 \quad \Leftrightarrow \quad \hat{\rho} = |\uparrow\rangle\langle\uparrow| ; \tag{5.6.4}$$

and similarly for the others. The full master equation is therefore taken as

$$\frac{\mathrm{d}}{\mathrm{d}t}\hat{\rho}(t) = \frac{i}{2}\Omega(t)[\hat{\sigma}^z, \hat{\rho}(t)] + \sum_{j=\pm,z} \Gamma_j(t)\left(\hat{\sigma}^j \hat{\rho}(t) \hat{\sigma}^{j\dagger} - \frac{1}{2}\{\hat{\sigma}^{j\dagger}\hat{\sigma}^j, \hat{\rho}(t)\}\right). \tag{5.6.5}$$

The natural operator basis $\left\{\hat{F}_k\right\}$ in this case is given by the normalized Pauli matrices $\hat{\sigma}^k/\sqrt{2}$ $(k = 0, x, y, z)$ where $\hat{\sigma}_0$ is the normalized 2×2 identity $\hat{\mathbb{1}}/\sqrt{2}$. Then, writing the master equation in vectorized form, as in Eq.(5.2.11), we find

$$\check{\mathscr{L}}(t) = -\frac{\Omega(t)}{\sqrt{2}}\check{\mathcal{H}}_z + \alpha(t)\left(\check{\mathcal{D}}_{xx} + \check{\mathcal{D}}_{yy}\right) + i\beta(t)\left(\check{\mathcal{D}}_{xy} - \check{\mathcal{D}}_{yx}\right) + 2\Gamma_z(t)\check{\mathcal{D}}_{zz} \tag{5.6.6}$$

where $\check{\mathcal{H}}_i$ and $\check{\mathcal{D}}_{ij}$ are defined in Eqs.(5.3.6a), (5.3.6b) and we have defined

$$\alpha(t) \equiv \frac{\Gamma_+(t) + \Gamma_-(t)}{2}; \quad \beta(t) \equiv \frac{\Gamma_+(t) - \Gamma_-(t)}{2}. \tag{5.6.7}$$

At this point, it is useful to introduce the combinations of super-operators

$$\check{\mathcal{D}}_{\uparrow;\downarrow} = \frac{1}{2}(\check{\mathcal{D}}_{xx} + \check{\mathcal{D}}_{yy} \mp i\check{\mathcal{D}}_{xy} \pm i\check{\mathcal{D}}_{yx}) \tag{5.6.8}$$

in terms of which the Liouvillean in Eq.(5.6.6) simply reads

$$\check{\mathscr{L}}(t) = -\frac{\Omega(t)}{\sqrt{2}}\,\check{\mathcal{H}}_z + \Gamma_+(t)\check{\mathcal{D}}_\uparrow + \Gamma_-(t)\check{\mathcal{D}}_\downarrow + 2\Gamma_z(t)\check{\mathcal{D}}_{zz}. \tag{5.6.9}$$

Moreover, the set of super-operators $\{\check{\mathcal{H}}_z, \check{\mathcal{D}}_\uparrow, \check{\mathcal{D}}_\downarrow, \check{\mathcal{D}}_{zz}\}$ forms a simple closed subalgebra having only

$$[\check{\mathcal{D}}_\uparrow, \check{\mathcal{D}}_\downarrow] = \check{\mathcal{D}}_\uparrow - \check{\mathcal{D}}_\downarrow \tag{5.6.10}$$

as a non-zero commutator.

We shall now provide an exact solution for the time-dependent Lindblad equation (5.6.5) using the rotating frame technique of Sec.5.4.2. We design a map $\check{W}(t)$ to $\mathcal{S}_{\text{aux}}$ in the form:

$$\check{W}(t) = \exp(f(t)\check{\mathcal{H}}_z)\,\exp(g_1(t)\check{\mathcal{D}}_\uparrow)\,\exp(g_2(t)\check{\mathcal{D}}_\downarrow)\,\exp(g_3(t)\check{\mathcal{D}}_{zz}) \tag{5.6.11}$$

with some (unknown) functions f, g_1, g_2, g_3.
Next, from Eqs.(5.4.24), (5.4.26) and computing the non-trivial blocks:

$$\begin{aligned}
\left[e^{g_1(t)\,\check{\mathcal{D}}_\uparrow}\right]\,\check{\mathcal{D}}_\downarrow\,\left[e^{-g_1(t)\,\check{\mathcal{D}}_\uparrow}\right] &= e^{-g_1(t)}\,\check{\mathcal{D}}_\downarrow + \left(1 - e^{-g_1(t)}\right)\check{\mathcal{D}}_\uparrow; \qquad (5.6.12)\\
\left[e^{g_2(t)\,\check{\mathcal{D}}_\downarrow}\right]\,\check{\mathcal{D}}_\uparrow\,\left[e^{-g_2(t)\,\check{\mathcal{D}}_\downarrow}\right] &= e^{-g_2(t)}\,\check{\mathcal{D}}_\uparrow + \left(1 - e^{-g_2(t)}\right)\check{\mathcal{D}}_\downarrow,
\end{aligned}$$

we obtain the set of first-order differential equations:

$$\frac{\mathrm{d}}{\mathrm{d}t}f(t) - \frac{1}{\sqrt{2}}(\Omega(t) - \Omega^{\text{aux}}) = 0; \tag{5.6.13a}$$

$$\frac{\mathrm{d}}{\mathrm{d}t}g_3(t) + 2(\Gamma_z(t) - \Gamma_z^{\text{aux}}) = 0; \tag{5.6.13b}$$

$$\begin{aligned}
\Gamma_+^{\text{aux}} = {}& \frac{\mathrm{d}}{\mathrm{d}t}g_1(t) + \left(1 - e^{-g_1(t)}\right)\,\frac{\mathrm{d}}{\mathrm{d}t}g_2(t)\\
&+ \left(1 + e^{-(g_1(t)+g_2(t))} - e^{-g_1(t)}\right)\Gamma_+(t) + \left(1 - e^{-g_1(t)}\right)\Gamma_-(t);
\end{aligned} \tag{5.6.13c}$$

$$\Gamma_-^{\text{aux}} = e^{-g_1(t)}\left(\frac{\mathrm{d}}{\mathrm{d}t}g_2(t) + \Gamma_+(t) + \Gamma_-(t)\right) - e^{-(g_1(t)+g_2(t))}\Gamma_+(t); \tag{5.6.13d}$$

where the values at $t = t_0$ of the functions f, g_1, g_2 and g_3 are specified through the choice of the initial state $|\hat{\rho}_{\text{aux}}(t_0)\rangle$ in $\mathcal{S}_{\text{aux}}$. Eqs. (5.6.13a) and (5.6.13b) are readily solvable while, taking the sum and the difference of (5.6.13c)-(5.6.13d), we obtain

$$\begin{aligned} r(t) &\equiv g_1(t) + g_2(t) \\ &= -\int^t \mathrm{d}t' \left((\Gamma_+(t') - \Gamma_+^{\text{aux}}) + (\Gamma_-(t') - \Gamma_-^{\text{aux}}) \right) \end{aligned} \tag{5.6.14}$$

and

$$\frac{\mathrm{d}}{\mathrm{d}t} y(t) + (\Gamma_+(t) + \Gamma_-(t)) y(t) - \Gamma_+(t) - e^{r(t)} \Gamma_-^{\text{aux}} = 0, \tag{5.6.15}$$

where $y(t) \equiv \exp(g_2(t))$.

For a periodic driving, we can conveniently require the condition (5.5.5) and look for a periodic solution of Eqs.(5.6.13). In this case, one finds the Floquet parameters:

$$\Omega^F = \overline{\Omega}, \qquad \Gamma_z^F = \overline{\Gamma}_z; \tag{5.6.16}$$

and

$$\Gamma_\pm^F(t_0) = \overline{\Gamma}_\pm \mp \delta\Gamma(t_0) \tag{5.6.17}$$

with Floquet shift of the polarizers

$$\delta\Gamma(t_0) = (1 - y(t_0))\overline{\Gamma}_+ + (e^{r(t_0)} - y(t_0))\overline{\Gamma}_-. \tag{5.6.18}$$

5.6.1 Counter-oscillating polarizers

As a first illustration, we consider the case of a periodic driving with polarizers:

$$\Gamma_\pm(t) = \overline{\Gamma}_\pm \pm A \sin(\omega t) \tag{5.6.19}$$

where $|A| \leq \overline{\Gamma}_\pm$ and $\omega \equiv 2\pi/\mathcal{T}$. For this setting, the solution of Eq.(5.6.15) is given by

$$y(t) = 1 + \frac{A}{\Gamma^2 + \omega^2} (\Gamma \sin(\omega t) - \omega \cos(\omega t)), \tag{5.6.20}$$

where $\Gamma \equiv \overline{\Gamma}_+ + \overline{\Gamma}_-$, and leads to a Floquet shift of the polarizers

$$\delta\Gamma(t_0) = \frac{A\omega\Gamma}{\Gamma^2 + \omega^2}. \tag{5.6.21}$$

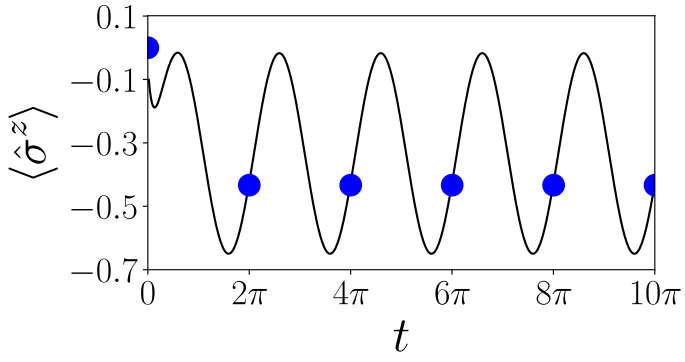

Figure 5.2: **Time evolution of the spin magnetization**. We show the evolution of $\langle\hat{\sigma}^z\rangle = \mathrm{tr}(\hat{\rho}(t)\,\hat{\sigma}^z)$ for the two-level open quantum system in Eq.(5.6.5) with counter-oscillating polarizers $\Gamma_+ = 2.0 + 0.5\sin(t)$, $\Gamma_- = 3.0 - 0.5\sin(t)$ and $\Gamma_z = 0$, $\Omega = \sqrt{2}(1-\cos(t))$. The numerical exact time evolution (*full line*) is compared with the stroboscopic evolution (*dots*) given by Eq.(5.6.21). The system is prepared at $t = 0$ in a state $\hat{\rho}(0) = \hat{\mathbb{1}}/2$.

In Fig.5.2, we show the time evolution of the magnetization of a single qubit subject to counter-oscillating polarizers (5.6.19) for a specific choice of the parameters in Eq.(5.6.5).
We now apply the high-frequency expansions derived in Sec.5.5.1 for the solution of this specific model. From Eq.(5.5.16) one obtains the Floquet parameters:

$$\delta\Gamma(t_0) = \frac{A\Gamma}{\omega} + \mathcal{O}(\omega^{-3})\,, \tag{5.6.22}$$

$\Omega^F = \overline{\Omega} + \mathcal{O}(\omega^{-3})$ and $\Gamma_z^F = \overline{\Gamma}_z + \mathcal{O}(\omega^{-3})$, in agreement with the exact solution (5.6.21). For the micromotion one has from Eq.(5.5.17):

$$\begin{aligned}\check{\mathcal{K}}(t,0) =& \frac{A}{\omega}[1-\cos(\omega t)]\left(\check{\mathcal{D}}_\uparrow - \check{\mathcal{D}}_\downarrow\right) \\ &+ \frac{A\sin(\omega t)}{\omega^2}\left(\Gamma\left(\check{\mathcal{D}}_\uparrow - \check{\mathcal{D}}_\downarrow\right) + \Delta\,\check{\mathcal{H}}_z\right) + \mathcal{O}(\omega^{-3}),\end{aligned} \tag{5.6.23}$$

setting $t_0 = 0$ and $\Omega = \overline{\Omega} + \Delta\cos(\omega t)$. The time evolution of the spin magnetization obtained in high-frequency approximation is shown in Fig.5.3 for different values of the driving frequency. As expected, the larger ω, the better the agreement with the exact solution.

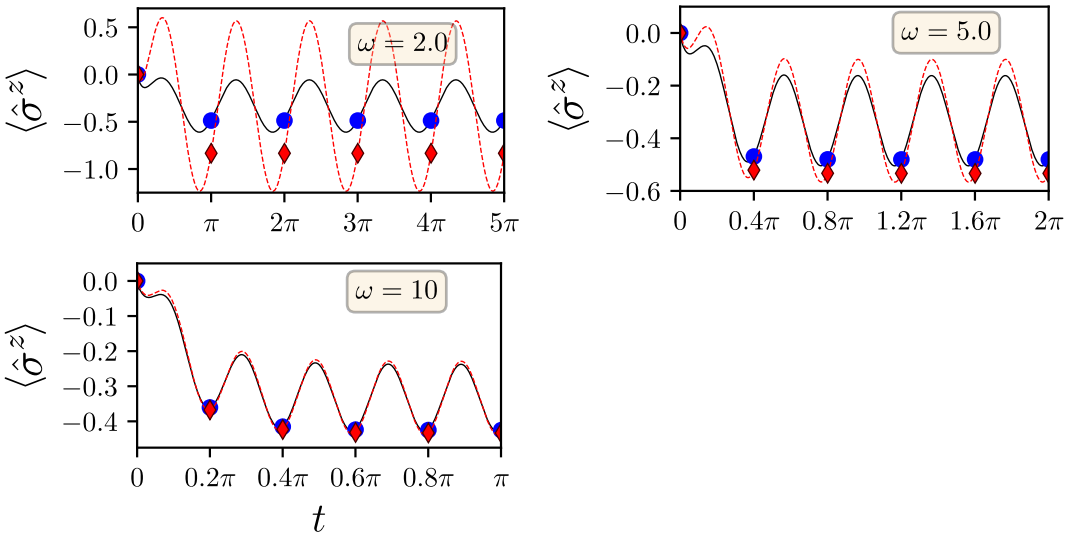

Figure 5.3: **Time evolution of the spin magnetization in high-frequency expansion.** Evolution of $\langle \hat{\sigma}^z \rangle = \mathrm{tr}(\hat{\rho}(t)\,\hat{\sigma}^z)$ for the single qubit in Eq.(5.6.5) with counter-oscillating polarizers $\Gamma_+ = 2.0 + 0.5\sin(\omega t)$, $\Gamma_- = 3.0 - 0.5\sin(\omega t)$ and with $\Gamma_z = 0$, $\Omega = \sqrt{2}(1-\cos(\omega t))$. The numerical exact time evolution (*full line*) is compared with the approximate time evolution (*dashed line*) obtained in high-frequency expansion at second order for three values of the driving frequency $\omega = 2.0,\ 5.0,\ 10$. The dots show the stroboscopic evolution (*circle*: exact, *diamond*: approximate). The system is prepared at time $t = 0$ in a state $\hat{\rho}(0) = \hat{\mathbb{1}}/2$.

5.6.2 Incoherent driving

Next, we provide an example of a non-periodic driving for the Lindblad evolution in Eq.(5.6.5) of a single qubit. In particular, we shall consider the case where $\Gamma_z = 0$, Ω is kept constant and where the system is incoherently driven by the polarizers:

$$\Gamma_+(t) = A(1 - \tanh(t/t_s))\,, \quad \Gamma_-(t) = A(1 + \tanh(t/t_s)) \tag{5.6.24}$$

that we plot in Fig.5.4a for different values of the time scale t_s of the driving. As we can see, the amplitudes $\Gamma_\pm(t)$ of the two polarizers cross each other at $t = 0$ leading to a change in the target state of the relaxation during the time evolution. In other words, at a given time t, the qubit will feel the resulting effect of the two competing drivings and thus it will try to follow a target state that is changing in time. This time evolution can be described with the help of

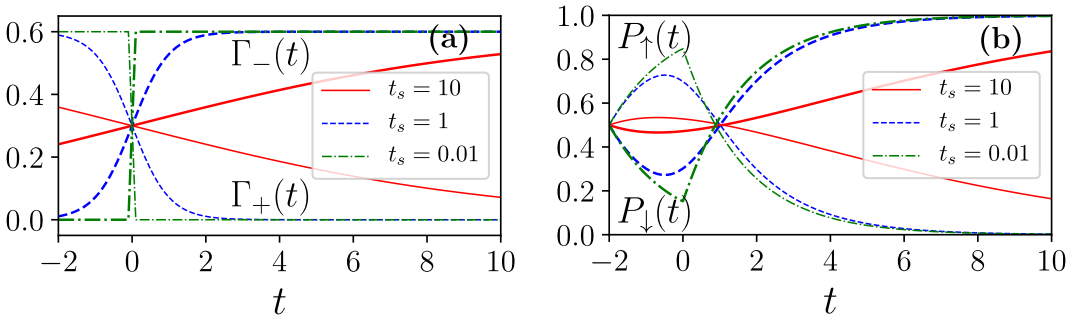

Figure 5.4: **Incoherent driving of a single qubit.** (a) The incoherent driving is made through the polarizers in Eq.(5.6.24). In the plot we show the time evolution of Γ_+ (*thin line*) and Γ_- (*bold line*) for three values of the time scale t_s, ranging from an adiabatic to a quench regime. The amplitude is set to the value $A = 0.3$. (b) Time evolution of the population (5.6.28) of the excited (ground) state in *thin line* (*bold line*) of a single qubit subject to the polarizers in Eq.(5.6.24). We prepare our system at $t_0 = -2$ in a high-temperature state $\hat{\rho}(t_0) = \hat{\mathbb{1}}_2/2$ with $A = 0.3$ and $\Omega = 1.0$. We clearly see that the system changes its target state when the amplitudes of the two lasers cross each other. This effect becomes sharper for short time scale t_s. In particular, in the quench regime (*dashed dotted line*) the population presents a cusp point at the crossover related to the sudden switch of the laser direction.

Eqs.(5.4.2),(5.4.3), which lead to the dynamical map:

$$\check{\Lambda}(t,t_0) = \exp(-\frac{\Omega}{\sqrt{2}}(t-t_0)\,\check{\mathcal{H}}_z)\,\exp(\pi_1(t)\,\check{\mathcal{D}}_\uparrow)\,\exp(\pi_2(t)\,\check{\mathcal{D}}_\downarrow) \tag{5.6.25}$$

where π_1, π_2 satisfy

$$\frac{\mathrm{d}}{\mathrm{d}t}\pi_1(t) + (1-e^{-\pi_1(t)})\frac{\mathrm{d}}{\mathrm{d}t}\pi_2(t) = \Gamma_+(t); \tag{5.6.26a}$$

$$e^{-\pi_1(t)}\,\frac{\mathrm{d}}{\mathrm{d}t}\pi_2(t) = \Gamma_-(t), \tag{5.6.26b}$$

with initial conditions $\pi_{1,2}(t_0) = 0$ and formal solutions

$$\pi_2(t) = \log\left(1 + \int_{t_0}^{t} \mathrm{d}t'\, e^{2A\,(t'-t_0)}\,\Gamma_-(t')\right), \tag{5.6.27a}$$

$$\pi_1(t) = -\pi_2(t) + 2A\,(t-t_0). \tag{5.6.27b}$$

Defining the projectors $P_\uparrow = |\uparrow\rangle\langle\uparrow|$ on the excited state and $P_\downarrow = |\downarrow\rangle\langle\downarrow|$ on the ground state, one can then follow the time evolution of the populations

$$P_\uparrow(t) = \mathrm{tr}\left(|\uparrow\rangle\langle\uparrow|\ \hat{\rho}(t)\right) = \mathrm{tr}\left(|\uparrow\rangle\langle\uparrow|\ \check{\Lambda}(t,t_0)\,\hat{\rho}(t_0)\right) \tag{5.6.28}$$

and similarly for $P_\downarrow(t)$, as shown in Fig.5.4b. As expected, the dynamics of the populations exchanges behavior when the direction of the resulting laser beam is inverted. This effect becomes sharper as we decrease t_s and eventually generates a non-analytical point in the quench regime $t_s \to 0$.

5.7 Quantum heat-engines

An interesting application of the Floquet-Lindblad formalism outlined in Sec.5.5 concerns the analysis of finite-time quantum heat-engines [Sco18a, Ali79, Kos14, Ali15, Rez06, Aba14, Kla17, Ros14, Cor14, Jar16, Sam17, dC14, Aba17, Aba18, Cam16, Elo17, Cot17, Mas18, Man18, Mic17, Man19].
A quantum heat-engine may be defined as a quantum open system capable to convert the thermal energy extracted from a hot source into a power output. To do so, an abstract quantum heat-engine needs:

1. an open quantum system $\mathcal{S}$ that is used as *working fluid*;
2. a *hot* and a *cold* thermal bath $\mathcal{R}$ through which the engine can extract work;
3. some periodic fields that determine its *operation cycle*.

An illustration of a quantum heat-engine is given in Fig.5.1.
It is easy to show that the points 1-3 can be readily implemented by considering a time-periodic Lindblad master equation. The points 1,3 are straightforward and will depend on the specific master equation that is considered. The design of a thermal bath with Lindblad dissipators requires instead a further comment. On one hand, any elementary dissipative process $\hat{L}_\alpha$ is associated to a target state of relaxation $\hat{\rho}$ defined through the condition:

$$\left[\hat{L}_\alpha\,\hat{\rho}\,\hat{L}_\alpha^\dagger - \frac{1}{2}\{\hat{L}_\alpha^\dagger\hat{L}_\alpha,\hat{\rho}\}\right] = 0. \tag{5.7.1}$$

On the other hand, a thermal bath at temperature T induces a relaxation towards a thermal distribution where the populations on each level satisfy a

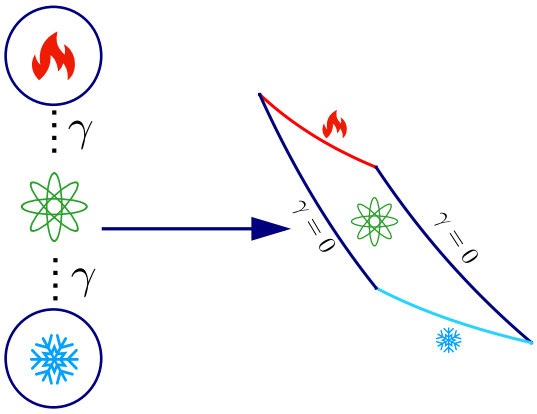

Figure 5.1: **Abstract quantum heat-engine**. Illustration of an abstract quantum heat-engine made out of: (i) an open quantum system that is used as working fluid (*green atom*); (ii) a hot (*red fire*) and a cold (*pale blue ice*) thermal bath; (iii) the time-periodic dependence of the Lindblad master equation which determines the cyclic evolution (e.g. a *Carnot cycle*, see Sec.5.7.2 and Sec.5.8.7).

detailed balance condition. For instance, in a two-level system we will have at thermal equilibrium:

$$\frac{P_{\downarrow}}{P_{\uparrow}} = \exp\left(\Omega/T\right) \tag{5.7.2}$$

with Ω the energy gap between the two states. Hence, one can easily see that imposing the detailed balance condition

$$\frac{\Gamma_{-}}{\Gamma_{+}} = \frac{P_{\downarrow}}{P_{\uparrow}} = \exp\left(\Omega/T\right) \tag{5.7.3}$$

on the relaxation coefficients $\Gamma_{\pm}$, the target state defined by the combined effect of the Lindblad dissipators $\hat{L}_{\pm}$ is the same of that of a thermal bath at temperature T. Such a picture extends similarly to more complicated systems.

The operation of these quantum devices relies on the existence of a *limit-cycle state*, where the system behaves cyclically during the time-evolution. Although it is easy to identify the basic elements of an abstract quantum heat-engine, understanding what is the state of the system within the cyclic dynamics and if this state can be eventually reached are non-trivial tasks. Quite remarkably, a clear answer to these questions can be provided by the Floquet generator $\check{\mathscr{L}}_F$ in Eq.(5.5.3).

First, the convergence to a cyclic evolution is directly associated to the spectrum

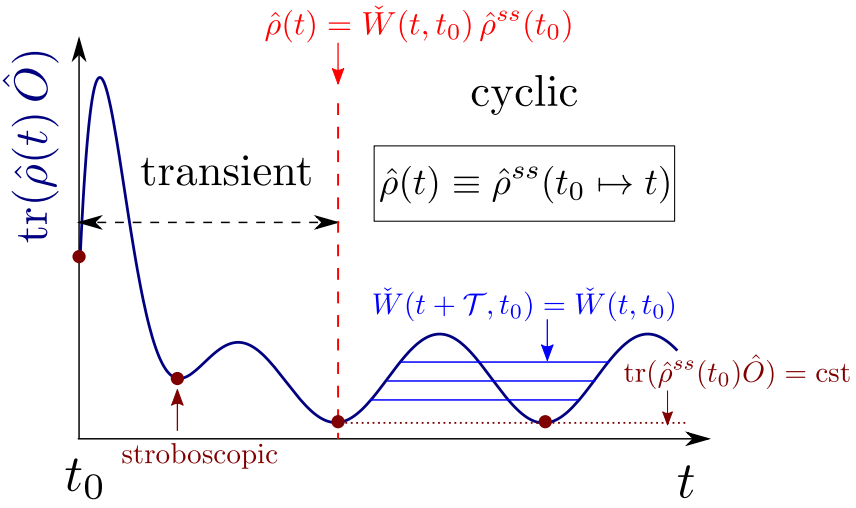

Figure 5.2: **Convergence towards a limit-cycle state.** Illustration of the time evolution of a generic observable $\langle \hat{O} \rangle = \mathrm{tr}(\hat{\rho}(t)\,\hat{O})$, with $\hat{O} \in \mathrm{end}(\mathscr{H}_S)$ a generic operator. After a transient regime, the dynamics converges towards a cyclic evolution where the state of the system reads $\rho(t) \equiv \hat{\rho}^{ss}(t \mapsto t_0)$.

of the Floquet-Liouvillean and, more precisely, the real part of its eigenvalues determines the time-scale of the transient regime.
Next, one has, by construction, that the zero-eigenstate of the Floquet-Liouvillean

$$\check{\mathscr{L}}_F(t_0)\,|\hat{\rho}^{ss}(t_0)\rangle = 0, \tag{5.7.4}$$

defines a stroboscopic steady-state of the time evolution i.e., a steady-state that is observed if we consider time steps of one period. Once the system is stroboscopically converged towards the steady-state $\hat{\rho}^{ss}(t_0)$, the dynamics becomes time-periodic with a limit-cycle state given by

$$|\hat{\rho}(t)\rangle = \check{W}(t,t_0)\,|\hat{\rho}^{ss}(t_0)\rangle\,. \tag{5.7.5}$$

Since $\check{W}(t)$ in Eq.(5.4.23) is chosen to be periodic, the micromotion generator $\check{W}(t,t_0)$ in Eq.(5.5.4) is also periodic in both its arguments and satisfies $\check{W}(t_0,t_0) = \hat{\mathbb{1}} \otimes \hat{\mathbb{1}}$. Hence, without loss of generality, we can follow the cyclic evolution by setting the intial time $t_0 \mapsto t$ so that the limit-cycle state will read:

$$\hat{\rho}(t) \equiv \hat{\rho}^{ss}(t_0 \mapsto t). \tag{5.7.6}$$

We conclude that all the relevant properties of the system within the cyclic evolution can be described solely in terms of the Floquet-Liouvillean. In par-

ticular, the convergence towards the cycle is dictated by its spectrum whereas the limit-cycle state is simply the zero-eigenstate of $\check{\mathscr{L}}_F(t_0 \mapsto t)$, provided that this state is unique. An illustration of convergence towards a cyclic evolution is given in Fig.5.2.

The operation cycle can be characterized through the time-evolution of thermodynamic quantities. In Lindblad approximation[§], the dynamics of an operator $\hat{O}(t) \in \mathrm{end}(\mathscr{H}_S)$ is generated by the Heisenberg master equation (see Eq.(5.1.39)):

$$\frac{\mathrm{d}}{\mathrm{d}t}\hat{O}(t) = \frac{\partial}{\partial t}\hat{O}(t) + i[\hat{H}(t), \hat{O}(t)] + \check{\mathcal{D}}^{\star}(t)\,\hat{O}(t), \tag{5.7.7}$$

where the dual Lindblad dissipator $\check{\mathcal{D}}^{\star}$ reads

$$\check{\mathcal{D}}^{\star}(t)\,\bullet = \sum_{k,l=1}^{n^2-1} \gamma_{kl}(t)\left(\hat{F}_l \,\bullet\, \hat{F}_k - \frac{1}{2}\{\hat{F}_l\,\hat{F}_k, \bullet\}\right). \tag{5.7.8}$$

Defining the internal energy of the system as $E(t) \equiv \langle \hat{H}(t) \rangle_{ss}$, with $\langle \bullet \rangle_{ss} \equiv \mathrm{tr}(\hat{\rho}^{ss}(t)\,\bullet)$, we have from Eq.(5.7.7)

$$\frac{\mathrm{d}}{\mathrm{d}t}E(t) = \left\langle \frac{\partial}{\partial t}\hat{H}(t) \right\rangle_{ss} + \left\langle \check{\mathcal{D}}^{\star}(t)\,\hat{H}(t) \right\rangle_{ss} \tag{5.7.9}$$

which is nothing but the quantum analogue of the first law of thermodynamics in a differential form [Ali79, Gev92]. Indeed, we may interpret the two terms in the r.h.s. of Eq.(5.7.9)

$$\mathcal{P}(t) = \left\langle \frac{\partial}{\partial t}\hat{H}(t) \right\rangle_{ss}, \quad \delta\mathcal{Q}(t) = \left\langle \check{\mathcal{D}}^{\star}(t)\,\hat{H}(t) \right\rangle_{ss}, \tag{5.7.10}$$

as the power output $\mathcal{P}$ and the heat flow $\delta\mathcal{Q}$ of the engine.
From the latter, one can eventually define the *efficiency* η of the quantum heat-engine as the ratio between the rate of work generated and the rate of thermal energy extracted from the bath i.e.,

$$\eta \equiv \frac{\mathcal{P}}{\delta\mathcal{Q}}. \tag{5.7.11}$$

For a wider understanding, we address the reader to Refs. [And17, Kos13, Ali18].

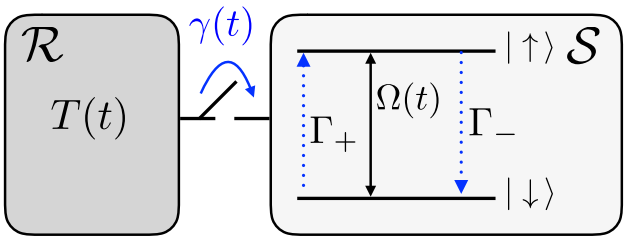

Figure 5.3: **Illustration of a two-level quantum heat-engine.** The Hamiltonian parameter $\Omega(t)$ tunes the energy gap between the ground state $|\downarrow\rangle$ and the excited level $|\uparrow\rangle$. The thermal bath is modeled as in Eq.(5.7.12) with a couple of polarizers Γ_+, Γ_-. The interactions of the system $\mathcal{S}$ with the thermal bath $\mathcal{R}$ are controlled by the interruptor γ.

5.7.1 Two-levels quantum heat-engine

We now apply the general results presented in Sec.5.7 for the concrete design of a quantum heat-engine operating with a working fluid composed of a single qubit [Gev92]. In particular, we consider the Lindblad evolution in Eq.(5.6.5) with $\Gamma_z = 0$ and with polarizers satisfying a detailed balance condition:

$$\frac{\Gamma_-}{\Gamma_+} = \exp(\Omega(t)/T(t))\,, \quad \forall t \geq t_0 \tag{5.7.12}$$

so that their combined effect mimic the relaxation properties induced by a thermal bath $\mathcal{R}$ with time-dependent temperature $T(t)$. A convenient parametrization of the thermal bath is

$$\Gamma_+(t) = \gamma(t)\, n(t)\,, \quad \Gamma_-(t) = \gamma(t)(1 - n(t)) \tag{5.7.13}$$

with

$$n(t) \equiv (1 + e^{\Omega(t)/T(t)})^{-1} \tag{5.7.14}$$

and a control parameter $\gamma(t)$ that allows us to couple (decouple) the system with the bath at different strokes. An illustration of the two-level quantum heat-engine is given in Fig.5.7.1.

Next, we compute the limit-cycle state of the Floquet-Liouvillean (see Sec.5.6):

$$\check{\mathscr{L}}_F(t_0) = -\frac{\overline{\Omega}}{\sqrt{2}}\,\check{\mathcal{H}}_z + \Gamma_+^F(t_0)\,\check{\mathcal{D}}_\uparrow + \Gamma_-(t_0)\,\check{\mathcal{D}}_\downarrow, \tag{5.7.15}$$

[§]That is, for weakly coupled and sufficiently large reservoir $\mathcal{R}$ so that the markovian approximation holds.

where the Floquet parameters $\Gamma^F_\pm$ are given in Eqs.(5.6.17) and (5.6.18). To do so, we consider the following basis of the vectorized space:

$$|\uparrow\rangle\langle\uparrow| \mapsto \begin{bmatrix}1\\0\\0\\0\end{bmatrix} ; \; |\uparrow\rangle\langle\downarrow| \mapsto \begin{bmatrix}0\\1\\0\\0\end{bmatrix} ; \; |\downarrow\rangle\langle\uparrow| \mapsto \begin{bmatrix}0\\0\\1\\0\end{bmatrix} ; \; |\downarrow\rangle\langle\downarrow| \mapsto \begin{bmatrix}0\\0\\0\\1\end{bmatrix} ; \tag{5.7.16}$$

such that the operators in end($\mathscr{H}_\mathcal{S}$) have a 4-vector representation, e.g.

$$\hat{\sigma}^x \mapsto \begin{bmatrix}0\\1\\1\\0\end{bmatrix} ; \; \hat{\sigma}^y \mapsto \begin{bmatrix}0\\i\\-i\\0\end{bmatrix} ; \; \hat{\sigma}^z \mapsto \begin{bmatrix}1\\0\\0\\-1\end{bmatrix} , \tag{5.7.17}$$

and super-operators are represented as 4×4 matrices. The Floquet-Liouvillean takes therefore the form:

$$\check{\mathscr{L}}_F(t_0) = \begin{bmatrix} -\Gamma^F_-(t_0) & 0 & 0 & \Gamma^F_+(t_0) \\ 0 & -\frac{1}{2}\Gamma - i\sqrt{2}\,\overline{\Omega} & 0 & 0 \\ 0 & 0 & -\frac{1}{2}\Gamma + i\sqrt{2}\,\overline{\Omega} & 0 \\ \Gamma^F_-(t_0) & 0 & 0 & -\Gamma^F_+(t_0) \end{bmatrix} \tag{5.7.18}$$

with $\Gamma \equiv \overline{\Gamma}_+ + \overline{\Gamma}_-$. The limit-cycle state is thus obtained from Eq.(5.7.4) and reads

$$\hat{\rho}^{ss}(t_0 \mapsto t) = \hat{F}_0 - \frac{\sqrt{2}}{\Gamma}\,\delta\Gamma(t)\,\hat{F}_3. \tag{5.7.19}$$

The convergence towards $\hat{\rho}^{ss}(t)$ is dictated by the real part of the eigenvalues of $\check{\mathscr{L}}_F$, that are

$$\mathrm{spec}(\check{\mathscr{L}}_F) = \left[0,\, -\Gamma,\, -\frac{1}{2}(\,\Gamma \pm i2\sqrt{2}\,\overline{\Omega})\right], \tag{5.7.20}$$

from which we specificy the time-scale τ of the transient regime to be $\tau = 2/\Gamma$. From the knowledge of the limit-cycle state (5.7.19), one can then compute the expectation value of thermodynamic quantities during the cyclic evolution. In particular, for the internal energy E one has

$$E(t) = \langle \hat{H}(t)\rangle_{ss} = \Omega(t)\frac{\delta\Gamma(t)}{\Gamma}, \tag{5.7.21}$$

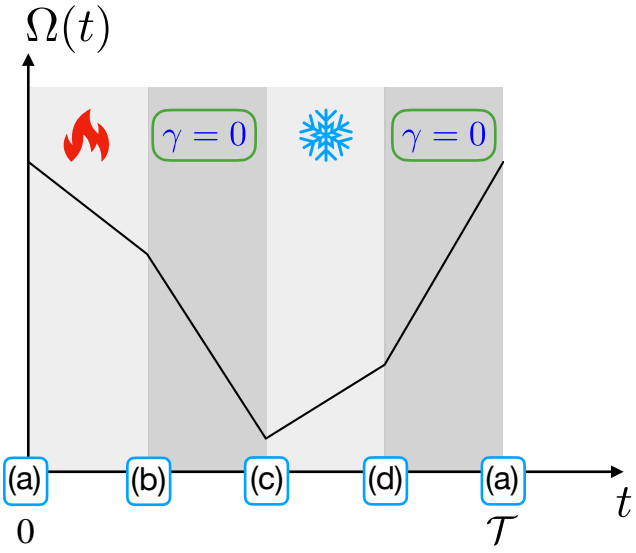

Figure 5.4: **Illustration of a Carnot cycle**. A Carnot cycle is made out of four strokes of duration $\mathcal{T}/4$: **a-b** (**c-d**) a hot (cold) isothermal expansion (compression) where the working parameter is decreasing (increasing), *light gray boxes*; **b-c** (**d-a**) an isentropic expansion (compression) where the system is detached from the bath $\gamma = 0$, *dark gray boxes*. In this figure the working parameter Ω is varied in time as a linear piecewise function, see Eq.(5.7.30).

and similarly

$$\mathcal{P}(t) = \left\langle \frac{\partial}{\partial t}\hat{H}(t) \right\rangle_{ss} = \left(\frac{\mathrm{d}}{\mathrm{d}t}\,\Omega(t)\right) \frac{\delta\Gamma(t)}{\Gamma}; \tag{5.7.22}$$

$$\delta\mathcal{Q}(t) = \left\langle \check{\mathcal{D}}^{\star}(\hat{H}(t)) \right\rangle_{ss} = 2\Omega(t)\,\frac{\Gamma_{+}^{F}(t)\,\Gamma_{-}^{F}(t)}{\Gamma}, \tag{5.7.23}$$

for the power output $\mathcal{P}$ and the heat flow $\delta\mathcal{Q}$ respectively.

5.7.2 Carnot cycle

To illustrate a concrete application of the previous results, we shall consider the operation of a finite-time two-level Carnot engine. The cycle is made of four strokes, which we assume have an equal duration $\mathcal{T}/4$:

(**a-b**) Hot isothermal expansion at T^{hot}

(**b-c**) Isentropic expansion

(**c-d**) Cold isothermal compression at T^{cold}

(**d-a**) Isentropic compression

For our specific model, expansions (compressions) mean decreasing (increasing) the level spacing through the parameter Ω. We shall consider a protocol where $\Omega(t)$ varies in a linear piecewise fashion, as sketched in Fig.5.4. The control function $\gamma(t)$ in Eq.(5.7.13) is set to

$$\gamma(t) = \{\, 1,\, 0,\, 1,\, 0 \,\}\,, \tag{5.7.24}$$

since the system evolves unitarily in the second and in the fourth stroke. Finally, the time-dependence of $T(t)$ is given by

$$T(t) = \left\{T^{hot},\, -\,, T^{cold},\, -\right\}, \quad T^{hot} > T^{cold} \tag{5.7.25}$$

where the notation "$-$" means that the specific value of the temperature in that interval is not physically relevant since the thermal bath is detached from the system.

Quasi-static reversibility limit

For large enough values of the driving period $\mathcal{T} \gg 1$, the evolution of the quantum heat-engine can be investigated by using standard equilibrium statistical mechanics. During the isothermal strokes the expectation value of the energy reads

$$E(t) = \langle \hat{H}(t) \rangle_{eq} = \frac{\Omega(t)}{2}\, \tanh(\frac{\Omega(t)}{2T}) \tag{5.7.26}$$

where $\langle \bullet \rangle_{eq} \equiv \mathrm{tr}(\hat{\rho}^{eq}\, \bullet)$ is the average computed with the thermal equilibrium density matrix $\hat{\rho}^{eq}$ at a fixed temperature T:

$$\hat{\rho}^{eq} = \frac{1}{2\cosh(\Omega(t)/T)} \begin{bmatrix} e^{-\Omega(t)/2T} & 0 \\ 0 & e^{\Omega(t)/2T} \end{bmatrix}. \tag{5.7.27}$$

On the other hand, in the isentropic strokes the evolution is unitary and any variation in the internal energy is due to a variation of the energy separation of the two levels:

$$E(t_2) = \frac{\Omega(t_2)}{\Omega(t_1)}\, E(t_1)\,, \tag{5.7.28}$$

as follows from the adiabatic theorem in standard quantum mechanics. We can see that depending on the driving protocol being used, the cycle may not have a reversible quasi-static limit. The reason is that, if by the end of the isentropic strokes (**c** and **a**) the value of the energies in Eq.(5.7.28) are not the same to those at thermal equilibrium in Eq.(5.7.26) with a hot and a cold temperature, then a dissipation inevitably will take place. The condition for the existence of a quasi-static reversibility condition is therefore obtained by imposing that [Sco18a, Sek00, Lek18]

$$\frac{T^{cold}}{T^{hot}} = \frac{\Omega(\mathbf{c})}{\Omega(\mathbf{b})} = \frac{\Omega(\mathbf{d})}{\Omega(\mathbf{a})}\,. \tag{5.7.29}$$

These conditions are usually referred to as *quasi-static reversibility*.

Finite-time operation

We now turn to the finite-time operation. With Eq.(5.7.29) in mind, we choose the unitary parameter Ω to vary linearly in the four strokes as:

$$\Omega(t) = \begin{cases} \frac{4(\Omega_b-\Omega_a)}{\mathcal{T}}t + \Omega_a \\ \frac{4(\Omega_c-\Omega_b)}{\mathcal{T}}t + 2\Omega_b - \Omega_c \\ \frac{4(\Omega_c-\Omega_d)}{\mathcal{T}}t + 3\Omega_c - 2\Omega_d \\ \frac{4(\Omega_a-\Omega_d)}{\mathcal{T}}t + 3\Omega_a - 4\Omega_d \end{cases} \tag{5.7.30}$$

with $\Omega_c = (T^{cold}/T^{hot})\Omega_b$ and $\Omega_d = (T^{cold}/T^{hot})\Omega_a$.

At this point, it only remains to compute explicitly the Floquet parameters $\Gamma^F_\pm(t)$ for the two-level quantum engine. Recall that the polarizers $\Gamma_\pm(t)$ are set as in Eq.(5.7.13) and $\Gamma^F_\pm(t)$ have the form (see Eq.(5.6.17) and (5.6.18)):

$$\Gamma^F_\pm(t) = \overline{\Gamma}_\pm \mp \delta\Gamma(t) \tag{5.7.31}$$

with the Floquet shift

$$\delta\Gamma(t) = (1-y(t))\overline{\Gamma}_+ + (e^{r(t)} - y(t))\overline{\Gamma}_- \tag{5.7.32}$$

where (see Eq.(5.6.13d) and (5.6.15))

$$r(t) = \int_{t_0}^{t} \mathrm{d}t'\ (\Gamma - \gamma(t'))\,; \tag{5.7.33a}$$

$$\frac{\mathrm{d}y(t)}{\mathrm{d}t} = \gamma(t)\left(y(t) - n(t) - e^{r(t)}(1-n(t))\right); \quad y(0) = y(\mathcal{T}). \tag{5.7.33b}$$

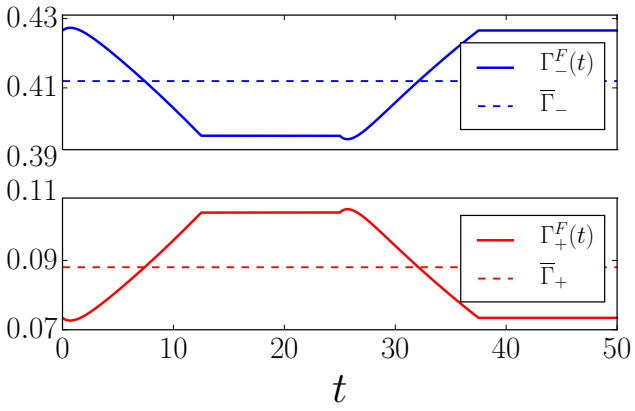

Figure 5.5: **Carnot engine: Floquet parameters.** Numerical results for the Floquet parameters in Eqs.(5.7.31) obtained by solving Eq.(5.7.33) with polarizers $\Gamma_\pm$ in Eq.(5.7.13) and energy level separation Ω in Eq.(5.7.30). We have set: $\Omega_a = 1.8$, $\Omega_b = 1.3$ and temperatures $T^{hot} = 1.0$, $T^{cold} = 0.5$. The driving period is $\mathcal{T} = 50$.

Hence, a numerical integration of Eq.(5.7.33) allows us to determine the Floquet parameters. We show the results in Fig.5.5.
From Eq.(5.7.21), one is then able to compute the cyclic evolution of the internal energy $E(t)$; the result is shown in Fig.5.6 for different values of the driving period $\mathcal{T}$. As expected, at large $\mathcal{T}$, one observes a convergence towards the quasi-static regime described before. All the deviations at finite-time operation from the quasi-static limit can be addressed to a non-equilibrium behavior of the device. The latter can be quantified through the deviations of the cycle area $\mathcal{A}$

$$\mathcal{A}(\mathcal{T}) \equiv \oint_{t\in[0,\mathcal{T}]} \mathrm{d}(1/\Omega(t))\, E(t), \tag{5.7.34}$$

from its quasi-static limit value $\mathcal{A}_{\rm qs}$

$$\mathcal{A}_{\rm qs} \equiv \oint \mathrm{d}(1/\Omega(t))\, E_{\rm qs}(t) \tag{5.7.35}$$

where $E_{\rm qs}(t)$ is given in Eqs.(5.7.26) and (5.7.28). Introducing the quantity

$$\delta_{\mathcal{A}} \equiv 1 - \frac{\mathcal{A}(\mathcal{T})}{\mathcal{A}_{\rm qs}}, \tag{5.7.36}$$

a numerical estimation of the cycle areas reveals that the approach to the equilibrium quasi-static operation is

$$\delta_{\mathcal{A}} \propto 1/\mathcal{T}, \tag{5.7.37}$$

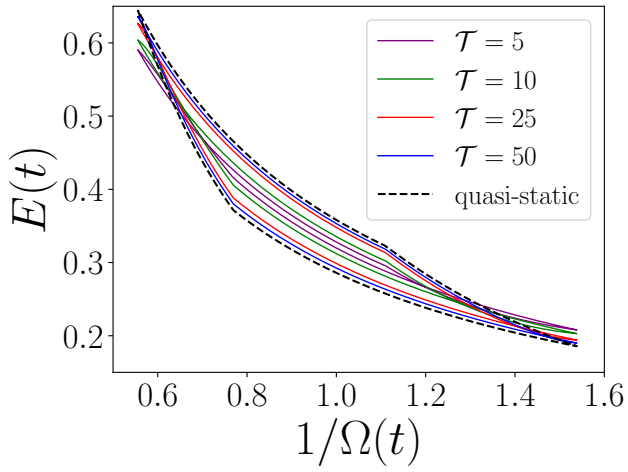

Figure 5.6: **Operation of a finite-time Carnot engine.** The plot shows the internal energy $E(t)$ as function of the compression $1/\Omega(t)$. In the figure we select Ω as in Eq.(5.7.30), setting $\Omega_a = 1.8$, $\Omega_b = 1.3$ and the thermal bath in Eq.(5.7.13) with $T^{hot} = 1.0$, $T^{cold} = 0.5$. We see that increasing the value of the driving period $\mathcal{T}$ (from the innermost to the outermost), the cycle converges towards its quasi-static limit.

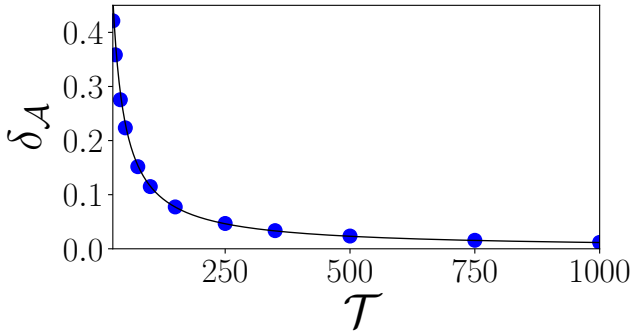

Figure 5.7: **Carnot cycle: convergence toward the quasi-static limit**. A numerical estimation of the deviations of the cycle areas $\delta_{\mathcal{A}}$ in Eq.(5.7.36) for the two-level Carnot engine in Fig.5.6. We see that the approach to the quasi-static limit is $\propto 1/\mathcal{T}$ with a proportionality constant $c = 11.6$, extracted from our fitting datas.

as shown in Fig.5.7.

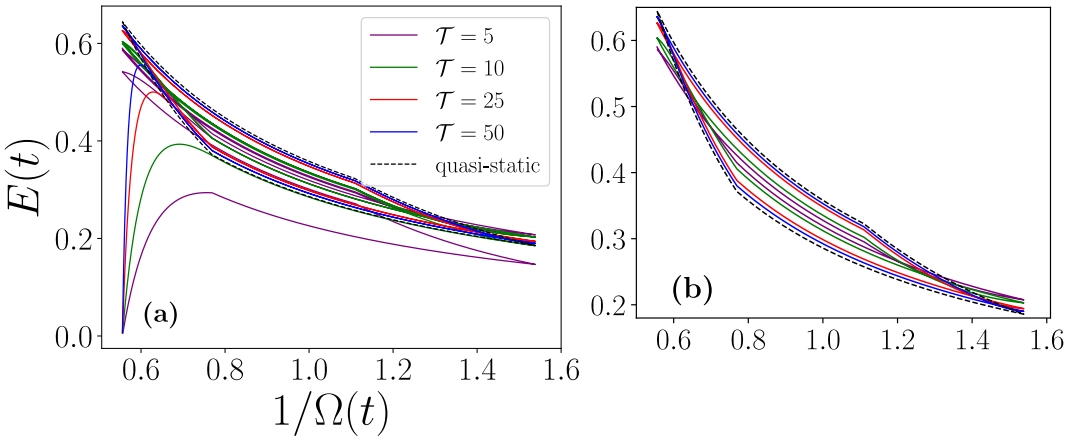

Figure 5.8: **Carnot engine: coherence vector formalism.** Operation of a finite-time Carnot engine obtained by a numerical solution of Eqs.(5.7.40) with initial state $\hat{\rho}(0) = \hat{\mathbb{1}}/2$. The plots show the internal energy $E(t)$ as function of the compression $1/\Omega(t)$. In the figures we have set $\Gamma_z = 0$, Ω in Eq.(5.7.30) with $\Omega_a = 1.8$, $\Omega_b = 1.3$ and the thermal bath as in Eq.(5.7.13) with $T^{hot} = 1.0$, $T^{cold} = 0.5$. (a) We show the solution in a time window $t \in [0, 3\mathcal{T}]$ for different values of the driving period $\mathcal{T}$. We can see that increasing the value of $\mathcal{T}$ (from the innermost to the outermost), the cycle matches its quasi-static limit. (b) Inset showing the time-evolution for $t > 2\mathcal{T}/\Gamma$ where the dynamics becomes cyclic. The result is then in perfect agreement with that of Fig.5.6.

Coherence vector formalism

We also provide an analysis of the two-level Carnot engine based on the matrix formulation of Sec.5.4.1. In the case $n = 2$, we can write the density matrix as

$$\hat{\rho}(t) = \begin{bmatrix} P_\uparrow(t) & a(t) - ib(t) \\ a(t) + ib(t) & 1 - P_\uparrow(t) \end{bmatrix} \tag{5.7.38}$$

(in the basis of $|i\rangle\langle j|$, $i, j = \uparrow, \downarrow$,) with a, b and $P_\uparrow$ real functions, and we obtain the coherence vector:

$$\vec{v}(t) = \frac{1}{\sqrt{2}} \begin{bmatrix} \mathrm{tr}(\hat{\rho}(t)\,\hat{\sigma}^x) \\ \mathrm{tr}(\hat{\rho}(t)\,\hat{\sigma}^y) \\ \mathrm{tr}(\hat{\rho}(t)\,\hat{\sigma}^z) \end{bmatrix} = \sqrt{2} \begin{bmatrix} a(t) \\ b(t) \\ P_\uparrow(t) - \frac{1}{2} \end{bmatrix}. \tag{5.7.39}$$

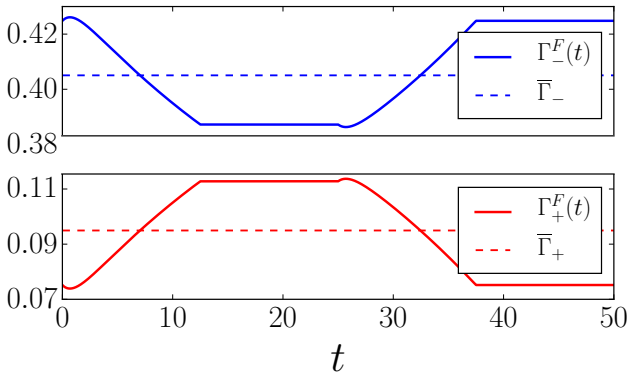

Figure 5.9: **Otto engine: Floquet parameters.** Numerical results for the Floquet parameters in Eqs.(5.7.31) obtained by solving Eq.(5.7.33) with polarizers in Eq.(5.7.13) and energy level separation Ω in Eq.(5.7.41), setting $\Omega_1 = 1.8$, $\Omega_2 = 1.3$. The temperature is varied as in Eq.(5.7.42), requiring quasi-static reversibility conditions (5.7.43) and chosing $T_a = 1.0$, $T_b = 1.5$. The driving period is $\mathcal{T} = 50$.

Next, for the case of Lindblad evolution (5.6.5), the Bloch equation (5.4.7) leads to the set of equations:

$$\frac{\mathrm{d}}{\mathrm{d}t}a(t) - \Omega(t)\, b(t) + (\alpha(t) + 2\Gamma_z(t))a(t) = 0; \tag{5.7.40a}$$

$$\frac{\mathrm{d}}{\mathrm{d}t}b(t) + \Omega(t)\, a(t) + (\alpha(t) + 2\Gamma_z(t))b(t) = 0; \tag{5.7.40b}$$

$$\frac{\mathrm{d}}{\mathrm{d}t}P_\uparrow(t) + 2\alpha(t)P_\uparrow(t) - (\alpha(t) + \beta(t)) = 0, \tag{5.7.40c}$$

with $\alpha(t) = \frac{1}{2}(\Gamma_+(t) + \Gamma_-(t))$ and $\beta(t) = \frac{1}{2}(\Gamma_+(t) - \Gamma_-(t))$.
If we set then $\Gamma_z = 0$ and $\Gamma_\pm$, Ω as in Eqs.(5.7.13), (5.7.30) respectively, a numerical integration of (5.7.40) allows to study the dynamics of the Carnot engine. The result for the internal energy E is shown in Fig.5.8a.
As we can see, a simple numerical integration of $\hat{\rho}(t)$ does not allow to know the limit-cycle state and thus the values of the thermodynamic quantities during the cyclic evolution. Quite nicely, if we plot the result for the internal energy for times $t > 2\mathcal{T}/\Gamma$ (compare with Eq.(5.7.20)), we can completely get ride of the transient regime and the result is found in perfect agreement with that of Fig.5.6, see Fig.5.8b.

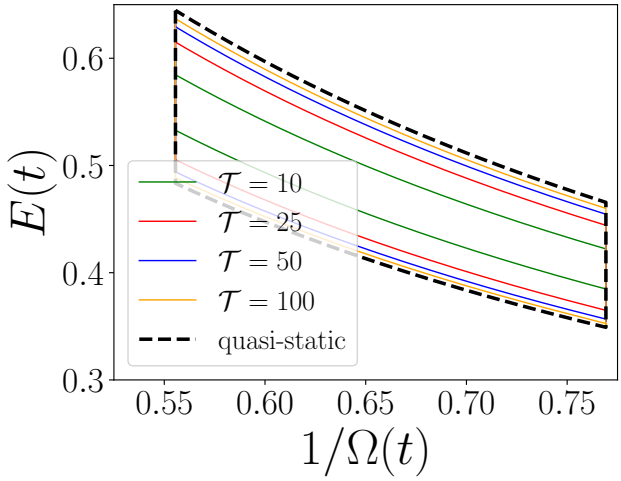

Figure 5.10: **Operation of a finite-time Otto engine.** The plot shows the internal energy $E(t)$ as function of the compression $1/\Omega(t)$. In the figure we select Ω as in Eq.(5.7.41), setting $\Omega_1 = 1.8$, $\Omega_2 = 1.3$ and the thermal bath in Eq.(5.7.13) with temperature in Eq.(5.7.42). We require quasi-static reversibility conditions (5.7.43) and we chose $T_a = 1.0$, $T_b = 1.5$. We see that increasing the value of the driving period $\mathcal{T}$ (from the innermost to the outermost), the cycle converges towards its quasi-static limit.

5.7.3 Otto cycle

Finally, we show that the Lindblad-Floquet solution of the two-level quantum heat-engine allows to engineer different cycles with just a few replacements. For instance, an Otto engine is obtained by replacing Ω in Eq.(5.7.30) with

$$\Omega(t) = \begin{cases} \Omega_1 \\ 2\Omega_1 - \Omega_2 + \frac{4(\Omega_2 - \Omega_1)}{\mathcal{T}} t \\ \Omega_2 \\ -3\Omega_1 + 4\Omega_2 + \frac{4(\Omega_1 - \Omega_2)}{\mathcal{T}} t \end{cases} \tag{5.7.41}$$

and the temperature in Eq.(5.7.25) with

$$T(t) = \begin{cases} \frac{4(T_b - T_a)}{\mathcal{T}} t + T_a \\ - \\ \frac{4(T_d - T_c)}{\mathcal{T}} t + 3T_c - 2T_d \\ - \end{cases} \tag{5.7.42}$$

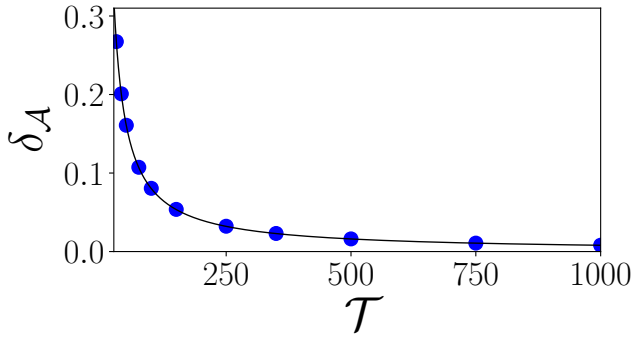

Figure 5.11: **Otto cycle: convergence toward the quasi-static limit**. A numerical estimation of the deviations of the cycle areas $\delta_{\mathcal{A}}$ in Eq.(5.7.36) for the two-level Otto engine in Fig.5.10. We see an approach $\delta_{\mathcal{A}} \propto 1/\mathcal{T}$ to the quasi-static limit with a proportionality constant $c = 8.02$, extracted from our fitting datas.

where the first and the third isothermal strokes are substituted by thermal isochoric strokes (i.e., with Ω kept constant). One can easily show that the quasi-static reversibility conditions now read

$$\frac{\Omega_2}{\Omega_1} = \frac{T(\mathbf{c})}{T(\mathbf{b})} = \frac{T(\mathbf{d})}{T(\mathbf{a})} \tag{5.7.43}$$

and are satisfied in Eq.(5.7.42) if $T_c = (\Omega_2/\Omega_1)T_b$, $T_d = (\Omega_2/\Omega_1)T_a$.
In Fig.5.9 and 5.10 we show the Floquet parameters and the operation of the Otto engine respectively, obtained by a numerical solution of Eq.(5.7.33). The deviations $\delta_{\mathcal{A}}$ in the cycle area from the quasi-static limit value are plotted in Fig.5.11 and decay as a power law $\delta_{\mathcal{A}} \sim \mathcal{O}(1/\mathcal{T})$ for large $\mathcal{T}$.

5.8 Application to a Harmonic Oscillator

We now consider the exactly solvable model of a single bosonic mode, described by a creation (annihilation) operator $\hat{a}^\dagger$ ($\hat{a}$), subject to an arbitrary time-dependent and Gaussian-preserving open system dynamics. Here we provide only the main ideas and results, leaving some of the technical details to the appendix 5.B.

5.8.1 Gaussian-preserving dynamics

To begin with, we construct a Gaussian-preserving dynamics for a single-bosonic mode subject to a squeezed thermal bath. In the following sections, we will make use of these results for the definition of the time-dependent Lindblad master equation.
Let us consider the Hamiltonian of a quantum harmonic oscillator (HO):

$$\hat{H} = \omega(\hat{a}^\dagger \hat{a} + \frac{1}{2}) \tag{5.8.1}$$

subject to the dissipation induced by the jump operators

$$\hat{L}_1 = \hat{a} \qquad \hat{L}_2 = \hat{a}^\dagger, \tag{5.8.2}$$

which give rise to the Lindblad dissipator

$$\begin{aligned}\check{\mathcal{D}}\,\hat{\rho} =& \gamma\,(n+1)\left(\hat{a}\,\hat{\rho}\,\hat{a}^\dagger - \frac{1}{2}\{\hat{a}^\dagger\hat{a},\hat{\rho}\}\right)\\ &+\gamma\,n\left(\hat{a}^\dagger\,\hat{\rho}\,\hat{a} - \frac{1}{2}\{\hat{a}\hat{a}^\dagger,\hat{\rho}\}\right).\end{aligned} \tag{5.8.3}$$

Here $\gamma \geq 0$ sets the damping rate of the HO and

$$n = \left(e^{\omega/T} - 1\right)^{-1} \tag{5.8.4}$$

is the mean number of excitations in a thermal bath at temperature T. It is easy to show that the Lindblad dissipator (5.8.3) has a target state:

$$\check{\mathcal{D}}\,\hat{\rho} = 0 \quad \Leftrightarrow \quad \hat{\rho} = \left(1 - e^{-\omega/T}\right)\exp\left(-\frac{\omega}{T}\,\hat{a}^\dagger\,\hat{a}\right), \tag{5.8.5}$$

which is nothing but a Gibbs thermal state at temperature T. Notice that this open system dynamics preserves Gaussian states since it involves terms which are quadratic in the bosonic operators, see e.g. [Wee12, Ser17]. Hence, the Lindblad evolution generated by (5.8.1), (5.8.3) is completely determined by the value of the second moments:

$$\langle\hat{a}^\dagger\,\hat{a}\rangle \quad \langle\hat{a}\,\hat{a}\rangle\,. \tag{5.8.6}$$

Next, we consider the effect of a squeeze radiation field that we treat as an external bath. The effect of squeezing on the open system dynamics (5.8.3) can be easily implemented by replacing the bosonic operators $\hat{a}^\dagger$, $\hat{a}$ with

$$\hat{a}_{\rm sq} \equiv \hat{S}(\lambda)\,\hat{a}\,\hat{S}^\dagger(\lambda) \qquad \hat{a}^\dagger_{\rm sq} \equiv \hat{S}^\dagger(\lambda)\,\hat{a}^\dagger\,\hat{S}(\lambda), \tag{5.8.7}$$

where $\hat{S}$ is the squeezing operator

$$\hat{S}(\lambda) \equiv \exp\left(\frac{1}{2}\lambda^* \,\hat{a}\,\hat{a} - \frac{1}{2}\lambda\,\hat{a}^\dagger\,\hat{a}^\dagger\right) \tag{5.8.8}$$

and $\lambda = |\lambda| e^{i\theta} \in \mathbb{C}$ is a squeezing parameter characterizing the bath. Due to the structure of the squeezing operator (5.8.8), $\hat{a}_{\rm sq}$, $\hat{a}^\dagger_{\rm sq}$ can be written as

$$\hat{a}_{\rm sq} = \cosh|\lambda|\,\hat{a} - e^{i\theta}\sinh|\lambda|\,\hat{a}^\dagger; \quad \hat{a}^\dagger_{\rm sq} = \cosh|\lambda|\,\hat{a}^\dagger - e^{-i\theta}\sinh|\lambda|\,\hat{a}, \tag{5.8.9}$$

with the help of BCH formulae (3.1.24). With this prescription, the Lindblad dissipator for the squeezed thermal bath will read:

$$\begin{aligned}\check{\mathcal{D}}\,\hat{\rho} =& \gamma\,(n+1)\left(\hat{a}_{\rm sq}\,\hat{\rho}\,\hat{a}^\dagger_{\rm sq} - \frac{1}{2}\{\hat{a}^\dagger_{\rm sq}\hat{a}_{\rm sq},\hat{\rho}\}\right)\\ &+\gamma\,n\left(\hat{a}^\dagger_{\rm sq}\,\hat{\rho}\,\hat{a}_{\rm sq} - \frac{1}{2}\{\hat{a}_{\rm sq}\hat{a}^\dagger_{\rm sq},\hat{\rho}\}\right),\end{aligned} \tag{5.8.10}$$

or, equivalently, in terms of the $\hat{a}$, $\hat{a}^\dagger$ operators [San17]:

$$\begin{aligned}\check{\mathcal{D}}\,\hat{\rho} =& \gamma\,(\tilde{n}+1)\left(\hat{a}\,\hat{\rho}\,\hat{a}^\dagger - \frac{1}{2}\{\hat{a}^\dagger\hat{a},\hat{\rho}\}\right) + \gamma\,\tilde{n}\left(\hat{a}^\dagger\,\hat{\rho}\,\hat{a} - \frac{1}{2}\{\hat{a}\hat{a}^\dagger,\hat{\rho}\}\right)\\ &-\gamma\,m\left(\hat{a}^\dagger\,\hat{\rho}\,\hat{a}^\dagger - \frac{1}{2}\{\hat{a}^\dagger\hat{a}^\dagger,\hat{\rho}\}\right) - \gamma\,m^*\left(\hat{a}\,\hat{\rho}\,\hat{a} - \frac{1}{2}\{\hat{a}\hat{a},\hat{\rho}\}\right),\end{aligned} \tag{5.8.11}$$

where we have defined

$$\tilde{n} + \frac{1}{2} \equiv (n+\frac{1}{2})\cosh(2|\lambda|) \tag{5.8.12}$$

and

$$m \equiv -(n+\frac{1}{2})e^{i\theta}\sinh(2|\lambda|). \tag{5.8.13}$$

Notice that the effect of the squeeze radiation field in Eq.(5.8.7) is equivalent to a Bogoliubov transformation of the operators $\hat{a}$, $\hat{a}^\dagger$. Therefore, one can interpret Eq.(5.8.11) as source of squeezing or thermal dissipative mechanisms, depending on the reference basis. Moreover, due to the quadratic structure of the super-operators (5.8.11), the target state of the open system dynamics is still a Gaussian state and so it will be completely characterized by the value of the covariances (5.8.6), see e.g. [Wee12, Ser17].

5.8.2 Effective Hamiltonian

The Hamiltonian of the system is chosen to be a generic quadratic form of the operators $\hat{a}$, $\hat{a}^\dagger$:

$$\hat{H}(t) = \omega(t)(\hat{a}^\dagger\,\hat{a} + \frac{1}{2}) + \frac{\lambda(t)}{2}\hat{a}\,\hat{a} + \frac{\lambda^*(t)}{2}\hat{a}^\dagger\,\hat{a}^\dagger, \tag{5.8.14}$$

where $\omega(t)$ and $\lambda(t)$ are arbitrary periodic functions satisfying $\omega(t)^2 > |\lambda(t)|^2$. In a mechanical picture, the Hamiltonian in Eq.(5.8.14) describes a situation where both the mass and the spring constant may be time-dependent.
To see this, let us rewrite $\hat{H}(t)$ in terms of position and momentum operators:

$$\hat{x} \equiv \frac{1}{\sqrt{2\eta}}(\hat{a}^\dagger + \hat{a}), \qquad \hat{p} \equiv i\sqrt{\frac{\eta}{2}}(\hat{a}^\dagger - \hat{a}). \tag{5.8.15}$$

where η is an arbitrary frequency scale setting the units of $\hat{x}$ and $\hat{p}$. In terms of these new variables and assuming λ to be real, the Hamiltonian (5.8.14) becomes

$$\hat{H}(t) = \frac{1}{2\eta}\left(\omega(t) - \lambda(t)\right)\,\hat{p}^2 + \frac{\eta}{2}\left(\omega(t) + \lambda(t)\right)\,\hat{x}^2. \tag{5.8.16}$$

Thus, we can see that the general Hamiltonian (5.8.14) corresponds to a mechanical oscillator where both the frequency and the mass are time-dependent. We also see that the more usual problem of a time-independent mass occurs when $\omega(t) - \lambda(t)$ is time-independent. In this case one may choose, without loss of generality, $\eta = \omega(t) - \lambda(t)$, leading to

$$\hat{H}(t) = \frac{1}{2}\left(\hat{p}^2 + \Omega(t)^2\,\hat{x}^2\right), \tag{5.8.17}$$

where

$$\Omega(t)^2 \equiv \omega(t)^2 - \lambda(t)^2 = \eta(\omega(t) + \lambda(t)). \tag{5.8.18}$$

Notice that in this situation one recovers precisely the setup of the Ermakov-Lewis theory, see Sec.4.5.

5.8.3 Super-operator content

The Hamiltonian (5.8.14) adds to $\check{\mathscr{L}}(t)$ three super-operators:

$$\check{\mathcal{H}}_0\ \bullet \equiv -i[\hat{a}^\dagger\,\hat{a},\ \bullet], \tag{5.8.19a}$$

$$\check{\mathcal{H}}_1\ \bullet \equiv -i[\hat{a}\,\hat{a},\ \bullet], \tag{5.8.19b}$$

$$\check{\mathcal{H}}_2\ \bullet \equiv -i[\hat{a}^\dagger\,\hat{a}^\dagger,\ \bullet]. \tag{5.8.19c}$$

In addition, we consider the general effects of Gaussian-preserving dissipation generated by

$$\check{\mathcal{D}}_1 \bullet \equiv \hat{a} \bullet \hat{a}^\dagger - \frac{1}{2}\{\hat{a}^\dagger \hat{a}, \bullet\}; \tag{5.8.20a}$$

$$\check{\mathcal{D}}_2 \bullet \equiv \hat{a}^\dagger \bullet \hat{a} - \frac{1}{2}\{\hat{a}\, \hat{a}^\dagger, \bullet\}; \tag{5.8.20b}$$

$$\check{\mathcal{D}}_3 \bullet \equiv \hat{a}^\dagger \bullet \hat{a}^\dagger - \frac{1}{2}\{\hat{a}^\dagger \hat{a}^\dagger, \bullet\}; \tag{5.8.20c}$$

$$\check{\mathcal{D}}_4 \bullet \equiv \hat{a} \bullet \hat{a} - \frac{1}{2}\{\hat{a}\, \hat{a}, \bullet\}. \tag{5.8.20d}$$

With these ingredients, we then parametrize our time-dependent Liouvillean as

$$\check{\mathscr{L}}(t) = \check{\mathcal{H}}(t) + \check{\mathcal{D}}(t), \tag{5.8.21}$$

where

$$\check{\mathcal{H}}(t) \equiv \omega(t)\, \check{\mathcal{H}}_0 + \frac{\lambda(t)}{2}\, \check{\mathcal{H}}_1 + \frac{\lambda^*(t)}{2}\, \check{\mathcal{H}}_2; \tag{5.8.22}$$

$$\begin{aligned}\check{\mathcal{D}}(t) \equiv &\gamma(t)\,(n(t)+1)\,\check{\mathcal{D}}_1 + \gamma(t)\, n(t)\, \check{\mathcal{D}}_2 \\ &- \gamma(t)\, m(t)\, \check{\mathcal{D}}_3 - \gamma(t)\, m^*(t)\, \check{\mathcal{D}}_4,\end{aligned} \tag{5.8.23}$$

with $\gamma(t)$, $n(t)$ and $m(t)$ time-periodic parameters satisfying $\gamma(t) > 0$ and $n(t)(n(t)+1) > |m(t)|^2$ [§].

Here $\gamma(t)$ represents the coupling strength to the bath, whereas $n(t)$ and $m(t)$ may represent both thermal and squeezing effects, depending on the choice of basis. For instance, if $\lambda(t) = 0$ then a thermal bath at a temperature T corresponds to $m(t) = 0$ and $n(t) = (e^{\omega(t)/T} - 1)^{-1}$. For the general Hamiltonian (5.8.14), on the other hand, the thermal bath is modeled by

$$n(t) + \frac{1}{2} = \frac{\omega(t)}{2\Omega(t)} \coth\left(\frac{\Omega(t)}{2T}\right), \quad m(t) = -\frac{\lambda(t)}{2\Omega(t)} \coth\left(\frac{\Omega(t)}{2T}\right), \tag{5.8.24}$$

where $\Omega^2(t) \equiv \omega^2(t) - \lambda^2(t)$.

Next, we apply the rotating frame transformation of Sec.5.4.2. The key property making this problem analytically tractable is that the seven super-operators

[§]It is easy to see that these conditions are required for the semi-positivity of the relaxation matrix.

$\{\{\check{\mathcal{H}}_j\}_{j=0}^2, \{\check{\mathcal{D}}_j\}_{j=1}^4\}$ form a closed algebra [Pei07] (see also [Rya13]). In particular, the sets $\{\check{\mathcal{H}}_j\}$ and $\{\check{\mathcal{D}}_j\}$, when taken separately, satisfy independent algebras:

$$[\check{\mathcal{H}}_0, \check{\mathcal{H}}_{1,2}] = \pm 2i\check{\mathcal{H}}_{1,2}; \qquad [\check{\mathcal{H}}_1, \check{\mathcal{H}}_2] = -4i\check{\mathcal{H}}_0; \tag{5.8.25a}$$

which is nothing but $\mathfrak{su}(1,1)$ (see the appendix 4.D), and

$$\begin{aligned} &[\check{\mathcal{D}}_1, \check{\mathcal{D}}_2] = -(\check{\mathcal{D}}_1 + \check{\mathcal{D}}_2); \qquad &&[\check{\mathcal{D}}_3, \check{\mathcal{D}}_4] = 0; \\ &[\check{\mathcal{D}}_1, \check{\mathcal{D}}_{3,4}] = -\check{\mathcal{D}}_{3,4}; \qquad &&[\check{\mathcal{D}}_2, \check{\mathcal{D}}_{3,4}] = \check{\mathcal{D}}_{3,4}. \end{aligned} \tag{5.8.25b}$$

Mixtures of the two sets, on the other hand, only produce elements of the latter:

$$\begin{aligned} &[\check{\mathcal{H}}_0, \check{\mathcal{D}}_{1,2}] = 0; \qquad &&[\check{\mathcal{H}}_0, \check{\mathcal{D}}_{3,4}] = \mp 2i\check{\mathcal{D}}_{3,4}; \\ &[\check{\mathcal{H}}_1, \check{\mathcal{D}}_{1,2}] = -2i\check{\mathcal{D}}_4; \qquad &&[\check{\mathcal{H}}_2, \check{\mathcal{D}}_{1,2}] = 2i\check{\mathcal{D}}_3; \\ &[\check{\mathcal{H}}_1, \check{\mathcal{D}}_3] = -2i(\check{\mathcal{D}}_1 + \check{\mathcal{D}}_2); \qquad &&[\check{\mathcal{H}}_1, \check{\mathcal{D}}_4] = 0; \\ &[\check{\mathcal{H}}_2, \check{\mathcal{D}}_4] = 2i(\check{\mathcal{D}}_1 + \check{\mathcal{D}}_2); \qquad &&[\check{\mathcal{H}}_2, \check{\mathcal{D}}_3] = 0. \end{aligned} \tag{5.8.25c}$$

This algebraic structure suggests that the operator $\check{W}(t)$ in Eq.(5.4.23) may be taken as

$$\check{W}(t) = \check{V}(t)\, \check{U}(t), \tag{5.8.26}$$

where

$$\check{V}(t) = \exp(g_1(t)\, \check{\mathcal{D}}_1)\ \exp(g_2(t)\, \check{\mathcal{D}}_2)\ \exp(g_3(t)\, \check{\mathcal{D}}_3)\ \exp(g_4(t)\, \check{\mathcal{D}}_4) \tag{5.8.27}$$

and

$$\check{U}(t) = \exp(r_0(t)\, \check{\mathcal{H}}_0)\ \exp(r_1(t)\, \check{\mathcal{H}}_1)\ \exp(r_2(t)\, \check{\mathcal{H}}_2). \tag{5.8.28}$$

Here $r_i(t)$ and $g_i(t)$ are the canonical coordinates which are to be suitably adjusted so as to make $\check{\mathscr{L}}_{\text{aux}}$ time-independent.

The problem is then solved sequentially. First one applies $\check{U}(t)$ and adjusts the $r_i(t)$ to make the unitary part time-independent. Then $\check{V}(t)$ is applied and the $g_i(t)$ are adjusted to deal with the dissipative part. In this section, we shall illustrate the procedure in the simpler case when $\omega = \lambda = 0$, that is, when only the dissipative terms are present. The general formulation is presented in Appendices 5.B.1 and 5.B.2 and the main results will be summarized in Sec.5.8.5 below.

5.8.4 Purely dissipative case

In the case $\omega = \lambda = 0$, the situation simplifies dramatically since only the dissipative part remains in the Liouvillean (5.8.21). Consequently, it suffices to choose $\check{U}(t) = \hat{\mathbb{1}} \otimes \hat{\mathbb{1}}$ in Eq.(5.8.26). To carry out the rotating frame transformation of Sec.5.4.2, it is necessary to evaluate products such as

$$\left[e^{g_1(t)\,\check{\mathcal{D}}_1}\right]\ \check{\mathcal{D}}_2\ \left[e^{-g_1(t)\,\check{\mathcal{D}}_1}\right] = e^{-g_1(t)}\,\check{\mathcal{D}}_2 + (e^{-g_1(t)} - 1)\check{\mathcal{D}}_1, \tag{5.8.29}$$

which can be found as usual, with the BCH formulae (3.1.24). Carrying out all computations we then find

$$\check{\mathscr{L}}_{\text{aux}} = C_1(t)\,\check{\mathcal{D}}_1 + C_2(t)\,\check{\mathcal{D}}_2 + C_3(t)\,\check{\mathcal{D}}_3 + C_4(t)\,\check{\mathcal{D}}_4, \tag{5.8.30}$$

where

$$C_2(t) = e^{-g_1(t)}\left[\dot{g}_2(t) - \gamma(t) + \gamma(t)\,e^{g_2(t)}\,(n(t)+1)\right]; \tag{5.8.31a}$$

$$C_1(t) = \dot{g}_1(t) - \dot{g}_2(t) + \gamma(t) + C_2(t); \tag{5.8.31b}$$

$$C_3(t) = e^{g_2(t)-g_1(t)}\left[\dot{g}_3(t) + \gamma(t)\,g_3(t) - \gamma(t)\,m(t)\right]; \tag{5.8.31c}$$

$$C_4(t) = e^{g_2(t)-g_1(t)}\left[\dot{g}_4(t) + \gamma(t)\,g_4(t) - \gamma(t)\,m^*(t)\right]. \tag{5.8.31d}$$

We now must choose time-periodic functions for the $g_i(t)$ which will make all $C_i(t)$ time-independent. We see that this may be accomplished by setting g_2, g_3 and g_4 to be the time-periodic solutions of

$$\dot{g}_2(t) - \gamma(t) + \gamma(t)\,e^{g_2(t)}\,(n(t)+1) = 0; \tag{5.8.32a}$$

$$\dot{g}_3(t) + \gamma(t)\,g_3(t) - \gamma(t)\,m(t) = 0; \tag{5.8.32b}$$

$$\dot{g}_4(t) + \gamma(t)\,g_4(t) - \gamma(t)\,m^*(t) = 0, \tag{5.8.32c}$$

which then imply $C_2 = C_3 = C_4 = 0$. Note also that $g_4 = g_3^*$. Finally, in order to make $C_1(t)$ time-independent, we may choose

$$g_1(t) = g_2(t) + \int_{t_0}^{t} \mathrm{d}t'\ (\overline{\gamma} - \gamma(t')) \tag{5.8.33}$$

where we have defined the time-average $\overline{\gamma} \equiv \langle\gamma\rangle_{\mathbf{t}}$. With this form for g_1 we then get $C_1 = \overline{\gamma}$ so that the rotating frame Liouvillean becomes simply

$$\check{\mathscr{L}}_{\text{aux}} = \overline{\gamma}\ \check{\mathcal{D}}_1. \tag{5.8.34}$$

Thus, in the rotating frame the system evolves as if coupled to a zero-temperature bath with damping rate $\overline{\gamma}$.

We see from Eq.(5.8.32b) that g_3 satisfies a linear differential equation, whereas the same is not true for g_2. However, if we change variables to

$$G_2(t) \equiv e^{-g_2(t)} - \frac{1}{2} \tag{5.8.35}$$

then Eq.(5.8.32a) becomes

$$\dot{G}_2(t) + \gamma(t) G_2(t) = \gamma(t)(n(t) + \frac{1}{2}) \tag{5.8.36}$$

which is linear in G_2. Thus, we conclude that, in the case of purely dissipative dynamics, all Floquet variables satisfy linear differential equations. We will see that when $\lambda(t) \neq 0$ in Eq.(5.8.14), this will no longer be the case.

Having found the functions which make $\check{\mathscr{L}}_{\text{aux}}$ time-independent, we now compute the Floquet-Liouvillean (5.5.3), with $\check{\mathscr{L}}_{\text{aux}}$ being given by (5.8.34). As a result, we find

$$\check{\mathscr{L}}_F(t_0 \mapsto t) = \overline{\gamma}(n_F(t)+1)\check{\mathcal{D}}_1 + \overline{\gamma}\, n_F(t)\check{\mathcal{D}}_2 - \overline{\gamma} m_F(t)\check{\mathcal{D}}_3 - \overline{\gamma} m_F^*(t)\check{\mathcal{D}}_4, \tag{5.8.37}$$

which has the same form as the original dissipator (5.8.23), but with time-independent damping $\overline{\gamma}$ and new parameters $n_F(t)$ and $m_F(t)$ which turn out to be simply given by

$$n_F(t) = G_2(t); \qquad m_F(t) = g_3(t). \tag{5.8.38}$$

Thus, in view of Eqs.(5.8.36) and (5.8.32b), we may recast the final result as the statement that the Floquet parameters are the time-periodic solutions of

$$\dot{n}_F(t) + \gamma(t)\, n_F(t) = \gamma(t)\, n(t); \tag{5.8.39a}$$

$$\dot{m}_F(t) + \gamma(t)\, m_F(t) = \gamma(t)\, m(t). \tag{5.8.39b}$$

These solutions then determine the value of the thermal noise and squeezing at any time t during the cyclic evolution. Notice that the time-dependence in $\check{\mathscr{L}}_F$ enters only as a parameter and all we require is the steady-state $\hat{\rho}^{ss}$ of $\check{\mathscr{L}}_F$ for a given t, see Eq.(5.7.4). This state turns out to be simply a squeezed thermal state (see e.g. [Wee12, Ser17]) defined by the covariances

$$\langle \hat{a}^\dagger \hat{a} \rangle_{ss} = n_F(t); \quad \langle \hat{a}\, \hat{a} \rangle_{ss} = m_F(t), \tag{5.8.40}$$

and where, as usual, $\langle \bullet \rangle_{ss} \equiv \text{tr}(\hat{\rho}^{ss}(t)\, \bullet)$.
Thus, once the periodic solutions of Eqs.(5.8.39a) and (5.8.39b) are found, one knows exactly the state in the cyclic regime.

5.8.5 General case

When $\lambda(t) \neq 0$ the situation becomes much more complicated. In this case we must use the full transformation $\check{W} = \check{V}\,\check{U}$ in Eq.(5.8.26). The procedure is applied sequentially, first dealing with the unitary part and then with the dissipative part. In this section we will focus only on the main results and leave the details of the calculations to the appendices 5.B.1 and 5.B.2.

Once the functions $r_i(t)$ and $g_i(t)$ in Eqs.(5.8.27) and (5.8.28) are properly adjusted, one finds the following surprisingly simple result for the rotating frame Liouvillean:

$$\check{\mathscr{L}}_{\text{aux}} = \overline{\Lambda}\,\check{\mathcal{H}}_0 + \overline{\gamma}\,\check{\mathcal{D}}_1, \tag{5.8.41}$$

where $\Lambda(t) \equiv \omega(t) + 2i\lambda(t)r_2(t)$. The variable $r_2(t)$ (which is part of the rotating frame transformation in Eq.(5.8.28)), turns out to play a special role, being the time-periodic solution of the *Riccati equation*:

$$\dot{r}_2(t) + 2i\omega(t)\,r_2(t) - 2\lambda(t)\,r_2^2(t) + \frac{\lambda^*(t)}{2} = 0, \tag{5.8.42}$$

which is the only non-linear equation in the problem.

The result in Eq.(5.8.41) is noteworthy. It shows that, in the generalized rotating frame, the system always evolves as a simple HO coupled to a zero-temperature bath with damping rate $\overline{\gamma}$. We also note that in general, $\overline{\Lambda}$ may be complex, which is the source of potential instabilities, as explained below.

Next, we obtain for the Floquet-Liouvillean (see Appendix 5.B.3):

$$\begin{aligned}\check{\mathscr{L}}_F(t) =& \omega_F(t)\,\check{\mathcal{H}}_0 + \frac{\lambda_F(t)}{2}\,\check{\mathcal{H}}_1 + \frac{\lambda'_F(t)}{2}\,\check{\mathcal{H}}_2 + \overline{\gamma}\,(n_F(t)+1)\,\check{\mathcal{D}}_1 \\ &+ \overline{\gamma}\,n_F(t)\,\check{\mathcal{D}}_2 - \overline{\gamma}\,m_F(t)\,\check{\mathcal{D}}_3 - \overline{\gamma}\,m'_F(t)\,\check{\mathcal{D}}_4.\end{aligned} \tag{5.8.43}$$

This therefore has the same form of the original Liouvillean (5.8.21), but with modified parameters $\omega_F, \lambda_F, \lambda'_F, n_F, m_F$ and m'_F, whose explicit forms are given in Eqs.(5.B.33a)-(5.B.33f). We note also that, in general, $\lambda'_F \neq \lambda_F^*$ and $m'_F \neq m_F^*$. However, this does not lead to unphysical results, as explained in the appendix 5.B.3.

The steady-state of $\check{\mathscr{L}}_F(t)$ is also a squeezed thermal state with covariances given by Eqs.(5.B.35a)-(5.B.35c). Thus, as in the purely dissipative case, knowing the Floquet-Liouvillean immediately allows us to know the state during cyclic evolution. We also call attention to the fact that the damping rate that appears in Eq.(5.8.43) is $\overline{\gamma}$, which implies that the steady-state will be unique irrespective of how small $\gamma(t)$, unless $\gamma(t) = 0$ at all times.

5.8.6 Connection with Ermakov-Lewis theory

When λ is a real function and $\eta \equiv \omega(t) - \lambda(t)$ is time-independent, we recover the more common mechanical situation of a harmonic oscillator $\hat{H}(t) = \frac{1}{2}(-\partial_x^2 + \Omega(t)^2 x^2)$, subject to a time-periodic frequency $\Omega^2(t) = \omega(t)^2 - \lambda(t)^2$. In this case we may define a new variable $\zeta(t)$ such that

$$r_2(t) \equiv \frac{i}{2} + \frac{\zeta(t)^2}{i + i\zeta(t)^2 + \zeta(t)\dot{\zeta}(t)/\eta}. \tag{5.8.44}$$

Then Eq.(5.8.42) implies that ζ will satisfy the Ermakov-Pinney equation

$$\ddot{\zeta}(t) + \Omega(t)^2\,\zeta(t) = \eta^2\,\zeta^{-3}(t), \tag{5.8.45}$$

which is exactly the same as in the unitary problem, see (4.4.9) of Chap.4. This equation always has a time-periodic solution, but it may either be real or such that ζ^2 is purely imaginary. The former case corresponds to a stable evolution whereas the latter is unitarily unstable (that is, it would be unstable in the absence of dissipation).
For a purely unitary evolution, these two regimes can be differentiated by the value of $\overline{\Lambda}$ appearing in Eq.(5.8.41), which is real in the unitarily stable phase and complex otherwise.

To know if a unitarily unstable solution will be stabilized by the presence of dissipation, we must look into the eigenvalues of $\check{\mathscr{L}}_{\text{aux}}$ in Eq.(5.8.41). Due to its simplicity, its eigenvalues can actually be found analytically and read

$$\text{spec}\left(\check{\mathscr{L}}_{\text{aux}}\right) = -\overline{\gamma}\,\frac{\alpha}{2} + 2i\,\overline{\Lambda}\,k \qquad \alpha = 0, 1, \ldots \tag{5.8.46}$$

where $k \in [-\frac{\alpha}{2}, \frac{\alpha}{2}]$, with $\Delta k = 1$. Hence, we find that the condition for the system to converge to a stable limit cycle is

$$\overline{\gamma} > 2|\text{Im}(\overline{\Lambda})|. \tag{5.8.47}$$

This formula provides a remarkably transparent method for determining the minimum amount of damping required to stabilize a cycle: one has to simply compare the output of the unitary evolution with the average damping. Notice that this result holds for any type of protocol, hence generalizing and simplifying the approach introduced in Refs. [Ins18, Ins16].

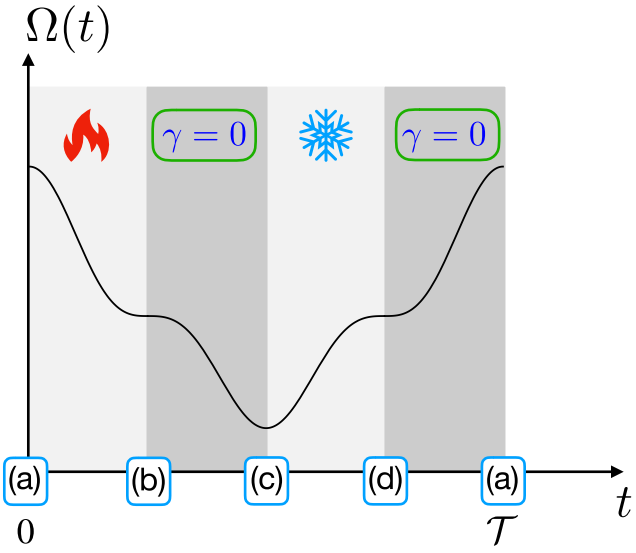

Figure 5.1: **Illustration of the Carnot cycle II**. We show a sketch of the Carnot cycle made with the HO (5.8.14) as working fluid and with continuous frequency modulation. Recall that the order of the cycle is: **a-b** (**c-d**) a hot (cold) isothermal expansion (compression) where the working parameter is decreasing (increasing), *light gray boxes*; **b-c** (**d-a**) an isentropic expansion (compression) where the system is detached from the bath $\gamma = 0$ and Ω is decreasing (increasing), *dark gray boxes*.

5.8.7 Example: Carnot cycle

Finally, to illustrate an application of the previous results, we present the operation of a finite-time Carnot engine operating under continuous frequency modulations, see Fig.5.1. We consider for simplicity the mechanical scenario where λ is real and $\eta = \omega(t) - \lambda(t)$ is time-independent, so that the frequency protocol is completely specified by $\Omega(t) = \omega(t)^2 - \lambda(t)^2$ (for concreteness we choose $\eta = \Omega(t_0)$). The order of the cycle is chosen as in Sec.5.7.2 and the four strokes of the cycle are taken to have the same duration of $\mathcal{T}/4$.

Quasi-static reversibility limit

Before we turn to the finite-time operation of the engine, it is necessary to review some properties of the quasi-static cycle. During an isothermal stroke,

the energy at any time will be given by

$$E(t) = \omega(t)(n(t) + \frac{1}{2}) + \lambda(t)\, m(t) = \frac{\Omega(t)}{2} \coth\left(\frac{\Omega(t)}{2T}\right) \tag{5.8.48}$$

with $E(t) \equiv \mathrm{tr}(\hat{\rho}^{eq}\, \hat{H}(t))$ and where $\hat{\rho}^{eq}$ is a thermal state defined through the covariances

$$\langle \hat{a}^\dagger \hat{a} \rangle_{eq} = n(t); \quad \langle \hat{a}\, \hat{a} \rangle_{eq} = m(t). \tag{5.8.49}$$

Notice that if $T \gg \Omega(t)$, we get the classical result $E \simeq T$. In fact, the classical harmonic oscillator behaves like an ideal gas, in the sense that the energy during the isothermal stroke is constant. Conversely, for the quantum oscillator, the energy depends on the frequency.
In the isentropic strokes, on the other hand, the evolution is purely unitary so that the quasi-static energy is obtained from the adiabatic theorem and reads

$$E(t_2) = \frac{\Omega(t_2)}{\Omega(t_1)}\, E(t_1). \tag{5.8.50}$$

From these results we may then write down the energy of the system at the end of each quasi-static stroke:

$$E(\mathbf{a}) = \frac{\Omega(\mathbf{a})}{\Omega(\mathbf{d})}\, E(\mathbf{d}); \tag{5.8.51a}$$

$$E(\mathbf{b}) = \frac{\Omega(\mathbf{b})}{2} \coth\left(\frac{\Omega(\mathbf{b})}{2T^{hot}}\right); \tag{5.8.51b}$$

$$E(\mathbf{c}) = \frac{\Omega(\mathbf{c})}{\Omega(\mathbf{b})}\, E(\mathbf{b}); \tag{5.8.51c}$$

$$E(\mathbf{d}) = \frac{\Omega(\mathbf{d})}{2} \coth\left(\frac{\Omega(\mathbf{d})}{2T^{cold}}\right). \tag{5.8.51d}$$

and the condition for the existence of a reversible quasi-static limit is therefore obtained by imposing that

$$E(\mathbf{a}) = \frac{\Omega(\mathbf{a})}{2} \coth\left(\frac{\Omega(\mathbf{a})}{2T^{hot}}\right), \tag{5.8.52}$$

and

$$E(\mathbf{c}) = \frac{\Omega(\mathbf{c})}{2} \coth\left(\frac{\Omega(\mathbf{c})}{2T^{cold}}\right). \tag{5.8.53}$$

This implies the quasi-static reversibility conditions (5.7.29).

Finite-time operation

Let us come back to the finite-time operation of the engine. Consistently with the quasi-static reversibility conditions (5.7.29), we choose for our cycle the frequency modulation

$$\Omega(t) = \Delta + \delta(t)\cos^3(2\pi t/\mathcal{T}), \tag{5.8.54}$$

where $\Delta = 1$ is a constant setting the overall energy scale and $\delta(t)$ is chosen so as to satisfy Eq.(5.7.29), which implies

$$\delta(t) = \begin{cases} \delta & \text{for } 0 < t < \frac{\mathcal{T}}{4}, \\ \frac{\Delta\delta}{\Delta+\delta} & \text{for } \frac{\mathcal{T}}{4} < t < \frac{3\mathcal{T}}{4}, \\ \delta & \text{for } \frac{3\mathcal{T}}{4} < t < \mathcal{T}. \end{cases} \tag{5.8.55}$$

In the results to be presented below, we have chosen for simplicity $\delta = 0.85$. The choice (5.8.54) for $\Omega(t)$ leads to a smooth function (only the third derivative is discontinuous), while still preserving the spirit of the Carnot cycle of having two expansion strokes followed by two compressions (see Fig.5.1). The damping rate was then chosen as $\gamma(t) = \{\gamma_0\,,\,0\,,\,\gamma_0\,,\,0\}$, as illustrated in Fig.5.1.

Finally, the Lindblad parameters $n(t)$ and $m(t)$ are chosen according to Eq.(5.8.24):

$$n(t) + \frac{1}{2} = \frac{\omega(t)}{2\Omega(t)}\coth\left(\frac{\Omega(t)}{2T(t)}\right), \quad m(t) = -\frac{\lambda(t)}{2\Omega(t)}\coth\left(\frac{\Omega(t)}{2T(t)}\right), \tag{5.8.56}$$

where $T(t)$ is given by $\left\{T^{hot}\,,\,-\,,T^{cold}\,,\,-\right\}$. The hot temperature is chosen as $T^{hot} = 1$ (in units of $\Delta = 1$). Then from Eq.(5.7.29) one finds that the cold bath must have a temperature

$$T^{cold} = \frac{\Delta}{\delta+\Delta}T^{hot} \simeq 0.54. \tag{5.8.57}$$

Examples of finite-time cycles are shown in Fig.5.2a, in which the gradual convergence towards the quasi-static limit can be clearly observed. In Fig.5.2b we present the efficiency and the output power. The analysis of the quasi-static work, heat and efficiency is presented in the appendix 5.D. As expected, when the cycle duration $\mathcal{T}$ becomes large the efficiency tends to the Carnot efficiency and the output power tends to zero. Maximum power output is attained at

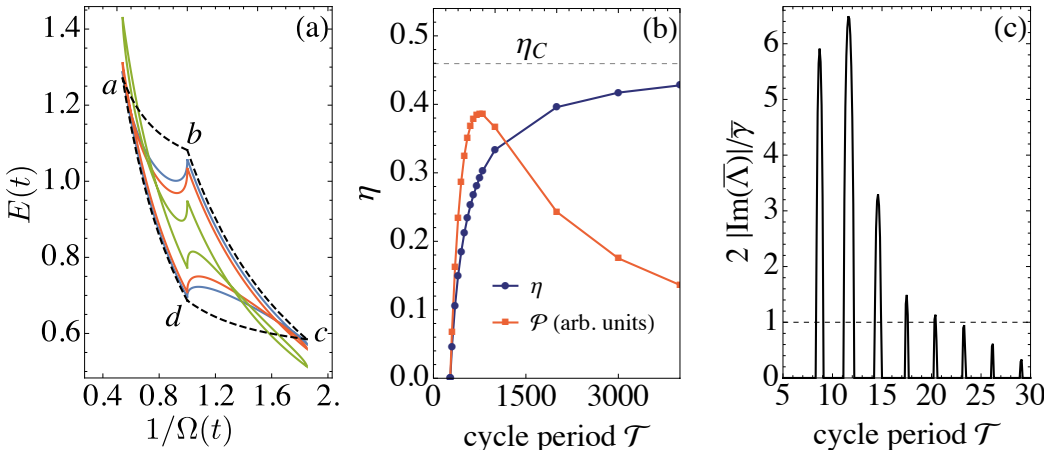

Figure 5.2: **Harmonic oscillator: operation of a finite-time Carnot engine.** The frequency modulation is chosen as in Eq.(5.8.54) setting $\Delta = 1$. Quasi-static reversibility requires that we choose $\delta(t)$ as in Eq.(5.8.55) with $\delta = 0.85$. Other parameters are $T^{hot} = 1$, $T^{cold} = 0.54$ and $\gamma = 0.03$ in the isothermal strokes (and zero otherwise). (a) Stable cycles in a $E(t)$ vs. $1/\Omega(t)$ diagram for periods $\mathcal{T} = 1000$, 700 and 300 (from outermost to innermost). The black dashed lines represent the corresponding quasi-static cycle. (b) Efficiency $\eta = \mathcal{P}/\delta\mathcal{Q}^{hot}$ (*blue circles*) and output power $\mathcal{P}$ (*red squares*; arbitrary units) as a function of the period $\mathcal{T}$. The uppermost dashed line corresponds to the classical Carnot efficiency $\eta_C = 1 - T^{cold}/T^{hot}$. Maximum power output is attained at $\mathcal{T} \sim 700$. (c) Stability analysis using Eq.(5.8.47), obtained by plotting $2|\mathrm{Im}(\overline{\Lambda})|/\overline{\gamma}$ vs. $\mathcal{T}$. When this quantity is larger than unity (*dashed line*) the cycle becomes unstable.

$\mathcal{T} \sim 700$.

Finally, we consider the stability of the cycle in Fig.5.2c, by studying Eq.(5.8.42) and the stability criteria (5.8.47). These results show that the regions of instability appear in the form of pulses, signifying a type of resonant behavior. The interesting aspect of these results is that it allows one to devise the necessary amount of dissipation required to create a stable cycle.

Appendix

5.A General properties of $\mathfrak{su}(n)$ generators

We briefly review some properties of the set $\left\{\hat{F}_k\right\}_{k=1}^{n^2-1}$ of the generators of $\mathfrak{su}(n)$:

- The commutator of two elements of $\{\hat{F}_k\}$ is

$$[\hat{F}_k, \hat{F}_l] = i \sum_{s=1}^{n^2-1} \mathrm{f}_{kls}\, \hat{F}_s \tag{5.A.1}$$

  where $\mathrm{f}_{abc} \equiv -i\mathrm{tr}([\hat{F}_a, \hat{F}_b]\, \hat{F}_c)$ is a completely antisymmetric tensor.

- The anticommutator of two elements of $\{\hat{F}_k\}$ is

$$\left\{\hat{F}_k, \hat{F}_l\right\} = 2\,\delta_{kl}\, \hat{F}_0 + \sum_{s=1}^{n^2-1} \mathrm{d}_{kls}\, \hat{F}_s \tag{5.A.2}$$

  where $\mathrm{d}_{abc} \equiv \mathrm{tr}(\{\hat{F}_a, \hat{F}_b\}\hat{F}_c)$ is a completely symmetric tensor.

- The product of two elements of $\{\hat{F}_k\}$ is

$$\hat{F}_k\, \hat{F}_l = \hat{F}_0\, \delta_{kl} + \frac{i}{2} \sum_{s=1}^{N^2-1} \mathrm{z}^*_{kls}\, \hat{F}_s\,, \qquad \mathrm{z}_{kls} \equiv \mathrm{f}_{kls} - i\mathrm{d}_{kls}\,, \tag{5.A.3}$$

  following from the Eqs. (5.A.1) and (5.A.2).

For the case $n = 2$, the set $\{\hat{F}_k\}$ reduces to the well-known ensemble of Pauli operators. Similarly, the set for $n = 3$ is given by the eight Gell-Mann matrices. However, the infinitesimal generators of $\mathfrak{su}(n > 3)$ are much less known. Therefore, we provide a general method for the derivation of the set $\{\hat{F}_k\}$ for any $n \geq 2$ [Geo82, Ali87]. Consider first the ensemble of $n \times n$ matrices P^{ik}:

$$\left(P^{ik}\right)_{\mu\nu} = \delta_{i\mu}\delta_{k\nu} \quad i, k, \mu, \nu = 1, \ldots, n \tag{5.A.4}$$

in which all the elements are zero except one. By definition, we have

$$\mathrm{tr}(P^{ik}\, P^{jl}) = \delta_{il}\delta_{kj}\,. \tag{5.A.5}$$

For $i < k$, we define the $\frac{n}{2}(n-1)$ real and the $\frac{n}{2}(n-1)$ imaginary combinations:

$$\mathcal{K}^{ik} = \frac{1}{\sqrt{2}}\left(P^{ik} + P^{ki}\right), \quad \mathcal{J}^{ik} = -\frac{i}{\sqrt{2}}\left(P^{ik} - P^{ki}\right) \tag{5.A.6}$$

whereas, using the elements P^{ii} we construct the $(n-1)$ traceless diagonal matrices

$$\mathcal{M}^q = \frac{1}{\sqrt{q(q+1)}} \sum_{k=1}^{q} \left(P^{kk} - q\, P^{q+1,q+1}\right) \tag{5.A.7}$$

with $q = 1, \ldots, n-1$. From Eq.(5.A.5), we see that the $n^2 - 1$ matrices $\mathcal{K}^{ik}, \mathcal{J}^{ik}, \mathcal{M}^q$ are orthogonal and thus they form a basis of $\mathfrak{su}(n)$.

5.B Further information for the HO example

5.B.1 Unitary part

In this appendix we consider the problem of tackling the full time-dependent Liouvillean (5.8.21). Using the transformation (5.8.26) in Eq.(5.4.20) leads to

$$\check{\mathscr{L}}_{\text{aux}} = \left(\frac{\mathrm{d}}{\mathrm{d}t}\check{V}\right)\check{V}^{-1} + \check{V}\left[\left(\frac{\mathrm{d}}{\mathrm{d}t}\check{U}\right)\check{U}^{-1} + \check{U}\,\check{\mathscr{L}}(t)\,\check{U}^{-1}\right]\check{V}^{-1}. \tag{5.B.1}$$

We will begin by dealing with the terms inside square brackets, corresponding to the unitary evolution. Carrying out the BCH expansions, as in Sec. 5.8.4, we find

$$\left(\frac{\mathrm{d}}{\mathrm{d}t}\check{U}\right)\check{U}^{-1} + \check{U}\,\check{\mathscr{L}}(t)\,\check{U}^{-1} = B_0(t)\,\check{\mathcal{H}}_0 + B_1(t)\,\check{\mathcal{H}}_1 + B_2(t)\,\check{\mathcal{H}}_2 + \check{\tilde{\mathcal{D}}}(t), \tag{5.B.2}$$

where $\check{\tilde{\mathcal{D}}}(t) \equiv \check{U}\,\check{\mathcal{D}}(t)\,\check{U}^{-1}$ (to be dealt with in Appendix 5.B.2) and

$$B_2(t) = e^{-2ir_0(t)}\left[\dot{r}_2(t) + 2i\omega(t)\,r_2(t) - 2\lambda(t)\,r_2^2(t) + \frac{\lambda^*(t)}{2}\right]; \tag{5.B.3a}$$

$$B_1(t) = -4r_1^2(t)\,B_2(t) + e^{2ir_0(t)}\left[\dot{r}_1(t) - 2i\omega(t)\,r_1(t) + 4\lambda(t)\,r_1(t)\,r_2(t) + \frac{\lambda(t)}{2}\right]; \tag{5.B.3b}$$

$$B_0(t) = -4ir_1(t)\,e^{2ir_0(t)}\,B_2(t) + \dot{r}_0(t) + \omega(t) + 2i\lambda(t)\,r_2(t). \tag{5.B.3c}$$

Next we adjust the functions r_0, r_1 and r_2 so as to make the unitary part of Eq.(5.B.2) time-independent. To accomplish this, we choose $r_1(t)$ and $r_2(t)$ to be the time-periodic solutions of

$$\dot{r}_2(t) + 2i\omega(t)\, r_2(t) - 2\lambda(t)\, r_2^2(t) + \frac{\lambda^*(t)}{2} = 0; \tag{5.B.4a}$$

$$\dot{r}_1(t) - 2i\omega(t)\, r_1(t) + 4\lambda(t)\, r_1(t)\, r_2(t) + \frac{\lambda(t)}{2} = 0, \tag{5.B.4b}$$

which then makes $B_1 = B_2 = 0$. Next, let

$$\Lambda(t) \equiv \omega(t) + 2i\lambda(t)\, r_2(t). \tag{5.B.5}$$

Then, to make $B_0(t)$ in Eq.(5.B.3c) time-independent we choose

$$r_0(t) = \int_{t_0}^{t} \mathrm{d}t' \left(\overline{\Lambda} - \Lambda(t')\right). \tag{5.B.6}$$

With these choices Eq.(5.B.2) becomes

$$\left(\frac{\mathrm{d}}{\mathrm{d}t}\check{U}\right)\check{U}^{-1} + \check{U}\,\check{\mathscr{L}}(t)\,\check{U}^{-1} = \overline{\Lambda}\,\check{\mathcal{H}}_0 + \check{\tilde{\mathcal{D}}}(t) \tag{5.B.7}$$

and, consequently, Eq.(5.B.1) reduces to

$$\check{\mathscr{L}}_{\text{aux}} = \left(\frac{\mathrm{d}}{\mathrm{d}t}\check{V}\right)\check{V}^{-1} + \check{V}\left[\overline{\Lambda}\check{\mathcal{H}}_0 + \check{\tilde{\mathcal{D}}}(t)\right]\check{V}^{-1}. \tag{5.B.8}$$

The next step is to now turn to the dissipative part and adjust $\check{V}(t)$ in order to make Eq.(5.B.8) time-independent. But before doing so it is useful to anticipate certain facts about r_1 and r_2. Eq.(5.B.4a) admits two types of solutions, representing unitarily stable (US) and unitarily unstable (UU) dynamics (by "unitarily" we refer to stability in the absence of dissipation). Let us define the variable

$$\sigma = \begin{cases} 1 & \text{unitarily stable (US)} \\ i & \text{unitarily unstable (UU)} \end{cases} \tag{5.B.9}$$

Then, the properties of the two phases are most readily distinguished by means of the following auxiliary variables:

$$J(t) \equiv 1 + 8r_1(t)\, r_2(t); \tag{5.B.10}$$

$$z(t) \equiv 1 + 4r_1(t)\, r_2(t) = \frac{1 + J(t)}{2}; \tag{5.B.11}$$

$$r_1'(t) \equiv r_2(t)\,(1 + 4r_1(t)\, r_2(t)) = r_2(t)\, z(t), \tag{5.B.12}$$

which are introduced to make the results that follow more self-contained. As will be discussed in Appendix 5.C, it turns out that

$$r_1'(t) = \sigma^2\, r_1^*(t), \tag{5.B.13}$$

and

$$J(t) = \sigma\, j, \qquad j \in \mathbb{R}. \tag{5.B.14}$$

Using also that $J^2 = 1 + 16 r_1\, r_1' = 1 + 16\sigma^2 |r_1|^2$ we find that

$$j^2 = 16|r_1|^2 + \sigma^2. \tag{5.B.15}$$

Moreover, combining these results we find

$$4|r_1|^2 = \sigma^2 \left(\frac{J^2-1}{4}\right) = \sigma^2 z(z-1). \tag{5.B.16}$$

Finally, it is worth mentioning that

$$z^* = \begin{cases} z & \sigma = 1 \\ 1-z & \sigma = -i \end{cases} \tag{5.B.17}$$

We can also use the above results to express r_2 in terms of r_1, z and j in various ways:

$$r_2 = \frac{\sigma^2\, r_1^*}{z} = \frac{\sigma\, j - 1}{8 r_1} = \frac{2\sigma^2\, r_1^*}{\sigma\, j + 1}. \tag{5.B.18}$$

In particular, it then follows that in the UU phase ($\sigma = -i$)

$$4|r_2|^2 = 1. \tag{5.B.19}$$

so $r_2(t)$ evolves in time as a pure phase.

5.B.2 Dissipative part

We now return to Eq.(5.B.8) and adjust the functions $g_i(t)$ in order to eliminate the remaining time-dependence. To do so we first need to compute $\check{\check{\mathcal{D}}}(t) = \check{U}\, \check{\mathcal{D}}(t)\, \check{U}^{-1}$. Using again the BCH expansions we find that $\check{\check{\mathcal{D}}}(t)$ has the same structure as $\check{\mathcal{D}}(t)$ in Eq.(5.8.23), but with modified parameters

$$\check{\check{\mathcal{D}}}(t) = \gamma(t)\,(\tilde{n}(t)+1)\,\check{\mathcal{D}}_1 + \gamma(t)\,\tilde{n}(t)\,\check{\mathcal{D}}_2 - \gamma(t)\,\tilde{m}(t)\,\check{\mathcal{D}}_3 - \gamma(t)\,\tilde{m}'(t)\,\check{\mathcal{D}}_4, \tag{5.B.20}$$

where

$$\tilde{n}(t)+\frac{1}{2}=J(t)\,(N(t)+\frac{1}{2})+2im(t)\,r_1(t)-2im^*(t)\,r_1'(t); \tag{5.B.21a}$$

$$\tilde{m}(t)=\left[M(t)-4ir_2(t)\,(n(t)+\frac{1}{2})-4m^*(t)\,r_2^2(t)\right]e{-}2ir_0(t); \tag{5.B.21b}$$

$$\tilde{m}'(t)=\left[m^*(t)\,z^2(t)+4ir_1(t)z(t)\,(n(t)+\frac{1}{2})-4m(t)\,r_1^2(t)\right]e^{2ir_0(t)}. \tag{5.B.21c}$$

In these formulas, we assume that we have already solved for the r_i, so that these correspond simply to new time-periodic parameters. In general, however, $\tilde{m}'(t)\neq\tilde{m}^*(t)$ and $n(t)$ may now be complex. Below in this subsection we will show how that can be amended.

We now see from this result that Eq.(5.B.8) falls under the same category of the problem treated in Sec. 5.8.4. In fact, carrying out all expansions we find

$$\check{\mathscr{L}}_{\rm aux}=\overline{\Lambda}\,\check{\mathcal{H}}_0+C_1(t)\,\check{\mathcal{D}}_1+C_2(t)\,\check{\mathcal{D}}_2+C_3(t)\,\check{\mathcal{D}}_3+C_4(t)\,\check{\mathcal{D}}_4, \tag{5.B.22}$$

where now

$$C_2(t)=e^{-g_1(t)}\left[\dot{g}_2(t)-\gamma(t)+\gamma(t)\,e^{g_2(t)}(\tilde{n}(t)+1)\right]; \tag{5.B.23a}$$

$$C_1(t)=\dot{g}_1(t)-\dot{g}_2(t)+\gamma(t)+C_2(t); \tag{5.B.23b}$$

$$C_3(t)=e^{g_2(t)-g_1(t)}\left[\dot{g}_3(t)+(\gamma(t)+2i\overline{\Lambda})\,g_3(t)-\gamma(t)\,\tilde{M}(t)\right]; \tag{5.B.23c}$$

$$C_4(t)=e^{g_2(t)-g_1(t)}\left[\dot{g}_4(t)+(\gamma(t)-2i\overline{\Lambda})\,g_4(t)-\gamma(t)\tilde{m}'(t)\right]. \tag{5.B.23d}$$

The only difference with respect to Eqs.(5.8.31a)-(5.8.31d) is the appearance of $\overline{\Lambda}$ and the fact that the physical parameters $(n(t)\,,\,m(t)\,,\,m^*(t))$ are now replaced by $(\tilde{n}(t)\,,\,\tilde{m}(t)\,,\,\tilde{m}'(t))$. Proceeding as before, we then obtain a time-independent $\check{\mathscr{L}}_{\rm aux}$ by setting

$$\dot{g}_2(t)-\gamma(t)+\gamma(t)\,e^{g_2(t)}(\tilde{n}(t)+1)=0; \tag{5.B.24a}$$

$$\dot{g}_3(t)+(\gamma(t)+2i\overline{\Lambda})\;g_3(t)=\gamma(t)\,\tilde{m}(t); \tag{5.B.24b}$$

$$\dot{g}_4(t)+(\gamma(t)-2i\overline{\Lambda})\;g_4(t)=\gamma(t)\,\tilde{m}'(t). \tag{5.B.24c}$$

and

$$g_1(t) = g_2(t) + \int_{t_0}^{t} \mathrm{d}t' \; (\overline{\gamma} - \gamma(t')). \tag{5.B.25}$$

We also define $G_2(t)$ exactly as in Eq.(5.8.35), which then gives

$$\dot{G}_2(t) + \gamma(t)\, G_2(t) = \gamma(t)\, (\tilde{n}(t) + \frac{1}{2}). \tag{5.B.26}$$

After setting all these functions, we then finally obtain

$$\check{\mathscr{L}}_{\text{aux}} = \overline{\Lambda}\, \check{\mathcal{H}}_0 + \overline{\gamma}\, \check{\mathcal{D}}_1. \tag{5.B.27}$$

which is Eq.(5.8.41).

In the above formulation we generally have $g_4 \neq g_3^*$ and G_2 complex. It is therefore convenient to use a new set of variables in which the physical meaning of these variables can be made clearer. The variable G_2 can be left as is. But it is convenient to use Eqs.(5.B.9)-(5.B.17) to rewrite Eq.(5.B.21a) as

$$\tilde{n}(t) + \frac{1}{2} = \sigma \Big\{ j(t)\, (n(t) + \frac{1}{2}) + 2im(t)\, r_1(t)\, \sigma^* - 2im^*(t)\, r_1^*(t)\, \sigma \Big\}. \tag{5.B.28}$$

The quantity inside brackets in Eq.(5.B.28) is now real by construction, so that $\tilde{n}(t) + \frac{1}{2} \propto \sigma$. Consequently, the same will be true for G_2. As will be seen below, G_2 always appears in products of the form $J(t)\, G_2(t) \propto \sigma^2$, which will therefore be real.

Next, we turn to g_3 and g_4. First we eliminate the dependence on r_0 by defining $\tilde{g}_3 \equiv e^{2ir_0}\; g_3$ and $\tilde{g}_4 \equiv e^{-2ir_0}\; g_4$. Because of Eq.(5.B.6) it then follows that Eqs.(5.B.24b) and (5.B.24c) are simply replaced by

$$\dot{\tilde{g}}_3(t) + (\gamma(t) + 2i\Lambda(t))\tilde{g}_3(t) = \\ \gamma(t) \Big[m(t) - 4ir_2(t)\, (n(t) + \frac{1}{2}) - 4m^*(t)\, r_2^2(t) \Big]; \tag{5.B.29a}$$

$$\dot{\tilde{g}}_4(t) + (\gamma(t) - 2i\Lambda(t))\tilde{g}_4(t) = \\ \gamma(t) \Big[m^*(t)\, z^2(t) + 4ir_1(t)\, z(t)(n(t) + \frac{1}{2}) - 4m(t)\, r_1^2(t) \Big]. \tag{5.B.29b}$$

That is, compared to Eqs.(5.B.24b) and (5.B.24c), $\overline{\Lambda}$ is replaced by Λ and the factors of $e^{\pm 2ir_0}$ are eliminated from Eqs.(5.B.21b) and (5.B.21c).

Next, we change variables to

$$G_3(t) \equiv z(t)\ \tilde{g}_3(t), \qquad G_4(t) \equiv \frac{\tilde{g}_4(t)}{z(t)}. \tag{5.B.30}$$

where, recall, $z = 1 + 4r_1\ r_2$ (compare with Eq.(5.B.11)). We then get

$$\dot{G}_3(t) + (\gamma(t) + 2i\omega(t) - \nu(t))G_3(t) = \gamma(t)\left[m(t)\ z(t) - 4i\sigma^2\ r_1^*(t)(n(t) + \frac{1}{2}) - \frac{4m^*(t)\ (r_1^*)^2(t)}{z(t)}\right]; \tag{5.B.31a}$$

$$\dot{G}_4(t) + (\gamma(t) - 2i\omega(t) + \nu(t))G_4(t) = \gamma_(t)\left[m^*(t)\ z(t) + 4ir_1(t)\ (n(t) + \frac{1}{2}) - \frac{4m(t)\ r_1^2(t)}{z(t)}\right]. \tag{5.B.31b}$$

where

$$\begin{aligned}\nu(t) &\equiv 4\lambda(t)\ r_2(t) + \frac{\dot{z}(t)}{z(t)} = 2\lambda(t)\ r_2(t) - \frac{2\lambda^*(t)\ r_1(t)}{z(t)} \\ &= \frac{2\lambda(t)\ \sigma^2\ r_1^*(t) - 2\lambda^*(t)\ r_1(t)}{z(t)}.\end{aligned} \tag{5.B.32}$$

In the US phase $\sigma = 1$ and $z^* = z$ so that $\nu^* = -\nu$. Consequently, we see that in this case $G_3^* = G_4$. In the UU phase, on the other hand, this is no longer true. However, in the UU phase a new symmetry appears. Namely, ir_1G_3 and $ir_1^*G_4$ become real. This can be seen by verifying that ir_1G_3 satisfies a linear real equation, so that the solution must also be real. To summarize:

- In the unitarily stable (US) case ($\sigma = 1$) we have $G_3 = G_4^*$ and $G_2 \in \mathbb{R}$.
- In the unitarily unstable (UU) case ($\sigma = i$) we have $(r_1G_3)^* = -(r_1G_3)$, $(r_1^*G_4)^* = -r_1^*G_4$ and $iG_2 \in \mathbb{R}$.

5.B.3 Floquet Liouvillean

The final step is to apply Eq.(5.5.3) to find the Floquet Liouvillean. The result is Eq.(5.8.43) with

$$\omega_F = \overline{\Lambda}\, J; \tag{5.B.33a}$$

$$\lambda_F = 4i\overline{\Lambda}\, r_1; \tag{5.B.33b}$$

$$\lambda'_F = -4i\bar{\Lambda}\, r'_1; \tag{5.B.33c}$$

$$n_F + \frac{1}{2} = J\, G_2 - \frac{2i}{\overline{\gamma}}\Big[r_1\, z(\overline{\gamma} + 2i\overline{\Lambda})\tilde{g}_3 - r_2(\overline{\gamma} - 2i\overline{\Lambda})\tilde{g}_4\Big]; \tag{5.B.33d}$$

$$m_F = 4ir'_1\, G_2 + \frac{1}{\overline{\gamma}}\Big[z^2(\overline{\gamma} + 2i\overline{\Lambda})\tilde{g}_3 - 4r_2^2(\overline{\gamma} - 2i\overline{\Lambda})\tilde{g}_4\Big], \tag{5.B.33e}$$

$$m'_F = -4ir_1\, G_2 + \frac{1}{\overline{\gamma}}\Big[- 4r_1^2(\overline{\gamma} + 2i\overline{\Lambda})\tilde{g}_3 + (\overline{\gamma} - 2i\overline{\Lambda})\tilde{g}_4\Big]. \tag{5.B.33f}$$

In these expressions, all quantities are to be evaluated at time t, which has been omitted for clarity.

The steady-state of the Floquet Liouvillean (5.8.43) is unique and corresponds to a squeezed thermal state which is completely characterized by the covariances

$$\langle \hat{a}^\dagger\, \hat{a}\rangle_{ss} + \frac{1}{2} = \frac{(n_F + \frac{1}{2})(\overline{\gamma}^2 + 4\omega_F^2) + m_F\lambda_F(2\omega_F + i\overline{\gamma}) + m'_F\lambda'_F(2\omega_F - i\overline{\gamma})}{\overline{\gamma}^2 + 4\omega_F^2 - 4\lambda_F\lambda'_F}; \tag{5.B.34a}$$

$$\langle \hat{a}\, \hat{a}\rangle_{ss} = \frac{m_F(\overline{\gamma}^2 - 2i\overline{\gamma}\omega_F - 2\lambda_F\lambda'_F) - 2m'_F\lambda'^2_F - \lambda'_F(2n_F + 1)(2\omega_F + i\overline{\gamma})}{\overline{\gamma}^2 + 4\omega_F^2 - 4\lambda_F\lambda'_F}; \tag{5.B.34b}$$

$$\langle \hat{a}^\dagger\, \hat{a}^\dagger\rangle_{ss} = \frac{m'_F(\overline{\gamma}^2 + 2i\overline{\gamma}\omega_F - 2\lambda_F\lambda'_F) - 2m_F\lambda_F^2 - \lambda_F(2n_F + 1)(2\omega_F - i\overline{\gamma})}{\overline{\gamma}^2 + 4\omega_F^2 - 4\lambda_F\lambda'_F}. \tag{5.B.34c}$$

Substituting the Floquet parameters Eqs.(5.B.33a)-(5.B.33f) into Eqs.(5.B.34a), (5.B.34c) we obtain

$$\langle \hat{a}^\dagger \hat{a} \rangle_{ss} + \frac{1}{2} = J\, G_2 - 2ir_1\, z\tilde{g}_3 + 2ir_2\tilde{g}_4; \tag{5.B.35a}$$

$$\langle \hat{a}\, \hat{a} \rangle_{ss} = 4ir_1'\, G_2 + z^2\tilde{g}_3 - 4r_2^2\tilde{g}_4; \tag{5.B.35b}$$

$$\langle \hat{a}^\dagger \hat{a}^\dagger \rangle_{ss} = -4ir_1 G_2 - 4r_1^2\tilde{g}_3 + \tilde{g}_4. \tag{5.B.35c}$$

In terms of the variables G_3 and G_4, defined in Eq.(5.B.30), these simplify even further to

$$\langle \hat{a}^\dagger \hat{a} \rangle_{ss} + \frac{1}{2} = JG_2 - 2i(r_1 G_3 - r_1' G_4); \tag{5.B.36a}$$

$$\langle \hat{a}\, \hat{a} \rangle_{ss} = 4ir_1'\, G_2 + z\, G_3 - \frac{4r_1'^2}{z} G_4; \tag{5.B.36b}$$

$$\langle \hat{a}^\dagger \hat{a}^\dagger \rangle_{ss} = -4ir_1 G_2 - \frac{4r_1^2}{z} G_3 + zG_4. \tag{5.B.36c}$$

It follows from this result, together with our previous discussion about G_2, G_3 and G_4, that in both the US and UU cases we will have $\langle \hat{a}^\dagger \hat{a} \rangle_{ss}$ real and $\langle \hat{a}\, \hat{a} \rangle_{ss} = \langle \hat{a}^\dagger \hat{a}^\dagger \rangle_{ss}^*$, as expected on physical grounds. This is a bit cumbersome to verify but can be done as follows.
In the US phase $r_1\, G_3 - r_1'\, G_4 = r_1\, G_3 - r_1^*\, G_3^*$ which is purely imaginary, hence making (5.B.36a) real. In the UU phase, on the other hand, $r_1\, G_3$ and $r_1^*\, G_4$ will independently be purely imaginary, hence leading to the same conclusion. One may proceed similarly when comparing (5.B.36b) and (5.B.36c). For instance, in the US phase $(z\, G_3 - 4r_1^{*2}\, G_4/z)^* = zG_4 - 4r_1^2\, G_3/z$, hence making $\langle \hat{a}\, \hat{a} \rangle_{ss}^* = \langle \hat{a}^\dagger \hat{a}^\dagger \rangle_{ss}$.
In the UU phase, on the other hand, one has to make use of Eq.(5.B.16), which in this case is written as $4|r_1|^2 = zz^*$. Then, since $G_3^* = -r_1 G_3/r_1^*$, it follows that $(zG_3)^* = -z^* r_1 G_3/r_1^* = -4r_1^2 G_3/z$. A similar calculation will hold for $4r_1^{*2} G_4/z$ so that, once again, we will have $\langle \hat{a}\, \hat{a} \rangle_{ss}^* = \langle \hat{a}^\dagger \hat{a}^\dagger \rangle_{ss}$.

5.C Stability of the Ermakov-Lewis theory

Let us analyze the connection between our results and the Ermakov-Lewis theory describing the unitary dynamics of a harmonic oscillator subject to a time-dependent frequency (see Chap.4).

As discussed in Sec. 5.8.2, this connection is established when $\eta = \omega(t) - \lambda(t)$ is time-independent, in which case we work instead with $\Omega(t)$ defined in Eq.(5.8.18). If we now let

$$r_1(t) = \frac{\zeta(t)\,\dot{\zeta}(t)}{4\eta(t)} - \frac{i}{8}\left[\frac{1}{\zeta^2(t)} - \zeta^2(t) + \frac{\dot{\zeta}^2(t)}{\eta^2}\right]; \tag{5.C.1}$$

$$r_2(t) = \frac{i}{2} + \frac{\zeta^2}{i(1+\zeta^2) + \zeta\dot{\zeta}/\eta}. \tag{5.C.2}$$

then one may verify that Eq.(5.B.4a) will be satisfied provided ζ is a time-periodic solution of the Ermakov-Pinney equation (5.8.45)

$$\ddot{\zeta} + \Omega(t)^2\zeta = \frac{\eta^2}{\zeta^3}. \tag{5.C.3}$$

This therefore serves to show that our calculations reproduce the Ermakov-Lewis theory as a particular case.

Eq.(5.8.45) always admits a time-periodic solution. However, this solution may be either real or such that ζ^2 is purely imaginary. The former corresponds to unitarily stable solutions whereas the latter are unitarily unstable (that is, they would be unstable in the absence of dissipation). This can now be used to demonstrate the facts stated below Eqs.(5.B.10) and (5.B.12). The quantities J and r_1' may be rewritten as

$$J(t) = 1 + 8r_1(t)\,r_2(t) = \frac{1}{2}\left(\frac{1}{\zeta^2(t)} + \zeta^2(t) + \frac{\dot{\zeta}^2(t)}{\eta^2}\right); \tag{5.C.4}$$

$$r_1'(t) = r_2(t)\,(1 + 4r_1(t)\,r_2(t)) = \frac{\zeta(t)\,\dot{\zeta}(t)}{4\eta} + \frac{i}{8}\left[\frac{1}{\zeta^2(t)} - \zeta^2(t) + \frac{\dot{\zeta}^2(t)}{\eta^2}\right]. \tag{5.C.5}$$

From the properties of ζ in the two phases it then readily follows that $J^* = J$ in the US phase and $J^* = -J$ in the UU phase (compare with Eq.(5.B.14)). Similarly, it follows that $r_1' = r_1^*$ in one case and $r_1' = -r_1^*$ in the other (compare with Eq.(5.B.13)).

5.D Heat, work and efficiency in the quasi-static case

In this appendix we discuss the quasi-static properties of the Carnot cycle of Sec.5.8.7. We take for the work rate the usual definition

$$\frac{\mathrm{d}\mathcal{W}}{\mathrm{d}t} \equiv \mathcal{P} = \left\langle \frac{\partial \hat{H}}{\partial t} \right\rangle = \dot{\omega}(t)(\langle \hat{a}^\dagger\, \hat{a}\rangle + \frac{1}{2}) + \frac{\dot{\lambda}(t)}{2}(\langle \hat{a}\, \hat{a}\rangle + \langle \hat{a}^\dagger \hat{a}^\dagger\rangle). \tag{5.D.1}$$

In the isentropic strokes no heat flows to the environment so that the total work performed becomes simply

$$\begin{aligned}\mathcal{W}_{\mathbf{bc}} &= E(\mathbf{c}) - E(\mathbf{b}) \\ &= \frac{\Omega(\mathbf{c})}{2}\coth\left(\frac{\Omega(\mathbf{c})}{2T^{cold}}\right) - \frac{\Omega(\mathbf{b})}{2}\coth\left(\frac{\Omega(\mathbf{b})}{2T^{hot}}\right);\end{aligned} \tag{5.D.2}$$

$$\begin{aligned}\mathcal{W}_{\mathbf{da}} &= E(\mathbf{a}) - E(\mathbf{d}) \\ &= \frac{\Omega(\mathbf{a})}{2}\coth\left(\frac{\Omega(\mathbf{a})}{2T^{hot}}\right) - \frac{\Omega(\mathbf{d})}{2}\coth\left(\frac{\Omega(\mathbf{d})}{2T^{cold}}\right).\end{aligned} \tag{5.D.3}$$

As for the isothermal strokes, we have

$$\langle \hat{a}^\dagger\, \hat{a}\rangle + \frac{1}{2} = n(t) + \frac{1}{2} = \frac{\omega(t)}{2\Omega(t)}\coth\left(\frac{\Omega(t)}{2T}\right); \tag{5.D.4}$$

$$\langle \hat{a}\, \hat{a}\rangle = m(t) = -\frac{\lambda(t)}{2\Omega(t)}\coth\left(\frac{\Omega(t)}{2T}\right), \tag{5.D.5}$$

where T means either T^{hot} or T^{cold}. The work rate then becomes

$$\frac{\mathrm{d}\mathcal{W}}{\mathrm{d}t} = \frac{\dot{\omega}(t)\,\omega(t) - \dot{\lambda}(t)\,\lambda(t)}{2\Omega(t)}\coth\left(\frac{\Omega(t)}{2T}\right). \tag{5.D.6}$$

But this may be written as

$$\frac{\mathrm{d}\mathcal{W}}{\mathrm{d}t} = T\frac{\mathrm{d}}{\mathrm{d}t}\log\left[\sinh\left(\frac{\Omega(t)}{2T}\right)\right]. \tag{5.D.7}$$

Integrating over the initial and final times of the stroke then yields the total work performed:

$$\mathcal{W}_{\mathrm{iso}} = T\log\left[\frac{\sinh(\Omega_f/2T)}{\sinh(\Omega_i/2T)}\right]. \tag{5.D.8}$$

In the classical limit $T \gg \Omega_{i,f}$ we get

$$\mathcal{W}_{\text{iso}} \simeq T \log\left(\frac{\Omega_f}{\Omega_i}\right). \tag{5.D.9}$$

The total work performed in each stroke will therefore be

$$\mathcal{W}_{\mathbf{ab}} = T^{hot} \log\left[\frac{\sinh(\Omega(\mathbf{b})/2T^{hot})}{\sinh(\Omega(\mathbf{a})/2T^{hot})}\right]; \tag{5.D.10a}$$

$$\begin{aligned}\mathcal{W}_{\mathbf{bc}} &= E(\mathbf{c}) - E(\mathbf{b}) \\ &= \frac{\Omega(\mathbf{c})}{2}\coth\left(\frac{\Omega(\mathbf{c})}{2T^{cold}}\right) - \frac{\Omega(\mathbf{b})}{2}\coth\left(\frac{\Omega(\mathbf{b})}{2T^{hot}}\right);\end{aligned} \tag{5.D.10b}$$

$$\mathcal{W}_{\mathbf{cd}} = T^{cold} \log\left[\frac{\sinh(\Omega(\mathbf{d})/2T^{cold})}{\sinh(\Omega(\mathbf{c})/2T^{cold})}\right];$$

$$\begin{aligned}\mathcal{W}_{\mathbf{da}} &= E(\mathbf{a}) - E(\mathbf{d}) \\ &= \frac{\Omega(\mathbf{a})}{2}\coth\left(\frac{\Omega(\mathbf{a})}{2T^{hot}}\right) - \frac{\Omega(\mathbf{d})}{2}\coth\left(\frac{\Omega(\mathbf{d})}{2T^{cold}}\right).\end{aligned} \tag{5.D.10c}$$

Moreover, the heat exchanged in $\mathbf{a} - b$ and $\mathbf{c} - d$ will be

$$\delta\mathcal{Q}^{hot} = E(\mathbf{b}) - E(\mathbf{a}) - \mathcal{W}_{\mathbf{ab}}; \tag{5.D.11}$$

$$\delta\mathcal{Q}^{cold} = E(\mathbf{d}) - E(\mathbf{c}) - \mathcal{W}_{\mathbf{cd}}. \tag{5.D.12}$$

From this one may now compute the efficiency of the quasi-static cycle

$$\eta = -\frac{\mathcal{W}_{\mathbf{ab}} + \mathcal{W}_{\mathbf{bc}} + \mathcal{W}_{\mathbf{cd}} + \mathcal{W}_{\mathbf{da}}}{\delta\mathcal{Q}^{hot}} = 1 + \frac{\delta\mathcal{Q}^{cold}}{\delta\mathcal{Q}^{hot}}. \tag{5.D.13}$$

However, due to Eq.(5.7.29) it follows that

$$\frac{\delta\mathcal{Q}^{cold}}{\delta\mathcal{Q}^{hot}} = -\frac{T^{cold}}{T^{hot}}, \tag{5.D.14}$$

therefore leading us to the Carnot efficiency

$$\eta_C \equiv 1 - \frac{T^{cold}}{T^{hot}}. \tag{5.D.15}$$

We emphasize that this result is only obtained if the constraint (5.7.29) is applied.

Concluding remarks

In this thesis we have analyzed some aspects regarding the non-equilibrium dynamics of closed and open quantum systems. In particular, we have considered those non-equilibrium situations which are generated by the presence of time-dependent external fields, focusing on the case of a slow driving across a quantum phase transition and on the case of a periodic driving.
More precisely, we have first investigated the non-equilibrium dynamics of a one-dimensional Tonks-Girardeau gas subject to a time-dependent harmonic trap potential. For this setup, we have shown that a trap-release protocol is actually equivalent to an inhomogeneous driving across the XX criticality.
The dynamics generated by a trap-frequency modulation has been solved with mainly two techniques: a perturbative expansion over the adiabatic evolution and an exact approach based on the use of Ermakov-Lewis dynamical invariants, in terms of which one finds that the time-evolved density can be written as a dynamical rescaling of the initial density profile. Numerical exact diagonalization has been carried out to check the analytical computations. Quasi-adiabatic expansions and the exact Ermakov-Lewis method are found in agreement for modest trap-size variations, where the perturbation theory is expected to hold. As an application, we have considered the case of a continuous frequency modulation with a $1/t$ protocol. In this case the dynamics of the Tonks-Girardeau gas shows an interesting discrete-time symmetry and it undergoes a series of plateaus distribuited log-periodically, where the expansion of the cloud surprisingly stops despite the continuous decreasing of the trap-frequency. We have also considered the effects of a time-periodic modulation of the trap-frequency. A classification of time-periodic harmonic Schrödinger operators on varying the trap-frequency allowed us to describe the possible dynamical evolutions of the bosonic cloud. We have found two main scenarios: a stable regime where the external forcing generates breathing modes and an unstable regime where the gas develops dynamical instabilities. We have shown that the key object for such study is the trace of the monodromy matrix $\mathbb{M}(\omega)$ of the Hill problem associated in the semi-classical limit with the harmonic Schrödinger operator. In particular, the stable regime corresponds to elliptic monodromies (for which $|\mathrm{tr}(\mathbb{M}(\omega))| < 2$) whereas hyperbolic monodromies ($|\mathrm{tr}(\mathbb{M}(\omega)| > 2$) lead to instabilities. Moreover, working out Floquet theory together with Ermakov-Lewis invariants for this setup, we have been able to

provide general results for the energy spectrum and for the N-particle density at large N.
Notice that these results are in agreement with general expectations for scale-invariant Fermi gases. An interesting sequel of this analysis could be to use the machinery of dynamical invariants to test the dynamical behavior of interacting integrable models, such as e.g. the XXZ Heisenberg chain. In this case one may lose scale invariance, due to the presence of an extra energy scale related to finite interactions. Therefore, a next step could be the analysis of the Gross-Pitaevskii regime of the Bose-Hubbard model, which is still suitable for a scaling description although different from that of the Tonk-Girardeau limit. We also mention that the Ermakov-Lewis invariants allow for a hydrodynamic interpretation (see e.g. [Mad26, Mad27] and [Tse11]). Hence, one expects to find a hydrodynamic description in agreement with the recent results [Ber16, CA16], when speaking about integrable models.

The last part of the thesis has dealt with markovian driven open quantum systems. Our goal was to extend Floquet theory to the case of a Lindblad evolution, exploiting the strict analogy of the vectorized Lindblad equation with a standard Schrödinger equation. At a first glance, one may be tempted to use Magnus expansions, from which approximate results are easily obtained in the case of a fast-oscillating driving. However, a part from the well-known problems of convergence that affect Magnus expansion already in a closed setup, complete-positivity and trace preservation properties of the reduced time-evolution may be lost when one truncates the Floquet-Liouvillean at lowest orders (which is typically done). Therefore, we have derived an exact method that encompasses known-problems related to Magnus expansions and that allows to write down an exact physical Floquet generator. The main idea that underlies our Lindblad-Floquet framework is rather simple: if we provide a closed algebraic structure, then formal BCH formulae can be re-summed exactly. We thus proved the existence of a closed algebra for a generic markovian open system with finite Hilbert space dimension and we have designed a generic time-dependent transformation to a time-independent frame where the dynamics is easily solved. Moving backwards to the physical system, one then has formal exact solutions for the time-evolution of the reduced density matrix. The advantage of such frame transformation consists in getting rid of the super-operator structure of the time-dependent master equation reducing the initial problem to the solution of a set of first-order differential equations. However, this method is limited by the possibility of handling a very complicated algebra. In practice, only subalgebras related to some specific problems

have been managed in our analysis. Moreover, the differential equations which encode the time-evolution of the system are generically highly non-linear and thus require a particular care to be solved.
Nevertheless, the Lindblad-Floquet framework results a very powerful tool in the analysis of time-periodic Lindblad equations. As shown in a few applications, it gives a transparent and simple manner to investigate the properties of the cyclic evolution and the convergence towards it. As a main application of Lindblad-Floquet, we have analyzed the operation of finite-time quantum heat-engine with a special focus on the Carnot cycle, where the time-dependence of the environment and of the system has to be considered simultaneously during the isothermal strokes. As a perspective, some optimization studies are needed to let these quantum devices to work at the maximum possible efficiency. This may be done considering a mixture of two bosonic modes that evolve with a Gaussian-preserving dynamics. In this way, the efficiency of the quantum machine can be tuned varying the fraction of the different species.
Regarding the existence of a Floquet description for a generic time-periodic Lindblad dynamics, further analysis are required, especially in light of the work in Ref. [Sch18b], where general conditions for the markovianity of the Floquet evolution have been pointed out. In fact, understanding the connection between the existence of periodic solutions for the canonical coordinates and the general conditions under which markovianity is preserved in the Floquet description remains still an open question.

Bibliography

[Aba14] Abah O and Lutz E [2014]. EPL, 106(2):20001.

[Aba17] Abah O and Lutz E [2017]. EPL, 118(4):40005.

[Aba18] Abah O and Lutz E [2018]. Phys. Rev. E, 98:032121.

[Abr64] Abramowitz M and Stegun I [1964]. *Handbook of Mathematical Functions*. Dover, New York.

[Acc15] Acconcia TV, Bonança MVS and Deffner S [2015]. Phys. Rev. E, 92:42148.

[Ali79] Alicki R [1979]. J. Phys. A: Math. Gen., 12(5):L103.

[Ali87] Alicki R and Lendi K [1987]. *Quantum dynamical semigroups and applications*. LNP0717. Springer.

[Ali12] Alicki R, Gelbwaser-Klimovsky D and Kurizki G [2012]. arXiv:1205.4552.

[Ali15] Alicki R and Gelbwaser-Klimovsky D [2015]. New J. of Phys., 17(11):115012.

[Ali18] Alicki R and Kossloff R [2018]. arXiv:1801.08314.

[And69] Andrews T [1869]. Philosophical Transactions of the Royal Society of London, 159:575–590.

[And09] Anderson GW, Guionnet A and Zeitouni O [2009]. *An Introduction to Random Matrices*. Cambridge University Press.

[And17] Anders J and Esposito M [2017]. New J. of Phys., 19(1):10201.

[Ara19] Araújo R, Wald S and Henkel M [2019]. J. Stat. Mech.: Theory and Experiment, 2019(5):053101.

[Ave85] Avenel O and Varoquaux E [1985]. Phys. Rev. Lett., 55(24):2704–2707.

[Bak02] Baker H [1902]. Proc. London Math. Soc., 1(34):347–360.

[Bar18] Barato AC and Chetrite R [2018]. J. Stat. Mech.: Theory and Experiment, 2018(5):53207.

[Bas18] Bastidas VM, Kyaw TH, Tangpanitanon J, Romero G, Kwek LC and Angelakis DG [2018]. New J. of Phys., 20(9):93004.

[Bau17] Bauer M, Bernard D and Jin T [2017]. SciPost Phys., 3:033.

[Bau19] Bauer M, Bernard D and Jin T [2019]. SciPost Phys., 6:45.

[Bav92] Bavli R and Metiu H [1992]. Phys. Rev. Lett., 69(13):1986–1988.

[Bcv14] Buča B and Prosen T [2014]. Phys. Rev. Lett., 112:067201.

[Bcv17] Buča B and Prosen T [2017]. Phys. Rev. E, 95:052141.

[Ber90] Berche B and Turban L [1990]. J. Phys. A: Math. Gen., 23(13):3029.

[Ber04] Berline N, Getzler E and Vergne M [2004]. *Heat Kernels and Dirac Operators*. Springer.

[Ber09] Berche B, Henkel M and Kenna R [2009]. J. Phys. Studies, (13):3201.

[Ber11] Bernier JS, Roux G and Kollath C [2011]. Phys. Rev. Lett., 106:200601.

[Ber12a] Bernard D and Doyon B [2012]. J. Phys. A: Math. Theor., 45(36):362001.

[Ber12b] Bernier JS, Poletti D, Barmettler P, Roux G and Kollath C [2012]. Phys. Rev. A, 85:033641.

[Ber16] Bertini B, Collura M, De Nardis J and Fagotti M [2016]. Phys. Rev. Lett., 117:207201.

[Ber17] Berdanier W, Kolodrubetz M, Vasseur R and Moore JE [2017]. Phys. Rev. Lett., 118(26):260602.

[Bet30] Bethe H [1930]. Annalen der Physik, 397(3):325–400.

[Bew06] Bewley GP, Lathrop DP and Sreenivasan KR [2006]. Nature, 441(7093):588–588.

[Bin87] Binder K [1987]. Reports on progress in physics, 50:783–859.

[Bin18] Binder F, Correa LA, Gogolin C, Anders J and Adesso G, editors [2018]. *Thermodynamics in the Quantum Regime*, volume 195. Springer International Publishing.

[Bit96] Bitko D, Rosenbaum TF and Aeppli G [1996]. Phys. Rev. Lett., 77(5):940–943.

[Bla08] Blanes S, Casas F, Oteo JA and Ros J [2008]. Phys. Rep., 470:151–238.

[Bou09] Bouchoule I, Van Druten NJ and Westbrook CI [2009]. arXiv:0901.3303.

[Bra06] Braaten E and Hammer HW [2006]. Phys. Rep., 428(5-6):259–390.

[Bre07] Breuer HP and Petruccione F [2007]. *The Theory of Open Quantum Systems*. Oxford University Press, USA.

[Bre16] Breuer HP, Laine EM, Piilo J and Vacchini B [2016]. Rev. Mod. Phys., 88:21002.

[Bru17] Brun Y and Dubail J [2017]. SciPost Phys., 2:012.

[Bru18] Brun Y and Dubail J [2018]. SciPost Phys., 4:37.

[Buk15] Bukov M, D'Alessio L and Polkovnikov A [2015]. Adv. in Phys., 64(2):139–226.

[CA16] Castro-Alvaredo OA, Doyon B and Yoshimura T [2016]. Phys. Rev. X, 6:041065.

[Cam97a] Campbell JE [1897]. Proc. London Math. Soc., 1(28):381–390.

[Cam97b] Campbell JE [1897]. Proc. London Math. Soc., (29):14.

[Cam10a] Campostrini M and Vicari E [2010]. Phys. Rev. A, 82(6):63636.

[Cam10b] Campostrini M and Vicari E [2010]. Phys. Rev. A, 81(2):23606.

[Cam14] Campostrini M, Nespolo J, Pelissetto A and Vicari E [2014]. Phys. Rev. Lett., 113:070402.

[Cam15a] Campbell S, De Chiara G, Paternostro M, Palma GM and Fazio R [2015]. Phys. Rev. Lett., 114(17):1–8.

[Cam15b] Campostrini M, Nespolo J, Pelissetto A and Vicari E [2015]. Phys. Rev. E, 91:052103.

[Cam15c] Campostrini M, Nespolo J, Pelissetto A and Vicari E [2015]. Phys. Rev. E, 91:022108.

[Cam16] Camati PA, Peterson JPS, Batalhão TB, Micadei K, Souza AM, Sarthour RS, Oliveira IS and Serra RM [2016]. Phys. Rev. Lett., 117(24):240502.

[Cap07] Capponi S, Roux G, Azaria P, Boulat E and Lecheminant P [2007]. Phys. Rev. B, 75:100503.

[Car96] Cardy J [1996]. *Scaling and Renormalization in Statistical Physics*. Cambridge press.

[Cas79] Casati G, Chirikov BV, Izraelev FM and Ford J [1979]. In *Stochastic Behavior in Classical and Quantum Hamiltonian Systems*, pages 334–352. Springer-Verlag, Berlin/Heidelberg.

[Cas01] Casas F, Oteo JA and Ros J [2001]. J. Phys. A: Math. Gen., 34(16):3379.

[Caz11] Cazalilla MA, Citro R, Giamarchi T, Orignac E and Rigol M [2011]. Rev. Mod. Phys., 83:1405–1466.

[Ces71] Cesari L [1971]. *Asymptotic Behavior and Stability Problems in Ordinary Differential Equations*. Springer Berlin Heidelberg.

[Cha12] Chandran A, Erez A, Gubser SS and Sondhi SL [2012]. Phys. Rev. B, 86(6):64304.

[Che10] Chen X, Ruschhaupt A, Schmidt S, Del Campo A, Guéry-Odelin D and Muga JG [2010]. Phys. Rev. Lett., 104(6):63002.

[Che17] Chen QY, Xu DF, Niu XH, Jiang J, Peng R, Xu HC, Wen CHP, Ding ZF, Huang K, Shu L, Zhang YJ, Lee H, Strocov VN, Shi M, Bisti F, Schmitt T, Huang YB, Dudin P, Lai XC, Kirchner S, Yuan HQ and Feng DL [2017]. Phys. Rev. B, 96:045107.

[Col09] Collura M, Karevski D and Turban L [2009]. J. Stat. Mech.: Theory and Experiment, 2009(08):P08007.

[Col10a] Coldea R, Tennant DA, Wheeler EM, Wawrzynska E, Prabhakaran D, Telling M, Habicht K, Smeibidl P and Kiefer K [2010]. Science, 327(5962):177–180.

[Col10b] Collura M and Karevski D [2010]. Phys. Rev. Lett., 104(20):200601.

[Col11] Collura M and Karevski D [2011]. Phys. Rev. A, 83(2):23603.

[Col12a] Collura M [2012]. *Non-equilibrium aspects in strongly correlated one-dimensional systems*. PhD Thesis - Université de Lorraine.

[Col12b] Collura M, Aufderheide H, Roux G and Karevski D [2012]. Phys. Rev. A, 86(1):13615.

[Col13a] Collura M, Sotiriadis S and Calabrese P [2013]. Phys. Rev. Lett., 110(24):245301.

[Col13b] Collura M, Sotiriadis S and Calabrese P [2013]. J. Stat. Mech.: Theory and Experiment, 2013(09):P09025.

[Col18] Collura M, Kormos M and Calabrese P [2018]. Phys. Rev. A, 97(3):33609.

[Cor14] Correa LA, Palao JP, Alonso D and Adesso G [2014]. Scien. Rep., 4:3949.

[Cot17] Cottet N, Jezouin S, Bretheau L, Campagne-Ibarcq P, Ficheux Q, Anders J, Auffèves A, Azouit R, Rouchon P and Huard B [2017]. Proc. Nat. Acad. Scien., 114(29):7561–7564.

[Cre09] Creffield CE [2009]. Phys. Rev. A, 79(6):63612.

[Cro09] Cronin AD, Schmiedmayer J and Pritchard DE [2009]. Rev. Mod. Phys., 81(3):1051–1129.

[Cro16] Crossno J, Shi JK, Wang K, Liu X, Harzheim A, Lucas A, Sachdev S, Kim P, Taniguchi T, Watanabe K, Ohki TA and Fong KC [2016]. Science, 351(6277):1058–61.

[Cub12] Cubitt TS, Eisert J and Wolf MM [2012]. Comm. in Math. Phys., 310(2):383–418.

[Da 10] Da Prato G and Zabczyk J [2010]. *Ergodicity for Infinite Dimensional Systems*. Cambridge University Press.

[D'A13] D'Alessio L and Polkovnikov A [2013]. Ann. Phys., 333:19–33.

[D'A16] D'Alessio L, Kafri Y, Polkovnikov A and Rigol M [2016]. Adv. in Phys., 65(3):239–362.

[Dai16] Dai CM, Shi ZC and Yi XX [2016]. Phys. Rev. A, 93(3):32121.

[Dai17] Dai CM, Li H, Wang W and Yi XX [2017]. arXiv:1707.05030.

[dC13] del Campo A and Zurek WH [2013]. International Journal of Modern Physics A, 29(8):49.

[dC14] del Campo A, Goold J and Paternostro M [2014]. Scien. Rep., 4:6208.

[Den09] Deng S, Ortiz G and Viola L [2009]. Phys. Rev. B, 80(24):241109.

[Den16] Deng S, Shi ZY, Diao P, Yu Q, Zhai H, Qi R and Wu H [2016]. Science, 353(6297):371–374.

[dlT22] de la Tour C [1822]. Ann. Chim. Phys., 21:127.

[dlT23] de la Tour C [1823]. Ann. Chim. Phys., 22:410.

[Dom07] Dominici D [2007]. Journal of Difference Equations and Applications, 13(12):1115–1128.

[Don18] Donvil B [2018]. J.Stat. Mech.: Theory and Experiment, (4):43104.

[Dub17] Dubail J, Stèphan J, Viti J and Calabrese P [2017]. SciPost Phys., 2:002.

[Dut15] Dutta A, Aeppli G, Chakrabarti BK, Divakaran U, Rosenbaum TF and Sen D [2015]. *Quantum Phase Transitions in Transverse Field Spin Models*. Cambridge University Press.

[Dzi10] Dziarmaga J [2010]. Adv. in Phys., 59(6):1063–1189.

[Eck15] Eckardt A and Anisimovas E [2015]. New J. of Phys., 17(9):93039.

[Eck17] Eckardt A [2017]. Rev. Mod. Phys., 89:011004.

[Efi70] Efimov V [1970]. Phys. Lett. B, 33(8):563–564.

[Elo17] Elouard C, Herrera-Martí D, Huard B and Auffèves A [2017]. Phys. Rev. Lett., 118:260603.

[Fis89] Fisher MPA, Weichman PB, Grinstein G and Fisher DS [1989]. Phys. Rev. B, 40:546–570.

[Flo83] Floquet G [1883]. Annales scientifiques de l'École normale supérieure, 12:47–88.

[Fol00] Folman R, Krüger P, Cassettari D, Hessmo B, Maier T and Schmiedmayer J [2000]. Phys. Rev. Lett., 84(20):4749–4752.

[Fré19] Frérot I and Roscilde T [2019]. Nature Communications, 10(1):577.

[Fun17] Funo K, Zhang JN, Chatou C, Kim K, Ueda M and del Campo A [2017]. Phys. Rev. Lett., 118:100602.

[Gem10] Gemmer J, Michel M and Mahler G [2010]. *Quantum Thermodynamics*, volume 784. Springer Berlin Heidelberg.

[Geo82] Georgi H [1982]. *Lie algebras in particle physics*. Frontiers in Physics. Addison Wesley Publishing Company, 2 edition.

[Gev92] Geva E and Kosloff R [1992]. J. Chem. Phys., 96(4):3054–3067.

[Gia03] Giamarchi T [2003]. *Quantum Physics in One Dimension*. Oxford.

[Gir60] Girardeau M [1960]. J. Math. Phys., 1(6):516.

[Gir65] Girardeau MD [1965]. Phys. Rev., 139(2B):B500–B508.

[Gol14] Goldman N and Dalibard J [2014]. Phys. Rev. X, 4(3):31027.

[Gol15] Goldman N, Dalibard J, Aidelsburger M and Cooper NR [2015]. Phys. Rev. A, 91:033632.

[Gor76] Gorini V, Kossakowski A and Sudarshan ECG [1976]. J. Math. Phys., 17(5):821–825.

[Gre02] Greiner M, Mandel O, Esslinger T, Hänsch TW and Bloch I [2002]. Nature, 415(6867):39–44.

[Gri17] Gritsev V and Polkovnikov A [2017]. SciPost Phys., 2(3):21.

[Gro91] Grossmann F, Dittrich T, Jung P and Hänggi P [1991]. Phys. Rev. Lett., 67(4):516–519.

[Gua14] Guarneri I, Casati G and Karle V [2014]. Phys. Rev. Lett., 113:174101.

[Had15] Haddadfarshi F, Cui J and Mintert F [2015]. Phys. Rev. Lett., 114(13):130402.

[Hal03] Hall BC [2003]. *Lie Groups, Lie Algebras, and Representations: An Elementary Introduction*. Springer-Verlag New York, 1 edition.

[Hal09] Haller E, Gustavsson M, Mark MJ, Danzl JG, Hart R, Pupillo G and Nägerl HC [2009]. Science, 325(5945):1224–1227.

[Hal10] Haller E, Hart R, Mark MJ, Danzl JG, Reichsöllner L, Gustavsson M, Dalmonte M, Pupillo G and Nägerl HC [2010]. Nature, 466:597 EP –.

[Har99] Harel G and Akulin VM [1999]. Phys. Rev. Lett., 82(1):1–5.

[Har15] Harris RJ [2015]. J. Stat. Mech.: Theory and Experiment, 2015(7):P07021.

[Har17] Hartmann M, Poletti D, Ivanchenko M, Denisov S and Hänggi P [2017]. New J. Phys., 19:83011.

[Hau06] Hausdorff F [1906]. Leipz. Ber., 58:19.

[Hen08] Henkel M [2008]. *Non-Equilibrium Phase Transitions*. Springer.

[Hen13] Henkel M [2013]. *Conformal Invariance and Critical Phenomena*. Springer.

[Hil86] Hill GW [1886]. Acta Mathematica, 8(0):1–36.

[Hil81] Hilhorst HJ and van Leeuwen JMJ [1981]. Phys. Rev. Lett., 47(17):1188–1190.

[Hof07] Hofferberth S, Lesanovsky I, Fischer B, Schumm T and Schmiedmayer J [2007]. Nature, 449:324 EP –.

[Igl93] Iglói F, Peschel I and Turban L [1993]. Adv. in Phys., 42(6):683–740.

[Ino13] Inomata A, Kuratsuji H and Gerry CC [2013]. *Path Integrals and Coherent States of SU(2) and SU(1,1)*. World Scientific.

[Ins16] Insinga A, Andresen B and Salamon P [2016]. Phys. Rev. E, 94:12119.

[Ins18] Insinga A, Andresen B, Salamon P and Kosloff R [2018]. Phys. Rev. E, 97:062153.

[Iti15] Itin AP and Katsnelson MI [2015]. Phys. Rev. Lett., 115:075301.

[Iwa16] Iwahori K and Kawakami N [2016]. Phys. Rev. B, 94(18):184304.

[Jar16] Jaramillo J, Beau M and Campo AD [2016]. New J. of Phys., 18(7).

[Joh12] Johansson J, Nation P and Nori F [2012]. Computer Physics Communications, 183(8):1760–1772.

[Joh13] Johansson J, Nation P and Nori F [2013]. Computer Physics Communications, 184(4):1234–1240.

[Jor28] Jordan P and Wigner E [1928]. Zeitschrift für Physik, 47(9):631–651.

[KÖ0] Kühner TD, White SR and Monien H [2000]. Phys. Rev. B, 61:12474–12489.

[Kag96] Kagan Y, Surkov EL and Shlyapnikov GV [1996]. Phys. Rev. A, 54(3):R1753—-R1756.

[Kam11] Kamleitner I and Shnirman A [2011]. Phys. Rev. B, 84(23):235140.

[Kan18] Kandelaki E and Rudner MS [2018]. Phys. Rev. Lett., 121(3):36801.

[Kap51] Kapitza PL [1951]. Sov. Phys JETP 21, 588.

[Kap65] Kapitza PL [1965]. Collected Papers of P.L. Kapitza pp: 714-725.

[Kar00] Karevski D, Turban L and Iglói F [2000]. J. Phys. A: Math. Gen., 33(14):2663–2673.

[Kar13] Karevski D, Popkov V and Schütz GM [2013]. Phys. Rev. Lett., 110:047201.

[Khe09] Khesin BA and Wendt R [2009]. *The geometry of infinite-dimensional groups*. Springer.

[Kho14] Khoromskaia D, Harris RJ and Grosskinsky S [2014]. J. Stat. Mech.: Theory and Experiment, 2014(12):P12013.

[Kib76] Kibble TWB [1976]. J. Phys. A: Math. Gen., 9(8):1387–1398.

[Kib80] Kibble T [1980]. Phys. Rep., 67(1):183–199.

[Kin04] Kinoshita T, Wenger T and Weiss DS [2004]. Science, 305(5687):1125–1128.

[Kin06] Kinoshita T, Wenger T and Weiss DS [2006]. Nature, 440:900 EP –.

[Kin14] Kinross A, Fu M, Munsie T, Dabkowska H, Luke G, Sachdev S and Imai T [2014]. Phys. Rev. X, 4(3):031008.

[Kir82] Kirillov AA [1982]. *Infinite dimensional lie groups; their orbits, invariants and representations. The geometry of moments*. Springer, Berlin, Heidelberg.

[Kis12] Kisil VV [2012]. *Geometry of Möbius Transformations*. Imperial College Press.

[Kla14] Klanjšek M [2014]. Physics, 7:74.

[Kla17] Klaers J, Faelt S, Imamoglu A and Togan E [2017]. Phys. Rev. X, 7:31044.

[Kno09] Knoop S, Ferlaino F, Mark M, Berninger M, Schöbel H, Nägerl HC and Grimm R [2009]. Nature Phys., 5(3):227–230.

[Kos11] Kosov DS, Prosen T and Žunkovič B [2011]. J. Phys. A: Math. Theor., 44(46):462001.

[Kos13] Kosloff R [2013]. Entropy, 15(6):2100–2128.

[Kos14] Kosloff R and Levy A [2014]. Ann. Rev. of Phys. Chem., 65(1):365–393.

[Kos17] Kos P and Prosen T [2017]. J. Stat. Mech.: Theory and Experiment, 2017(12):123103.

[Kra71] Kraus K [1971]. Ann. Phys., 64:311–335.

[Kra06] Kraemer T, Mark M, Waldburger P, Danzl JG, Chin C, Engeser B, Lange AD, Pilch K, Jaakkola A, Nägerl HC and Grimm R [2006]. Nature, 440(7082):315–318.

[Kui74] Kuipers L and Niederrieter H [1974]. *Uniform distribution of sequences.* Wiley.

[Lan15] Langen T, Geiger R and Schmiedmayer J [2015]. Ann. Rev. of Cond. Matt. Phys., 6(1):201–217.

[Laz14] Lazarides A, Das A and Moessner R [2014]. Phys. Rev. Lett., 112(15):150401.

[Lek18] Lekscha J, Wilming H, Eisert J and Gallego R [2018]. Phys. Rev. E, 97(2):22142.

[Ler18] Lerose A, Marino J, Gambassi A and Silva A [2018]. arXiv:1803.04490.

[Lew67] Lewis HR [1967]. Phys. Rev. Lett., 18(13):510–512.

[Lew68] Lewis HR [1968]. J. Math. Phys., 9(11):1976–1986.

[Lew69] Lewis HR and Riesenfeld WB [1969]. J. Math. Phys., 10(8):1458–1473.

[Lew82] Lewis HR and Leach PGL [1982]. J. Math. Phys., 23(12):2371–2374.

[Li03] Li D and Liang Y [2003]. Nonlinear Analysis: Theor., Meth. & App., 52(4):1095–1109.

[Li18] Li C, Zhou T, Mazets I, Stimming HP, Zhu Z, Zhai Y, Xiong W, Zhou X, Chen X and Schmiedmayer J [2018]. arXiv:1804.01969.

[Lie61] Lieb EH, Schultz T and Mattis D [1961]. Ann. Phys., 16:407–466.

[Lin75] Lindblad G [1975]. Comm. in Math. Phys., 40(2):147–151.

[Lin76] Lindblad G [1976]. Comm. in Math. Phys., 48(2):119–130.

[Lja07] Ljapunov AM [1907]. Annales de la faculté des science de Toulouse, 2 série, 9:203–474.

[Lor17] Lorenzo S, Marino J, Plastina F, Palma GM and Apollaro TJG [2017]. Scien. Rep., 7(1):5672.

[Luc16] Lucas A, Crossno J, Fong KC, Kim P and Sachdev S [2016]. Phys. Rev. B, 93:075426.

[Ma00] Ma SK [2000]. *Modern Theory of Critical Phenomena.* Westview Press.

[Mad26] Madelung E [1926]. Die Naturwissenschaften, 14(45):1004–1004.

[Mad27] Madelung E [1927]. Zeitschrift fi£ · r Physik, 40(3-4):322–326.

[Mag66] Magnus W and Winkler S [1966]. *Hill's equation.* Courier Corporation.

[Mag18] Magazzù L, Denisov S and Hänggi P [2018]. Phys. Rev. E, 98:022111.

[Man18] Manzano G [2018]. The European Physical Journal Special Topics, 227(3-4):285–300.

[Man19] Manzano G, Silva R and Parrondo JMR [2019]. Phys. Rev. E, 99:042135.

[Mas18] Masuyama Y, Funo K, Murashita Y, Noguchi A, Kono S, Tabuchi Y, Yamazaki R, Ueda M and Nakamura Y [2018]. Nature Comm., 9(1):1291.

[Mic17] Micadei K, Peterson JPS, Souza AM, Sarthour RS, Oliveira IS, Landi GT, Batalhão TB, Serra RM and Lutz E [2017]. arXiv:1711.03323.

[Mik16] Mikami T, Kitamura S, Yasuda K, Tsuji N, Oka T and Aoki H [2016]. Phys. Rev. B, 93:144307.

[Min05] Minguzzi A and Gangardt DM [2005]. Phys. Rev. Lett., 94(24):240404.

[Moa08] Moan PC and Niesen J [2008]. Found. of Computational Math., 8(3):291–301.

[Mon17a] Monthus C [2017]. J. Stat. Mech.: Theory and Experiment, 2017(4):043303.

[Mon17b] Monthus C [2017]. J. Stat. Mech.: Theory and Experiment, 2017(4):043302.

[Muk09] Mukherjee V and Dutta A [2009]. J. Stat. Mech.: Theory and Experiment, 2009(05):P05005.

[Nai17] Naidon P and Endo S [2017]. Rep. Prog. Phys., 80(5):056001.

[Pei07] Peixoto De Faria JG [2007]. European Physical Journal D, 42(1):153–162.

[Pel02] Pelissetto A and Vicari E [2002]. Phys. Rep., 368:549.

[Pel18a] Pelissetto A, Rossini D and Vicari E [2018]. Phys. Rev. E, 97:052148.

[Pel18b] Pelissetto A, Rossini D and Vicari E [2018]. Phys. Rev. E, 98:032124.

[Pel18c] Pelissetto A, Rossini D and Vicari E [2018]. Phys. Rev. B, 97:094414.

[Pet00] Petrov DS, Shlyapnikov GV and Walraven JTM [2000]. Phys. Rev. Lett., 85(18):3745–3749.

[Pfe70] Pfeuty P [1970]. Ann. Phys., 57:79–90.

[Pfe71] Pfeuty P and Elliott RJ [1971]. J. Phys. C: Solid State Physics, 4(15):2370–2385.

[Pin50] Pinney E [1950]. Proc. American Math. Soc., 1:681.

[Pit16] Pitaevskii L and Stringari S [2016]. *Bose-Einstein Condensation and Superfluidity*. Oxford University Press.

[Pla07] Platini T, Karevski D and Turban L [2007]. J. Phys. A: Math. Theor., 40(7):1467.

[Ple17] Plekhanov K, Roux G and Le Hur K [2017]. Phys. Rev. B, 95:045102.

[Pol11] Polkovnikov A, Sengupta K, Silva A and Vengalattore M [2011]. Rev. Mod. Phys., 83(3):863–883.

[Pop13] Popkov V, Karevski D and Schütz GM [2013]. Phys. Rev. E, 88:062118.

[Pro08] Prosen T and Pižorn I [2008]. Phys. Rev. Lett., 101:105701.

[Pro11a] Prosen T [2011]. Phys. Rev. Lett., 106:217206.

[Pro11b] Prosen T and Ilievski E [2011]. Phys. Rev. Lett., 107(6):60403.

[Rah03a] Rahav S, Gilary I and Fishman S [2003]. Phys. Rev. A, 68(1):13820.

[Rah03b] Rahav S, Gilary I and Fishman S [2003]. Phys. Rev. Lett., 91(11):110404.

[Rau02] Rau ARP and Wendell RA [2002]. Phys. Rev. Lett., 89(22):220405.

[Rau03] Rau ARP and Zhao W [2003]. Phys. Rev. A, 68(5):52102.

[Rau05] Rau ARP and Zhao W [2005]. Phys. Rev. A, 71(6):63822.

[Ray64] Rayfield GW and Reif F [1964]. Phys. Rev., 136(5A):A1194–A1208.

[Rei13] Reichl L [2013]. *The transition to chaos: conservative classical systems and quantum manifestations*. Springer Science & Business Media.

[Rei18] Reimer V, Pedersen KGL, Tanger N, Pletyukhov M and Gritsev V [2018]. Phys. Rev. A, 97(4):43851.

[Rez06] Rezek Y and Kosloff R [2006]. New J. of Phys., 8:83.

[Rib19] Ribeiro P and Prosen T [2019]. Phys. Rev. Lett., 122:010401.

[Rig07] Rigol M, Dunjko V, Yurovsky V and Olshanii M [2007]. Phys. Rev. Lett., 98:050405.

[Ros14] Rossnagel J, Abah O, Schmidt-Kaler F, Singer K and Lutz E [2014]. Phys. Rev. Lett., 112(3):30602.

[Ros18] Rossini D and Vicari E [2018]. Phys. Rev. E, 98:062137.

[Rou10] Roux G [2010]. Phys. Rev. A, 81:053604.

[Rug19] Ruggiero P, Brun Y and Dubail J [2019]. SciPost Phys., 6:51.

[Rus12] Russomanno A, Silva A and Santoro GE [2012]. Phys. Rev. Lett., 109(25):257201.

[Rya13] Ryabov A, Dierl M, Chvosta P, Einax M and Maass P [2013]. J. Phys. A: Math. Theor., 46(7):1–12.

[Sac11a] Sachdev S [2011]. *Quantum Phase Transitions*. Cambridge University Press, 2ed. edition.

[Sac11b] Sachdev S and Keimer B [2011]. Physics Today, 64(2):29–35.

[Sam17] Samuelsson P, Kheradsoud S and Sothmann B [2017]. Phys. Rev. Lett., 118(25):256801.

[San17] Santos JP, Landi GT and Paternostro M [2017]. Phys. Rev. Lett., 118:220601.

[Sch64] Schultz TD, Mattis DC and Lieb EH [1964]. Rev. Mod. Phys., 36:856–871.

[Sch11] Schollwöck U [2011]. Annals of Physics, 326(1):96–192.

[Sch18a] Schemmer M, Bouchoule I, Doyon B and Dubail J [2018]. Phys. Rev. Lett., 122(9):090601.

[Sch18b] Schnell A, Eckardt E and Denisov S [2018]. arXiv:1809.11121.

[Sco17] Scopa S and Karevski D [2017]. J. Phys. A: Math. Theor., 50(42):425301.

[Sco18a] Scopa S, Landi GT and Karevski D [2018]. Phys. Rev. A, 97(6):62121.

[Sco18b] Scopa S, Unterberger J and Karevski D [2018]. J. Phys. A: Math. Theor., 51(18):185001.

[Sco19] Scopa S, Landi GT, Hammoumi A and Karevski D [2019]. Phys. Rev. A, 99:022105.

[Sek00] Sekimoto K, Takagi F and Hondou T [2000]. Phys. Rev. E, 62(6):7759–7768.

[Ser17] Serafini A [2017]. *Quantum continuous variables : a primer of theoretical methods*. CRC Press.

[Shi65] Shirley JH [1965]. Phys. Rev., 138(4B):B979–B987.

[Si10] Si Q and Steglich F [2010]. Science, 329(5996):1161–6.

[Son97] Sondhi SL, Girvin SM, Carini JP and Shahar D [1997]. Rev. Mod. Phys., 69(1):315–333.

[Spo80] Spohn H [1980]. Rev. Mod. Phys., 52(3):569–615.

[Sze39] Szegö G [1939]. *Orthogonal polynomials*. American Mathematical Society.

[Tak14] Takekoshi T, Reichsöllner L, Schindewolf A, Hutson JM, Le Sueur CR, Dulieu O, Ferlaino F, Grimm R and Nägerl HC [2014]. Phys. Rev. Lett., 113(20):205301.

[Tap18] Tapias Arze SE, Claeys PW, Castillo IP and Caux JS [2018]. arXiv:1804.10226.

[Tjo70] Tjon JA [1970]. Phys. Rev. B, 2:2411–2421.

[Tse11] Tsekov R [2011]. Ann. Univ. Sofia, Fac. Chem., 102-103:185–188.

[Tsv16] Tsvelik AM and Zaliznyak IA [2016]. Phys. Rev. B, 94:075152.

[Unt10] Unterberger J [2010]. Confluentes Mathematici, 02(02):217–263.

[Unt12] Unterberger J and Roger C [2012]. *The Schrödinger-Virasoro Algebra*. Springer Berlin Heidelberg.

[Voj03] Vojta M [2003]. Rep. Prog. Phys., 66(12):2069–2110.

[Wal16] Wald S and Henkel M [2016]. J. Phys. A: Math. Theor., 49(12):125001.

[Wal18] Wald S, Landi GT and Henkel M [2018]. J. Stat. Mech.: Theory and Experiment, 2018(1):013103.

[Wan17] Wang L, Fu Z, Sun J, Liu M, Yi W, Yi C, Luo Y, Dai Y, Liu G, Matsushita Y, Yamaura K, Lu L, Cheng JG, Yang Yf, Shi Y and Luo J [2017]. Quantum Materials, 2(1):36.

[Web03a] Weber T, Herbig J, Mark M, Nägerl HC and Grimm R [2003]. Science, 299(5604):232–235.

[Web03b] Weber T, Herbig J, Mark M, Nägerl HC and Grimm R [2003]. Phys. Rev. Lett., 91(12):123201.

[Wee12] Weedbrook C, Pirandola S, García-Patrón R, Cerf NJ, Ralph TC, Shapiro JH and Lloyd S [2012]. Rev. Mod. Phys., 84(2):621–669.

[Wen13] Wendenbaum P, Collura M and Karevski D [2013]. Phys. Rev. A, 87(2):23624.

[Wil17] Wilde MM [2017]. *Quantum Information Theory*. Cambridge University Press, 2 edition.

[Wol08] Wolf MM, Eisert J, Cubitt TS and Cirac JI [2008]. Phys. Rev. Lett., 101(15):150402.

[Yan52] Yang CN [1952]. Phys. Rev., 85:808–816.

[Zac09] Zaccanti M, Deissler B, D'Errico C, Fattori M, Jona-Lasinio M, Müller S, Roati G, Inguscio M and Modugno G [2009]. Nature Phys., 5(8):586–591.

[Zal04] Zaliznyak IA, Woo H, Perring TG, Broholm CL, Frost CD and Takagi H [2004]. Phys. Rev. Lett., 93(8):87202.

[Zel67] Zeldovich BY [1967]. Soviet Physics JETP, 24(5):1006.

[ZJ12] Zinn-Justin J [2012]. *Quantum Field Theory and Critical Phenomena*. Clarendon press - Oxford.

[Zur85] Zurek WH [1985]. Nature, 317:505 EP –.

[Zur05] Zurek WH, Dorner U and Zoller P [2005]. Phys. Rev. Lett., 95(10):3–6.

UNIVERSITÉ DE LORRAINE

Résumé détaillé de la Thèse
présentée pour obtenir le grade de
Docteur en Physique
par
Stefano Scopa
LPCT - Université de Lorraine, Nancy

Dynamique des systèmes quantiques en basses dimensions guidée hors équilibre

Membres du Jury:

Président du jury:

Malte Henkel,	LPCT - Université de Lorraine, Nancy

Rapporteurs :

Tomaž Prosen,	University of Ljubljana
Cécile Monthus,	IPhT CNRS-CEA - Université Paris-Saclay

Examinateurs :

Rosemary J. Harris,	Queen Mary University of London
Denis Bernard,	ENS Paris
Guillaume Roux,	LPTMS - Université Paris Sud

Directeur de Thèse :

Dragi Karevski,	LPCT - Université de Lorraine, Nancy

Cette thèse analyse certains aspects de la dynamique hors équilibre de systèmes quantiques unidimensionnels, lorsqu'ils sont soumis à des champs externes dépendant du temps. Nous considérons plus particulièrement le cas des forçages périodiques, et le cas d'une variation temporelle lente d'un paramètre de l'Hamiltonien qui permet de traverser une transition de phase quantique.
La première partie contient une présentation des notions, des modèles et des outils nécessaires pour comprendre la suite de la thèse, avec notamment des rappels sur les modèles quantiques critiques (en particulier sur les chaines de spin et sur le modèle de Bose-Hubbard), le mécanisme de Kibble-Zurek, et la théorie de Floquet.

Ensuite, nous étudions la dynamique hors équilibre d'un gaz de bosons dans un potentiel harmonique dépendant du temps.
Plus en détail, on considère théoriquement un Hamiltonien de Bose-Hubbard en présence d'un potentiel de piège harmonique $V(j,t) = \frac{1}{2}\omega^2(t)j^2$:

$$\hat{H}(t) = -w\sum_j \left(\hat{a}^\dagger_{j+1}\hat{a}_j + \text{h.c.}\right) + \frac{U}{2}\sum_j \hat{n}_j(\hat{n}_j - 1) + \sum_j \left(V(j,t) - \mu\right)\hat{n}_j,$$

où les opérateurs $\hat{a}_j$, $\hat{a}^\dagger_j$ obéissent aux relations de commutation standard pour les bosons et $\hat{n}_j = \hat{a}^\dagger_j\hat{a}_j$ est l'opérateur nombre de bosons sur un site j. Ce choix est motivé par des configurations expérimentales, où les échantillons d'atomes froids sont généralement confinés dans l'espace par la présence de ces potentiels de piège.
Nous considérons également la limite des interactions fortes $U/w \gg 1$ - la limite de *Tonks-Girardeau*, dans laquelle le système de bosons peut être ramené à un système fermionique libre par une transformation de Jordan-Wigner. Il s'ensuit donc qu'un gaz Tonks-Girardeau peut être décrit par l'Hamiltonien de la chaine du spin xx:

$$\hat{H}(t) = \sum_{i,j} \hat{c}^\dagger_i\, A_{ij}(t)\, \hat{c}_j,$$

où $\hat{c}^\dagger_j$, $\hat{c}_j$ sont des opérateurs fermioniques et

$$A_{ij}(t) = (V(j,t) - \mu)\delta_{ij} - w\left(\delta_{i,j+1} + \delta_{i+1,j}\right).$$

Ce système montre une transition quantique de phase ($\mu = \mu_c$) d'une phase de l'isolant de Mott ($|\mu| > 1$) à un superfluide ($|\mu| < 1$), guidé par le potentiel chimique μ. Pour notre configuration, $\mu_{\text{eff}}(j,t) = \mu - V(j,t)$ s'avère être

un potentiel chimique efficace, en raison du potentiel du piège. Nous avons donc étudié le cas $\mu = \mu_c$, où retirer le potentiel de confinement $V(j,t) \to 0$ correspond au passage de la transition de phase non homogène.
Dans le cas de variations lentes du potentiel du piège, on peut étudier l'évolution temporelle du système en approximation adiabatique, où l'état du système pour N particules, préparé à l'équilibre à un instant t_0, est donné à un instant $t > t_0$ à partir de l'état fondamental correspondant au Hamiltonien instantané:

$$|\Psi(t)\rangle = |\Psi_0(t)\rangle = \sum_{q<N} \hat{\eta}_q^\dagger(t)\,|0\rangle\,.$$

Ici, $\hat{\eta}_q^\dagger$ est l'opérateur de création de quasi-particules obtenu après une diagonalisation canonique du système.
Après, nous avons calculé les déviations hors équilibre de l'évolution adiabatique, où l'état du système est écrit:

$$|\Psi(t)\rangle \simeq e^{-i\int_{t_0}^{t} \mathrm{d}s\; E_0(s)} \left(|\Psi_0(t)\rangle + \sum_{p\geq N} \sum_{k<N} a_{pk}(t)\; |\Psi_0[\underline{k}, p](t)\rangle \right),$$

obtenu au moyen d'un developpement perturbatif à l'ordre dominant. Ici, $|\Psi_0[\underline{k}, p](t)\rangle = \hat{\eta}_p^\dagger(t)\hat{\eta}_k(t)\,|\Psi_0(t)\rangle$ est l'état fondamental dans lequel une particule passe d'une position $k < N$ à $p \geq N$ avec une amplitude de transition $a_{pk}(t)$, qui a été calculée analytiquement.
Nous avons quantifié les effets de non-équilibre sur l'évolution adiabatique en calculant le profil de densité du système $\rho(j,t) = \langle\Psi(t)|\hat{c}_j^\dagger\hat{c}_j|\Psi(t)\rangle$, comme illustré dans la Fig. 5.1. Ensuite, nous avons présenté des résultats exacts pour l'évolution temporelle du profil de densité, obtenus avec l'utilisation des invariants dynamiques d'Ermakov-Lewis. Les résultats s'écrivent

$$\rho(j,t) = \frac{1}{\zeta(t)} \sum_{k<N} |\psi_k(\frac{x}{\zeta(t)}, t_0)|^2,$$

où ψ_k est une fonction de Hilbert-Hermite (solution d'un oscillateur harmonique quantique 1d) et ζ est une solution de l'équation:

$$\ddot{\zeta}(t) + \omega^2(t)\zeta(t) = \frac{\omega^2(t_0)}{\zeta^3(t)}.$$

Plus en détail, nous nous sommes concentrés sur deux types de protocoles de fréquence de piège $\omega(t)$: **(i)** le cas $\omega(t) = \lambda/t$ (pour $t \geq 1$) et **(ii)** le cas du forçage périodique $\omega(t) = \omega(t + 2\pi)$.

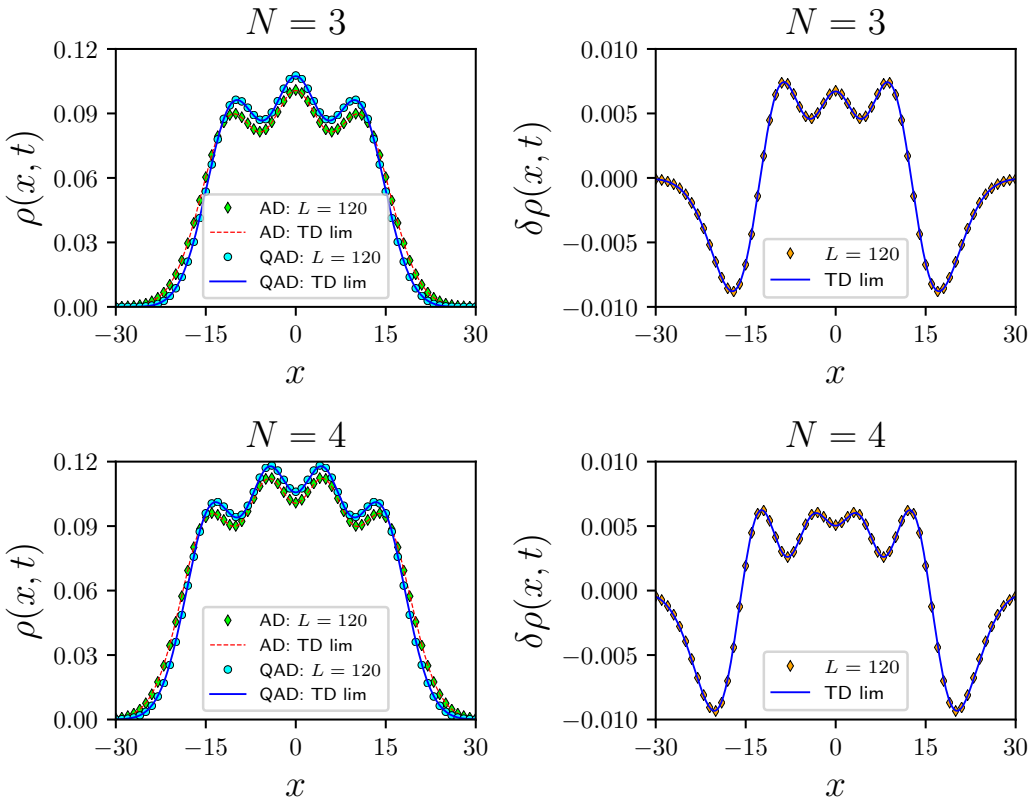

Figure 5.1: Corrections du profil de densité adiabatique pour un système de $N = 3, 4$ particules. Les résultats sont obtenus analytiquement et numériquement avec la méthode de diagonalisation exacte.

Le premier cas présente un phénomÃÍne intéressant appelé expansion d'Efimov (voir Fig. 5.2) tandis que le second cas peut conduire à un régime stable ou instable, en fonction du type de fréquence périodique $\omega(t) = \omega(t + 2\pi)$ (voir Fig. 5.3).

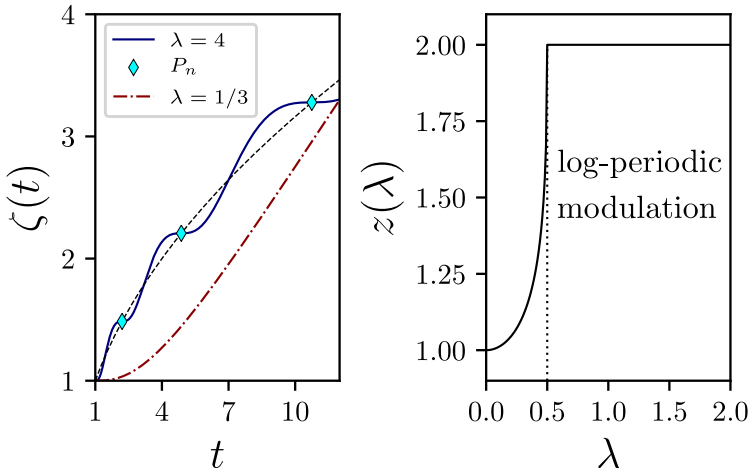

Figure 5.2: Evolution temporelle du profil de densité pour une modulation de la fréquence du piège égale à $\omega(t) = \lambda/t$ (pour $t \geq 1$). L'expansion du gaz est contrôlée par la fonction $\zeta(t)$ (*à gauche*) obtenue analytiquement avec la théorie d'Ermakov-Lewis. En particulier, nous avons trouvé deux régimes contrôlés par la valeur de λ: (**i**) un régime de basse fréquence initiale, $\lambda < 1/2$, dans lequel il existe une expansion continue du gaz avec une loi à puissance asymptotique $\zeta \sim t^{1/z(\lambda)}$ ($z(\lambda)$ *à droite*) et (**ii**) un régime à haute fréquence initiale, $\lambda > 1/2$, dans lequel des modulations log-périodiques sont présentes. Ces modulations log-périodiques conduisent à l'émergence de plateaux P_n autour desquels la dilatation du gaz s'arrête.

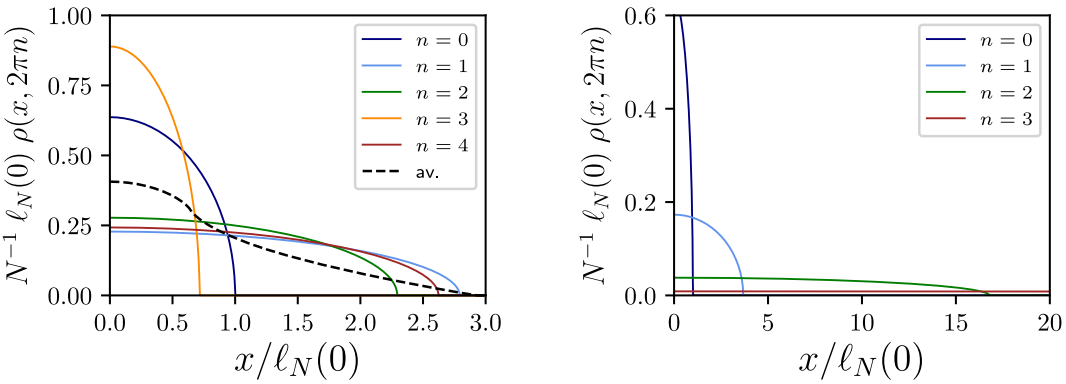

Figure 5.3: Evolution temporelle du profil de densité pour une modulation périodique de la fréquence du piège $\omega(t) = \omega(t + 2\pi)$. Nous avons montré que deux types de scénarios sont possibles: (**i**) (*à gauche*) l'évolution est stable et le gaz développe des oscillations. (**ii**) (*à droite*) l'évolution est instable et le gaz se dilate rapidement en ignorant la présence du piège.

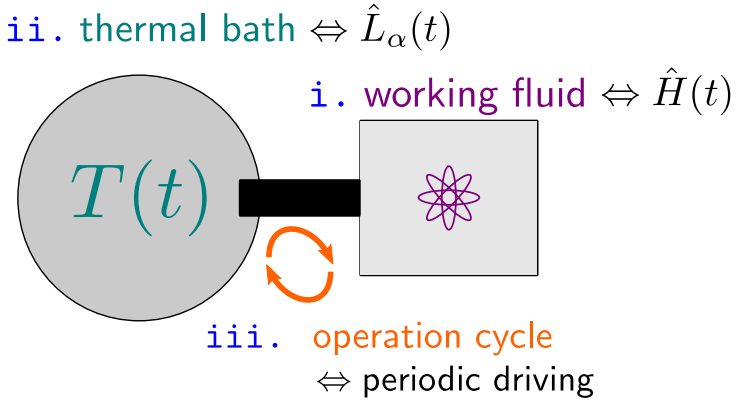

Figure 5.4: Illustration d'un moteur thermique quantique: (**i**) le fluide de travail est modélisé avec un Hamiltonien dépendant du temps $\hat{H}(t)$ qui interagit avec (**ii**) un réservoir à température $T(t)$, reproduit avec l'utilisation appropriée des opérateurs $\hat{L}_\alpha(t)$. (iii) Le cycle thermodynamique est donc déterminé par un protocole spécifique pour $\hat{H}(t)$ et $T(t)$.

Enfin, nous analysons la dynamique hors équilibre des systèmes quantiques ouverts en approximation de Markov. Pour faire ça, nous avons considéré l'évolution temporelle de la matrice de densité réduite $\hat{\rho}$ générée par l'équation de Lindblad

$$\frac{\mathrm{d}}{\mathrm{d}t}\hat{\rho}(t) = -i[\hat{H}(t), \hat{\rho}(t)] + \sum_\alpha \left(\hat{L}_\alpha(t)\hat{\rho}(t)\hat{L}_\alpha^\dagger(t) - \frac{1}{2}\{\hat{L}_\alpha^\dagger(t)\hat{L}_\alpha(t), \hat{\rho}(t)\} \right)$$

où le premier terme à droite, $-i[\hat{H}, \hat{\rho}]$, génére l'évolution de Liouville pour le système tandis que le second terme considère les mécanismes de dissipation entre le système quantique et l'environnement. Ici, le mécanisme de dissipation est mis en œuvre par l'intermédiaire d'opérateurs de *jump* $\hat{L}_\alpha(t)$, dont la structure et le nombre sont généralement choisis avec des considérations phénoménologiques. Nous avons formulé une méthode algébrique pour obtenir des solutions exactes de lâĂŹ équation de Lindblad dependant du temps. Cette méthode est basée sur la définition d'une carte $\check{W}(t)$ qui transporte le problème initial dans un nouveau système de référence $\hat{\rho} \overset{\check{W}}{\mapsto} \hat{\rho}_{\text{eff}}$, où l'évolution est générée par une équation de Lindblad indépendante du temps, et peut donc être, facilement résolue.

Enfin, nous nous sommes concentrés sur le cas d'un Hamiltonien $\hat{H}(t) = \hat{H}(t+\mathcal{T})$ et d'un environnement $\hat{L}_\alpha(t) = \hat{L}_\alpha(t+\mathcal{T})$ périodiques.

En particulier, nous avons formulé une nouvelle théorie de Floquet afin d'obtenir des solutions exactes des équations de Lindblad périodiques. Ce formalisme de Lindblad-Floquet est enfin utilisé pour obtenir une caractérisation exacte du fonctionnement en temps fini des machines thermiques quantiques (voir Fig.4).